NEURONAL CHANGES IN THE HIPPOCAMPUS OF POST-STROKE SURVIVORS

Elizabeth Gemmell
MRes. Neuroscience, BSc Hons Biomedical Science

Neurovascular Research Group
Institute for Ageing and Health
Newcastle University
Campus for Ageing and Vitality
Newcastle Upon Tyne
NE4 5PL

Dissertation submitted for the degree of Doctor of Philosophy in
Newcastle University
November, 2013

Abstract

Background: Delayed post-stroke dementia (PSD) affects up to 50% of all stroke survivors, developing months or years after the initial stroke. However, the underlying mechanisms which cause PSD are unclear. Hippocampal atrophy is associated with PSD and vascular dementia, and hippocampal neurons are known to be particularly vulnerable in stroke and cerebrovascular disease. This work aimed to identify neuropathological characteristics and mechanisms contributing to cognitive decline in post-stroke survivors, focusing on the involvement of regional specific hippocampal neurons.

Methods: Post-mortem brain tissue from the prospective CogFAST study was analyzed to compare pathological changes in stroke survivors who developed PSD with those who maintained normal cognitive function (PSND). Tissue from elderly controls and pathologically defined dementia groups; Alzheimer's disease (AD), vascular dementia (VaD), mixed AD with VaD (MD); were also analysed for comparison with different disease aetiologies. Histological and immunohistochemical staining with quantitative image analysis and 3D morphometric analysis was carried out in paraffin-embedded sections, and protein immunoblotting was used in frozen hippocampal tissue.

Key findings: Neuronal volumes in hippocampal subfields CA1-4 were reduced in PSD, VaD and AD subjects compared to elderly controls and PSND. Neuronal volume was also related to post-stroke cognitive function. There were no differences in dendritic length-density, hippocampal myelin loss, or autophagy markers between PSD and PSND. However, neuronal volumes were related to hippocampal tau pathology burden, reactive astrocyte density and myelin density in the alveus. Interestingly, the PSND subjects had greater burden of hippocampal amyloid-β than PSD. There were no quantitative differences in markers for astrocytes or microglia between the post-stroke groups.

Conclusion: These findings suggest that neuronal volume loss is associated with post-stroke and ageing-related dementia. There were no relationships between the observed neuronal changes and AD pathology in stroke survivors, suggesting an important role for cerebrovascular disease processes.

Acknowledgements

First and foremost, I would like to thank my supervisor Professor Raj Kalaria for giving me the opportunity to complete a PhD in this exciting area of research, and for his support, knowledge and enthusiasm which has helped to inspire my work.

I would like to give special thanks to Mr. Arthur Oakley for his advice and support throughout my PhD, and for his great sense of humour, generosity, and tales of his time in research which have made my time with the Neurovascular Research group especially enjoyable.

I would not have been able to complete my PhD without the help of my colleagues and good friends, particularly Dr. Lucy Craggs, Dr. Ahmad Khundakar, and Janet Slade who taught me the essential research skills I acquired during my PhD. I wish to extend my gratitude to Ros Hall and Mary Johnson for their assistance and expert advice in neuroanatomy and histological techniques. I would also like to thank Edward Tam, Georgina Smalley and Sukhraj Tiwana, and all the staff at the Newcastle Brain Tissue Resource for their assistance during my studies. None of this research would have been possible without the generosity of the patients and families involved in the Cognitive Function After Stroke study, and I hope my work will help to inspire further important research in this field.

Finally I would like to thank Dean Smith and my family for always supporting and encouraging me through my studies, and to let them know how much I appreciate all that they have done to help me achieve my PhD.

My PhD was funded by the Medical Research Council as part of the Lifelong Health and Wellbeing Initiative at the Centre for Brain Ageing and Vitality.

Lizzie Gemmell

November, 2013

Contents

NEURONAL CHANGES IN THE HIPPOCAMPUS OF POST-STROKE SURVIVORS i

Chapter 1. Introduction 1

1.1 Ageing, stroke and dementia 1

1.1.1 Post-stroke dementia 1

1.2 Causes of delayed post-stroke dementia 3

1.2.1 Cerebrovascular disease (CVD) 4

1.2.2 Alzheimer's disease (AD) 7

1.2.3 Mixed dementia: CVD and AD 11

1.2.4 Ageing 12

1.3 The Cognitive Function After Stroke (CogFAST) study 14

1.3.1 Study design 14

1.3.2 Key CogFAST study findings 16

1.3.3 Hippocampal microvascular changes in delayed PSD 17

1.4 The hippocampus in post-stroke dementia 18

1.4.1 Hippocampal atrophy and dementia 18

1.4.2 The hippocampus and memory 19

1.4.3 Hippocampal anatomy and circuitry 20

1.4.4 Pyramidal neurons in the Cornu Ammonis 23

1.4.5 Differential subfield vulnerability in PSD 26

1.4.6 Neurodegeneration and autophagy 27

1.5 The role of neuroglia in neurodegeneration 28

1.5.1 Astrocytes 29

1.5.2 Microglia....33
1.5.3 Oligodendrocytes....34
1.6 Aims and hypotheses....36
Chapter 2. Materials and Methods....37
2.1 Introduction....37
2.2 Subject selection and clinical diagnosis....37
2.2.1 CogFAST study design....37
2.2.2 Neuropathological assessment and dementia diagnoses....38
2.2.3 Subject demographics and pathological findings....40
2.3 Tissue acquisition....41
2.4 Paraffin-embedded tissue preparation....42
2.4.1 Sectioning, dewaxing and mounting....42
2.5 Histology....44
2.5.1 Cresyl Fast Violet (CFV)....44
2.5.2 Luxol Fast Blue (LFB)....44
2.5.3 Haematoxylin and Eosin (H & E)....45
2.6 Standard immunohistochemistry (IHC) protocol....45
2.7 Image analysis....48
2.7.1 Image capture....48
2.7.2 Image Pro analysis....48
2.7.3 Image Pro analysis of LFB stained sections and myelin index calculations 49
2.7.4 Astrocyte counts....50

2.7.5 2.7.5 3D Stereology for neuronal density and volume 50

2.7.6 3D stereology for dendritic length-density 53

2.8 Protein analysis in frozen hippocampal tissue 54

2.8.1 Tissue extraction 54

2.8.2 DC protein assay 55

2.8.3 Protein separation by SDS-PAGE 56

2.8.4 Protein immunoblotting 57

2.9 Baboon model of acute chronic cerebral hypoperfusion 59

2.10 Statistical analyses 61

Chapter 3. Neuronal Volume and Density Changes in Post-Stroke and Ageing Related Dementias 62

3.1 Introduction 62

3.1.1 Measuring neuronal volume and density using 3D stereology 63

3.2 Aims 64

3.3 Methods 64

3.3.1 3D stereological analysis of neuronal volumes and densities 64

3.3.2 Statistical analyses 65

3.4 Results 65

3.4.1 Subject demographics 65

3.4.2 Neuronal density in PSD and ageing-related dementias 66

3.4.3 Neuronal volumes in PSD and ageing-related dementias 68

3.4.4 Clinicopathological correlations 71

3.4.5 Neuronal changes in younger versus elderly controls 73

3.4.6 Neuronal changes in a baboon model of acute cerebral hypoperfusion .75

3.5 Discussion 77

3.5.1 Reduced neuronal volumes in post-stroke and ageing-related dementias 77

3.5.2 Neuronal volumes and densities in different disease processes.....78

3.5.3 Comparison with previous studies.....79

3.5.4 Limitations of neuronal volume and density measurements 80

3.5.5 Neuronal volumes in middle-aged and elderly controls.....81

3.5.6 Neuronal volumes were reversibly reduced in acute cerebral hypoperfusion 82

3.6 Conclusions.....83

Chapter 4. Neurodegenerative Processes in Stroke Survivors 84

4.1 Introduction.....84

4.1.1 Hippocampal Alzheimer's-type pathology.....84

4.1.2 Dysfunctional autophagy in AD and CVD.....86

4.2 Aims 89

4.3 Materials and methods 89

4.3.1 IHC and image analysis.....89

4.3.2 Semi-quantitative rating of hippocampal Aβ pathology.....89

4.3.3 Semi-quantitative rating of hippocampal tau pathology.....90

4.3.4 Statistical analyses 90

4.4 Results 93

4.4.1 AD pathology.....93

4.4.2 Autophagy markers 96

4.4.3 Correlations between autophagy markers 99

4.4.4 Clinicopathological correlations 100

4.5 Discussion 100

4.5.1 Hippocampal AD pathology 100

4.5.2 Autophagy markers 102

4.6 Conclusions 104

Chapter 5. Hippocampal Dendritic Changes in Post-Stroke and Ageing-Related Dementias 105

5.1 Introduction 105

5.1.1 Dendrites and dendritic spines 105

5.1.2 Techniques used to study dendrite morphology: Golgi staining 106

5.1.3 Techniques used to study dendrite morphology: MAP2 IHC 107

5.1.4 Dendritic changes after ischemia 107

5.1.5 Synapse loss in AD and stroke 109

5.2 Aims 111

5.3 Materials and methods 112

5.3.1 IHC 112

5.3.2 Image Pro analysis of MAP2 in the pyramidal layer 112

5.3.3 Novel 3D analysis of dendritic length density in the stratum radiatum . 112

5.3.4 Investigation of CA layers stained for MAP2 and other post-synaptic proteins 112

5.3.5 Protein immunoblots of synaptic markers 113

5.3.6 Statistical analysis 113

5.4 Results 114

5.4.1 MAP2 2D image analysis 114

5.4.2 MAP2 dendritic length density 117

5.4.3 Visual investigation of MAP2 and post-synaptic markers 118

5.4.4 MAP2 and drebrin staining in perfused non-human primate model 122

5.4.5 Protein immunoblots of synaptic markers 124

5.5 Discussion 126

5.5.1 MAP2 in the pyramidal layer 126

5.5.2 MAP2 dendritic length density in the stratum radiatum 126

5.5.3 MAP2 and AD pathology 129

5.5.4 Visual investigation of MAP2, drebrin and PSD-95 staining 129

5.5.5 Pre- and post-synaptic proteins in frozen hippocampal tissue 130

5.6 Conclusions 132

Chapter 6. Hippocampal white matter changes and involvement of astrocytes and microglia 134

6.1 Introduction 134

6.1.1 White matter changes in the alveus 134

6.1.2 Neuroglia in stroke and AD 138

6.2 Aims 141

6.3 Methods 142

6.3.1 Histological and IHC staining 142

6.3.2 Image analysis 142

6.3.3 Statistical analysis 145
6.4 Results 146
6.4.1 White matter changes in the alveus 146
6.4.2 Neuronal dMBP staining 148
6.4.3 Neuronal pyknosis rating 150
6.4.4 Astrocyte density 151
6.4.5 Microglia 158
6.5 Discussion 160
6.5.1 White matter damage 160
6.5.2 Astrocyte densities 162
6.5.3 Microglia 164
6.6 Conclusions 165
Chapter 7. Discussion 167
7.1 Introduction 167
7.2 Neuronal atrophy as a mechanism contributing to cognitive impairment 168
7.3 Investigating mechanisms causing neuronal atrophy 169
7.3.1 Alzheimer's disease pathology 169
7.3.2 Autophagy 169
7.3.3 Neuronal connectivity; dendrites, dendritic spines and synapses 170
7.3.4 White matter changes in ageing and CVD 172
7.3.5 Role of astrocytes and microglial activation 173
7.4 General strengths and limitations 174
7.4.1 Unique strengths of the CogFAST cohort 174

7.4.2 Additional factors to consider 174

7.4.3 Limitations associated with human post-mortem studies of age-associated dementia 175

7.5 Future Directions 176

7.5.1 Short-term studies 176

7.5.2 Medium-term studies 177

7.5.3 Long-term studies 178

7.6 Conclusions 179

Chapter 8. Appendix 180

Figure and table legends

Figure 1.1 Progression of delayed post-stroke dementia over time. TIA = transient ischaemic attack, NFT = neurofibrillary tangle, CAA = cerebral amyloid angiopathy. 4

Figure 1.2. Common pathological characteristics of AD and VaD. A, Hyperphosphorylated tau pathology in the hippocampus of an AD subject, visualized using antibodies to AT8; B, amyloid plaques in the hippocampus of an AD subject, visualized using antibodies to 4G8; C, Cerebral amyloid angiopathy (CAA), arrows show Aβ deposition in capillaries; D, atherosclerotic changes in the left carotid artery of an elderly subject (C and D adapted from Grinberg and Thal, 2010); E, normal blood vessel in elderly subject; F, Arteriolosclerotic blood vessel in a subject with SVD, demonstrating splitting of concentric smooth muscle cell layers 10

Figure 1.3 The CogFAST study design. Mean survival time from stroke to death was 6.72 years (Allan *et al.*, 2011). CT = X-ray computed tomography scan, MMSE = Mini Mental State Exam, CAMCOG = Cambridge Cognitive Examination, DSM = Diagnostic and Statistical Manual of mental disorders. 15

Figure 1.4 Hippocampal atrophy in an Alzheimer's disease and control subject. Thinning of the cortex and enlarging of ventricles is also evident in the AD brain, contributing to overall brain atrophy. 19

Figure 1.5. Diagram showing the location of the hippocampus in the medial temporal lobe and the differences between episodic and semantic memory. 20

Figure 1.6 A, Transverse section of the hippocampus stained using cresyl fast violet to visualize neuronal soma and neuronal subfields: The CA4 subfield is completely enclosed by the dentate gyrus, the CA3 begins at the 'mouth' of the DG and contains larger and more uniformly oriented neurons, the CA2 neurons are larger, rounder and densely packed in a narrow band, and the CA1 widens out to a broad band of more dispersed, smaller pyramidal neurons. The CA1/subiculum border is harder to visually identify, and is generally considered to begin where the distribution of neurons becomes more patchy in the straighter band of cells towards the entorhinal cortex. B, Major circuits of information processing in the hippocampus. Orange arrows represent the traditional trisynaptic loop involving the DG - CA3 - CA1; Blue arrows represent the

disynaptic loop involving the CA3 - CA1; Yellow arrows represent the disynaptic loop involving the CA2 – CA1; the green arrow represents the monosynaptic temporoammonic pathway from the EC to CA1. The black arrow in the CA3 represents its highly reciprocal connections (Jones and McHugh, 2011).....22

Figure 1.7. Layers of the Cornu Ammonis. Str = stratum, SO = stratum oriens, SP = stratum pyramidal, SR = stratum radiatum. Adapted from (Duevernoy, 2005).....24

Figure 1.8. Hippocampal subfields visualized using immunohistochemistry to detect dendritic protein MAP2.....25

Figure 1.9. GFAP-positive astrocytes in the CA1 visualized using nickel-DAB. A, Protoplasmic astrocyte; B, Fibrous astrocyte in the alveus, surrounded by other GFAP-immunopositive processes; C, Astrocytes and astrocytic endfeet around a blood vessel. A, B Scale bar = 50µm; C, Scale bar = 100µm.....33

Figure 1.10 Activated microglia in the CA1 of an AD subject, visualized using IHC to CD68. Scale bar = 50µm. 34

Figure 1.11. A, Diagram of an oligodendrocyte forming myelin sheath around an axon; B, Characteristic regular, small, darkly stained nuclei of oligodendrocytes in the alveus, section stained using LFB for myelin and haematoxylin to visualize nuclei. Scale bar = 50µm. 35

Figure 2.1. A, Levels 18 and 19 according to the Newcastle Brain Map (Perry and Oakley, 1993); B, Close-up of hippocampal formation at level 18 with clearly identifiable dentate gyrus and CA regions in a section stained with cresyl-fast violet..43

Figure 2.2. Example screen capture of image analysis using Image Pro. Histogram-based segmentation is performed to highlight in red all immunopositive staining.....48

Figure 2.3 Diagrams demonstrating how images were taken throughout the alveus of LFB/CFV stained hippocampal sections. A, Red squares represent individual images taken at 10x magnification; B The alveus was delineated as one subfield for myelin index analysis. 49

Figure 2.4. CA1 stratum pyramidal stained for ALDH1L1 with 3x4 counting grid overlay. Scale bar = 100µm.....50

Figure 2.5. CA1 Stratum pyramidal stained for ALDH1L1 with3x4 counting grid overlay. Scale bar = 100µm. 50

Figure 2.6. A, Diagram depicting the optical disector box within a 30µm thick tissue section; B, Representative image of a CA1 pyramidal neuron being measured using the nucleator tool: N indicates non-pyramidal neuron; P, pyramidal neuron; G, glial cell. Red and green lines delineate the disector frame. Scale bar = 10µm. 52

Figure 2.7. Representative images of the spherical probe used to measure dendritic length density. A-C, as the focal plane moved downwards through the z-axis dendrites were measured when an in focus dendrite crossed the sphere boundary (red circle). 54

Figure 2.8. Flow diagram depicting stages of frozen tissue extraction (A,B), the protein assay (C) and making up running sample (D).WH = whole homogenate; RS = running sample. 56

Figure 2.9. A, Papio anubis; B, Diagram showing the sites of ligation for three vessel occlusion surgery (3VO). 60

Figure 3.1. Diagram demonstrating the differences between 2D and 3D stereological analysis of neuronal volumes and densities. The left diagram shows how neurons would be viewed within a thick tissue section using 3D stereology. The right diagram shows how 2D analysis would result in inaccurate area measurements from profiles of each neuron, and demonstrates how larger neurons would be over-counted using this technique (3 neurons, 5 profiles). 63

Figure 3.2. Neuronal densities in CA1-4 and ECV. PSND = post-stroke non-demented, PSD = delayed post-stroke dementia, VaD = vascular dementia, MD = mixed vascular and Alzheimer's dementia, AD = Alzheimer's disease; *indicate difference to controls, + indicate difference compared to PSND; $p < 0.05$. 68

Figure 3.3. Neuronal volumes in CA1-4 and ECV. PSND = post-stroke non-demented, PSD = delayed post-stroke dementia, VaD = vascular dementia, MD = mixed vascular and Alzheimer's dementia, AD = Alzheimer's disease; *indicate difference to controls, + indicate difference compared to PSND; Red = $p < 0.05$, blue = $p < 0.01$. 70

Figure 3.4. Neuronal volume as a percentage of control means. 71

Figure 3.5. CA2 neuronal volumes were positively correlated with total CAMCOG scores (A) and memory sub-scores (B), with subjects with total CAMCOG score < 40 and memory score < 10 excluded. o = PSD; x = PSND. 72

Figure 3.6 CA1 and CA2 neuronal densities (A) and volumes (B) in elderly and younger controls. Red asterisk indicates significant difference compared to controls.....74

Figure 3.7. A, CA1 and CA2 Neuronal volumes in a baboon model of cerebral hypoperfusion at different survival times post-surgery; 1D = 1 day, 2D = 2 day, 3D = 3 day, 7D = 7 day, 14D = 14 days, 28D = 28 days post-surgery. Blue circles = left hemisphere (contralateral to surgery), green circles = right hemisphere (ipsilateral to surgery); B, Representative images of normal CA1 neurons in sham animal (top panel) and pyknotic CA1 neurons in 3 day animal (bottom panel), Scale bar = 50µm; C, CA1 neuronal volumes were negatively correlated with % pyknotic neurons in CA1 (r = -0.654, p < 0.001). 76

Figure 4.1. Diagram of the key mechanisms in cerebrovascular disease, Aβ and tau pathology relating to neuronal dysfunction and autophagy. 86

Figure 4.2 Thal staging (Thal *et al.*, 2006) of amyloid β and criteria for modified Thal Stages. EC = entorhinal cortex, DG = dentate gyrus. 91

Figure 4.3. Representative images of hippocampal Aβ pathology stained using 4G8, taken at 2.5x magnification. Thal stages are numbered 1-4 in white, modified Thal stages are numbered 1-11 in black. 92

Figure 4.5. Box plots of semi-quantitative ratings of Aβ (A) and hyperphosphorylated tau staining (B) in the CA1. Red lines show differences between groups (Mann-Whitney U test p<0.05). 94

Figure 4.6. Representative images demonstrating the variability of AT8-positive staining in the CA1 in subjects with different Braak scores. A = PSND, Braak stage 1; B = PSND, Braak stage 5, C = PSD, Braak stage 3; D = AD, Braak stage =6.Scale bar = 50um. 95

Figure 4.7. Box plots showing CA1 % Per Area and Mean IOD results for A, LC3; B, Beclin-1; C, P62. Red lines indicate significant differences $p < 0.05$, dashed lines indicated $p < 0.1$. 97

Figure 4.8 Representative images of CA1 stained for LC3 (A, D, G), Beclin-1 (B, E, H) and P62 (C, F, I) in PSND (A, B, C) PSD (D, E, F) and AD (G, H, I). Bar = 50µm 98

Figure 5.1. The CA1 stratum radiatum in a section stained for MAP2. 112

Figure 5.2 A, Box-plots of CA1 and CA2 MAP2 % Area (%PA) staining and IOD; B, Negative correlations between MAP2 %PA and post-mortem delay. 115

Figure 5.3. Images demonstrating variability in CA1 MAP2 staining in the pyramidal layer between subjects within the same group. A, B = Controls; C, D = PSND; E, F = PSD; G, H = AD. Scale bar = 100µm. 116

Figure 5.4. Dendritic length density in CA1 stratum radiatum. 118

Figure 5.5 Representative images of the different types of hippocampal layer staining using MAP2. A, mottled stratum radiatum; B, Even staining across all layers; C, Patchy stratum moleculare, pale neuronal staining; D, solid stratum molecular of CA layer, pale stratum moleuclare of DG, dark neuronal staining; E, 'Stringy' stratum radiatum; F Few MAP2 positive dendrites in stratum radiatum. Scale bar = 200µm. 119

Figure 5.7 Variability in staining for MAP2 in hippocampal layers; (A, B), Drebrin (C, D) and PSD-95 (E, F) in two PSND subjects with similar PMD, Fixation and Braak stage; A, C, E PMD = 48h, Fixation = 7 weeks, Braak stage = 3; B, D, F PMD = 46h, Fixation = 12 weeks, Braak stage = 3. Scale bar = 200µm 120

Figure 5.6 Variability in pyramidal layer staining for MAP2 (A, B), Drebrin (C, D) and PSD-95 (E, F) in two PSND subjects with similar PMD, fixation length and Braak stage; A, C, E PMD = 48h, Fixation = 7 weeks, Braak stage = 3; B, D, F PMD = 46h, Fixation = 12 weeks, Braak stage = 3. Scale bar = 100µm 120

Figure 5.8 A, B, MAP2 staining in sham baboon; C, D, MAP2 staining in 7-day baboon; E, F, drebrin staining in sham baboon; G, H, drebrin staining in 7-days post-surgery baboon. A, C, E scale bar = 200µm; B, D, F scale bar = 100µm. 123

Figure 5.9. Box-plot and representative protein immunoblots probed for A, pre-synaptic protein SNAP-25; B, Post-synaptic protein PSD-95; C, Pre-synaptic protein synaptophysin. Dotted red line indicates trend to significant difference ($p < 0.1$). S = loading standard, C = control. 125

Figure 5.10. Representative image of CA1 pyramidal layer stained for non-phosphorylated MAP2 from (Cotter *et al.*, 2000). Lines represent linear probes. Scale bar = 50µm. 128

Figure 6.1 A, Diagram of the alveus in the hippocampal formation (dark blue), adapted from (Duevernoy, 2005); B, Image of a hippocampal section stained using LFB to visualize myelin in the alveus, with CFV counterstain to visualize neuronal cell bodies in the pyramidal layers and dentate gyrus. 137

Figure 6.2. Comparing methods to identify astrocytes in the CA2 subfield of a control subject. A, using antibodies to Aldh1L1, DAB stained brown with a very pale hematoxylin counterstain; B, antibodies to GFAP, nickel-DAB stained black, with no counterstain although neurons are still visible in the pyramidal layer as pale brown. There are noticeably fewer astrocytes positive for GFAP (B) than Aldh1L1 (A), particularly in the pyramidal layer. SR = stratum radiatum, PL = pyramidal layer, A = alveus. Scale bar = 100µm. 140

Figure 6.3. Representative images of the alveus stained using LFB to visualize myelin. A, PSND; B, PSD; C, PSD; D PSND. Scale bar = 100µm. 143

Figure 6.4 Representative images of dMBP staining rating in the alveus (CA1). A, 0 = none; B, 1 = mild; C, 2 = moderate; D, 3 = severe. Scale bar = 100µm. 144

Figure 6.5 Pyramidal neurons in the CA1 stained using H&E. A, Pyknotic appearing pyramidal neurons (PSD); B, normal appearing pyramidal neurons with clear nucleolus (PSND). Scale bar large images = 50µm, small images = 10µm. 144

Figure 6.6 A, Area of myelin stained using LFB in the alveus adjacent to CA1 (%PA); B, and CA2 (%PA); C, Area of the CA1 alveus immunoreactive for dMBP (%PA); D, Mean intensity (IOD) of dMBP staining in the CA1 alveus. 147

Figure 6.7 Comparison of dMBP immunopositive staining and LFB myelin staining in serial sections from the same cases. Numbers indicate rating score where 0 = none, 1 = mild, 2 = moderate, 3 = severe. There were no relationships between dMBP and myelin damage. Scale bar = 100µm. 149

Figure 6.8. Immunopositive dMBP staining in soma of CA1 neurons in controls (A, B) and PSD (C), Scale bar = 50µm; D, box plots of neuronal dMBP immunoreactivity in CA1 and CA2. 150

Figure 6.9. Diagram showing the areas where astrocyte densities were calculated. Section from a PSND subject, stained to visualize Aldh1L1. 151

Figure 6.10. GFAP-positive astrocyte density in A, CA1 pyramidal layer; B, CA2 pyramidal layer; C, CA1 stratum radiatum; D, CA2 stratum radiatum; E, Negative correlation between GFAP-positive astrocyte density and dendritic length density in the CA1 stratum radiatum; F, Positive correlation between astrocyte density and CA1 neuronal volume. Dotted red lines indicate trend to significant difference ($p < 0.1$), solid red lines indicate significant difference ($p < 0.05$). 153

Figure 6.11 Representative images of Aldh1L1-positive astrocytes stained brown using DAB (A, C, E) and GFAP-positive astrocytes stained black using nickel-DAB (B, D, F). A and B are from the CA1 stratum radiatum / moleculare of an AD subject; C and D are from the CA1 stratum radiatum / moleculare of a PSND subject; E and F are high-power representative images of Aldh1L1-positive astrocytes and GFAP-positive astrocytes in the CA1 of the PSND subject. Scale bar in A-D = 100µm, E-F = 50µm. ...154

Figure 6.12. Aldh1L1-positive astrocyte densities in the CA1 stratum radiatum (A) and pyramidal layer (B), and CA4 (C); D, Correlation between CA1 pyramidal layer Aldh1L1-positive astrocyte density and global vascular pathological burden. 155

Figure 6.13 A, Correlations between Aldh1L1- and GFAP-positive astrocyte densities in CA1 and CA2; B, Graph showing ratio of Aldh1L1 : GFAP positive astrocyte densities in the different layers analysed. Asterisks indicate significant difference to the PSD group. SR = stratum radiatum, PL= pyramidal layer, A = alveus. 157

Figure 6.14. Representative images of CD68 immunostaining in the CA1 of PSND (A, C) and AD subject (B, D). A-B Scale bar = 100µm, C-D Scale bar = 50µm. E, Box-plots of CD68 mean IOD in the CA1 and CA2. Dotted line indicates trend to significant difference (p = 0.059).....159

Figure 8.1. Neuronal densities (A) and volumes (B) in hippocampal subfields of controls. Error bars ±2SE.....181

Figure 8.2. Neuronal densities in a baboon model of cerebral hypoperfusion at different survival times post-surgery; 1D = 1 day, 2D = 2 day, 3D = 3 day, 7D = 7 day, 14D = 14 days, 28D = 28 days post-surgery. White bars = left hemisphere (contralateral to surgery), grey bars = right hemisphere (ipsilateral to surgery).....182

Figure 8.3 Unusual and different patterns of P62 staining. A, AD outlier (high IOD); B, spherical staining in the alveus of a PSD subject; C, intense spherical staining in the CA1 of a PSND subject; D, spherical staining in the CA2 of a control subject; E, Plaque-like staining in an AD subject; F, tangle like staining in the CA2 of an AD subject. Scale bar A-D = 100µm, E = 200µm, F = 50µm. 186

Figure 8.4. Differences in dentate gyrus staining for MAP2. A, control; B, PSD; C and D, PSND. Scale bar = 100µm.....188

Figure 8.5 Images of subjects with different MAP2 staining and different Braak stages: A = PSND, Braak stage 5; B = PSND, Braak stage 1; C and D = AD, Braak stage 6.....189

Figure 8.6. dMBP-positive neurons in the temporal cortex of control subjects with intense hippocampal dMBP neuronal immunostaining (A, C) and pale/little hippocampal dMBP neuronal immunostaining (B, D). A-B, Scale bar = 100µm, C-D scale bar = 50µm.....190

Figure 8.7. GFAP-positive astrocyte density in the CA1 and CA2 stratum radiatum....193

Figure 8.8 Astrocytes in the pyramidal layer and alveus of A) AD subject and B) PSD subject (Braak score 2, CERAD score 0). GFAP was visualized using IHC with Nickel-DAB. Scale bar = 100µm.....194

Table 1.1 Comparison of the development and distribution of Amyloid-β and tau pathology in AD. * = from (Thal *et al.*, 2002), ** = from (Braak and Braak, 1991).....8

Table 1.2. Common risk factors for AD and VaD (de la Torre, 2002).....12

Table 1.3 Summary of clinical assessments performed in the CogFAST study. CAMCOG = cognitive part of the Cambridge Examination for Mental Disorders of the elderly (CAMDEX) (de Koning *et al.*, 1998); DSM = Diagnostic and Statistical Manual of mental disorders ; CDR = Clinical Dementia Rating; Barthel ADL = Index to measure performance in activities of daily living. 14

Table 2.1. Subject demographics of all stroke subjects analysed. PSND = post-stroke non-demented, PSD = delayed post stroke dementia; PMD = post-mortem delay. 40

Table 2.2. Subject demographics of all subjects analysed. VaD = Vascular dementia, MD = mixed vascular dementia and Alzheimer's disease, AD = Alzheimer's disease; PMD = post-mortem delay.....41

Table 2.3. List of antibodies and methods used for immunohistochemistry. MAb = monoclonal antibody; PAb = polyclonal antibody; F = formic acid antigen retrieval; M = microwave antigen retrieval; P = pressure cooker antigen retrieval method; NHS = normal horse serum; NGS = normal goat serum. 47

Table 2.4 Location and numbers of images and grid squares in which astrocyte counts were performed. 50

Table 2.5. Protocol for making two 20 x 10cm acrylamide gels. 57

Table 2.6. List of antibodies and concentrations used for protein immunoblots. Blots were incubated with primary antibodies at 4C overnight. 59

Table 3.1 Subject demographics. PSND = post-stroke non-demented, PSD = delayed post-stroke dementia, VaD = vascular dementia, MD = mixed vascular and Alzheimer's dementia, AD = Alzheimer's disease, PMD = post mortem delay, N/A = information not available for the majority of control subjects. 66

Table 3.2. Correlations between CA neuronal volumes and CAMCOG scores and sub-scores. Ns = not significant. When correlations were corrected for multiple comparisons (20 tests), the cut-off for significance was reduced to $p < 0.0025$.....73

Table 3.3. Subject demographics in elderly vs. younger controls. 73

Table 4.1 Demographics of subjects studied for Aβ and tau pathology. Slightly fewer subjects were analysed for tau pathology (Controls n = 10, PSND n = 19, PSD n = 10, VaD n = 13, MD n = 13, AD n = 11). 93

Table 4.2. Correlations between different methods used to rate Alzheimer type pathology. Pale blue indicates $p < 0.05$, dark blue indicates $p < 0.01$. 94

Table 4.3 Demographics of subjects investigated using LC3 and Beclin-1. 96

Table 4.4. Demographics of subjects investigated using P62. 96

Table 4.5. Correlations between LC3, Beclin-1 and P62 image analysis results. Light grey highlights correlations significant at $p < 0.05$. Dark grey highlight correlations that remained significant after correcting for multiple testing ($p < 0.00074$). 99

Table 5.1 Demographics of subjects analysed with 2D Image Pro analysis of MAP2 immunostaining. 114

Table 5.2. Demographics of subjects studied using 3D stereology to quantify dendritic length-density. 117

Table 5.3. Demographics of subjects analysed for synaptic proteins in frozen hippocampal tissue. 124

Table 6.1 Demographics of groups analysed for LFB, dMBP and pyknosis rating studies. 146

Table 6.2 Correlations between dMBP staining in the alveus and neuronal soma (pyramidal layer). Dark blue highlights correlations $p < 0.01$, mid blue highlights $p < 0.05$, pale blue highlights trends to correlations $p < 0.1$. 148

Table 6.3. Group demographics of subjects analysed using astrocyte counts. 151

Table 6.4. Group demographics of subjects analysed using CD68 to visualise activated microglia. 158

Table 8.1 Numerical values for neuronal volume and density measures. PS = post-stroke; Std. = standard. 180

Table 8.2. Hippocampal neuronal volumes in CA1-4 and ECV as percentage of control means. 181

Table 8.3 Hippocampal neuronal densities in CA1-4 and ECV as percentage of control means. 181

Table 8.4. Correlations between neuronal volumes in hippocampal subfields CA1- CA4. 182

Table 8.5 Numerical values for neuronal volume and density measures in baboon model cohort. Right = right hippocampus, left = left hippocampus. 183

Table 8.6 Frequency tables for ratings of amyloid and tau pathology. 184

Table 8.7 Numerical values for image analysis of autophagy markers LC3, Beclin-1 and P62 in CA1 and CA2. %PA = percentage of the area of interest positively stained; IOD = integrated optical density (intensity of stain); Std = standard. 185

Table 8.8 Numerical values for MAP2 dendritic length-density (DLD) and image analysis. %PA = percentage of area of interest positive stained; IOD = integrated optical density; Std. = standard. 187

Table 8.9 Frequency tables for ratings of myelin integrity in the alveus. 191

Table 8.10 Numerical data from investigation into Aldh1L1- and GFAP-positive astrocyte densities. Mean = mean astrocyte density per 0.8mm^2; Std = standard; SR = stratum radiatum; PL = pyramidal layer; WM = white matter (alveus). 192

Abbreviations

2D	Two-dimensional
2-VO	Two vessel occlusion
3D	Three-dimensional
3-VO	Three vessel occlusion
AD	Alzheimer's disease
APES	Aminopropyltriethoxysilane
APP	Amyloid precursor protein
AV	Autophagic vacuole
Aβ	Amyloid-β
BSA	Bovine serum albumin
CA1-4	Cornu Ammonis 1-4
CAA	Cerebral amyloid angiopathy
CAMCOG	Cambridge Examination for Mental Disorders in the Elderly
CERAD	Consortium to Establish a Registry for Alzheimer's Disease
CFV	Cresyl fast violet
CogFAST	Cognitive Function After Stroke
CT	Computed Tomography
CVD	Cerebrovascular disease
DAB	3,3'-Diaminobenzidine
DC	Detergent compatible
DG	Dentate gyrus
DLB	Dementia with Lewy Bodies
dMBP	Degraded myelin basic protein
DSM	Diagnostic and Statistical Manual of Mental Disorders
DTI	Diffusion tensor imaging
DTT	Dithiothreitol
EC	Entorhinal cortex
ECV	Entorhinal cortex layer V
GABA	γ-Aminobutyric acid
GFAP	Glial fibrillary acidic protein
H&E	Haematoxylin and eosin
IHC	Immunohistochemistry
IOD	Integrated optical density
LFB	Luxol fast blue
MCAO	Middle cerebral artery occlusion
MCI	Mild cognitive impairment
MD	Mixed dementia
MRI	Magnetic resonance imaging
MTL	Medial temporal lobe
NBTR	Newcastle Brain Tissue Resource

NFT	Neurofibrillary tangle
NMDA	N-methyl-D-aspartate
NT	Neuropil thread
PBS	Phosphate-buffered saline
PL	Pyramidal layer
PMD	Post-mortem delay
PS	Post-stroke
PSD	Post-stroke dementia
PSND	Post-stroke non-demented
SDS	Sodium Dodecyl Sulphate
SDS-PAGE	Sodium Dodecyl Sulphate - Polyacrylamide Gel electrophoresis
SE	Standard error
SR	Stratum radiatum
SVD	Small vessel disease
TBS	tris-buffered saline
TEMED	N,N,NI,NI-tetramethyl-ethyledediamine
TIA	Transient ischaemic attack
VaD	Vascular dementia
VCI	Vascular cognitive impairment
WM	White matter
WMH	White matter hyperintensities
WML	White matter lesions
2D	Two-dimensional
2-VO	Two vessel occlusion
3D	Three-dimensional
3-VO	Three vessel occlusion

List of Original Publications

This thesis is based on the following original publications and some unpublished data:

I. Gemmell, E., Bosomworth, H., Allan, L., Hall, R., Khundakar, A., Oakley, A.E., Deramecourt, V., Polvikoski, T.M., O'Brien, J.T. and Kalaria, R.N. (2012). **Hippocampal Neuronal Atrophy and Cognitive Function in Delayed Poststroke and Aging-Related Dementias,** Stroke, 43(3), pp. 808-814.

II. Gemmell, E., Tam, E., Allan, L., Hall, R., Khundakar, A., Oakley, A.E., Thomas, A., Deramecourt, V., and Kalaria, R. N. (2014) **Neuronal Volumes in Hippocampal Subfields CA3 and CA4 in Delayed Post-stroke and Ageing-Related Dementias,** Journal of Neuropathology & Experimental Neurology, *In press.*

Chapter 1. Introduction

1.1 Ageing, stroke and dementia

The incidence of stroke and dementia increase exponentially with age, which has profound implications for the global ageing population (Burton *et al.*, 2004; Pendelbury, 2009). It is predicted that one fifth of the world's population will be over 60 years old by 2050, and 115 million people will have dementia (Luengo-Fernandez *et al.*, 2010; Prince *et al.*, 2013). Ageing and stroke are the first and second greatest risk factors for dementia, and one third of people will suffer from stroke and/or dementia during their lifetime (Gorelick and Nyenhuis, 2013).

In the UK, 30% of people over 80 years old have dementia, and as many again are affected by cognitive impairment not meeting the criteria for dementia diagnosis (O'Brien *et al.*, 2003). As the number of elderly people in the UK continues to rise over the next 20 years, the number of people affected is predicted to increase by a further 40%. Stroke prevalence in over 75-year-olds is also increasing; from 9% in 1994 to 13% in 2006 (*Stroke Statistics 2009*, 2009). Although improvements in healthcare and intervention strategies have succeeded in reducing mortality after stroke, this has been associated with a simultaneous increase in post-stroke dementia diagnoses, as more elderly people survive to become at higher risk of developing dementia (Ukraintseva *et al.*, 2006).

Dementia can have a devastating impact on patients and their families, and the growing prevalence of dementia also puts a significant strain on the economy and healthcare system(Luengo-Fernandez *et al.*, 2010). It is therefore becoming increasingly critical that effective therapies and preventative strategies are developed to reduce the risk of dementia. With this in mind, this study aimed to further current understanding of the causes of dementia in elderly stroke survivors.

1.1.1 Post-stroke dementia

Dementia is a clinical syndrome characterised by progressive decline in memory and at least one other cognitive domain, severe enough to interfere with performing the

tasks of daily life (*Americal Psychiatric Association: Diagnostic and Statistical Manual of Mental Disorders, Fourth Edition*, 2000). Age-related dementia is commonly caused by neurodegenerative diseases which develop within brain cells, and cerebrovascular disease which causes brain injury by restricting blood supply to brain cells. The most common cause of dementia is Alzheimer's disease, a neurodegenerative disease which accounts for around 60% of all dementia cases (Luengo-Fernandez *et al.*, 2010). Vascular dementia (VaD) is caused by cerebrovascular disease (CVD) and is generally considered to be the second most common form of dementia accounting for at least 30% of dementia cases (Román, 2002a). Strokes are caused by CVD, therefore post-stroke dementia is considered a type of VaD. Recently, the term vascular cognitive impairment (VCI) has also been introduced to encompass all types of cognitive dysfunction attributed to CVD (O'Brien *et al.*, 2003). VaD is commonly used for research purposes to describe a more extreme form of VCI (Grysiewicz and Gorelick, 2012). Additionally the term VCI-no dementia can be used to describe less severe cognitive impairment caused by CVD (Moorhouse and Rockwood, 2008).

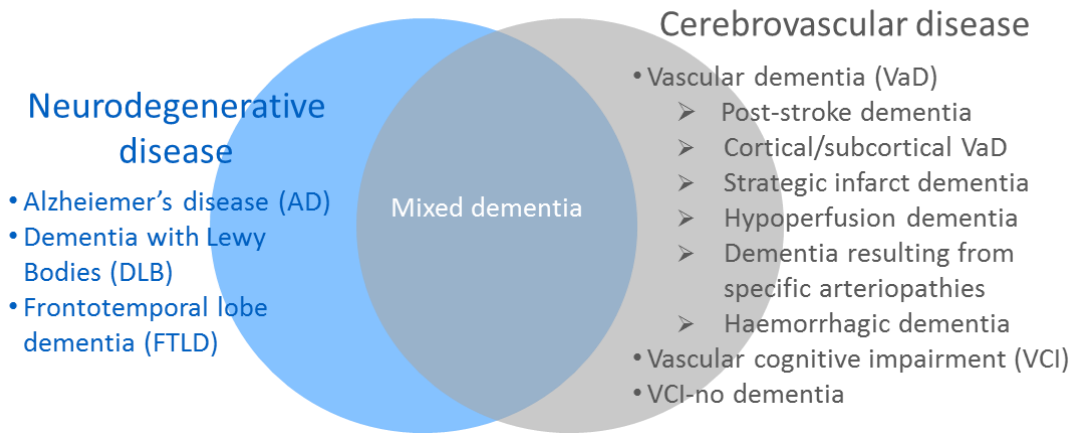

Figure 1.1 Common causes of dementia in the elderly. The three most common dementias caused by neurodegenerative diseases are Alzheimer's disease, Dementia with Lewy Bodies (DLB), and Frontotemporal dementia (FTD). Dementia caused by CVD is known as VaD, which encompasses numerous subtypes based on type of lesion and vessel affected (O'Brien *et al.*, 2003).

In addition to these common causes of dementia, rarer diseases and syndromes can also result in dementia and dementia-like symptoms. Parkinson's disease dementia (PDD) accounts for 2% of dementia cases in the UK, and is strongly associated with

older age, with a study finding the prevalence of dementia in Parkinson's patients over 80 years old to be 69% (compared to 0% in patients under 50 years)(Mayeux *et al.*, 1992). PDD develops secondary to the motor symptoms, and is related to Lewy body disease resulting in dementia that is very similar to DLB (Apaydin *et al.*, 2002). Other conditions linked to dementia in the elderly include rare hereditary neurodegenerative diseases (e.g. Huntington's disease) and cerebrovascular diseases (e.g. CADASIL [Cerebral Autosomal-Dominant Arteriopathy with Subcortical Infarcts and Leukoencephalopathy], the most common hereditary stroke disorder), infection with HIV (human immunodeficiency virus, which can cause neurocognitive impairment and dementia) or prion protein (Creutzfeld-Jakob disease), multiple sclerosis and corticobasal degeneration. Additionally, dementia-like symptoms may have treatable reversible causes such as metabolic dysfunction (e.g. hypothyroidism), nutritional disorders (e.g. vitamin B-6 or B-12 deficiencies), dehydration, brain infections (e.g. meningitis or untreated syphilis), and normal pressure hydrocephalus. However, these rarer causes of dementia account for only 5% of the dementia cases in the UK ('Factsheet: Rarer Causes of Dementia,' 2012), and were not investigated in this thesis.

1.2 Causes of delayed post-stroke dementia

Ischaemic strokes account for 90% of all strokes, and occur when an artery in the brain is occluded, restricting the supply of oxygen and nutrients to a region of the brain.[1] The clinical presentation of stroke depends on the size and location of the blood vessel and area of the brain affected. Studies have shown that around 25% of stroke survivors develop dementia within the first 3 months post-stroke (Barba *et al.*, 2000; Desmond *et al.*, 2000), indicating that the stroke damaged a large area of the brain critical for cognitive function. It is unclear why the risk of dementia remains substantially higher in non-demented stroke survivors compared to stroke-free controls, as few studies have followed stroke survivors beyond two years post-stroke, and even fewer have investigated pathological mechanisms in elderly stroke survivors (Kokmen *et al.*, 1996; Allan *et al.*, 2011).

[1] Haemorrhagic strokes are the second most common cause of stroke, and occur when a major artery in the brain is ruptured. This study focussed on the cause of dementia after ischaemic strokes.

Dementia which develops several months to years after a stroke is commonly described as delayed post-stroke dementia (PSD), and may involve both CVD and neurodegenerative disease (Figure 1.1). Reports of the cumulative incidence of delayed PSD developing more than one year post-stroke have ranged from 7.4% in population-based studies of first ever stroke, to 41% when pre-stroke dementia was included (Pendlebury and Rothwell, 2009; Allan *et al.*, 2011). Age, multiple vascular lesions, the characteristics of the first stroke, and presence of several risk factors are strongly associated with long-term risk of dementia post-stroke (Altieri *et al.*, 2004; Allan *et al.*, 2011), however, the precise mechanisms accelerating cognitive decline are unclear. Greater understanding of these mechanisms is needed for the prevention and management of delayed PSD.

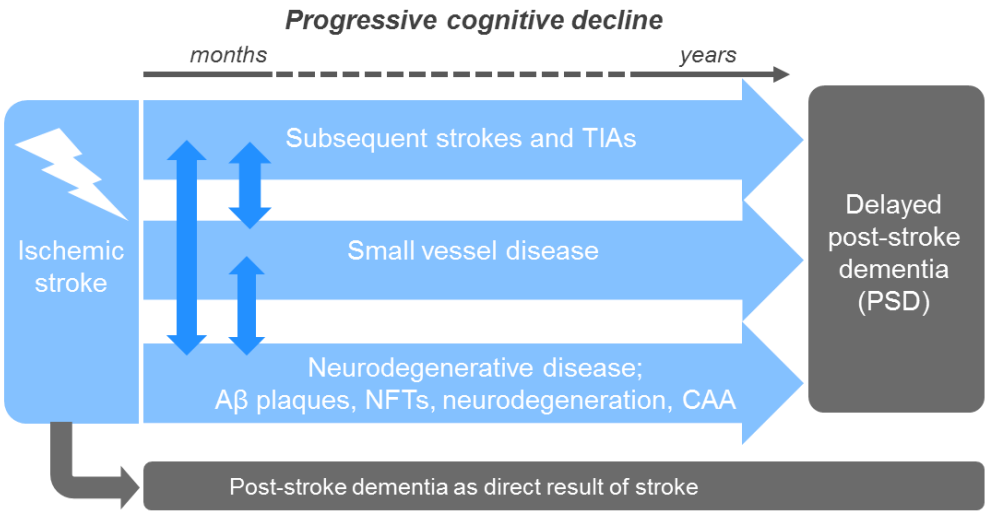

Figure 1.1 Progression of delayed post-stroke dementia over time. TIA = transient ischaemic attack, NFT = neurofibrillary tangle, CAA = cerebral amyloid angiopathy.

1.2.1 Cerebrovascular disease (CVD)

Cerebrovascular disease (CVD) can cause vascular dementia through single strategic infarcts (post-stroke dementia), multiple infarcts (multi-infarct dementia), and the accumulation of multiple smaller lacunes and hypoperfusive lesions. Hypoperfusion and infarction damages neurons and glia as they do not receive the oxygen and trophic factors required for normal functioning (Zlokovic, 2011). As neurons are the fundamental unit of information processing, loss or damage to neurons and neuronal

connections results in impaired cognition. The subtype of CVD, total volume of cerebral infarction and functional tissue loss, and location of the lesions are considered to be the major determinants of dementia in CVD (Leys *et al.*, 1999).

Cerebrovascular lesions may be categorised as large or atherothrombolic and small-vessel events. Large-vessel events involving the carotid arteries and circle of Willis restrict blood flow to larger areas of the brain resulting in a greater volume of functional tissue loss, and are generally associated with high mortality, morbidity and severe cognitive and/or physical impairment. Cognitive impairment may result from single strategic infarcts, where an infarct damages functionally critical areas of the brain. Strategic areas commonly affected include: the angular gyrus, thalamus, basal forebrain, bilateral involvement of the basal ganglia and thalamus, posterior cerebral artery territories including the ventral-medial temporal lobe, hippocampus, occipital structures and thalamus, and anterior cerebral artery territories (Román, 2002b). Strokes which destroy greater than 50 – 100ml of tissue (Tomlinson *et al.*, 1970), or result in large peri-lesional incomplete ischaemic areas involving white matter, and large periventricular white matter ischaemic lesions are also considered major risk factors for PSD (Román, 2002b).

Changes in smaller arteries and temporary occlusions causing transient ischaemic attacks (TIAs) are associated with stepwise or insidious cognitive decline. Pathological changes to small vessels are assumed to cause stenosis and occlusions leading to chronic hypoperfusion and infarction of the surrounding brain tissue (Kalaria *et al.*, 2004). The build-up of small lesions progressively damages increasing volumes of brain tissue to cause insidious cognitive decline to VaD. Subcortical lacunar infarctions caused by small vessel disease (SVD) may also cause stroke-like clinical symptoms when they develop in strategic locations (Bailey *et al.*, 2012).

It is widely accepted that CVD causes a spectrum of changes in the brain that can be viewed on MRI as white matter hyperintensities (WMH) (Kalaria and Ihara, 2013). However, WM degeneration may also be caused by primary axonal degeneration occurring as a result of neuron loss or damage in the grey matter (Capizzano *et al.*, 2004). Imaging studies have demonstrated that WM changes tend to occur in fibres within the frontal lobes (Tullberg *et al.*, 2004) and disrupt the frontal cortical-

subcortical circuits that underlie executive functions. The frontal lobe is more vulnerable to WM changes than the temporal lobe (Tullberg *et al.*, 2004), which fits with current understanding of the relationship between frontal lobe changes and impairments in attention and executive functions that are frequently observed in patients with VaD.

CVD causes vessel changes through three main disease mechanisms; atherosclerosis, small vessel disease, and cerebral amyloid angiopathy (Grinberg and Thal, 2010). Atherosclerosis is a degenerative vessel disorder caused by the accumulation of blood-borne lipids such as cholesterol in vessel walls. Atherosclerotic plaques, which commonly develop in medium to large arteries, can cause cerebral thrombosis due to narrowing of the blood vessel lumen, or rupture and cause vessel occlusion or an embolism occluding a smaller artery (Grinberg and Thal, 2010). Thromboembolic events are generally considered to cause up to 50% of all ischaemic strokes (Ferrer *et al.*, 2008), and the occlusion of internal carotid arteries and those of the circle of Willis are thought to explain ≤15% of VaD (Kalaria, 2012).

Cerebral small vessel disease (SVD) describes disease processes which impair blood flow in small perforating cerebral arterioles, capillaries and venules. Pathological small vessel wall alterations in SVD include arteriosclerosis (thickening and hardening of vessel walls), lipohyalinosis (wall thickening and lumen narrowing), fibrinoid necrosis (fibrin plugs in vessel lumen and walls) and perivascular tissue changes caused by blood-brain barrier dysfunction (leakage of toxic substances and metabolites out of the vessels)(Wardlaw *et al.*, 2003). SVD lesions such as lacunar infarcts (<20mm diameter), lacunes (3 -15mm fluid-filled cavities in the basal ganglia or white matter), microbleeds, and white matter hyperintensities (indicative of demyelination or dilated perivascular spaces) are visible using neuroimaging and post-mortem histopathological techniques (Wardlaw, 2008; Pantoni, 2010; Wardlaw *et al.*, 2013).

Cerebral amyloid angiopathy (CAA) is characterized by deposits of amyloid-β protein (Aβ) protein in vessel walls and is a common feature of ageing and AD (Grinberg and Thal, 2010). CAA is believed to be caused by disrupted clearance of Aβ through the perivascular space, resulting in the build-up of Aβ near the basement membrane (Weller *et al.*, 2009). Capillary CAA can occlude or disrupt blood flow and result in

infarctions or hypoperfusion, and can damage blood vessel walls causing haemorrhages (Grinberg and Thal, 2010).

The relationship between the size, type and location of cerebrovascular lesions and cognitive dysfunction are not well understood. Until recently, the prevalence of VaD was often underestimated as dementia diagnosis criteria was biased towards AD, emphasizing memory impairment as an essential symptom (Román, 2002a), although memory impairments tend to develop later in VaD (Desmond *et al.*, 1999). The high specificity and low sensitivity for diagnosis of VaD therefore meant that many VaD subjects were misdiagnosed with other forms of dementia (Wetterling *et al.*, 1996). This directed the focus of dementia research on AD, leaving the role of vascular lesions in dementia comparatively understudied. In addition, the frequent co-occurrence of AD with vascular pathology meant that AD was interpreted as being the primary cause of dementia while the role of CVD was overlooked. Although these issues are now being addressed, there are currently no standardized neuropathological criteria to quantify vascular lesions. This has resulted in differing procedures for pathological examination of VaD being used in different laboratories, making comparison between studies difficult (Jellinger, 2007). Furthermore, there are no set criteria for a pathological diagnosis of VaD, which has hindered the understanding of the relationships between vascular lesion burden and cognitive impairment.

1.2.2 Alzheimer's disease (AD)

Between 19-61% of stroke survivors who develop PSD also have a high burden of Alzheimer's disease (AD) pathology (Leys *et al.*, 2005), which implicates AD in the pathogenesis of delayed PSD. AD is clinically characterized by impairment in short-term and spatial memory, which becomes more severe as the disease progresses and other cognitive domains become impaired. The pathological hallmarks of AD are amyloid-β (Aβ) plaques, neurofibrillary tangles (NFTs), neuropil threads (NTs), and neuritic plaques. AD is also associated with neuronal and synaptic loss, CAA and gliosis (Attems and Jellinger, 2012).

One of the characteristic features of AD are cortical Aβ plaques, which are large insoluble extracellular aggregates of Aβ peptides, formed by the cleavage of the transmembrane amyloid precursor protein (APP) by β and **γ** secretases into $A\beta_{40}$ and

$A\beta_{42}$ peptides. In AD there is a pathological increase in extracellular Aβ concentration, believed to be due to increased Aβ production and impaired Aβ clearance. Age related vascular changes are thought to contribute to decreased clearance by impairing the ability of the perivascular drainage system to remove Aβ (Kalaria, 2010). $A\beta_{42}$ peptides aggregate to form cortical plaques, first developing in the neocortex and hippocampus, then spreading in a well-defined hierarchical pattern throughout the brain as the disease progresses (described in Table 1.1). $A\beta_{40}$ peptides accumulate in vessel walls and cause CAA in 80 – 100% of all AD patients (Grinberg and Thal, 2010).

The other characteristic features of AD are neurofibrillary tangles (NFTs) and neuropil threads (NTs), intracellular aggregates of abnormal tau protein in neuronal soma and neurites. Tau is a microtubule-associated protein which binds to and stabilises microtubules, however in AD tau becomes hyperphosphorylated and aggregates as paired helical filaments and larger NTs in axons and dendrites and NFTs in the soma (Goedert, 2006). These aggregates are therefore a sign of impaired microtubule function, impaired axonal transport and neuronal dysfunction. Hyperphosphorylated tau pathology first appears in the trans-entorhinal and entorhinal regions, and then spreads in a hierarchical pattern throughout the brain, which can be divided into six stages according to Braak and Braak, 1996 (Table 1.1). Tangle formation is associated with neuron death (Gómez-Isla *et al.*, 1997) and cognitive impairment in AD (Braak and Braak, 1996; Ince, 2001; Rössler *et al.*, 2002; Giannakopoulos *et al.*, 2003).

Phase	**Amyloid-β pathology***	**NFT and neuropil threads****
I II	Neocortex Hippocampus and entorhinal cortex	Trans-entorhinal and entorhinal regions
III IV	Basal ganglia, thalamus, hypothalamus Brainstem nuclei	Hippocampus
V VI	Pons and cerebellum	Neocortex

Table 1.1 Comparison of the development and distribution of Amyloid-β and tau pathology in AD. * = from (Thal *et al.*, 2002), ** = from (Braak and Braak, 1991).

A definitive diagnosis of AD is only confirmed after post-mortem examination. Until recently, diagnosis was based upon the semi-quantitative rating of 'frequent' neuritic plaques – Aβ plaques containing degenerating neurites – according to the CERAD score (Consortium to Establish a Establish a Registry for Alzheimer's Disease)(Mirra *et al.*, 1991), and Braak stage V/VI of NFTs (Braak and Braak, 1991). Montine et al. have now updated these guidelines to include more detailed methods to assess and report coexisting disease pathology such as vascular lesions; to incorporate staging of Aβ deposits, NFTs, and neuritic plaques; and to recognize that AD pathology can also develop in subjects without cognitive impairment (Montine *et al.*, 2012).

The causative relationship between the two pathological hallmarks of AD remains unclear. Over the last 20 years, the amyloid cascade hypothesis has dominated Alzheimer's disease research, postulating that Aβ deposits trigger AD processes and are the cause of neuron and synapse loss, mediated by the formation of tau pathology (Hardy and Higgins, 1992). However, studies found that Aβ plaque burden was not closely related to dementia symptoms or neurodegeneration, and it is not uncommon for elderly individuals with severe Aβ pathology to maintain normal cognitive function (Braak and Braak, 1991). In addition, plaque development follows a different pattern to tau pathology during disease progression (Table 1.1)(Attems and Jellinger, 2012). Furthermore, although the vast majority of research into AD treatments has focussed on clearing Aβ aggregates from the brain, no drugs designed to prevent or reverse amyloid accumulation have passed Phase III clinical trials (Karran *et al.*, 2011). Therefore, the original amyloid hypothesis has been modified to propose that soluble oligomers of Aβ may be the toxic component that directly injures synapses and neurites (Hardy and Selkoe, 2002). Further discussion on the role of AD pathology in neuronal and cognitive dysfunction is continued in Chapter 4.

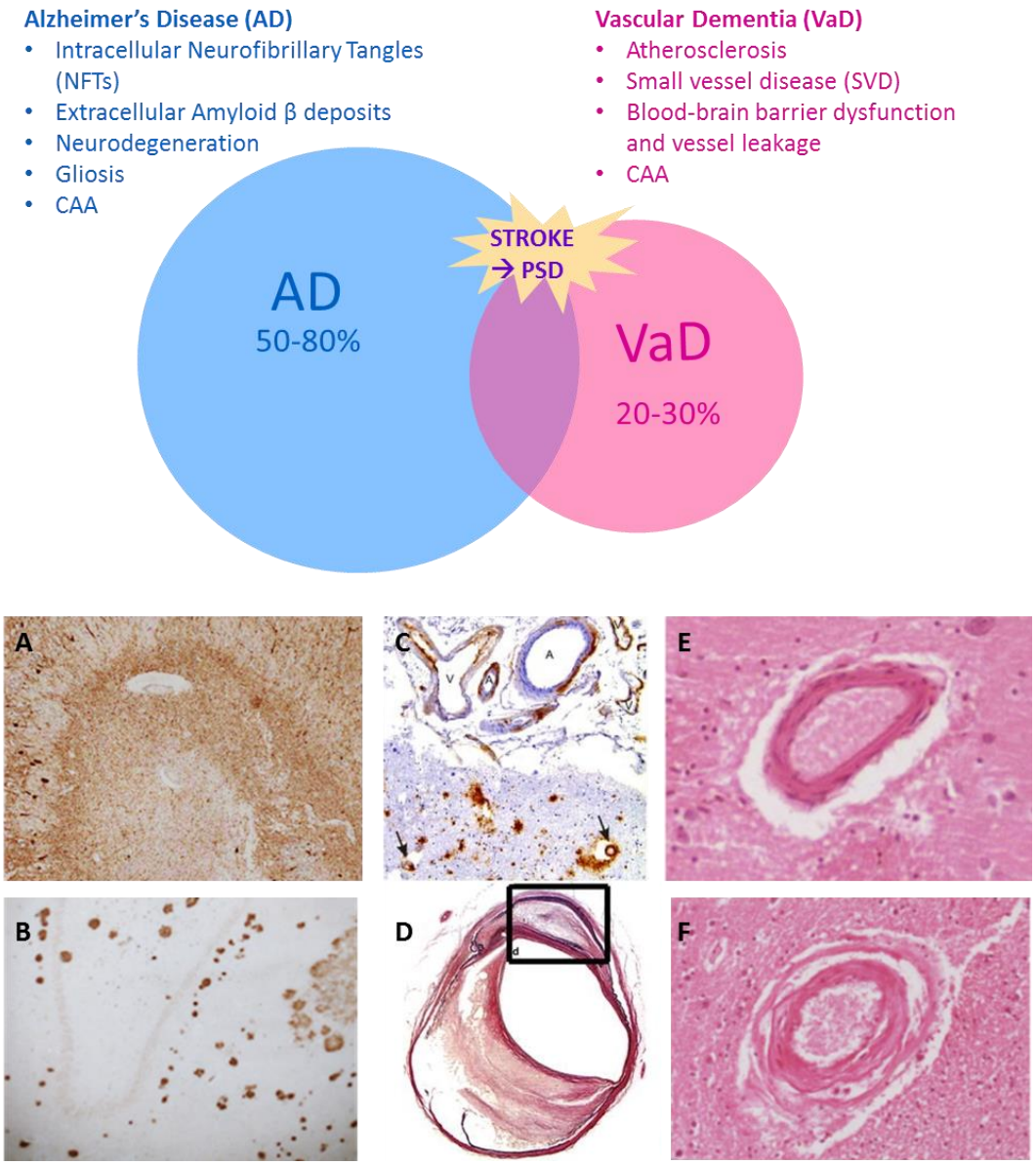

Figure 1.2. Common pathological characteristics of AD and VaD. A, Hyperphosphorylated tau pathology in the hippocampus of an AD subject, visualized using antibodies to AT8; B, amyloid plaques in the hippocampus of an AD subject, visualized using antibodies to 4G8; C, Cerebral amyloid angiopathy (CAA), arrows show Aβ deposition in capillaries; D, atherosclerotic changes in the left carotid artery of an elderly subject (C and D adapted from Grinberg and Thal, 2010); E, normal blood vessel in elderly subject; F, Arteriolosclerotic blood vessel in a subject with SVD, demonstrating splitting of concentric smooth muscle cell layers .

1.2.3 Mixed dementia: CVD and AD

Large epidemiological and neuroimaging studies have consistently found that dementia subjects often have a mixture of both neurodegenerative and vascular lesions. Around 30-50% of VaD patients have coexisting AD pathology, and over 30% of AD cases have co-existing cerebrovascular pathology (Snowdon *et al.*, 1997; Kalaria and Ballard, 1999; Wharton *et al.*, 2011; Kling *et al.*, 2013). The extent to which these disease processes influence and interact with one another is unclear, although the importance of CVD in the pathogenesis of AD is now becoming more widely recognized (Ruitenberg *et al.*, 2005; Bell and Zlokovic, 2009; Uh *et al.*, 2010; Chen *et al.*, 2011a). Studies have found that hypoperfusion is associated with amyloid plaque accumulation, suggesting that SVD processes can also trigger AD mechanisms (Sojkova *et al.*, 2008; Huang *et al.*, 2012). Conversely, AD pathology can also cause vascular damage, as cerebral capillary degeneration has been found in practically all AD subjects examined post-mortem (de la Torre, 2002). The co-existence of AD and CVD lesions have been found to have additive effect on cognitive function, further supporting the hypothesis that these pathological processes are synergistic and cumulative (Nagy *et al.*, 1997; Snowdon *et al.*, 1997; Zekry *et al.*, 2002; Toledo *et al.*, 2013). The involvement of CVD processes in AD is also evident in the number of shared risk factors for AD and VaD, many of which are traditionally associated with atherosclerosis or cardiovascular disease (Table 1.2)(Gorelick, 2004; Kling *et al.*, 2013). The increased vulnerability of stroke survivors to dementia has therefore been suggested to be due to the ischaemic cascade triggering or exacerbating widespread neurodegenerative processes (Kalaria, 2000; Lee *et al.*, 2005; Cumming and Brodtmann, 2011).

Risk Factors for AD and VaD	
Demographic:	Older age Low education
Cardiovascular:	Hypertension/hypotension Smoking Diabetes mellitus Hyperlipidaemia High serum homocysteine Atherosclerosis
Genetic	ApoE ε4

Table 1.2. Common risk factors for AD and VaD (de la Torre, 2002).

1.2.4 Ageing

The strongest risk factor for stroke and dementia is increasing age, which implicates changes that occur in the ageing brain as important mechanisms in the pathogenesis of PSD. Various changes associated with impaired structural and functional integrity of the cerebral vasculature have been reported in ageing, including reduced cerebral blood flow, decreased capillary density, microvascular fibrosis, basement membrane thickening (with or without Aβ deposits), loss/elongation of endothelial cells, and impaired blood-brain barrier function (Farkas and Luiten, 2001; Chen *et al.*, 2011a). The effect of these vessels changes are evident in the increase in number of white matter lesions with ageing, from below 20% in people under 30, to 100% of 71-80 year olds (Christiansen *et al.*, 1994). Elderly people are also more likely to have greater numbers of vascular risk factors which place additional strain on the cerebrovasculature, and have been shown to have robust effects on brain anatomy and function in non-demented elderly individuals (Aine *et al.*, 2014).

Accumulation of Alzheimer-type pathology also frequently occurs in normal ageing without cognitive impairment (Braak and Braak, 1991). Several studies have demonstrated this, including a large community-based study which found that similar proportion of demented and non-demented elderly subjects had mild/moderate Aβ pathology (49% and 53% respectively), with equivalent levels of vascular pathology (Ince, 2001). The Nun Study, a large longitudinal study of a homogeneous cohort of elderly nuns, found that 40% of subjects with the levels of Alzheimer's pathology required for a diagnosis of AD were not demented (Snowdon *et al.*, 1997).

Differences in cognitive ability in elderly subjects with similar levels of brain pathology have been attributed to differences in brain and cognitive reserve (Barulli and Stern, 2013). Epidemiological and experimental studies have consistently found that greater cognitive reserve is protective against dementia, assessed through variables such as education, socioeconomic status and engagement in intellectually stimulating social activities (Barulli and Stern, 2013). However, cognitive reserve is a hypothetical concept and not directly measurable, relying on these proxy variables to estimate cognitive reserve (Jones *et al.*, 2011). Brain reserve is a similar concept which relates differential susceptibility to disease pathology to differences in brain capacity, such as greater brain size, number of neurons, or neuronal plasticity (Barulli and Stern, 2013), which has been implicated in brain ageing (Burke and Barnes, 2006). As age-related decline in brain structure and function make the brain more vulnerable to further insults, brain and cognitive reserve are likely to have important roles in maintaining cognition through protecting from or compensating for neuronal damage and dysfunction.

Therefore, elderly stroke survivors are likely to already have some degree of vascular and neurodegenerative changes, varying in severity from 'normal' ageing to pre-clinical AD, which will influence the cognitive outcome after stroke. Injury caused by stroke may significantly lower the threshold of damage required to cause dementia by reducing brain reserve, making stroke survivors vulnerable to additional age-associated change or disease mechanisms. The precise mechanisms contributing to delayed PSD, developing over the long-term after stroke, still require elucidation (Allan *et al.*, 2011).

1.3 The Cognitive Function After Stroke (CogFAST) study

1.3.1 Study design

The Cognitive Function After Stroke (CogFAST) study was set up in 1999 to investigate the risk factors and substrates dementia after stroke. The study recruited 355 non-demented stroke survivors over 75 years old to prospectively study the evolution of cognitive changes after stroke, particularly focussing on identifying and understanding the causes of delayed PSD. Due to the strict exclusion criteria precluding anyone who had severe cognitive impairment or disabilities at three months post-stroke, it was unlikely that CogFAST participants had suffered large vessel strokes. Therefore, CogFAST subjects were likely to have experienced smaller strokes, TIAs or strategic lacunar infarcts. Study participants received annual clinical and neuropsychological evaluations from baseline three months post-stroke to provide information about cognitive changes over time (Table 1.1). A subset of participants also received MRI (magnetic resonance imaging) scans to assess volumetric and cerebral blood flow changes. Over 60 participants have now donated their brain for post-mortem research into the pathological mechanisms causing VCI in stroke survivors. Full details of the recruitment criteria and study design are described in Figure 1.3 and in Chapter 2 (page 37).

Standard clinical assessments	**Vascular risk factors identified**
Cardiovascular history and examination	Angina, myocardial infarct, stroke, transient ischaemic attack
Neurological history and examination	
Blood pressure	Hypertension, hypotension
Blood chemistry	Atrial fibrillation, hyperlipidaemia, diabetes mellitus
Neuropsychological assessment	**Cognitive domain assessed**
CAMCOG (Cambridge Assessment Mental Disorders in the Elderly, Section B)	Global cognitive performance, with subscales of memory, orientation and executive function
CDR computerized battery	Composite of sub scales for power of attention
DSM IV	Dementia diagnosis
CDR and Barthel ADL	To assist dementia diagnosis

Table 1.3 Summary of clinical assessments performed in the CogFAST study. CAMCOG = cognitive part of the Cambridge Examination for Mental Disorders of the elderly (CAMDEX) (de Koning *et al.*, 1998); DSM = Diagnostic and Statistical Manual of mental disorders ; CDR = Clinical Dementia Rating; Barthel ADL = Index to measure performance in activities of daily living.

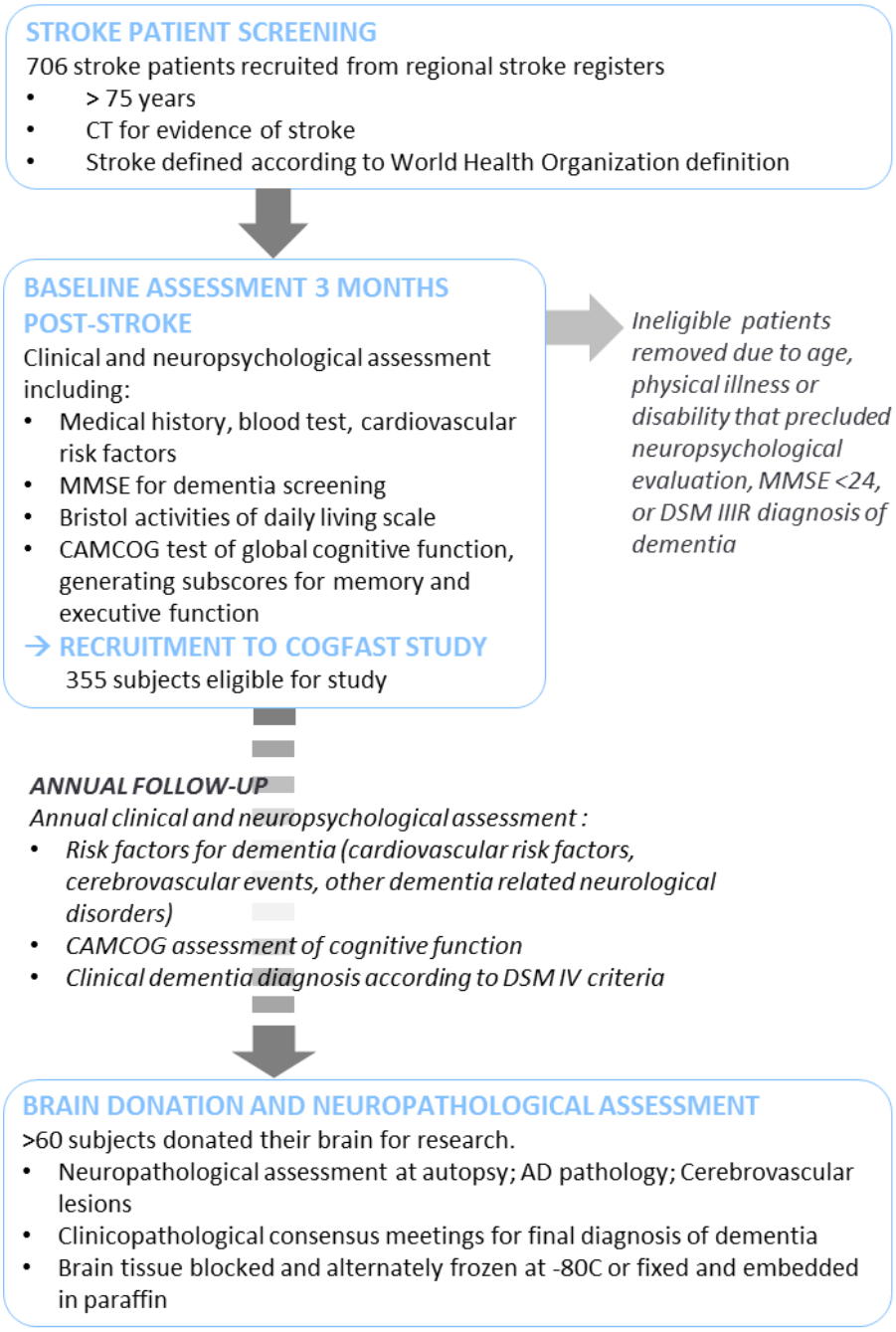

Figure 1.3 The CogFAST study design. Mean survival time from stroke to death was 6.72 years (Allan *et al.*, 2011). CT = X-ray computed tomography scan, MMSE = Mini Mental State Exam, CAMCOG = Cambridge Cognitive Examination, DSM = Diagnostic and Statistical Manual of mental disorders.

1.3.2 Key CogFAST study findings

The CogFAST study has generated several important findings that were particularly relevant to my studies. The study found that during the first 15 months post-stroke, 50% of participants showed initial improvement in cognitive function, ~40% remained stable, and ~10% developed delayed PSD (Ballard, 2003). However, despite the vast majority of subjects demonstrating initial improvements or cognitive stability, the long-term risk of dementia remained increased compared to stroke-free elderly subjects; by three years post-stroke 21% of stroke survivors had developed dementia and by seven years 39.5% had developed PSD (Allan *et al.*, 2011). Incidence of delayed PSD was calculated to be 6.32 cases per 100 person years (Allan *et al.*, 2011). Volumetric MRI investigations found that development of post-stroke cognitive impairment was associated with medial temporal lobe (MTL) atrophy (Allan *et al.*, 2011), and that PSD subjects had smaller hippocampal volumes compared to non-demented stroke survivors and controls, demonstrating similar hippocampal atrophy to AD subjects (Firbank *et al.*, 2011). All stroke survivors had a greater volume of white matter hyperintensities (WMH) compared to controls, however, the volume of WMH was not a predictor of subsequent cognitive decline (Firbank *et al.*, 2007). Volume of WMH in the temporal lobe was associated with memory impairment, and frontal WMH were associated with deficits in attention and processing speed but not executive dysfunction (Burton *et al.*, 2004).

These findings confirmed that long-term risk of dementia was increased in stroke survivors from the CogFAST cohort and was associated with structural changes in the MTL and hippocampus. This was initially assumed to be due to the stroke triggering or exacerbating AD processes, as atrophy of the MTL and hippocampus is traditionally associated with AD (Gosche *et al.*, 2002). However, when PSD subjects came to autopsy, the majority met neuropathological criteria for VaD, suggesting that AD processes were not the most important determinant of post-stroke cognition (Kalaria *et al.*, 2004). No previous studies had investigated neuropathological outcomes in older stroke survivors, although the finding of substantial vascular pathology in delayed PSD subjects supported the theory that dementia after stroke may be caused by on-going vascular pathological mechanisms including large and small vessel disease (Allan *et al.*, 2011). Allen et al. suggested that these pathological findings may also

reflect the inclusion criteria requiring cognitively intact elderly people over 75 years old, with at least one clinically detectable stroke, which may have excluded people with significant co-existing neurodegenerative pathology. As a previous study had found that PSD predicted poor long-term survival (Melkas *et al.*, 2009), it was surprising to find that there were no differences in mean survival time between demented and non-demented stroke survivors who came to autopsy (mean survival time = 6.72 years, 95% confidence intervals = 6.38–7.05) (Allan *et al.*, 2011).

In the CogFAST cohort, the presence of three or more cardiovascular risk factors (particularly ischaemic heart disease and hypertension), poor CAMCOG memory and executive function scores at baseline, previous disabling stroke, depression and older age were found to be significant predictors for death or dementia (Allan *et al.*, 2011). The PSD group had non-significantly greater mean number of infarcts compared to the PSND group (4.5 ±2.8(SD) vs. 3.9 ±2(SD)), and a greater percentage of PSD subjects had >3 microinfarcts in four regions (50% vs. 41%, p = 0.05) (Allan *et al.*, 2011). However, due to study limitations, Allen et al. were not able to accurately establish whether further strokes had occurred at follow-up, or whether different types of stroke or arterial territories involved were associated with increased likelihood of developing delayed PSD (Allan *et al.*, 2011).

Overall, the CogFAST study has confirmed that the long-term prognosis for survival and cognitive function in older stroke survivors is poor, although it is encouraging to find that risk of dementia is highly related to modifiable vascular risk factors. Neuroimaging findings indicated that the MTL and hippocampus were key structures involved in the pathogenesis of post-stroke dementia, as atrophy of these regions was associated with poor cognitive outcome. However, the underlying mechanisms causing these structural and functional changes in delayed PSD remain unclear. Therefore, my studies focussed on exploring pathological mechanisms in the hippocampus to further current understanding of the cellular substrates of hippocampal atrophy and cognitive impairment in delayed PSD.

1.3.3 Hippocampal microvascular changes in delayed PSD

A parallel study of delayed PSD in CogFAST subjects recently investigated changes to hippocampal microvasculature stroke survivors, AD and VaD subjects (Burke *et al.*,

2013). They found there was an increase in vascular density in PSD and AD subjects, and that the PSND group had a larger mean vessel diameter than all the other groups. These findings suggested that there was an increase in the proportion of smaller vessels in AD and PSD compared to PSND, which may indicate the development of new microvessels. However, interpretation of these findings is difficult and the role of tissue atrophy cannot be ruled out as a possible cause of increased vessel density in AD and PSD (Burke *et al.*, 2013). The differences in hippocampal microvasculature between demented and non-demented stroke survivors may reflect a cerebrovascular response which protected non-demented stroke survivors from cognitive decline; however, the mechanisms involved are unclear. As this study of hippocampal microvascular changes in CogFAST stroke survivors was run in parallel to my studies, my work focussed on the relationship between neuronal pathology and post-stroke cognitive impairment.

1.4 The hippocampus in post-stroke dementia

1.4.1 Hippocampal atrophy and dementia

There is considerable evidence that the pathological changes in the hippocampus are central to the development of cognitive impairment in ageing and dementia caused by CVD and neurodegenerative disease (Grysiewicz and Gorelick, 2012). Until recently, hippocampal atrophy was considered a specific marker of AD, reflecting neuronal death driven by NFT pathology (Gosche *et al.*, 2002; Zarow *et al.*, 2005). However, there is growing evidence that MTL and hippocampal atrophy are also associated with cognitive impairment caused by CVD, including ischaemic vascular dementia (Barber *et al.*, 1999; Bastos-Leite *et al.*, 2007; Scher *et al.*, 2011), dementia caused by SVD (Barber *et al.*, 2000; Kril *et al.*, 2002b), hereditary SVD (O'Sullivan *et al.*, 2009) and PSD (Jokinen *et al.*, 2004; Firbank *et al.*, 2007; Pendlebury and Rothwell, 2009).

Hippocampal atrophy has also been related to more subtle memory impairments in subjects with mild cognitive impairment (MCI) (Grundman *et al.*, 2003), and increases the risk of dementia in cognitively normal elderly subjects (Den Heijer *et al.*, 2006). Recent MR diffusion tensor imaging (DTI) studies have suggested that hippocampal

volumetric changes are preceded by disruption of tissue integrity and/or loss of neuronal fibres in MCI, AD and SVD (Fellgiebel and Yakushev, 2011; den Heijer *et al.*, 2012; van Norden *et al.*, 2012). These findings indicate that early disease mechanisms begin in the hippocampus, therefore understanding the basis of these changes will be critical for the development of strategies to prevent further deterioration.

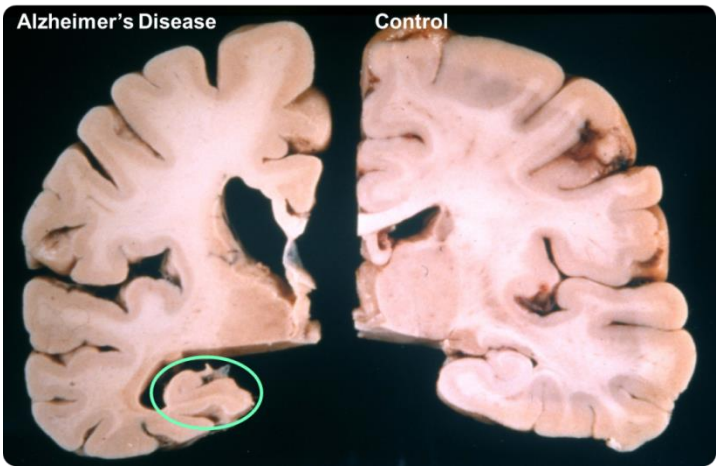

Figure 1.4 Hippocampal atrophy in an Alzheimer's disease and control subject. Thinning of the cortex and enlarging of ventricles is also evident in the AD brain, contributing to overall brain atrophy.

1.4.2 The hippocampus and memory

The hippocampus is a unique part of the cerebral cortex located within the MTL (Figure 1.5). This region of the brain was first recognized as having an essential role in memory nearly 60 years ago, when Scoville and Milner documented the case of patient HM who suffered severe anterograde amnesia following bilateral MTL resection (Scoville and Milner, 2000). Extensive lesion and neuroimaging studies have now firmly established that MTL structures are critical for memory function and in particular declarative memory, the conscious recall of knowledge based around personal experiences (Eichenbaum, 2003). Declarative memory can be further sub-divided into semantic memory (knowledge), and episodic memory (relating to specific personal experiences) (Figure 1.5). This distinction is mirrored within the structure of the MTL, as the hippocampus is central to episodic memory function, whereas semantic memory processing occurs outside the hippocampus (Tulving and Markowitsch, 1998; Binder *et al.*, 2009). The hippocampal formation has extensive reciprocal connections with other areas of the brain involved in memory such as the thalamus, basal forebrain and amygdala, and also receives information from sensory and association cortices (Swanson, 1982). Outputs project to the neocortex, frontal cortex, anterior cingulate

cortex and basal ganglia, where the information is used in higher-order cognitive functions and in storing long-term memories (Redgrave *et al.*, 1999; Tamminga, 2005).

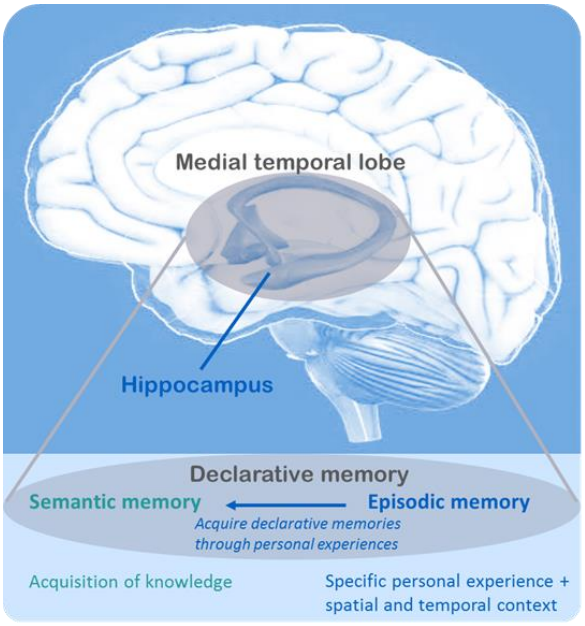

Figure 1.5. Diagram showing the location of the hippocampus in the medial temporal lobe and the differences between episodic and semantic memory.

1.4.3 Hippocampal anatomy and circuitry

The hippocampus has a unique and relatively simple structure composed of single layers of pyramidal neurons arranged along the transverse axis, curving around the dentate gyrus (DG), a dense v-shaped band of granule neurons (Figure 1.6 A). The pyramidal neuronal layers are divided into four subfields called the Cornu Ammonis 1-4 (CA1-4), described in Figure 1.6. Neuroimaging studies have found associations between volume reductions in specific CA subfields and different memory impairments, suggesting they each have a different role in memory processing. CA4/DG volumes were related to memory consolidation and retrieval in elderly subjects (Mueller *et al.*, 2010) whereas loss of CA1 volume was related to impairments in delayed recall in AD and temporal lobe epilepsy (Kerchner *et al.*, 2012). The DG is thought to have a key role in differentiating inputs to the hippocampus, which then converge and are reinforced in the highly reciprocal CA3 subfield (Schmidt *et al.*, 2012).

The entorhinal cortex (EC) forms the main interface between the hippocampus and the neocortex, and like other cortical regions can be divided into six layers. Layers II and III contain projection neurons which receive inputs from across the brain and carry out the first stage of memory processing before information is sent to the hippocampus

(Figure 1.6 B)(Canto *et al.*, 2008). Therefore, the superficial and deep layers of the EC can generally be considered as discrete input/output regions, although studies show the layers of the EC are highly interconnected therefore this is likely to be an over-simplification (Canto *et al.*, 2008).

The intrahippocmapal circuit is a complex network of hippocampal neuronal connections arranged along the transverse axis of the hippocampus (Cenquizca and Swanson, 2007). Information is received from cortical inputs via EC layer II neurons projecting to the DG and CA3, and layer III projecting to the CA1 and subiculum. Historically, models of hippocampal circuitry have focussed on sequential steps of information processing, creating a well-defined trisynaptic hippocampal loop from the DG – CA3 – CA1. However, anatomical, neurophysiological and behavioural studies have established that this is a considerable over-simplification, as the hippocampus contains multiple circuits, allowing conversion and comparison of combinations of raw and processed information in a highly interconnected 3D network (van Strien *et al.*, 2009; Jones and McHugh, 2011). Based upon recent findings, four major overlapping circuits of information processing have been proposed: (1) the trisynaptic loop involving the DG - CA3 - CA1, (2) a disynaptic loop involving the CA3 - CA1, (3) a disynaptic loop involving the CA2 – CA1, and (4) the monosynaptic temporoammonic pathway from the EC to CA1 (Figure 1.6) (Jones and McHugh, 2011). Therefore, information converges on the CA1 subfield, and is then output via the subiculum back to the EC (layers V and VI), parahippocampal and neocortical areas (Jones and McHugh, 2011).

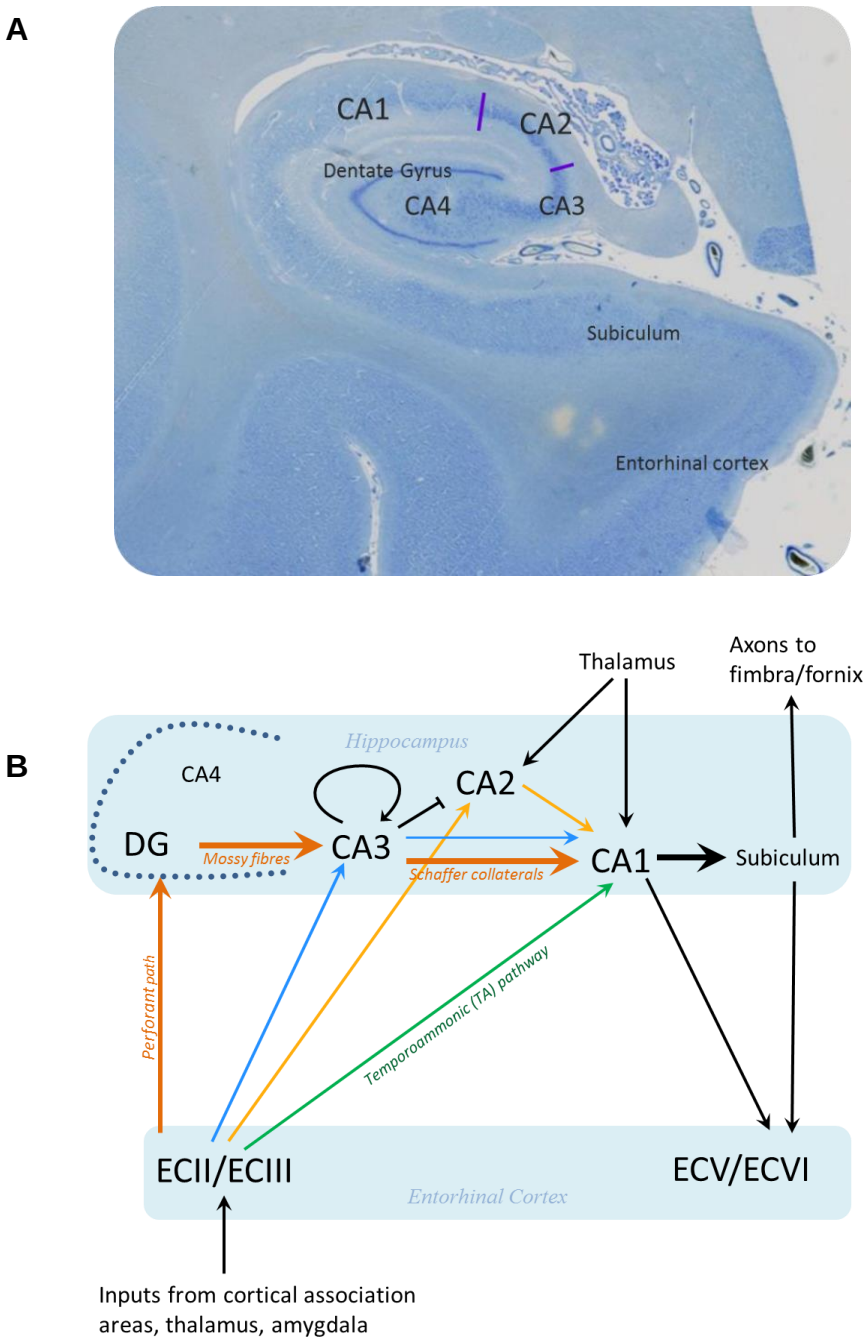

Figure 1.6 A, Transverse section of the hippocampus stained using cresyl fast violet to visualize neuronal soma and neuronal subfields: The CA4 subfield is completely enclosed by the dentate gyrus, the CA3 begins at the 'mouth' of the DG and contains larger and more uniformly oriented neurons, the CA2 neurons are larger, rounder and densely packed in a narrow band, and the CA1 widens out to a broad band of more dispersed, smaller pyramidal neurons. The CA1/subiculum border is harder to visually identify, and is generally considered to begin where the distribution of neurons becomes more patchy in the straighter band of cells towards the entorhinal cortex.
B, Major circuits of information processing in the hippocampus. Orange arrows represent the traditional trisynaptic loop involving the DG - CA3 - CA1; Blue arrows represent the disynaptic loop involving the CA3 - CA1; Yellow arrows represent the disynaptic loop involving the CA2 – CA1; the green arrow represents the monosynaptic temporoammonic pathway from the EC to CA1. The black arrow in the CA3 represents its highly reciprocal connections (Jones and McHugh, 2011).

1.4.4 Pyramidal neurons in the Cornu Ammonis

Pyramidal neurons are highly specialized cells comprised of a characteristic triangular soma, a highly branched axon arising from the base of the soma, and two distinct dendritic domains arising from the base and apex of the soma. Excitatory inputs largely synapse with the dendrites at specialized post-synaptic structures called dendritic spines, whereas the majority of inhibitory GABAergic inputs synapse on the axon and soma (Spruston, 2008). Pyramidal neurons have several relatively short basal dendrites, in contrast to the apical dendrite which connects the soma to a more distant tuft, with branching dendrites along its length (Spruston, 2008). The precise characteristics of dendritic trees vary between regions, allowing neurons to integrate and process signals differently according to their functional role. Dendrites are highly plastic and undergo constant remodelling, which is now widely believed to underlie the biological basis of learning and memory in the brain (Spronsen and Hoogenraad, 2010). Changes to the structural and functional connectivity of the hippocampus are therefore thought to be critically involved in the development of the clinical symptoms of dementia. Dendritic and axonal changes in PSD and ageing-related dementias are discussed in detail in Chapters 5 and 6.

The CA subfields can be divided into six layers which are defined according to which part of the CA pyramidal neurons they contain (Figure 1.7). The alveus contains axons of pyramidal neurons; the stratum oriens contains the basal dendritic trees and inhibitory neurons; the stratum pyramidale contains the soma of pyramidal neurons; the stratum radiatum contains the main branch of the apical dendrites; and the stratum lacunosum and stratum moleculare contain the apical dendritic tufts and synaptic inputs (Duevernoy, 2005). The dentate gyrus (DG) can be divided into three layers: the stratum moleculare, which blends with the molecular layer of the CA regions; the stratum granulosum, containing small, round, densely packed soma of granular neurons; and the polymorphic layer which borders the CA4 containing mossy cells and fibres (Amaral *et al.*, 2007).

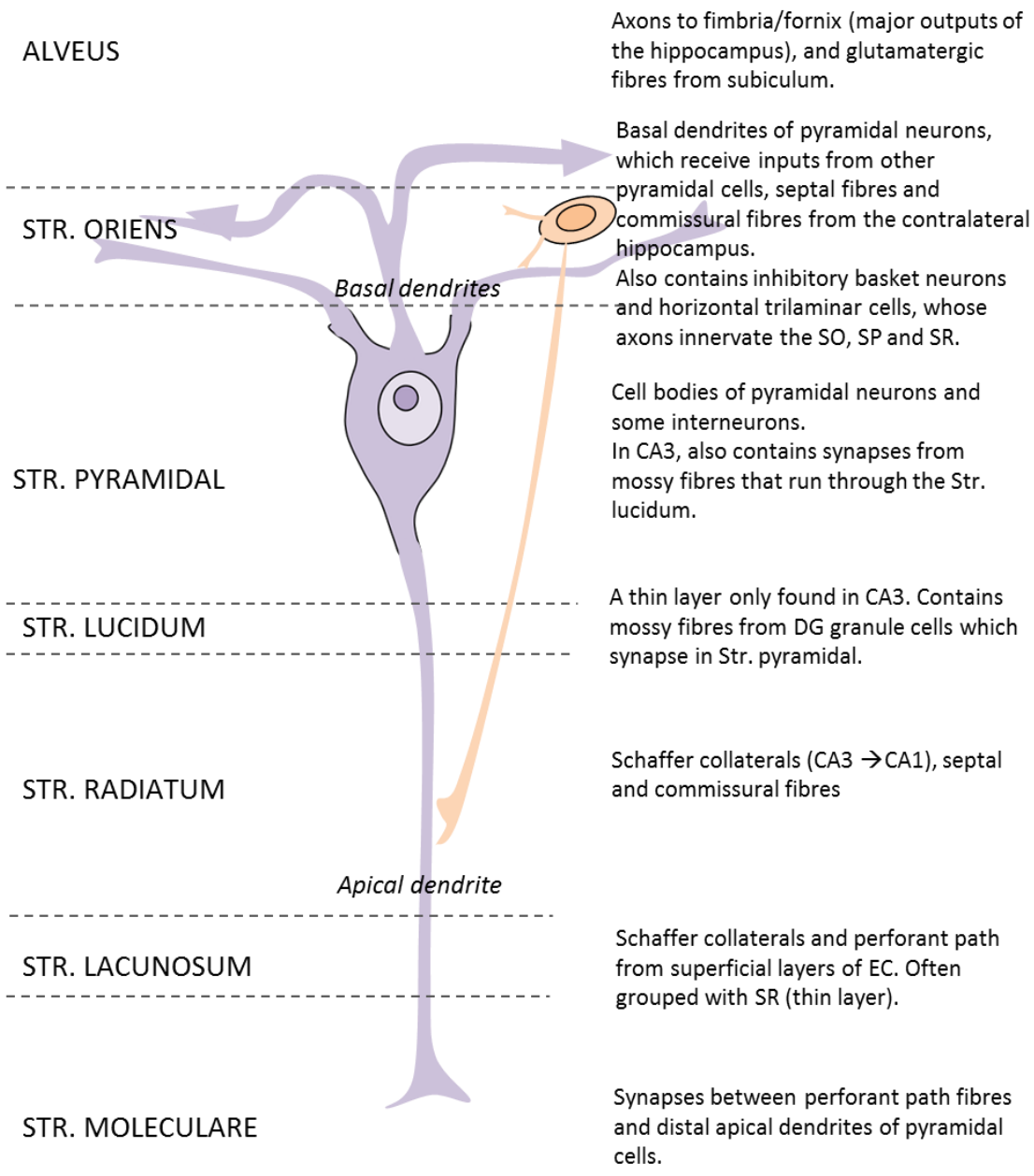

Figure 1.7. Layers of the Cornu Ammonis. Str = stratum, SO = stratum oriens, SP = stratum pyramidal, SR = stratum radiatum. Adapted from (Duevernoy, 2005).

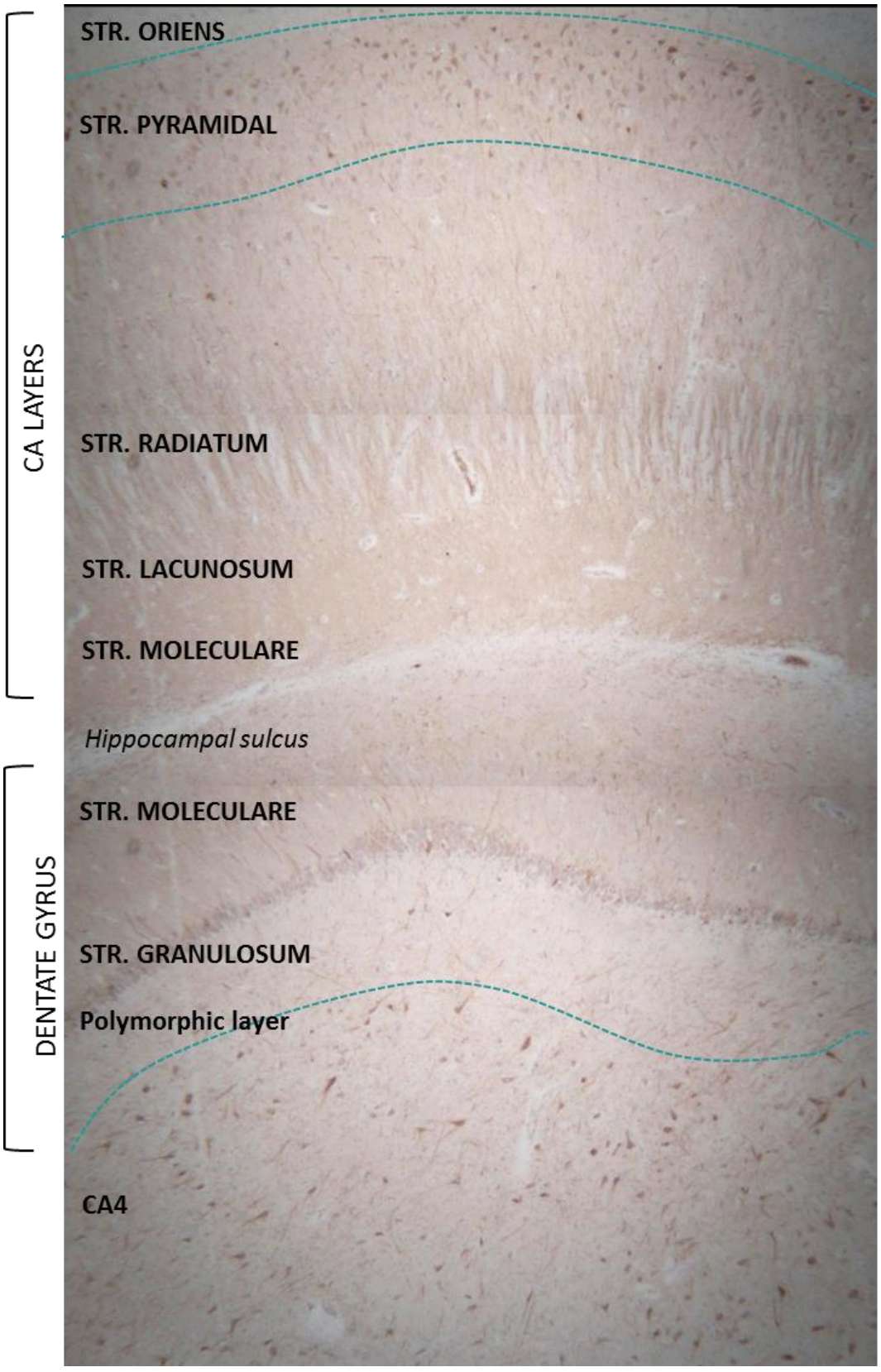

Figure 1.8. Hippocampal subfields visualized using immunohistochemistry to detect dendritic protein MAP2.

1.4.5 Differential subfield vulnerability in PSD

Hippocampal atrophy is thought to be caused by loss of neurons, as studies have shown that neurons in the largest hippocampal subfield, the CA1, are particularly vulnerable to injury and neurodegeneration in AD and hypoxia-ischemia (Kril *et al.*, 2002a; Kril *et al.*, 2004; Zarow *et al.*, 2005). However, the precise mechanisms causing hippocampal atrophy and dysfunction in PSD are unclear. During ischemia, neurons can be damaged through a combination of hypoxia, hypoglycaemia, and glutamate excitotoxicity (Larsen *et al.*, 2006). Reduced blood flow to neurons also causes an imbalance in neurotrophic and apoptotic signals which may lead to neurodegeneration (Banasiak *et al.*, 2000). Studies of animal models of transient cerebral ischemia have reported delayed post-ischaemic cell death with CA1 neurons starting to degenerate 2-3 days after ~15 minute ischemia, peaking at one week after the event (Kirino, 1982). These changes are associated with increased extracellular glutamate concentration suggesting that neurons are lost due to excitotoxic mechanisms (Ruan *et al.*, 2006). Excitotoxicity has also been implicated in neurodegeneration in AD (Hynd *et al.*, 2004; Mishizen-Eberz *et al.*, 2004).

Excitotoxicity is a process by which neurons become overexcited by high levels of extracellular glutamate at synapses, which activates NMDA receptors and causes calcium ion influx, triggering a cascade of catabolic processes causing cell damage and apoptotic cell death (Olney and Sharpe, 1969; Ankarcrona *et al.*, 1995). NMDA receptors are highly expressed in hippocampal neurons, which is assumed to contribute to the increased vulnerability to excitotoxic injury (Mishizen-Eberz *et al.*, 2004). Within the hippocampus, CA1 pyramidal neurons are particularly susceptible to NMDA-induced-excitotoxicity, whereas neurons in other CA subfields and the DG are more resistant. This selective sensitivity of CA1 neurons is not well understood, though the high density of NMDA NR_2B subunits in CA1 neurons suggests they may be involved (Chen *et al.*, 2007). Additionally, because hippocampal network activity culminates in the CA1 region, neuronal excitability during hypoxia-ischemia may be particularly high in CA1 neurons (Butler *et al.*, 2010).

In contrast, the CA2 subfield is considered the resistant subfield, as neurons do not appear to be lost from this region in AD or CVD. This may be related to their structure

and connectivity; CA2 neurons have distinct dendritic morphology, connectivity and basal membrane properties compared to CA1 neurons (Jones and McHugh, 2011) and do not appear to be sequentially activated as part of the classic 'trisynaptic loop' of hippocampal circuitry. Furthermore, CA2 neurons do not exhibit experimentally induced plasticity as readily as CA1 or CA3 neurons, which has been attributed to increased calcium buffering (Jones and McHugh, 2011), which may also protect against hyper-excitability. The differential vulnerability of the CA1 and CA2 neurons in ageing, hypoxia and AD means that studies comparing neuronal changes in the CA1 and CA2 subfields within the same section and subject can regard the CA2 neurons as an internal control for any changes observed in CA1 (i.e. if changes are only observed in the CA1 subfield, they must represent pathological changes rather than an artefact of tissue processing).

1.4.6 Neurodegeneration and autophagy

The major mechanisms of neuronal cell death after ischemia are apoptosis and necrosis, and both have been implicated in delayed neuronal death in the hippocampus after hypoxic-ischaemic injury (Hara and Mori, 2000). Additionally, macroautophagy (autophagy)[2], a degradation pathway for organelles and long-lived proteins too large to be degraded by the ubiquitin-proteasome-system, is also triggered in neurons after hypoxic and excitotoxic injury, and excessive or imbalanced induction can contribute to neuronal cell death (Cherra III and Chu, 2008). However, autophagy may also provide a neuroprotective mechanism in the early stages of injury (Carloni *et al.*, 2008).

Dysfunctional autophagy has been implicated in AD, ischemia and ageing, and autophagy has a role in maintaining neuronal function and morphology. During autophagy, proteins become enclosed in double-membraned autophagic vacuoles (AVs), which fuse with lysosomes in the soma to degrade the proteins **Error! Reference source not found.**(Kragh *et al.*, 2012). Under normal conditions autophagy is highly efficient in neurons; therefore neurons contain very few AVs. During cell starvation,

[2] Two other forms of autophagy also exist; chaperone-mediated autophagy and microautophagy. Macroautophagy is the most extensively studied and has been implicated in ageing and dementia, and is commonly simply referred to as 'autophagy'. Levine, B. and Kroemer, G. (2008) 'Autophagy in the Pathogenesis of Disease', *Cell*, 132(1), pp. 27-42.

stress or injury, autophagy is upregulated to degrade non-essential proteins and release amino acids that can then be recycled for stress adaptation or to maintain ATP production (Levine and Kroemer, 2008; Johansen and Lamark, 2011). Autophagy is therefore considered to provide a neuroprotective response in neurodegenerative disease and hypoxic-ischaemic injury (Nixon, 2006; Mariño *et al.*, 2011).

The two most commonly studied proteins involved in autophagy are LC3 (microtubule associated protein 1, light chain 3) and Beclin-1. During the initiation of autophagy, LC3-I becomes anchored to the AV membrane to form LC3-II, a specific marker for autophagosomes (Mizushima, 2004). Beclin-1 is involved in the recruitment of the membranes which form the autophagosomes, and also interacts with anti-apoptotic protein Bcl-2 as an upstream gatekeeper of apoptosis (Liang 1998). Under stress conditions, Beclin-1 dissociates from Bcl-2 and induces autophagy, providing a cytoprotective mechanism to avoid cell death (Maiuri *et al.*, 2010). In ageing neurons there is an accumulation of non-functional cellular components which is associated with a decline in autophagic degradation (Salminen and Kaarniranta, 2009). Ageing and early AD have been associated with a decline in Beclin-1 levels (Cherra III and Chu, 2008; Pickford *et al.*, 2008; Rohn *et al.*, 2011), however it is unclear whether ageing-associated impairments in autophagy are the cause of, or result from, impaired fusion with lysosomes and clearance of AVs (Levine and Kroemer, 2008). Further discussion on the role of autophagy in neuronal injury continued in Chapter 4.

1.5 The role of neuroglia in neurodegeneration

Over the last 20 years there have been considerable advances in our understanding of the role of neuroglial cells – astrocytes, oligodendrocytes and microglia – in brain organization and function (Giaume *et al.*, 2007). These cells, particularly astrocytes, express many of the same receptors as neurons, receive synaptic inputs, release gliotransmitters and form networks, maintain the blood-brain barrier, provide the brain's main defence against injury and infection, and can act as pluripotent neural precursors for adult neurogenesis (Giaume *et al.*, 2007). With such pivotal roles in

brain homeostasis and function, pathological changes to neuroglia in CVD and AD are likely to contribute to cognitive decline post-stroke and in ageing-related dementias.

1.5.1 Astrocytes

Astrocytes are the most numerous type of glial cell in the brain and are distributed in a homogeneous non-overlapping manner with each astrocyte occupying a distinct territory. It is believed that astrocytes may be as heterogeneous as neurons (Barres, 2008), although they have historically been defined using two main sub-types based on their location and morphology. Protoplasmic astrocytes are found in the grey matter and have a characteristic spherical cell body with several tortuous branched stem processes which are evenly extended around the cell body in all directions and contact synapses and blood vessels. Fibrous astrocytes are found in the white matter, and have a more oblong cell body, with longer, less ramified fibre-like processes mainly extending in two opposite directions which contact nodes of Ranvier and blood vessels (Sofroniew and Vinters, 2010).

Recently, additional classes of primate-specific glial fibrillary acidic protein (GFAP) positive astrocytes have been identified. Interlaminar astrocytes are found in layer 1, and extend tortuous processes from the pial surface across several millimetres to terminate in layers 2 – 4 (Colombo and Reisin, 2004). Protoplasmic astrocytes (the most common) are found in layers 2 – 6, and extend processes in all directions. A recent study also identified varicose projection astrocytes, which appear to be higher-order-primate-specific, and are sparsely found in layers 5 -6. These projection astrocytes extend approximately 1mm long straight processes within the deep layers of the cortex, characterised by varicosities every 10µm. Interestingly, these processes were found to extend in all directions and did not maintain the non-overlapping domain organisation. As many of the processes from these varicose projection astrocytes were found to contact vessels, it was suggested that these astrocytes may play a role in coordinating functional hyperemia across large areas (Oberheim *et al.*, 2009). The precise role of these different sub-types remains unclear, although it has been suggested that the complexity and diversity of cortical astrocytes is an evolutionary adaptation underlying the increased processing power of the human brain (Oberheim *et al.*, 2006).

In addition, GFAP positive radial neuronal stem cells (NSCs), found in the subventricular zone of the lateral ventricles and subgranular zone of the dentate gyrus in the adult brain, have been referred to as a sub-type of astrocyte (Doetsch *et al.*, 1999). However, these cells significantly differ from astrocytes as in morphology, chemical phenotype and physiological characteristics, and are the predominant source of adult neurogenesis, whereas protoplasmic and fibrous astrocytes are highly differentiated and specialized cells that do not exhibit neurogenic potential (Imura *et al.*, 2006; Sofroniew and Vinters, 2010). Therefore, it has been suggested that these cells simply be considered radial NSCs rather than a subtype of mature astrocyte to maintain clear functional distinctions between different cell types (Sofroniew and Vinters, 2010).

Role of astrocytes in synapse function

During development, astrocytes play an important role in synapse formation, maintenance and pruning, and are involved in guiding developing axons (Powell and Geller, 1999; Barres, 2008). Protoplasmic astrocyte processes envelop all synapses, and in the hippocampus and cortex each astrocyte is estimated to contact hundreds of dendrites from several neurons (Halassa *et al.*, 2007). Astrocytes have an important role in maintaining synapses through regulating ion concentrations and scavenging excess neurotransmitters and waste products from the extracellular space. In addition, astrocytes respond to neurotransmitters including glutamate through increased intracellular calcium levels (Porter and McCarthy, 1996). Studies have shown that these astrocytic calcium waves develop in well-defined receptive fields and are sharply tuned for orientation and spatial-frequency, indicating that astrocytes act quasi-independently with a small number of neurons surrounding them (Schummers *et al.*, 2008). Astrocytes are also believed to regulate synaptic transmission through the release of gliotransmitters, which gave rise to the 'tripartate synapse' hypothesis which suggests that astrocytes have a central role in synaptic activity and information processing in neuronal networks (Perea *et al.*, 2009). Through this function, astrocytes have also been suggested to increase network complexity required for higher brain functions (Giaume *et al.*, 2007).

Role of astrocytes in the neurovascular unit

Astrocytic endfeet surround the basal lamina of blood vessels allowing them to selectively take up blood components into the brain and regulate local blood flow in response to changes in neuronal activity (Koehler *et al.*, 2009). A recent functional MRI study demonstrated that changes to blood flow in response to stimuli were dependent on astrocyte function (Schummers *et al.*, 2008). Astrocytes produce molecular mediators (prostaglandins, nitric oxide, arachidonic acid) to coordinate the increase or decrease in blood vessel diameter. Astrocytes are therefore an essential component of the neurovascular unit (Hawkins and Davis, 2005), and are involved in maintaining the blood-brain barrier, although their precise mechanism is not well understood (Sofroniew and Vinters, 2010).

In addition to these functions, astrocytes contain the major brain store of glycogen, which they use to transfer glucose metabolites to adjacent neurons through gap-junctions during periods of high neuronal activity or hypoglycaemia, to be used aerobically as fuel to maintain neuronal activity (Brown and Ransom, 2007; Schousboe *et al.*, 2010). Astrocyte glycogen content is modulated by transmitters including glutamate (mediated by AMPA receptors), allowing the transfer of metabolic substrates to be directly linked to neuronal activity (Rouach *et al.*, 2008).

Astrocytes in stroke and AD

The central role of astrocytes in brain homeostasis means that it is now widely accepted that astrocytes must be deeply involved in the pathogenesis of neurological diseases, although there is currently little understanding of their precise role (Rodríguez *et al.*, 2009). Astrocytes near to a brain lesion such as an infarct can respond by become reactive and proliferating to isolate the damaged tissue, restore the blood brain barrier and help re-model brain circuitry around the lesion, which may result in the formation of a permanent glial scar. In sites distant from the focal damage, astrocytic reactive changes are less drastic and are involved in remodelling of neuronal networks (Rodríguez *et al.*, 2009).

Astrocytes have been implicated in the modulation of neuronal excitotoxicity stimulated by ischemia (Beauquis *et al.*, 2013), through their role in buffering ions to maintain neuronal excitability, maintaining extracellular glutamate concentration, and

their resistance to hypoxic injury (Nedergaard and Dirnagl, 2005; Giaume *et al.*, 2007). Astrocytic malfunction has been suggested to contribute to delayed neuronal death after ischemia as astrocytes are normally highly resistant to hypoxia, and if astrocytes are lost, neurons are not likely to be able to survive (Nedergaard and Dirnagl, 2005). Astrocytes protect neurons from excitotoxic cell death after ischemia through acting as a glutamate sink, maintaining extracellular ion concentrations to prevent neuronal depolarization, and providing the main antioxidant protection in brain tissue (Rodríguez *et al.*, 2009). If these functions become impaired they can exacerbate neurodegeneration due to the reversal of the glutamate uptake system, blood-brain barrier dysfunction and impaired blood flow, and secondary neuronal death after astrocyte death (Giaume *et al.*, 2007). One study has shown there was rapid depletion of glutamine synthetase, a key enzyme in the detoxification of glutamate, from astrocytes in vulnerable regions including the CA1 after hypoxic insult (Lee *et al.*, 2010). The loss of glutathione synthetase was therefore suggested to be an early pathological mechanism impairing the ability of astrocytes to protect neurons from excitotoxic injury, and potentially contributing to excitotoxic neurodegeneration in regions vulnerable to hypoxia (Lee *et al.*, 2010).

In AD, astrocytes have also been implicated in excitotoxic cell death, and become reactive and take up large amounts of Aβ and neuronal debris surrounding plaques (Ong *et al.*, 2013). Different types of astrocytes are likely to be differentially vulnerable to AD pathology. One study found that interlaminar astrocytes were more vulnerable to AD pathology in the neocortex, demonstrating a loss of interlaminar processes, whereas intralaminar processes became more reactive in severe AD. However, the relationship between loss of the interlaminar processes and the density of neuritic plaques was inconsistent (Colombo *et al.*, 2002). Further discussion of the role of astrocytes in stroke and dementia is continued in Chapter 6.

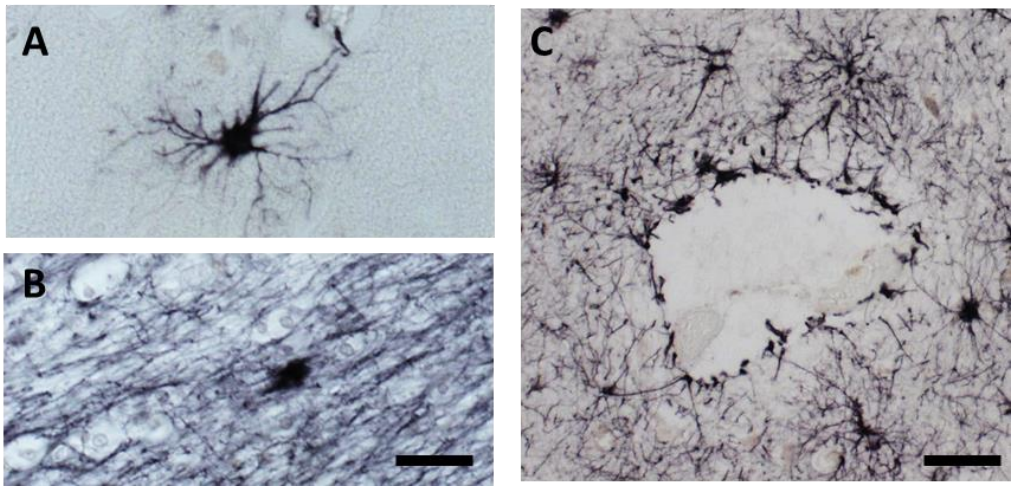

Figure 1.9. GFAP-positive astrocytes in the CA1 visualized using nickel-DAB. A, Protoplasmic astrocyte; B, Fibrous astrocyte in the alveus, surrounded by other GFAP-immunopositive processes; C, Astrocytes and astrocytic endfeet around a blood vessel. A, B Scale bar = 50µm; C, Scale bar = 100µm.

1.5.2 Microglia

Microglia are the most abundant immune cells in the brain and therefore make up the brain's major defence mechanism against injury and disease. Bone-marrow derived microglia invade the brain during embryonic and early postnatal development (Cuadros and Navascués, 1998). Under normal conditions, microglia are distributed throughout the neuropil and appear 'ramified' with a small soma and numerous thin branched processes which contact neurons, astrocytes, axon terminals, dendritic spines and blood vessels. These processes regularly extend and retract within their territory (Nimmerjahn *et al.*, 2005; Giaume *et al.*, 2007) to monitor the status of the environment and cleanse the extracellular fluid of metabolites and toxic factors (Fetler and Amigorena, 2005). Ramified microglia have been implicated in promoting synapse formation through the production of microglial brain-derived neurotrophic factor (BDNF) (Parkhurst *et al.*, 2013), and their processes have been shown to contact multiple synapse-associated elements during normal conditions, particularly transient dendritic spines, and these microglial-synapse interactions were found to be regulated by experience. Therefore, microglia may also play an active role in modifying or eliminating synapses in the healthy brain (Tremblay *et al.*, 2010).

Microglia are very sensitive to pathological changes in the brain. When activated, microglia undergo biochemical and morphological changes to extend thickened processes to the damaged site. Process tips in contact with the lesion broaden and together form a tight mesh to seal the damage. These processes are then retracted, and microglia become highly motile phagocytic cells that migrate to the site of injury (Davalos *et al.*, 2005). Microglia are stimulated by cytokines, neurotransmitters, neurotoxins, extracellular matrix molecules and proteases in areas undergoing inflammation, and synthesises cytokines, chemokines, complement, reactive oxygen species and neurotrophins that may have a neurotoxic or protective effect on nearby cells (Raivich and Banati, 2004).

Microglia may also recruit blood-borne macrophages which are indistinguishable from the rod-shaped reactive microglia which accumulate at the site of injury (Perego *et al.*, 2011), where they phagocytose debris such as that from apoptotic cells (Dihné *et al.*, 2001). Reactive microglia have been shown to accumulate around amyloid plaques (Bolmont *et al.*, 2008) and in delayed neuronal death following ischemia, resulting in sustained secretion of inflammatory mediators which may exacerbate disease processes and neuronal dysfunction/death (Lees, 1993). The role of microglia in stroke and dementia is discussed further in Chapter 6.

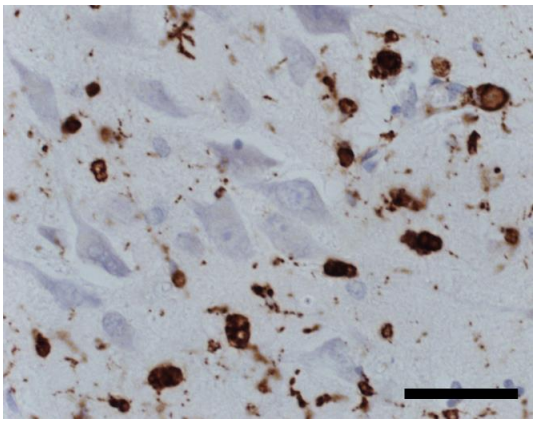

Figure 1.10 Activated microglia in the CA1 of an AD subject, visualized using IHC to CD68. Scale bar = 50µm.

1.5.3 Oligodendrocytes

Oligodendrocytes are the most numerous cell type in the white matter and have a critical role in axonal function, with each oligodendrocyte myelinating 30 – 40 axons. Oligodendrocytes form myelin sheathes by wrapping multiple layers of highly

specialized extensions of their plasma membrane around axons, forming tightly stacked layers of lipid bilayers which provides electrical insulation around the axon. This myelination is essential for axon function, as it increases axon conduction speed up to 100-fold, and reduces energy consumption by restricting the surface area for action potentials to less than 0.5% of the axonal surface (Nave, 2010). Oligodendrocytes also communicate with axons and have a critical role in maintaining axon integrity, as oligodendrocyte dysfunction leads to axonal degeneration (Simons and Trajkovic, 2006).

Oligodendrocytes express glutamate receptors and transporters and are therefore particularly sensitive to excitotoxic insults which are mediated by glutamate receptors (Giaume *et al.*, 2007). This is particularly relevant in stroke, as transient oxygen and glucose deprivation has been shown to be directly linked to oligodendrocyte excitotoxicity (Alberdi *et al.*, 2005), which induces oxidative stress, mitochondrial damage and cell death (Sánchez-Gómez *et al.*, 2003). Therefore, the loss of oligodendrocytes after ischaemic injury results in loss of myelin, axon dysfunction and ultimately axon loss. Interestingly, models of stroke which induced brief transient ischaemia demonstrated rapid oligodendrocyte death, followed by a subsequent increase in the number of immature oligodendrocytes bordering the affected regions. This suggests that the loss of oligodendrocytes may be compensated for by the proliferation of new oligodendrocytes (Mandai *et al.*, 1997; Petito *et al.*, 1998).

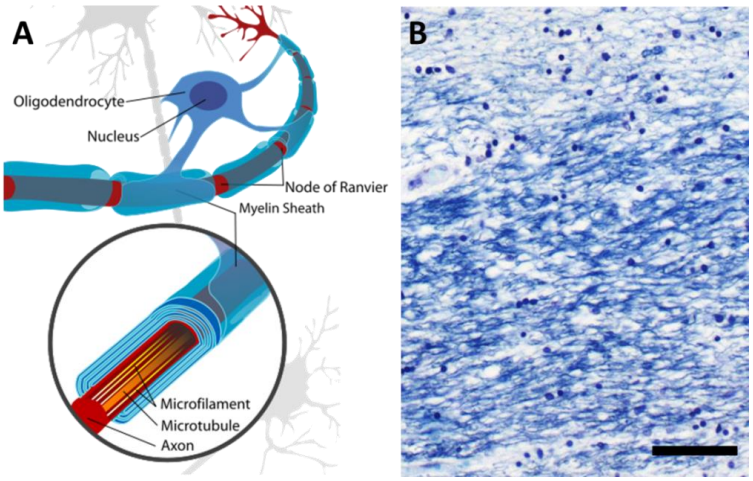

Figure 1.11. A, Diagram of an oligodendrocyte forming myelin sheath around an axon; B, Characteristic regular, small, darkly stained nuclei of oligodendrocytes in the alveus, section stained using LFB for myelin and haematoxylin to visualize nuclei. Scale bar = 50µm.

1.6 Aims and hypotheses

This study investigated neuronal changes in differentially vulnerable hippocampal subfields in stroke survivors from the CogFAST cohort in relation to clinicopathological findings. The main research aims were to:

- Identify novel pathological features discriminating subjects who had developed delayed post-stroke dementia from those who maintained cognitive function after stroke.
- Investigate possible mechanisms related to clinical and pathological changes in PSD, or associated with a protective role in PSND subjects.
- Elucidate the importance of different disease processes by comparing findings in post-stroke subjects with pathologically confirmed pure 'AD' and 'VaD' subjects, as well as cognitively normal elderly controls.

My main hypotheses for each chapter are described below:

- For the study described in Chapter 3, I hypothesised that hippocampal neuron loss and reductions in neuronal soma volume may contribute to cognitive impairment after stroke and hippocampal atrophy.
- In Chapter 4, I hypothesised that a greater burden of hippocampal AD pathology and dysfunctional autophagy may be associated with neuronal atrophy and cognitive impairment after stroke.
- In Chapter 5, I hypothesised that loss of apical dendritic arbour and synapses would be associated with neuronal volume reductions and cognitive impairment caused by greater CVD or degenerative disease mechanisms.
- In Chapter 6, I hypothesised that damage to hippocampal axons may be related to neuronal volume changes and cognitive impairment after stroke. I also hypothesised that pathological changes to astrocytes and microglia may be related to neuronal changes, disease pathology, and cognitive impairment.

Chapter 2. Materials and Methods

2.1 Introduction

The main focus of this study was to compare pathological changes and disease mechanisms in stroke survivors who developed PSD with those who maintained normal cognitive function. To achieve this, tissue was analysed from subjects from the CogFAST study and compared with elderly controls and pathologically defined dementia groups (AD, VaD and mixed AD with VaD).

Tissue from a non-human primate (baboon) model of acute cerebral hypoperfusion was also analysed to provide insight into acute neuronal changes in an experimental animal model of CVD. The model also allowed comparison between immersion fixed (human) and perfusion fixed (baboon) tissue to determine the influence of post mortem delay on the results observed in human tissue.

2.2 Subject selection and clinical diagnosis

2.2.1 CogFAST study design

Stroke patients over 75 years old were recruited from hospital-based stroke registers in North East England providing they were not demented according to DSM-IIIR (Diagnostic and Statistical Manual of Mental Disorders, Third Edition, Revised) criteria, did not show signs cognitive impairment at baseline three months after stroke, and had no disabilities that would impair cognitive testing (Allan *et al.*, 2011). A total of 355 eligible stroke patients gave written informed consent to participate in the Cognitive Function After Stroke (CogFAST) study. Ethical approval was given by the Joint Ethics Committee of Newcastle and North Tyneside Health Authority, Newcastle University and Northumbria University.

Medical histories were documented for all CogFAST participants. The mean age at baseline was 80 (SD ±4.1 (SD)) and the median number of baseline cardiovascular risk factors was 2 (range 1-3)(Ballard *et al.*, 2003b). Additional details on the clinical

characteristics of the CogFAST cohort are described in detail in (Ballard *et al.*, 2003a; Ballard *et al.*, 2003b).

All participants received annual clinical and cognitive follow-up assessments including the Mini Mental State Exam (MMSE)(Folstein *et al.*, 1975) to screen for dementia and the Cambridge Cognitive Examination (CAMCOG) section B, the cognitive and self-contained part of the Cambridge Examination for Mental Disorders of the Elderly (Roth *et al.*, 1986), described in section 1.3 (page 14). The CAMCOG test generated a global cognitive score (/107) and subscores for memory (/27) and executive function (/28). Mean global CAMCOG score at baseline was 85.1 (SD ±8.96). Additional details of all components of the follow-up battery are described in (Allan *et al.*, 2011). Over 60 patients who came to autopsy donated their brains for further research.

2.2.2 Neuropathological assessment and dementia diagnoses

Final diagnoses of VaD, AD or MD were based on both clinical (Diagnostic and Statistical Manual of Mental Disorders, Fourth Edition criteria for dementia) and neuropathological data at clinicopathological consensus meetings. Clinical diagnosis of dementia was made if there was evidence of memory impairment and one or more of aphasia, agnosia or disturbance of executive function severe enough to cause significant impairment in social or occupational functioning and represent a significant decline from a previous level of functioning. A clinical diagnosis of AD was made when in addition to these deficits, the course was characterized by gradual onset and continuing cognitive decline, and the cognitive deficits could not be attributed to other central nervous system, systemic or substance-induced conditions or delirium. A clinical diagnosis of VaD was made when in addition to the cognitive deficits, subjects demonstrated evidence of focal neurological signs or laboratory evidence of cerebrovascular disease related to the disturbance (*Americal Psychiatric Association: Diagnostic and Statistical Manual of Mental Disorders, Fourth Edition*, 2000).

Neuropathological assessment of all CogFAST subjects and VaD, AD and MD subjects was carried by out by experienced neuropathologists (T. M. Polvikoski, R. Perry and J. Attems) using standard protocols including visual inspection of macroscopic and microscopic infarcts, CERAD rating of neuritic plaques and Braak staging of tau pathology (Mirra *et al.*, 1991; Braak and Braak, 1996), as described in Section 1.2.2.

CERAD diagnostic criteria are based on semi-quantitative assessment of neocortical neuritic plaques (with thickened silver-positive neurites) which generates an age-related plaque score, which is integrated with clinical information to determine the level of certainty of the diagnosis of AD. Overall distribution of vascular amyloid deposition and proportion of plaques containing amyloid cores was also noted (Mirra *et al.*, 1991). Pathological diagnosis of AD was made with Braak stage V-VI and moderate-severe CERAD scores in the absence in significant vascular pathology (Kalaria *et al.*, 2004). Pathological diagnosis of VaD was assigned if there was evidence of multiple or cystic infarcts, lacunae, microinfarcts and small vessel disease, with Braak stage <IV and absence of other primary neurodegenerative disease. Pathological diagnosis of MD was assigned if there was evidence of CVD severe enough to cause VaD, together with sufficient AD pathology for a diagnosis of AD. Although control subjects were not psychologically assessed before death, they did not show any evidence of neurological disease or cognitive impairment. A vascular disease severity rating was also carried out in CogFAST subjects, generating scores for global vascular pathology (/20) and hippocampal subscores (/4). This method rated cerebrovascular lesions including arteriolosclerosis, amyloid angiopathy, perivascular hemosiderin leakage, perivascular spaces dilation, myelin loss and cortical micro- (<0.05cm) and large-infarcts (>0.5cm) on a 0-3 scale as described in (Deramecourt *et al.*, 2012).

2.2.3 Subject demographics and pathological findings

	PSND	PSD
Total number analysed	26	19
Age, years Mean (range)	84.8 (78-94)	87.4 (76-98)
Gender % Male	57.7	47.4
Post mortem delay, hours Mean (range)	40.4 (10-96)	41.2 (10-96)
Fixation length, weeks Mean (range)	10.2 (2-32)	8.16 (4-14)
CAMCOG score /120 Mean (range)	88.5 (76-99)	62.5 (24-80)
Pathological diagnosis	N/A	12 = VaD, 7 = MD
Time from stroke-death, months Mean (±2SE)	55.6 ±10.1	63.0 ±12.1
Braak stage Median (range)	2 (1-5)	3 (0-6)
CERAD score Median (range)	1 (0-2)	1 (0-3)
Vascular pathology score Global mean (range)	12.6 (7-16)	11.6 (6-17)
APOE E4 allele	0 = 14, 1 = 11, unknown = 1	0 = 13, 1 = 4, unknown = 1

Table 2.1. Subject demographics of all stroke subjects analysed. PSND = post-stroke non-demented, PSD = delayed post stroke dementia; PMD = post-mortem delay.

	Controls	VaD	MD	AD
Total number analysed	31	13	17	19
Age, years Mean (range)	81.8 (71-98)	84.8 (71-97)	84.1 (72-94)	82 (70-91)
PMD, hours Mean (range)	27.9 (8-67)	51.6 (24-84)	37.8 (11-72)	35.6 (5-72)
Fixation length, weeks Mean (range)	15.8 (4-105)	15 (4-52)	16.7 (3-40)	8.4 (2-24)
Braak stage Median (range)	3 (0-5)	2 (1-4)	5 (1-6)	5.5 (4-6)
CERAD score Median (range)	0 (0-3)	1 (0-2)	3 (1-3)	3 (2-3)

Table 2.2. Subject demographics of all subjects analysed. VaD = Vascular dementia, MD = mixed vascular dementia and Alzheimer's disease, AD = Alzheimer's disease; PMD = post-mortem delay.

2.3 Tissue acquisition

All brain tissues were obtained from the Newcastle Brain Tissue Resource, except four controls which were obtained from the Medical Research Council London Brain Bank for Neurodegenerative diseases (Institute of Psychiatry, London, UK) which were analysed chapter 3. Ethical approval was granted by Newcastle Upon Tyne Hospitals Trust ethics committees for post-mortem research on brain tissue.

Tissue from a total of 45 stroke survivors from the CogFAST study was analysed (26 PSND and 19 PSD). After post-mortem examination, brains from subjects in the CogFAST study were cut into 1cm thick coronal slices and subdissected into blocks which were alternately fixed in 10% buffered formalin or frozen at -80C. There were no evidence of lesions in any of the chosen hippocampal blocks and sections were taken from either the left or right hippocampus in each case. Standard protocols for fixation, subdissection and processing were used for all other brains (Perry *et al.*, 1990).Tissue from a total of 125 cases was used for these studies, subject demographics are presented in Table 2.2 and Table 2.2.

2.4 Paraffin-embedded tissue preparation

After immersion fixation blocks were processed (dehydrated in alcohol and cleared in xylene), and embedded in paraffin wax. Unless stated otherwise, standard protocols described below were used for all tissue sectioning, dewaxing and mounting.

2.4.1 Sectioning, dewaxing and mounting

Sections were cut using a Shandon FinesseE+ rotary microtome from predefined paraffin-embedded hippocampal blocks as close as possible to coronal level 18-20 according to the Newcastle Brain Map (Perry and Oakley, 1993). This level was defined as between the pregeniculate nucleus and the pulvinar at which the emergence of the ventricle is visible (Figure 2.1 A), where the dentate gyrus and CA regions 1-4 are clearly identifiable (Figure 2.1 B).

To make slides more adhesive for tissue sections, clean slides were immersed in acetone for 5 minutes, drained of excess fluid then placed in a 2% solution of APES (3 aminopropyl triethoxysilane) in acetone for 5 minutes. After draining, excess reagent was removed by gently dipping slides in fresh distilled water. Slides were dried at 45°C and stored until use.

Before staining, sections were rehydrated through two 10 minute changes of xylene and decreasing concentrations of alcohol for 1 minute each in 100%, 95%, 75% and 50%, then washed in water for 5 minutes.

After staining, sections were dehydrated in 95% ethanol for 1 minute and two changes of 100% ethanol for 2 minutes each. Sections were then immersed in two changes of xylene for a minimum of 2 minutes each before coverslips were applied with DPX.

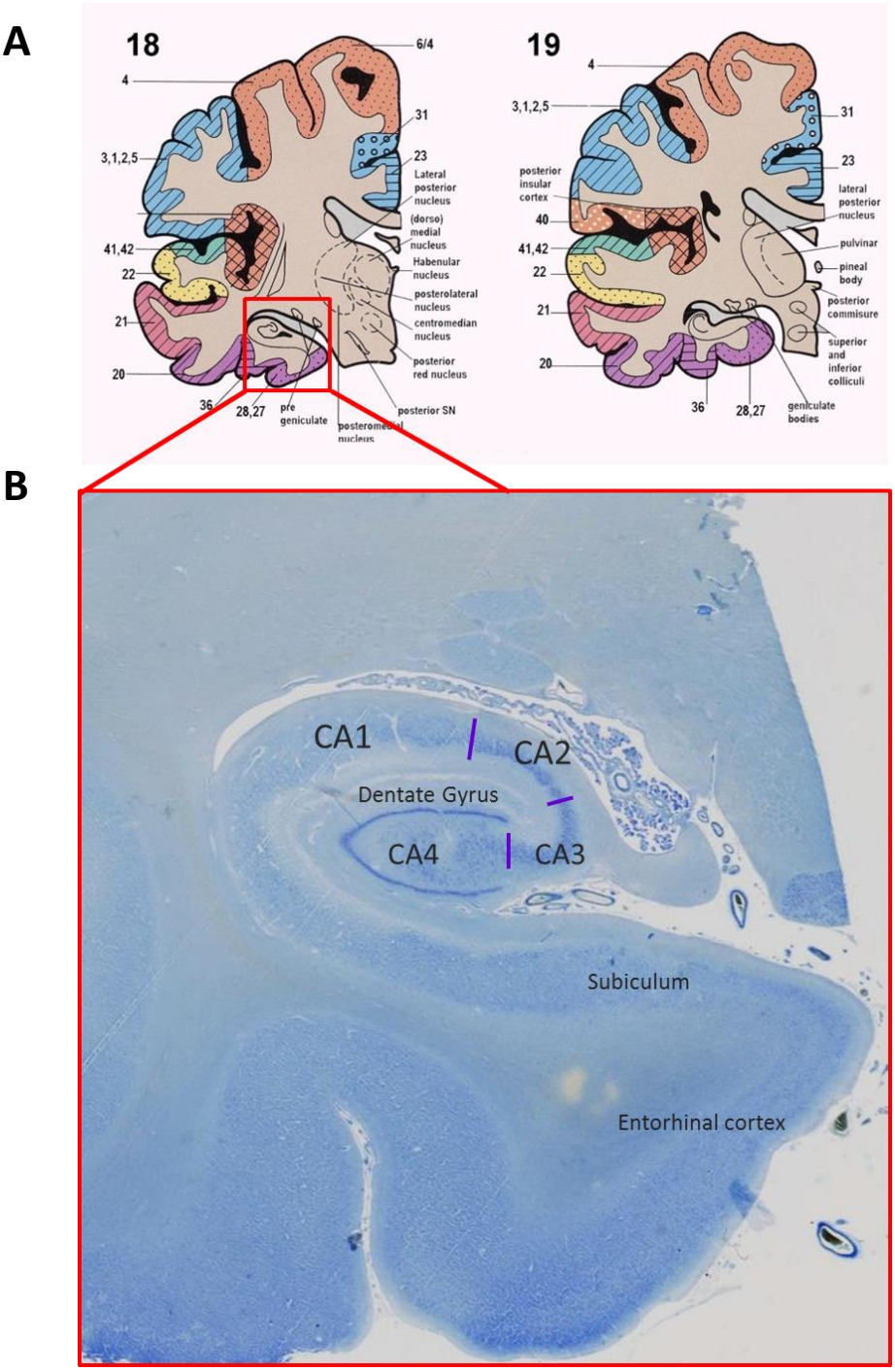

Figure 2.1. A, Levels 18 and 19 according to the Newcastle Brain Map (Perry and Oakley, 1993); B, Close-up of hippocampal formation at level 18 with clearly identifiable dentate gyrus and CA regions in a section stained with cresyl-fast violet.

2.5 Histology

2.5.1 Cresyl Fast Violet (CFV)

Cresyl Fast Violet (CFV) was used to stain tissue to visualise neuronal soma, nuclei and nucleoli. Sections were dewaxed and rehydrated to 95% alcohol for 1 minute, immersed in 1% acid alcohol for 5 minutes and rinsed in 3 changes of deionized water. Sections were incubated for 5 minutes in CFV solution pre-heated to 60°C, then cooled for 5 minutes. CFV solution was made using 20-25mls stock solution (0.2% w/v cresyl fast violet in deionized water) in 500mls deionized water and 500mls acetate buffer (13.5mls acetic acid, 23.5g sodium acetate to 2000mls in deionized water, pH 4.5). Sections were differentiated in 95% alcohol until the background was pale purple. Staining consistency was checked under a microscope before sections were dehydrated, cleared in xylene and mounted.

2.5.2 Luxol Fast Blue (LFB)

Luxol Fast Blue (LFB) is a copper phthalocyanine dye that is attracted to the lipoproteins of the myelin sheath which stains myelinated axons deep blue, therefore, LFB was used to visualize myelin in tissue sections. Sections were dewaxed and rehydrated to 95% ethanol, then incubated for 2 hours in LFB stain (1g of Luxol fast blue and 5mls of 10% acetic acid in 1000mls of 95% alcohol) preheated to 60C. Sections were cooled for 10 minutes, then washed in 70% ethanol for 1 minute. Sections were then differentiated in 4 cycles of; 1 minute in distilled water, 10 seconds in $LiCoO_3$ and 1 minute in 70% ethanol. After 4 cycles of differentiation sections were viewed under a microscope to assess staining. If the grey matter still appeared blue, sections were differentiated further until the grey matter appeared clear. When sections were consistently stained they were immersed in water ready for the CFV counterstain. Sections were immersed in CFV solution (0.1% CFV in 1% acetic acid) for 2 minutes at room temperature, washed in distilled water and differentiated in 95% ethanol. Sections were checked for staining consistency before being dehydrated, cleared in xylene and mounted.

2.5.3 Haematoxylin and Eosin (H & E)

Haematoxylin and eosin (H & E) was used to visualize cell nuclei in blue and other eosinophilic structures in shades of red, pink and orange. Sections were dewaxed and rehydrated to water then immersed in haematoxylin solution for 3 minutes (5g haematoxylin, 0.5g sodium iodate, 40ml glacial acetic acid, 300ml glycerine, 700ml distilled water). After a wash in tap water, sections were dipped in 1% acid alcohol for 40 seconds and washed again in water. Sections were then immersed in ammonia tap water for 1 minute and washed in water. Sections were then immersed in eosin for 3 minutes (10g eosin, 0.25g phloxine, 0.25g erytheosin, 1000ml 20% alcohol). After being washed in tap water sections were differentiated in 95% ethanol to remove excess stain. Slides were checked under a microscope for staining consistency before mounting.

2.6 Standard immunohistochemistry (IHC) protocol

All immunohistochemical staining was performed using the following protocol unless stated otherwise. To minimize staining variability, wherever possible all sections stained with each antibody were stained simultaneously. Table 2.3 details the antigen retrieval method, buffer, block and antibody concentrations used in each experiment.

Paraffin-embedded sections were dewaxed rehydrated to water. Antigen retrieval was performed using one of the following techniques:

- For microwave antigen retrieval, sections were simmered in sodium citrate solution (diluted in deionized water from a 10x stock solution of 2.94g trisodium citrate in 1 litre of distilled water, pH 6) for 11 minutes in the microwave. Sections were left in the solution to cool for 20 minutes and washed in tap water.
- For pressure cooker antigen retrieval, sections were immersed in boiling 10mM citrate buffer (pH 6) and cooked under pressure for ~8 minutes until pressure was reached. Sections were then rinsed in tap water.
- For formic acid antigen retrieval, sections were dipped in 40% formic acid, then immersed in concentrated formic acid (10ml 99% formic acid in 90ml distilled

water, pH 2) for 4 hours (in a sealed container in a fume hood). Sections were then dipped in 40% formic acid and transferred to running tap water for 10 minutes.

After antigen retrieval, endogenous peroxidase activity was quenched using 0.3% hydrogen peroxide in buffer for 15 minutes. The buffers used were tris-buffered saline with 0.5% Triton-X (TBS-TX, 12g tris and 81g NaCl in 10l distilled water, pH 7.6), or phosphate buffered saline with 0.5% Triton-X (PBS-TX, 2.76g $NaH_2PO4.1H_20$, 11.36g Na_2HPO_4 anhydrous, 85g NaCl, in 10l distilled water, pH 7.2).

After three washes in buffer, sections were incubated for 30 minutes at room temperature in blocking serum diluted in buffer. Excess solution was removed then sections were incubated overnight at 4C with the primary antibody. Sections were then washed in three changes of buffer, then incubated with 0.5% secondary antibody (biotinylated Universal antibody, Vector Vectastain Universal kit) and 1.5% blocking serum (15µl per 1ml TBS-TX) for 30 minutes at room temperature. Sections were washed in three changes of buffer then incubated with 20µls Avidin DH (reagent A) and 20µls of the paired biotinylated enzyme (Reagent B) from the Vector Vectastain kit per 1ml TBS-TX. Sections were washed in three changes of buffer and visualized with diaminobenzidine (DAB) for 5 minutes (100mg DAB and 167µl hydrogen peroxide per 400ml TBS). A pale haematoxylin counterstain was often used to visualize cell nuclei.

The method used to visualize GFAP differed slightly from this standard protocol, as nickel-DAB was used in the final stage. After the final wash in buffer (PBS-TX), sections were washed in acetate buffer (3.4g sodium acetate trihydrate per 250ml distilled water, to pH 6 with acetic acid). Following this wash, a nickel-DAB solution (2.5g di-ammonium nickel-sulphate, 100ml acetate buffer, 50mg DAB, 40mg ammonium chloride, 200mg beta-D-glucose, 100µl glucose oxidase) was pipetted onto the sections and incubated for 10 minutes. Slides were then washed in acetate buffer, before being dehydrated, cleared in xylene and mounted.

Antibody	Target	Manufacturer (product code)	Species	Concen-tration	Antigen retrieval	Block	Buffer
4G8	Amyloid β, APP	Signet (9220-10)	Mouse (MAb)	1:1000	F	1.5% NHS	TBS-Tx
ALDH1L1	Astrocytes	eBioscience (14-9595)	Mouse (MAb)	1:500	M	5% NHS	PBS-Tx
AT8	Hyperphos-phorylated tau	Autogen Bioclear (90206)	Mouse (MAb)	1:2000	M	1.5% NHS	TBS-Tx
Beclin-1	Autophagic vacuoles	Abgent (AM1818a)	Mouse (MAb)	1:100	M	5% NHS	TBS-Tx
CD68	Microglia	Dako (M7013)	Mouse (MAb)	1:400	2xM	1.5% NHS	TBS-Tx
dMBP	Degraded myelin basic protein	Millipore (AB5864)	Rabbit (PAb)	1:2000	M	1.5% NGS	TBS-Tx
Drebrin	Dendritic spine protein	MBL (D029-3)	Mouse (MAb)	1:200	M	1.5% NHS	TBS-Tx
GFAP	Reactive astrocytes	Dako (Z0334)	Rabbit (PAb)	1:8000	M	5% NGS	PBS-Tx
LC3	Autophagic vacuoles	Abgent (AP1801a)	Rabbit (PAb)	1:100	M	5% NGS	TBS-Tx
MAP2	Dendrites	Sigma (M4403)	Mouse (MAb)	1:2000	M	5% NHS	TBS-Tx
P62	Protein aggregates	BD Transduction Laboratories (610832)	Mouse (MAb)	1:600	P	1.5% NHS	TBS-Tx
PSD-95	Post-synaptic protein	Abcam (AB 19258)	Rabbit (PAb)	1:750	M	3% NGS	TBS-Tx

Table 2.3. List of antibodies and methods used for immunohistochemistry. MAb = monoclonal antibody; PAb = polyclonal antibody; F = formic acid antigen retrieval; M = microwave antigen retrieval; P = pressure cooker antigen retrieval method; NHS = normal horse serum; NGS = normal goat serum.

2.7 Image analysis

2.7.1 Image capture

All analyses were carried out blind to diagnosis. Unless stated otherwise, images were captured using a Zeiss Axioplan2 brightfield microscope through x5, x10, x20 or x40 planar using a Lumenera Infinity 2 digital camera (Lumenera Corporation). Low-power images were taken using a Zeiss Axio Scope A1 brightfield microscope through x2.5 N-Achroplan lenses using a Lumenera Infinity 2 digital camera (Lumenera Corporation). All images were white balanced and captured using Infinity Capture software.

2.7.2 Image Pro analysis

Images were analysed using Image Pro Plus 6.3 (Media Cybernetics). The area of interest was delineated on-screen using the wand tool and the size of the area selected was recorded. Histogram based analysis was used to measure the number of pixels stained ('per area', PA) and intensity of stain (integrated optical density, IOD), as determined by the operator when only positive staining was highlighted and background was excluded (Figure 2.2). Using the sum of each of the three measures further calculations generated the measures reported in this thesis: Percent of the area of interest positively stained, 'Percent area (%PA)' *= Per Area x 100;* Mean intensity of stain per pixel, 'Integrated Optical Density (IOD)' *= 255 – (sumIOD/area).* The mean % PA and IOD were then calculated for each subject from the images taken.

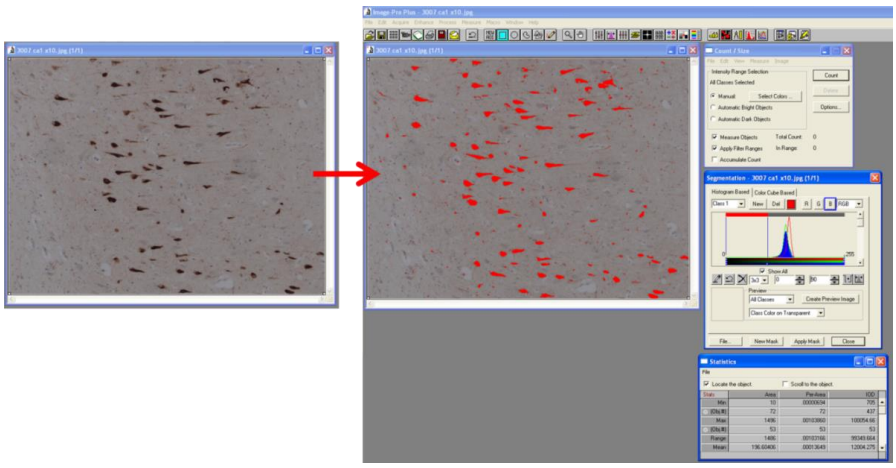

Figure 2.2. Example screen capture of image analysis using Image Pro. Histogram-based segmentation is performed to highlight in red all immunopositive staining.

2.7.3 Image Pro analysis of LFB stained sections and myelin index calculations

10µm thick sections stained using LFB were viewed at 10X magnification. Five images were taken of the alveus adjacent to the CA1 and four images were taken of the alveus adjacent to the CA2, evenly sampled along the length of the alveus (Figure 2.3A). An image was also taken from the white matter deep to the EC for comparison. An area equivalent to 300 x 900 pixels was delineated within the alveus in each image, and measurement for %PA and IOD were calculated for the region of interest in image.

Myelin index was calculated across the alveus using methods described in (Yamamoto *et al.*, 2009) and (Ihara *et al.*, 2010). Images of the hippocampus were taken at low power using an Epson Perfection V700 Photo duel lens system scanner. A standardized area (0.33 x 0.43 pixels) was defined around the hippocampus and captured at 12800 DPI (dots per inch). The alveus was delineated using the Image Pro wand tool. The range of blue stain intensity for each individual section was determined between 0 and 255 (where 0 = black and 255 = white, as Image Pro is set up for fluorescent analysis). This range was divided into four quartiles, and within each quartile the median IOD was calculated and multiplied by %PA to generate the myelin index (Figure 2.3B).

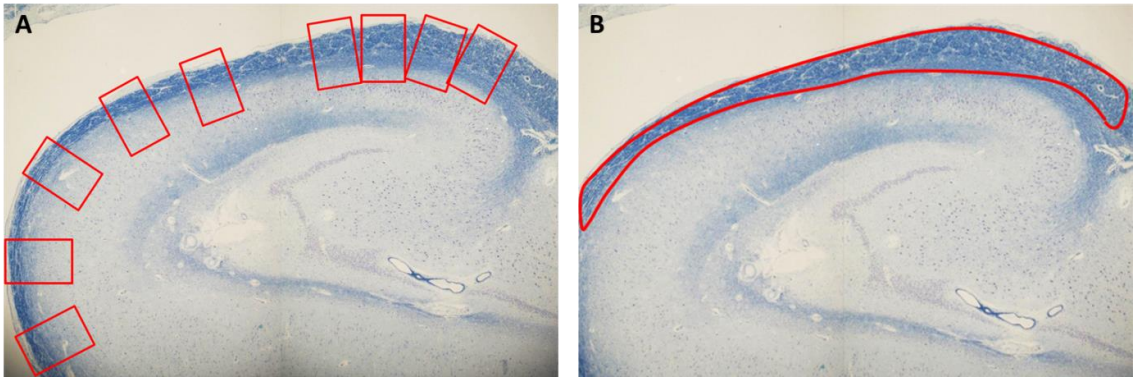

Figure 2.3 Diagrams demonstrating how images were taken throughout the alveus of LFB/CFV stained hippocampal sections. A, Red squares represent individual images taken at 10x magnification; B The alveus was delineated as one subfield for myelin index analysis.

2.7.4 Astrocyte counts

Sections were stained using IHC for GFAP and ALDH1L1 to visualize astrocytes. Images were captured at 10x magnification and viewed using Image Pro Plus 6.3. A 3x4 grid was placed over images, where each square covered an area equivalent to 280µm x 280µm (78400µm^2)(Figure 2.5). Astrocytes within squares covering regions of interest were counted provided they did not touch the bottom or left borders of the counting grid. Numbers of images and squares analysed within different layers of the hippocampus are shown in Table 2.4. The number of grid squares analysed was decided based on the size of the region available for analysis in all sections.

2.7.5 CA Region	CA Layer	Number of images	Number of grid squares analyzed per image	Total number of squares analyzed per layer
CA1	Alveus	5	2	
	Stratum Pyramidal	5	2	
	Stratum Radiatum	5	3	
CA2	Alveus	1	2	2
	Stratum Pyramidal	1	2	2
	Stratum Radiatum	1	2	2
CA3	Stratum Radiatum	1	2	2
CA4	Stratum Pyramidal	4	4	16

Figure 2.5. CA1 Stratum pyramidal stained for ALDH1L1 with3x4 counting grid overlay. Scale bar = 100µm.

Table 2.4 Location and numbers of images and grid squares in which astrocyte counts were performed.

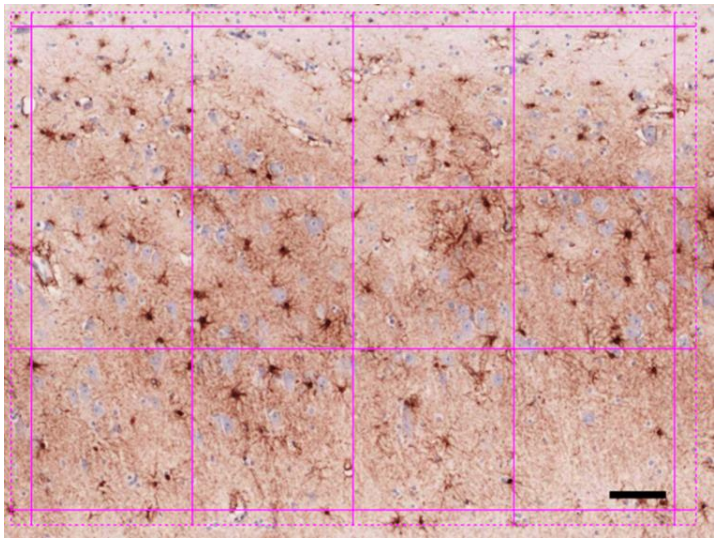

Figure 2.4. CA1 stratum pyramidal stained for ALDH1L1 with 3x4 counting grid overlay. Scale bar = 100µm.

2.7.5 3D Stereology for neuronal density and volume

A 3D stereological technique was used to measure neuronal density and volume as described in (Gemmell *et al.*, 2012). Three 30µm serial sections from each case were stained using CFV. Sections were viewed on a computer screen using a Zeiss Axioplan Photomicroscope with a Pixelink PL-B623CF colour digital camera. To define the area of interest, sections were viewed through a 2.5x objective lens and the investigator delineated CA1/CA2/CA3/CA4/ECV on-screen using stereological analysis software (Visiopharm Integration System, Hørsholm, Denmark). CA regions were clearly distinguishable based on the distribution and size of pyramidal neurons as described previously (Section 1.4.3, p20) and in (Duevernoy, 2005); CA4 neurons were enclosed within the v-shaped dentate gyrus (DG), CA3 neurons were larger and extended as a broad band of closely packed cells from the 'mouth' of the DG, CA2 neurons were in a much thinner band of large, densely packed and darkly stained neurons, CA1 neurons were in the widest band of more dispersed neurons. The CA1/subiculum border was identified when the distribution of neurons appeared more patchy in the straighter band of cells towards the entorhinal cortex (Figure 2.1B). Entorhinal cortex layer V (ECV) neurons were identified as a thin band of darkly stained large to medium sized pyramidal neurons, bordered superficially by a sparse layer as described by Canto et al. 2008 (Canto *et al.*, 2008).

A uniform random sampling procedure was applied to select approximately 33 frames within the area of interest using a motorised stage (Prior ProScan II; Prior Scientific Instruments Ltd, Cambridge, UK) with an accuracy of 1µm. Therefore approximately 100 frames per region were analysed within the three sections per case. Sections were analysed at 100x magnification using an oil immersion objective with a numerical aperture of 1.25. Each disector probe had an x-y area of 2548.66µm^2 and a z depth of 18µm, to ensure that a guard volume => 4µm was excluded from analysis at the top and bottom of the section. A Heidenhain z-axis microcator (Heidenhain GB Ltd, London, UK), accurate to 0.5µm was used to precisely measure disector depth and tissue thickness every 10 frames (mean section thickness = 26.3µm).

Neuron density was calculated using the optical disector method (Sterio, 1984). Pyramidal neurons were identified by their characteristic triangular soma, Nissl stained cytoplasm and darkly stained single nucleolus (Rajkowska *et al.*, 2005). The following

equation was used to calculate neuron density per tissue section, from which a mean density per case could be calculated:

$$Density\ (pyramidal\ neurons\ per\ mm^3) = \left[\frac{Neuron\ Count\ in\ CA1\ or\ CA2}{(No.Disector\ Boxes * Disector\ Frame\ Area * Disector\ Box\ Depth)}\right] * 10^7$$

The soma of each counted neuron was measured using an independent uniform random orientated Nucleator probe (Figure 2.6)(Gundersen and Jensen, 1987), which therefore did not take into account the volume of axons or dendrites. Volumes of neurons were estimated based on six randomly projected lines from the nucleolus. Approximately 150 neurons were analysed per subfield per case. A pilot study was performed to ensure that the average sampling error reached a satisfactory level demonstrating a high level of precision and that the observed variation could be attributed to biological variation. Using the Gundersen Jenesn method, the mean coefficient of error (CE) for neuron density was calculated to determine the level of sampling (methodological) error (Gundersen and Jensen, 1987):

$$CE^2 = \left\{\frac{\sum(I^2)}{(\sum I)^2} + \frac{\sum(Volume^2)}{\sum(Volume^2)} - \frac{2\sum(1 * Volume)}{(\sum I * \sum Volume)}\right\} * \left(\frac{n}{n-1}\right)$$

*Where I = Neurons counted; Volume = Reference area *(sampling frame density)^2 * section depth; N = number of frames.*

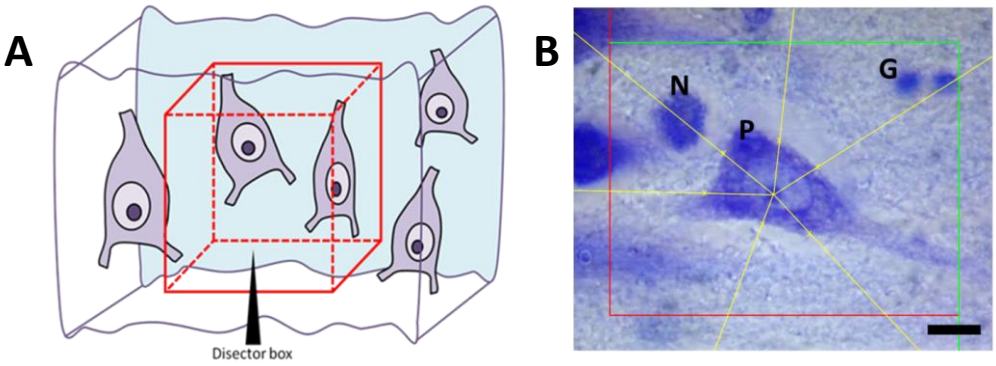

Figure 2.6. A, Diagram depicting the optical disector box within a 30µm thick tissue section; B, Representative image of a CA1 pyramidal neuron being measured using the nucleator tool: N indicates non-pyramidal neuron; P, pyramidal neuron; G, glial cell. Red and green lines delineate the disector frame. Scale bar = 10µm.

2.7.6 3D stereology for dendritic length-density

A 3D stereological technique was used to calculate the length-density of dendrites in the CA1 stratum radiatum. This technique had previously been applied to estimate the length-density of the hippocampal microvasculature in CogFAST subjects (Burke *et al.*, 2013). Fifteen 30µm thick sections were cut from pre-defined paraffin-embedded hippocampal blocks. Three sections were then selected from this series at 5 section intervals, thus sampling through a total of 450µm of hippocampal tissue. Sections were then stained using IHC for MAP2 to visualise dendrites. Sections were viewed using a Zeiss Axiolab brightfield microscope and 5x and 100x objectives and a JVC digital camera attached to a computer. The area of interest (stratum radiatum) was defined at 5x magnification using the Stereologer 2000 software (Stereologer, WV, USA) by drawing round the area on-screen. The software applied a stratified-random sampling procedure to select ~45 frames within the defined region of interest. Frames were viewed at 100x magnification with a numerical aperture of 1.25 under oil immersion.

A spherical probe 18µm in diameter was used to measure the length-density of dendrites. Spherical probes are ideal to estimate the length of anisotrophic structures such as dendrites, as spheres are isotropic in three-dimensions (Gokhale, 1990). Viewed from above, the probe appeared as a circle of increasing and then decreasing diameter as the focal plane was moved through the z-axis. The operator marked whenever a dendrite came into focus intersecting the sphere border (Figure 2.7). Average section thickness was 23.4µm, ensuring a guard volume =>2µm was excluded from analysis at the top and bottom of each section. A pilot study was initially carried out to establish that analysing ~45 frames per case gave an acceptable coefficient of error demonstrating high level of accuracy (CE = 0.066 ±0.02SE). The software then calculated length density (L_v) from the number of dendrites intersecting the probe (ΣQ) within the area of the sampling probe (ΣA) using the equation
$L_v = 2(\Sigma Q / \Sigma A)$ (Mouton, 2002).

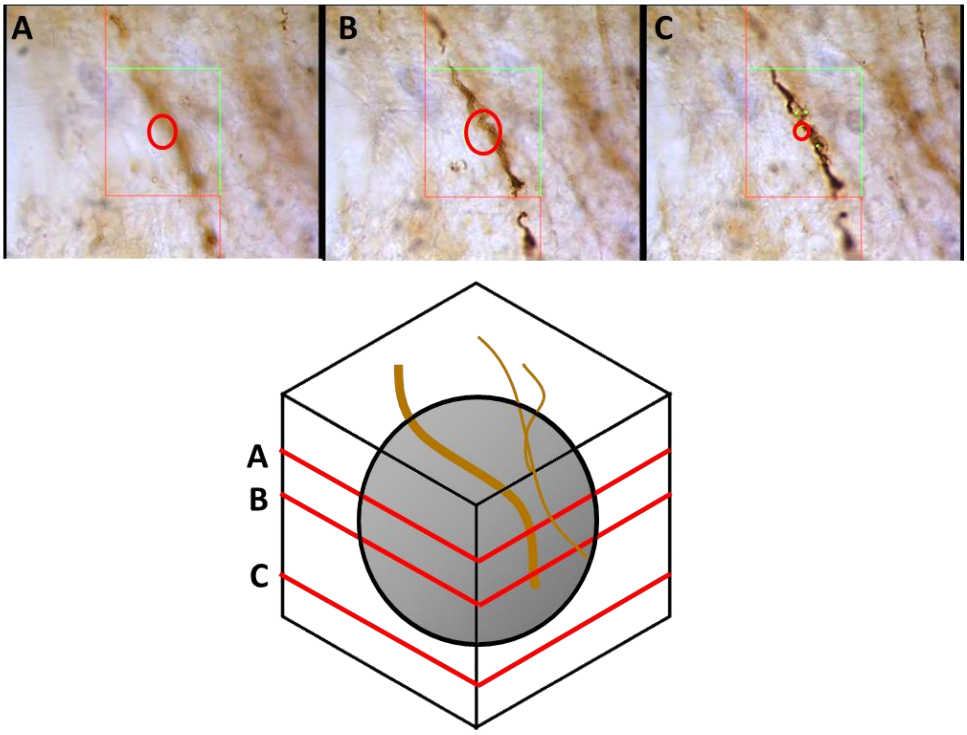

Figure 2.7. Representative images of the spherical probe used to measure dendritic length density. A-C, as the focal plane moved downwards through the z-axis dendrites were measured when an in focus dendrite crossed the sphere boundary (red circle).

2.8 Protein analysis in frozen hippocampal tissue

Analysis of protein levels in frozen hippocampal tissue was carried out using a protein immunoblotting technique. Proteins were separated by gel electrophoresis (SDS-PAGE) and transferred to a nitrocellulose membrane to allow protein detection by immunoprobing with antibodies. This method allowed comparison of protein levels between disease groups using frozen tissue which therefore removed the effect of tissue processing and fixation.

2.8.1 Tissue extraction

Cryostat sections of 20µm and 100µm thickness were cut from frozen hippocampal blocks at level 18-20 according to the Newcastle Brain Map and stored at -80C. Each 20µm section was stained with CFV for visualisation of tissue structure. Frozen sections were taken down through decreasing concentrations of alcohol to water (1 minute in 100%, 95%, 75%, 50% ethanol and 5 minutes in water). Sections were immersed in acid alcohol for 5 minutes and incubated in pre-heated CFV solution in acetate buffer at

60C for 20 minutes, then left to air dry for 15 minutes. Sections were differentiated in 95% alcohol for 30 seconds and checked for staining consistency, then dehydrated, cleared and mounted.

Using the CFV stained 20µm section as a visual guide (Figure 2.8), the hippocampus was rapidly dissected from two 100µm thick frozen sections and homogenized in 200µls of ice-cold extraction buffer (50mM Tris-Hcl, 5mM ethylene glycol tetraacetic acid (EGTA), 10mM enthylenemide tetra-acetic acid (EDTA), pH 7.4, following established method (Kirvell *et al.*, 2010)). The buffer also contained protease and phosphatase inhibitors to block endogenous protease and phosphatase activity (Thermo Scientific Halt Protease Inhibitor Cocktail product #78430 and Halt Phosphatase Inhibitor Cocktail, product #78428). The tissue was then homogenized by rapidly repeat pipetting, vortexing and using a Hamilton Gastight 1µl micro-syringe until the solution ran smooth. Samples were kept on ice during homogenization. These whole homogenate samples were then stored at -20°C.

2.8.2 DC protein assay

Protein concentration was determined using the DC (detergent compatible) protein assay kit (BioRad). The DC assay is a colorimetric assay based on the Lowry assay (Lowry *et al.*, 1951), which has been modified to save time. Six protein standards covering the working range of the DC assay were made up using Bovine Serum Albumin (BSA) at 0.2, 0.4, 0.5, 0.6, 0.8 and 1mg/ml and stored at -20C between assays. Samples were diluted 1:10 and 1:20 times in extraction buffer for the DC assay. 5µl of the protein standards and 5µl of each diluted sample were added in triplicate to a 96 well plate. BioRad DC protein assay solutions A (25µl) and B (200µl) were added sequentially to each well and the plate was incubated at room temperature for 15 minutes. The intensity of the colour was detected colorimetrically by absorption at 750nM using a FLUOstar Omega plate reader (BMG Labtech). Mean absorbances were calculated for standards and samples. A standard curve of absorbance versus concentration was constructed from the known standards, allowing determination of sample protein concentrations from the equation of the curve.

2.8.3 Protein separation by SDS-PAGE

Proteins in the samples were separated by molecular weight (MW) using SDS-PAGE (Sodium Dodecyl Sulphate - Polyacrylamide Gel electrophoresis). Running samples were prepared by diluting 100µl of whole homogenate from each sample in 100µl SDS-mix-DTT (20%w/v glycerol, 12.5% v/v 1M Tris-Hcl, pH 6.8, 3% w/v SDS (Sodium Dodecyl Sulphate), 15.4% w/v Dithiothreitol (DTT) and a few grains of bromophenol blue). Reducing agents in this solution denatured the tertiary structure of proteins for separation of proteins by electrophoresis. From the calculated concentrations of the whole homogenate, samples were diluted further with a 50:50 SDS-mix-DTT: water to make running samples with a standardized concentration of 2µg/µl. Samples with concentrations already below 2µg/µl were not diluted further, instead the volume loaded into the gel was adjusted maintain constant amount of protein loaded. Before loading, all running samples were vortexed and microcentrifued to ensure a homogeneous mix.

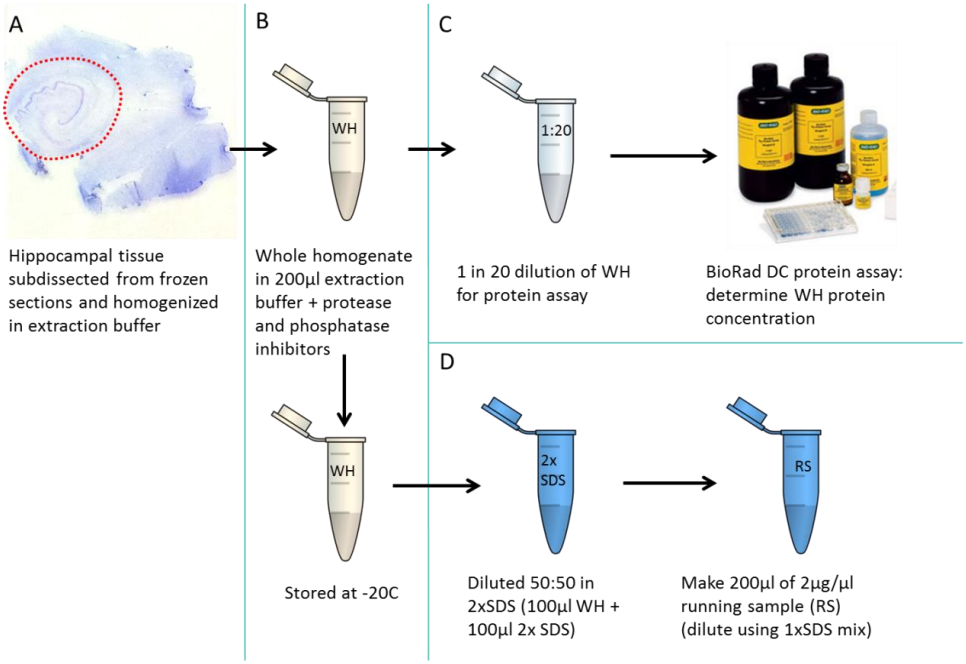

Figure 2.8. Flow diagram depicting stages of frozen tissue extraction (A,B), the protein assay (C) and making up running sample (D).WH = whole homogenate; RS = running sample.

Acrylamide gels 10cm long and 1.5mm thick were made according to details in Table 2.5. To make the plug, 120µl 10% ammonium persulphate (AMPS) and 60µl N,N,N^{I},N^{I}-tetramethyl-ethyledediamine (TEMED) were added to 10mls of the main gel solution,

which was mixed by inversion and then quickly poured into two casts. After five minutes the plugs were set and excess solution was removed with 3MM paper. To make the main gel, 400µl 10% (w/v) AMPS and 40µl TEMED were added to the remaining 40mls of main gel solution and poured into the casts, leaving room for the stack and combs. A few ml of water saturated butanol was added to ensure the surface set smoothly while the gel was left to set for 15-30 minutes. Once set, water saturated butanol was washed off with distilled water, and excess water was removed with 3MM paper. The stack was prepared from 3.4mls acrylamide, 2.52mls 1M Tris-HCl pH 6.8, 200µl 10% SDS and made up to 20mls with water. When ready, 200µl 10% AMPS and 20µl TEMED were added to the stack solution, which was quickly poured into the casts and 24-well combs were inserted. Gels were left for >30 minutes to completely set. Combs were then carefully removed and wells were washed out with distilled water before being placed in the running module.

Gels were run using an upright electrophoresis tank (Complete OmniPAGE Mini Wide system, SLS) at 150V constant in fresh running buffer (16.66g Tris, 144 g glycine, 10g SDS, to 2l with distilled water) for 50 minutes or until the blue dye had run into the plug. 10µl of pre-stained molecular weight marker (Spectra Multicolor Broad Range Protein Ladder, Thermo Scientific) was used to demonstrate the distance moved by known molecular weight (MW) protein standards, ranging from 10-260 kDa. A standard mix made from all running samples was also loaded three times per gel to assess variation within and between gels. The amount of protein loaded is described for individual experiments.

	6%	**8%**	**10%**	**12%**
Target protein molecular weight (kDa)	100-300	50-200	20-100	10-50
Acrylamide (mls)	10	13.3	16.7	20
2M Tris-HCl pH 8.8 (mls)	9.4	9.4	9.4	9.4
10% SDS (mls)	0.5	0.5	0.5	0.5
Water		Made up to 50mls		

Table 2.5. Protocol for making two 20 x 10cm acrylamide gels.

2.8.4 Protein immunoblotting

Nitrocellulose membranes of 0.45mm thickness were hydrated in distilled water and western blot buffer (5% w/v isopropanol, 0.4M glycine, 2.5mM Tris buffer) for 10 minutes each. Gels were removed from the SDS-PAGE casts and soaked in western blot buffer for 5 minutes. The western blot stack was constructed from layers of; sponge,

Whatman 3MM paper soaked in western blot buffer, the gel, the nitrocellulose membrane, a second layer of Whatman 3MM paper and sponge. These were compressed inside the cassette, which was immersed the transfer tank filled with western blot buffer with the gel towards the negative electrodes. The buffer was kept cool using a system running 16°C cool water through pipes immersed in the tank. A constant current of 350mA was applied for 120 minutes to ensure complete transfer.

After transfer, membranes were dried on fresh blotting paper and the position of molecular weight markers were marked on in permanent pen. The membranes were washed in TBS-T for 5 minutes (20mM Tris HCL, pH 7.5, 150mM NaCl, 0.1% w/v Tween 20). Membranes were then immersed in Ponceau stain for 1 minute (0.5% w/v ponceau S, 5% w/v trichloracetic acid), and rinsed in distilled water to check for successful protein transfer. The ponceau stain was removed using TBS-T.

Enhanced chemiluminescent (ECL) assay for protein detection

Proteins on the nitrocellulose membrane were detected using immunoprobing technique. To remove non-specific binding sites the nitrocellulose membrane was immersed in 5% w/v non-fat dried milk (Marvel) in TBS-T for 30 minutes at room temperature and gently mixed on a platform shaker. The membranes were then incubated with the primary antibody in 5% non-fat dried milk on a platform shaker overnight at 4C. After six 5 minute washes in 1% non-fat dried milk in TBS-T, membranes were incubated for 1 hour with the horse radish peroxidase conjugated secondary antibody (1:2000 dilution in 5% non-fat dried milk in TBS-T). The membranes were then washed in six 5 minute washes in 1% non-fat dried milk in TBS-T, with a final wash in TBS-T.

The membranes were then dried on fresh blotting paper, laid on a glass plate and incubated with a chemiluminescent substrate solution for 5 minutes (reagents A and B in a 1:1 ratio, Thermo Scientific, SuperSignal West Pico kit). A clear plastic sheet was then laid over the membrane to keep it moist. Membranes were imaged using a Fujifilm Luminescent Image Analyzer LAS4000 System cooled to -30C. Membranes were exposed for varying lengths of time to achieve optimal signal detection for analysis.

Quantification of protein blots

The optical density of bands was measured using ImageJ image analysis software. Raw data were normalized to the optical density of β-tubulin. The amount of signal detected was corrected between gels using the mean value from the standards loaded on gels. Data were expressed as the optical density of the band for each protein sample loaded.

Primary antibody	Target	Manufacturer (Product code)	Species	Concentration	Secondary antibody
PSD-95	Post-synaptic protein	Abcam (AB 19258)	Rabbit	1:1000	Anti-rabbit (1:2000)
SNAP-25	Pre-synaptic vesicles	*Affiniti* Research Products, UK	Mouse	1:2000	Anti-mouse (1:2000)
SY38	Pre-synaptic vesicles	Cymbus (MAB5258-20UG)	Mouse	1:2000	Anti-mouse (1:2000)
α/B-Tubulin	Loading control	Cell Signalling (2148S)	Rabbit	1:1000	Anti-rabbit (1:2000)

Table 2.6. List of antibodies and concentrations used for protein immunoblots. Blots were incubated with primary antibodies at 4C overnight.

2.9 Baboon model of acute chronic cerebral hypoperfusion

The non-human primate model (baboons) have comparable vascular and brain anatomy, morphology, cellular physiology and biochemistry to the human brain, and develop Aβ and tau pathology with ageing, allowing greater insight into pathophysiological mechanisms of human brain disorders than rodent models can provide.

Eighteen male olive baboons (*Papio anubis*) over 10 years old weighing 15-20kg underwent permanent three vessel occlusion (3VO) surgery where the left vertebral and both internal carotid arteries were ligated under deep anaesthesia (Figure 2.9). Animals were left to recover for 1, 3, 7, 14 or 28 days post-surgery before being euthanized with ketamine (Baneux *et al.*, 1986). Three age, weight and sex matched

baboons received sham surgery where they were anaesthetised and underwent surgery but no vessels were ligated. Sham animals were left for 24 hours to recover before being euthanized. Before being euthanized, animals were sedated and perfused with 4% buffered paraformaldehyde. The brains were removed and post-fixed in 4% buffered paraformaldehyde. The brains were then dissected into blocks, processed and embedded in paraffin wax.

Surgery was performed by Dr. M. Ndung'U at the Institute of Primate Research, National Museums of Kenya. Funding for this study was obtained from US and Japanese sources, therefore ethical approval was granted through the ethical committee at the Institute for Primate Research, Kenyan Museums, Kenya. Permission to import and use tissues in the UK was obtained from Defra (Department for Environment, Food and Rural Affairs) under a CITES (Convention on International Trade in Endangered Species of Wild Fauna and Flora) institutional agreement. Newcastle University biological safety officers were fully aware of the importation and use of the material in the Institute for Ageing and Health, Newcastle University.

Ten and 30µm thick sections were cut from paraffin embedded blocks containing the hippocampus at level A. 13.5- A.11 according to the Stereotaxic Atlas of the Brain of the Baboon (Davis and Huffman, 1968). Sections were cut and stained using the same methods as described for human tissue.

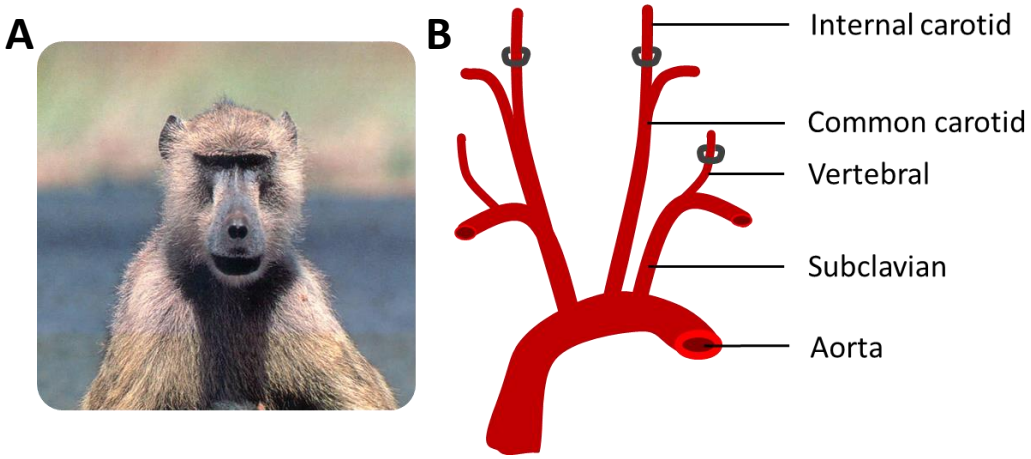

Figure 2.9. A, Papio anubis; B, Diagram showing the sites of ligation for three vessel occlusion surgery (3VO).

2.10 Statistical analyses

Statistical analyses were carried out using SPSS v.19. Before using parametric tests, data were checked for normal distribution using the Shapiro-Wilk test and homogeneity of variance using Levene's test.

Normally distributed data were analysed using the following parametric tests; ANOVA with post-hoc Tukey's to compare group means, Pearson's correlation to find relationships between variables, and paired T-test to compare related means.
When data were not normally distributed data were analysed using the following non-parametric tests; Kruskall Wallis and Mann-Whitney tests to compare groups, Spearman's correlation to find relationships between variables (and ordinal variables), and Wilcoxon signed rank test to compare related means. Corrections for multiple testing were carried out using the Bonferroni adjustment, by dividing the chosen alpha level ($p < 0.05$) by the number of tests carried out, to determine the p value cut-off for significance. Interpretation of significance using both cut-off points is discussed.

Associations between categorical data were analysed using Pearson χ^2 test or Fisher's Exact test with Phi and Cramer's V.

Chapter 3. Neuronal Volume and Density Changes in Post-Stroke and Ageing Related Dementias

3.1 Introduction

Hippocampal atrophy is associated with cognitive impairment in AD, VaD and dementia caused by familiar small vessel disease (Bastos-Leite *et al.*, 2007; O'Sullivan *et al.*, 2009; Frisoni *et al.*, 2010; Scher *et al.*, 2011). MTL atrophy was also found to be a predictor of delayed PSD in stroke survivors from the CogFAST cohort (Firbank *et al.*, 2007). Historically, the cause of reduced tissue volume and associated cognitive impairment was believed to be neurodegeneration. This was based upon studies demonstrating reduced neuronal numbers in hippocampal subfields in VaD (Kril *et al.*, 2002b; Zarow *et al.*, 2008), AD (Giannakopoulos *et al.*, 1996; Kril *et al.*, 2002b; Rössler *et al.*, 2002; Zarow *et al.*, 2005) mixed VaD and AD (Zarow *et al.*, 2005), and animal models of ischaemic stroke (Kirino, 1982; Olson and McKeon, 2004). In support of this theory, neuron number was shown to be related to hippocampal volume in ageing and AD (Kril *et al.*, 2004). Therefore, I reasoned that greater neurodegeneration may account for the more severe cognitive decline and structural brain changes in stroke survivors who developed delayed PSD compared to those who maintained normal cognitive function.

However, there is growing evidence that neuron loss is not the only factor that contributes to brain atrophy and functional decline. Studies into MCI and early dementia have found that hippocampal atrophy and cognitive decline develop before any significant loss of hippocampal neurons (Apostolova *et al.*, 2010; Leal and Yassa, 2013). In addition, although hippocampal atrophy is associated with memory impairment in AD and normal ageing (Apostolova *et al.*, 2011), studies have found that there is limited neuron loss with age (West *et al.*, 1994; Pakkenberg *et al.*, 2003) and neurodegeneration in AD may only make a weak contribution to tissue atrophy (Rössler *et al.*, 2002). Furthermore, conflicting reports of CA1 neuron loss in VaD suggest other mechanisms contribute to tissue atrophy and cognitive dysfunction in CVD (Kril *et al.*, 2002b; Korbo *et al.*, 2004; Zarow *et al.*, 2005). There is now growing

interest in changes to neuronal architecture as a possible mechanism causing tissue atrophy and cognitive dysfunction through loss of structural connectivity and neuronal dysfunction (Terry *et al.*, 1987; Swaab *et al.*, 1994; Morrison *et al.*, 2002; Freeman *et al.*, 2008; Fjell and Walhovd, 2010). Therefore, I also investigated changes to neuronal soma volumes as an indicator of neuronal dysfunction, to explore whether changes to neuronal morphology were related to post-stroke cognitive impairment.

3.1.1 Measuring neuronal volume and density using 3D stereology

Historically, studies of neuron loss and neuronal volumes relied on counting and measuring neuronal profiles in thin tissue sections. However, these methods result in over-counting of larger neurons whose profiles appeared across several serial sections, and neuronal volume estimations were based on assumptions about the shape, size and orientation of neurons (Gundersen *et al.*, 1988; Mayhew and Gundersen, 1996). To remove this bias, 3D stereology was developed to use thicker tissue sections (>30µm), allowing neurons to be viewed as whole particles within the tissue. Neurons are then only counted when a unique point within the cell comes into focus (e.g. the nucleolus), ensuring each neuron is only counted once. Neuronal volumes are also estimated from this standardized central point using the 'nucleator' tool (Gundersen *et al.*, 1988), (described in detail in section 2.7.5). 3D stereology is now recognized as the gold standard technique for quantitatively measuring cell density and size, as it has been proven to generate more accurate and consistent results compared to earlier 2D methods (West, 1999; Baddeley, 2001; West and Slomanka, 2001; Schmitz and Hof, 2007).

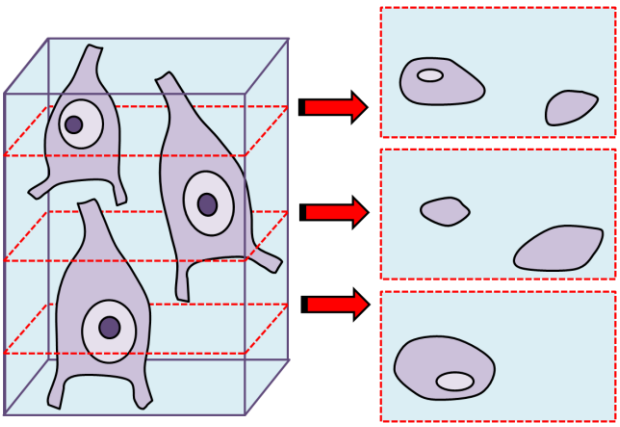

Figure 3.1. Diagram demonstrating the differences between 2D and 3D stereological analysis of neuronal volumes and densities. The left diagram shows how neurons would be viewed within a thick tissue section using 3D stereology. The right diagram shows how 2D analysis would result in inaccurate area measurements from profiles of each neuron, and demonstrates how larger neurons would be over-counted using this technique (3 neurons, 5 profiles).

3.2 Aims

This study investigated neuronal densities and volumes in hippocampal CA subfields and entorhinal cortex layer V (ECV) in stroke survivors from the CogFAST cohort, using 3D stereological techniques, to determine whether neuronal volume or density changes were related to post-stroke cognitive function. Hippocampal neurons in the CA subfields are known to be differentially vulnerable to age-associated disease processes. Therefore, I also analysed hippocampal neurons in elderly controls, VaD, AD and MD subjects to provide insight into the role of different disease processes in neuronal changes.

In addition, neuronal volumes and densities were analysed in a small number of younger, cognitively normal controls to investigate the effect of ageing on neuronal volumes. Normal ageing is associated with brain atrophy, however 3D stereological studies have not found any evidence of neuron loss in healthy ageing, suggesting that changes to neuronal morphology and function may contribute to normal age-associated cognitive decline (West and Slomanka, 2001).

Neuronal volumes and densities were also measured in a non-human primate (baboon) model of chronic cerebral hypoperfusion (described in full in section 2.9, page 59), to gain insight into whether there were acute changes to neuronal volume or density at different time points after hypoxic injury.

3.3 Methods

3.3.1 3D stereological analysis of neuronal volumes and densities

Neuronal volumes and densities were measured using the optical disector and nucleator techniques in three 30µm thick hippocampal tissue sections per subject, stained using cresyl fast violet (CFV) to view neuronal cell bodies and nucleoli (described on page 44).

3.3.2 Statistical analyses

CA1 and CA2 neuronal volume and density data were not normally distributed, and were therefore analysed using non-parametric tests; group means were compared using the Kruskal-Wallis test and pairwise comparisons were performed using the Mann-Whitney U test. CA3 and CA4 neuronal volumes and densities were normally distributed and were analysed using one-way ANVOA with post-hoc Tukey's test. Relationships between variables were correlated using Spearman's rank correlation.

3.4 Results

3.4.1 Subject demographics

Subject demographics are presented in Table 3.1. The control group had significantly shorter PMD than PSND, PSD, VaD and AD groups, and longer fixation length than the PSD and AD groups ($p < 0.05$). The mixed dementia (MD) group had a significantly longer fixation length than PSND and PSD ($p < 0.05$). However, no relationships were found between PMD or fixation length and neuronal volume or density results. Coefficient of error values for neuronal volume and density measurements were within the acceptable range in all regions, demonstrating a high level of precision: neuronal volume in CA1 $p = 0.04$, CA2 $p = 0.02$, CA3 $p=0.052$ and CA4 $p=0.073$; neuronal density in CA1 $p = 0.06$, CA2 $p = 0.002$, CA3 $p=0.051$ and CA4 $p=0.07$.

	n	Age, years Mean (range)	PMD, hours Mean (range)	Fixation length, weeks Mean (range)	Braak Stage Median (range)	CERAD score Median (range)	Vascular pathology Mean (range)
Controls	14	81.1 (72-92)	27.9 (8-67)	15.8 (8-67)	N/A	N/A	N/A
PSND	22	84 (78-94)	40.4 (10-96)	10.2 (2-32)	2 (1-5)	1 (0-2)	12.6 (7-16)
PSD	15	87.7 (80-98)	41.2 (10-96)	8.2 (4-14)	3 (0-6)	1 (0-3)	12.3 (8-17)
VaD	13	85.5 (71-97)	51.2 (24-84)	15 (4-52)	2 (1-4)	1 (0-2)	13.8 (12-15)
MD	17	84 (72-94)	37.8 (11-72)	16.8 (3-40)	5 (4-6)	3 (1-3)	10.4 (6-14)
AD	13	83.7 (70-91)	39.4 (5-83)	8.40 (2-24)	5.5 (4-6)	3 (2-3)	5.5 (5-6)

Table 3.1 Subject demographics. PSND = post-stroke non-demented, PSD = delayed post-stroke dementia, VaD = vascular dementia, MD = mixed vascular and Alzheimer's dementia, AD = Alzheimer's disease, PMD = post mortem delay, N/A = information not available for the majority of control subjects.

3.4.2 Neuronal density in PSD and ageing-related dementias

Numerical values for group means and standard deviations are shown in Appendix Table 8.1Figure 8.1. CA1 neuronal densities were different between the groups [H (2) = 33.2, $p < 0.001$] (Figure 3.2). Compared to controls, CA1 neuronal density was reduced in the PS group ($p = 0.025$), PSND ($p = 0.027$), VaD ($p = 0.012$), MD ($p < 0.001$), and AD groups ($p = 0.001$). The MD and AD groups had lower neuronal density than the PSND group ($p < 0.001$ and $p = 0.015$ respectively). There were no differences in CA1 neuronal density between the PSD and PSND groups ($p = 0.643$). CA2, CA3, CA4 and ECV neuronal densities were not different between groups. In control subjects, neuron densities were greatest in CA2 and ECV > CA1 and CA3 > CA4 (shown in Appendix, Figure 8.1).

Neuronal densities were positively correlated between CA1 and CA2 ($r = 0.311$, $p = 0.005$), CA1 and CA4 ($r = 0.317$, $p = 0.003$), CA1 and ECV ($r = 0.247$, $p = 0.037$), CA3 and ECV ($r = 0.481$, $p < 0.001$). In the post-stroke subjects only, CA3 neuronal densities were only correlated with ECV neuronal density ($r = 0.503$, $p = 0.02$). There were trends to negative correlations between neuronal volume and density in CA3 ($r = -0.373$, $p = 0.08$) and CA4 ($r = -0.403$, $p = 0.051$).

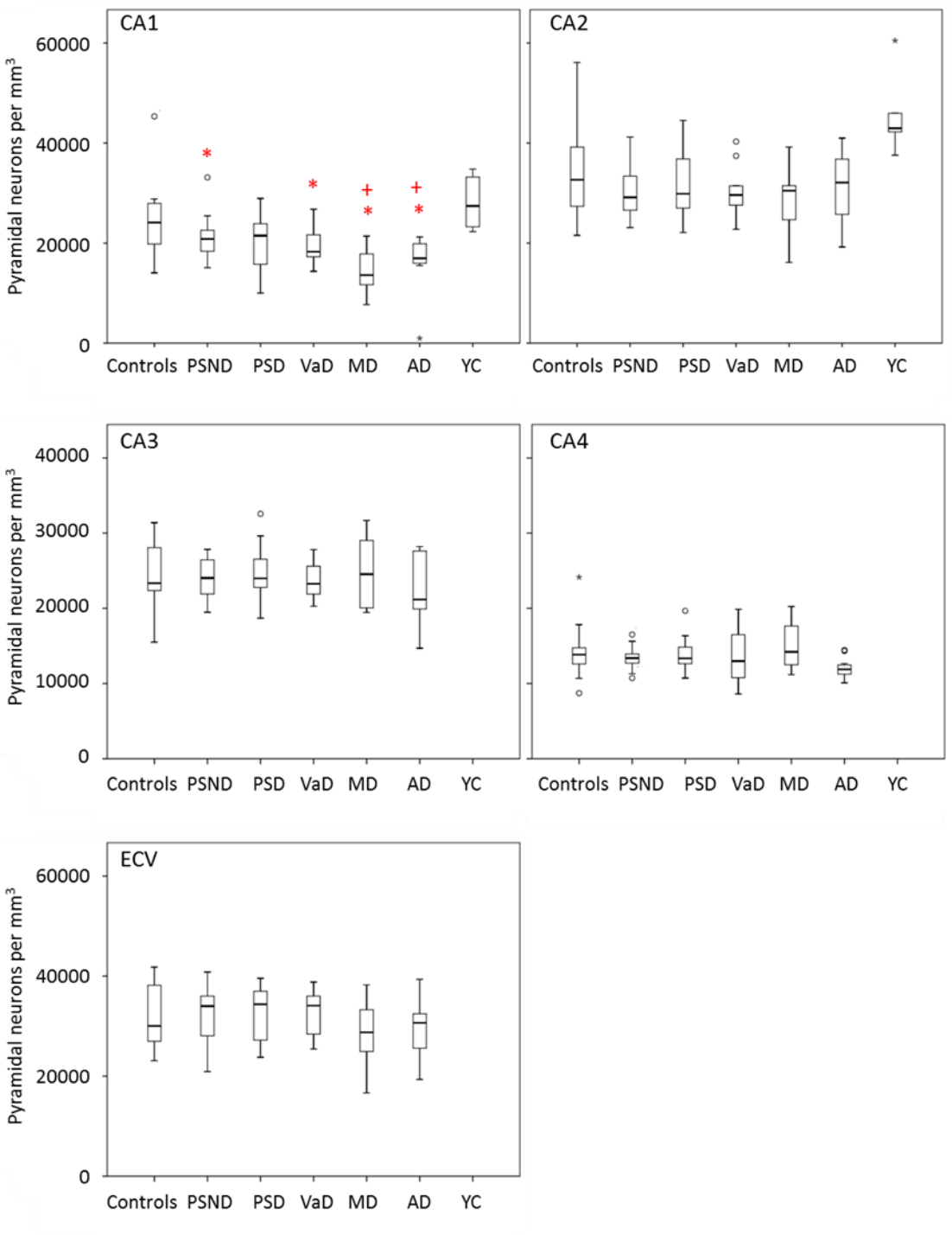

Figure 3.2. Neuronal densities in CA1-4 and ECV. PSND = post-stroke non-demented, PSD = delayed post-stroke dementia, VaD = vascular dementia, MD = mixed vascular and Alzheimer's dementia, AD = Alzheimer's disease; *indicate difference to controls, + indicate difference compared to PSND; $p < 0.05$.

3.4.3 Neuronal volumes in PSD and ageing-related dementias

CA1 neuronal volumes were different between the groups [H (5) = 14.1, p = 0.015].

CA1 neuronal volumes were reduced in VaD (p = 0.047), mixed dementia (p = 0.039)

and AD (p = 0.037) compared to controls. Compared to the PSND group, CA1 neuronal volumes were reduced in all dementia groups (PSD p = 0.028, VaD p = 0.026, MD p = 0.009 and AD p = 0.01). There were no differences in neuronal volume between the PSND group and controls.

CA2 neuronal volumes were different between the groups [H (5) = 19.1, p = 0.002]. CA2 neuronal volumes were reduced in all dementia groups; PSD p = 0.014, VaD p = 0.021, MD p = 0.003 and AD p = 0.016. Compared to the PSND group, CA2 neuron volumes were also reduced in all dementia groups (PSD p = 0.009, MD p = 0.003 and AD p = 0.019, and there was a trend to significance with the VaD group (p = 0.08). There were no differences between the PSND and controls.

CA3 neuronal volumes were different between the groups [F (5, 60) = 6.3, p < 0.001]. Compared to controls, CA3 neuronal volumes were reduced in PSD (p = 0.065) and MD (p < 0.001). Compared to the PSND group, CA3 neuronal volumes were reduced in PSD (p = 0.043), MD (p < 0.001). MD CA3 neuronal volumes were also lower than VaD (p = 0.04).

CA4 neuronal volumes were different between the groups [F (5, 61) = 9.4, p < 0.001]. Compared to controls, CA4 neuronal volumes were reduced in PSD (p < 0.001), MD (p < 0.001), AD (p = 0.001), and there was a trend to significance with the VaD group (p = 0.089). Compared to the PSND group, CA4 neuronal volumes were reduced in PSD (p = 0.001), MD (p < 0.001), and there was a trend to significance in AD (p = 0.052). MD CA4 neuronal volumes were also lower than VaD (p = 0.025).

ECV neuronal volumes were different between the groups [H (5) = 24.2, p < 0.001]. Compared to controls and PSND, ECV neuron volumes were reduced in MD (p < 0.001 and p < 0.001 respectively) and AD (p = 0.007 and p = 0.018 respectively). MD and AD ECV neuronal volumes were also reduced compared to PSD (p =0.002, p = 0.034) and VaD (p = 0.001, p = 0.04). MD neuronal volumes were reduced compared to AD (p = 0.047).

Neuronal volumes were highly correlated between all regions (Table 8.4).

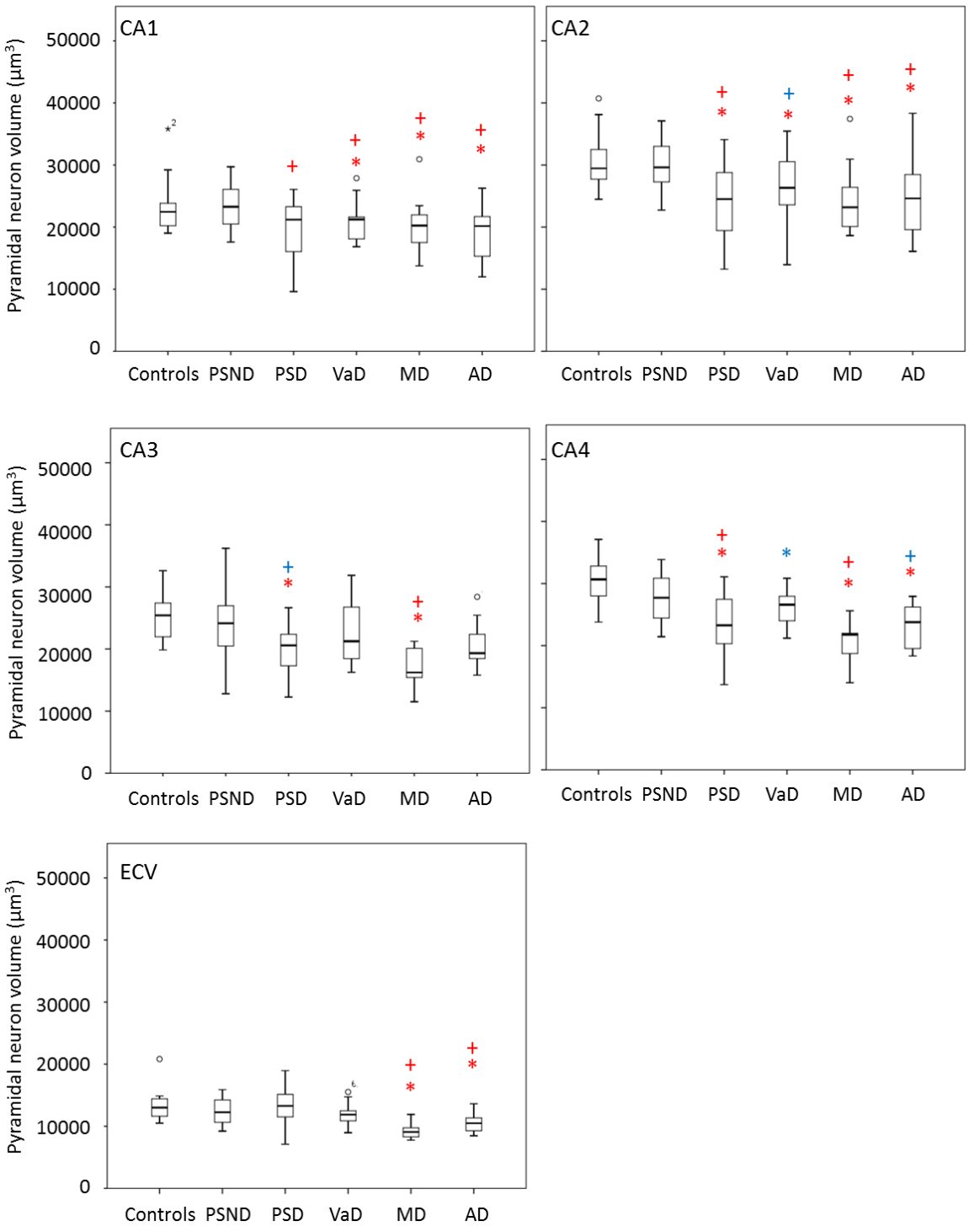

Figure 3.3. Neuronal volumes in CA1-4 and ECV. PSND = post-stroke non-demented, PSD = delayed post-stroke dementia, VaD = vascular dementia, MD = mixed vascular and Alzheimer's dementia, AD = Alzheimer's disease; *indicate difference to controls, + indicate difference compared to PSND; Red = $p < 0.05$, blue = $p < 0.01$.

When neuronal volumes were calculated as a percentage of control means they were 10-28% smaller in the disease groups (Figure 3.4) (values in Appendix Table 8.2). Neuronal volumes were positively correlated between all regions ($p < 0.05$, values in Appendix Table 8.4). There were no differences in neuronal volumes or densities between male and female subjects in any subfield, or between results obtained from the right and left hippocampus. CA2 neuronal volumes were weakly negatively correlated with age ($r = -0.226$, $p = 0.019$). Control subjects neuronal volumes were greatest in CA2 and CA4 > CA3 and CA1 > ECV (shown in Appendix Figure 8.1).

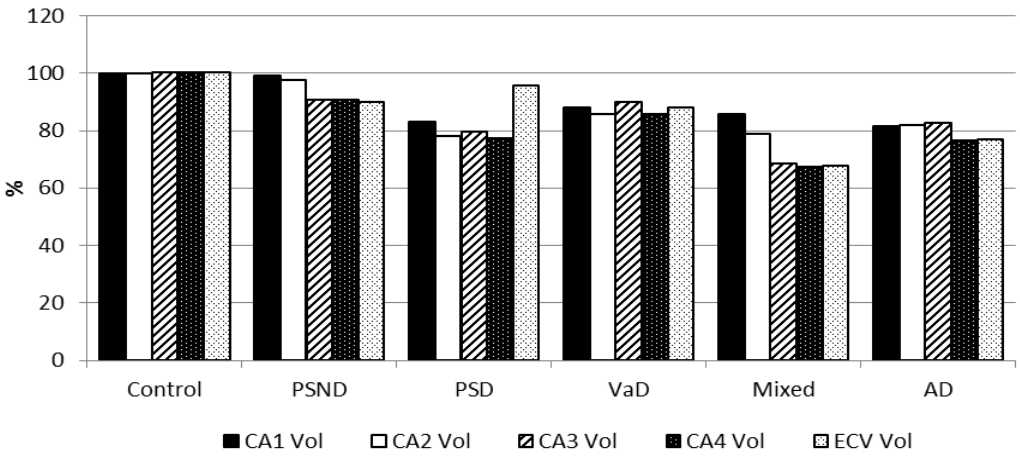

Figure 3.4. Neuronal volume as a percentage of control means.

3.4.4 Clinicopathological correlations

CAMCOG scores were positively correlated with neuronal volumes in CA1-4, and memory sub-scores were correlated with CA2 neuronal volumes (Figure 3.5)(Table 3.2). When subjects with total CAMCOG < 40 (and any sub-scores = 0) were excluded due to possible inaccurate cognitive test scorings, these correlations remained significant at $p > 0.05$ (all $r > 0.3$). When subjects with memory sub-scores scores of 0 were excluded, memory sub-score correlations with CA2 neuronal volumes remained significant ($r > 0.4$, $p < 0.02$) except learning ($r = 0.352$, $p = 0.052$). Neuronal densities were not correlated with CAMCOG scores in any region.

CA1 neuron density was negatively correlated with Braak stage and CERAD scores (r = -0.379, p = 0.002 and r = -0.392, p = 0.001 respectively). CA2, ECV and CA4 neuronal volumes were negatively correlated with Braak stage (r = -0.392, p = 0.003; r = -0.395, p = 0.004 and r = -0.274, p = 0.036 respectively) and CA2 and ECV volumes were negatively correlated with CERAD score (r = -0.261, p = 0.059 and r = -0.419, p = 0.002).

Global vascular pathology was not correlated with neuronal volumes or densities in any region.

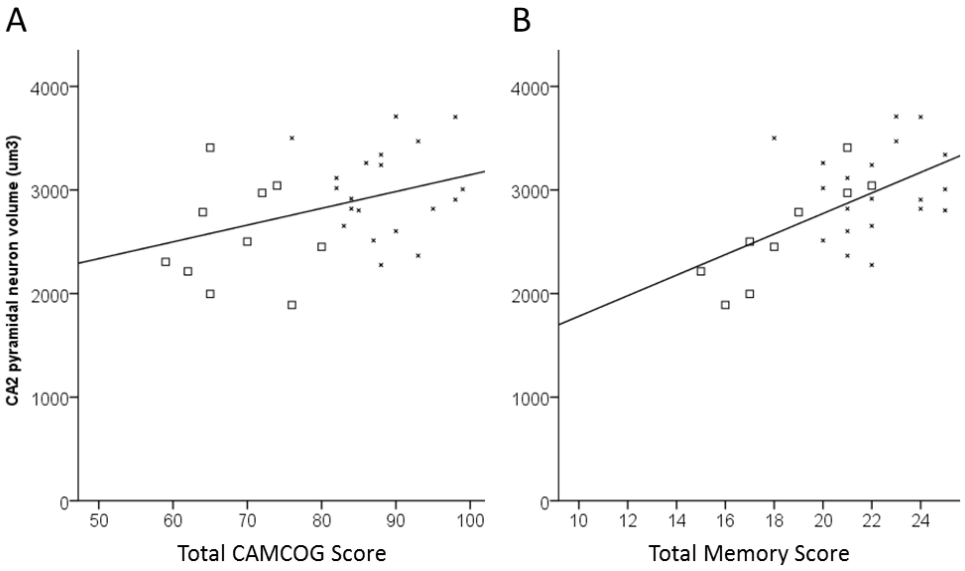

Figure 3.5. CA2 neuronal volumes were positively correlated with total CAMCOG scores (A) and memory sub-scores (B), with subjects with total CAMCOG score < 40 and memory score < 10 excluded. o = PSD; x = PSND.

		CA1 Volume	CA2 Volume	CA3 Volume	CA4 Volume
CAMCOG total	R p	0.399, 0.01	0.445, 0.007	0.526, 0.012	0.572, 0.004
Memory total	R p	Ns	0.481, 0.006	Ns	Ns
Recent memory	R p	Ns	0.692, < 0.001	Ns	Ns
Remote memory	R p	Ns	0.428, 0.016	Ns	Ns
Learning	R p	Ns	0.352, 0.052	Ns	Ns

Table 3.2. Correlations between CA neuronal volumes and CAMCOG scores and sub-scores. Ns = not significant. When correlations were corrected for multiple comparisons (20 tests), the cut-off for significance was reduced to $p < 0.0025$.

3.4.5 Neuronal changes in younger versus elderly controls

Elderly controls were significantly older than younger controls ($p < 0.001$). There were no significant differences in PMD or Fixation length between groups (Table 3.3).

There were no significant differences in neuronal volume in younger compared to elderly controls. CA2 neuronal density was greater in younger controls compared to elderly controls ($p = 0.009$) (Figure 3.6).

	n	**Age, years** Mean (range)	**PMD, hours** Mean (range)	**Fixation, weeks** Mean (range)
Elderly controls	14	81.1 (72-92)	27.9 (8-67)	15.8 (8-67)
Younger controls	5	48.8 (27-59)	32 (19-41)	59.8 (5-210)

Table 3.3. Subject demographics in elderly vs. younger controls.

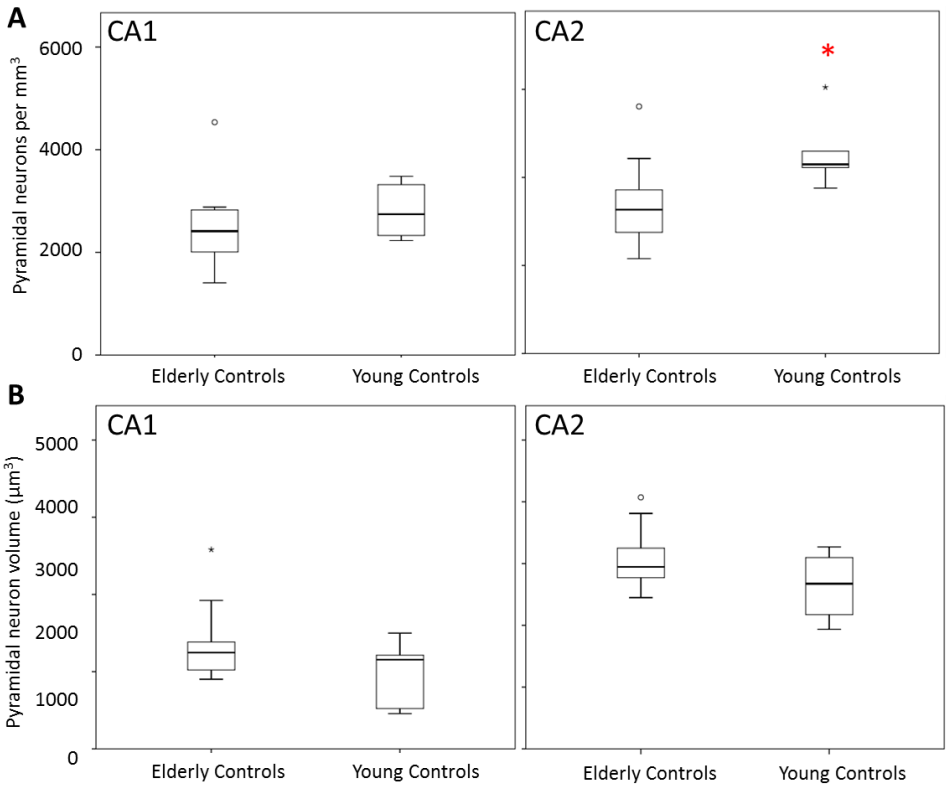

Figure 3.6 CA1 and CA2 neuronal densities (A) and volumes (B) in elderly and younger controls. Red asterisk indicates significant difference compared to controls.

3.4.6 Neuronal changes in a baboon model of acute cerebral hypoperfusion

Numerical values for mean neuronal volumes and densities are presented in Appendix Table 8.5. When neuronal volume measurements from the left and right hemispheres were combined, there was a difference in CA1 neuronal volumes between groups ($H(5) = 13.25$, $p = 0.021$). The sham group had greater CA1 neuronal volumes than the 3 day ($p = 0.041$), 7 day ($p = 0.026$) and 14 day groups ($p = 0.004$). The 28 day group CA1 neuronal volumes were greater than 14 day ($p = 0.002$).

When results were separated by hemisphere, no statistical analyses were performed between groups as there were only three animals per time point, limiting the validity and interpretation of statistical analyses. Neuronal volumes were very similar in the ipsi- and contra-lateral hemispheres (Figure 3.7 A), and the results indicated that neuronal volumes in the CA1 and CA2 were reduced in both hemispheres in the 1 day, 3 day, 7 day and 14 day groups compared to the sham animals, whereas the 28 day group had larger neuronal volumes equivalent to those in the sham group. Mean neuronal densities were not different at different time points post-surgery (Appendix Figure 8.2), although when statistical analyses were performed on the combined hemisphere data, CA2 neuronal densities were lower in the 3 day group compared to the sham group ($p = 0.015$).

Neuronal volumes were also related to data from a previous study using sections from the same block, where all neurons within the CA1 were rated as appearing ‘pyknotic’ or ‘healthy’ (Figure 3.7 B)(unpublished results). From this, the percentage of pyknotic neurons within the CA1 was calculated. CA1 and CA2 neuronal volumes were negatively correlated with the percentage of pyknotic neurons (CA1 $r = -0.654$, $p < 0.001$; CA2 $r = -0.465$, $p = -0.465$) (Figure 3.7 C).

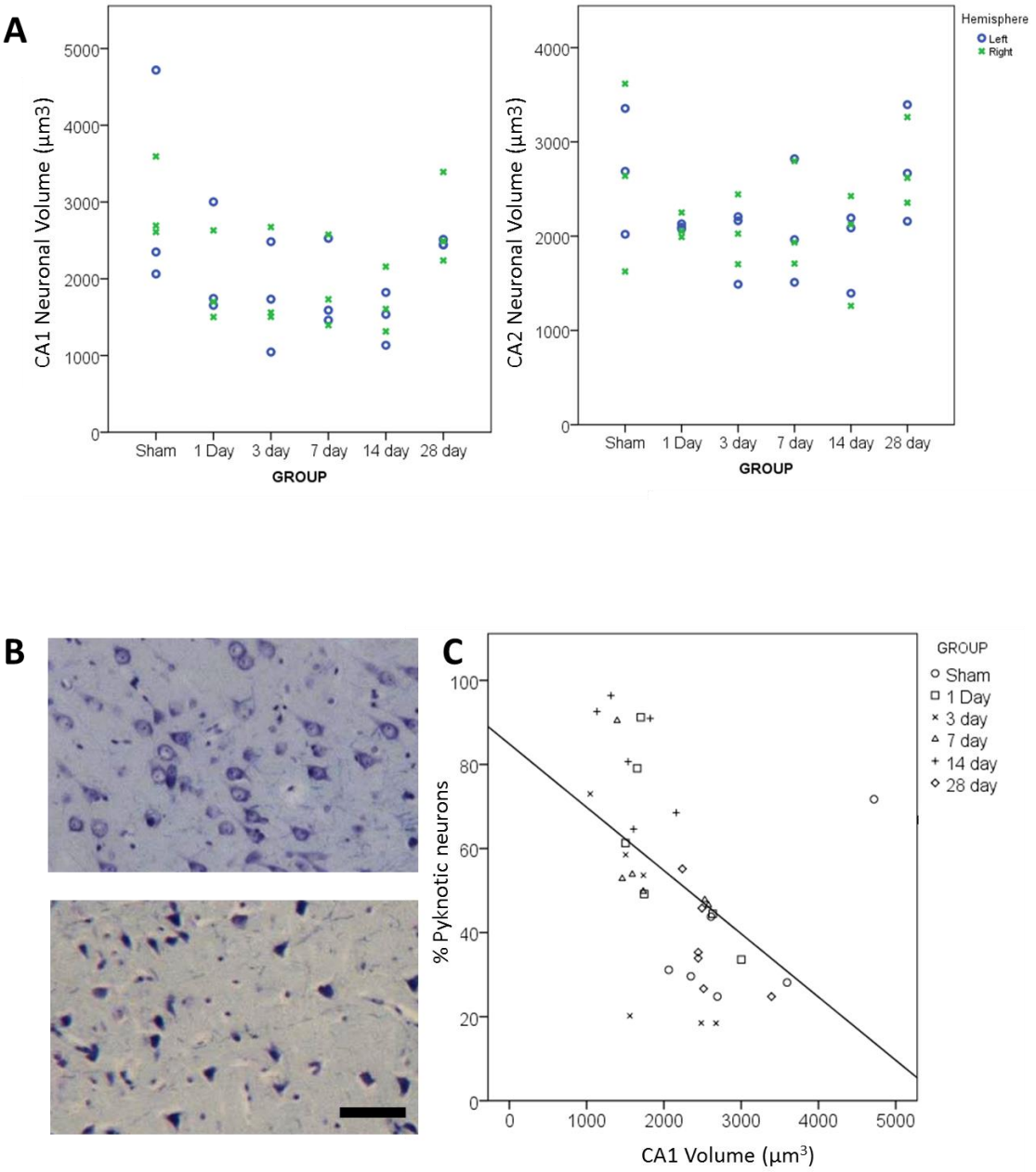

Figure 3.7. A, CA1 and CA2 Neuronal volumes in a baboon model of cerebral hypoperfusion at different survival times post-surgery; 1D = 1 day, 2D = 2 day, 3D = 3 day, 7D = 7 day, 14D = 14 days, 28D = 28 days post-surgery. Blue circles = left hemisphere (contralateral to surgery), green circles = right hemisphere (ipsilateral to surgery); B, Representative images of normal CA1 neurons in sham animal (top panel) and pyknotic CA1 neurons in 3 day animal (bottom panel), Scale bar = 50µm; C, CA1 neuronal volumes were negatively correlated with % pyknotic neurons in CA1 ($r = -0.654$, $p < 0.001$).

3.5 Discussion

3.5.1 Reduced neuronal volumes in post-stroke and ageing-related dementias

Hippocampal neuronal volumes were reduced by 10-20% in the CA subfields of stroke survivors who developed delayed PSD compared to PSND subjects, and decreased neuronal volumes were related to lower CAMCOG scores in stroke survivors. These results provide novel evidence that decreased neuronal volumes were associated with post-stroke cognitive impairment, and suggest that decreased neuronal volumes reflect mechanisms contributing to cognitive decline. This finding was supported by similar observations in the other types of dementia, where neuronal volumes in CA1, CA2 and CA4 were also ~20% reduced in AD, VaD and MD compared to PSND and controls.

In contrast to the neuronal volumes, there were no differences in hippocampal neuronal densities between PSND and PSD subjects, although both groups had lower CA1 neuron density than controls. This finding was consistent with previous reports of CA1 neuron loss after ischaemic stroke; however it was surprising not to find any association between lower neuron density and lower CAMCOG scores or PSD, as I had reasoned that neuron loss was likely to contribute to the observed MTL atrophy and dementia in stroke survivors. Although unexpected, this finding complements the neuronal volume results as it implies that differing mechanisms in the surviving neurons were important in determining cognitive outcome after stroke.

It was surprising to find that only CA2 neuronal volumes were related to memory sub-scores in stroke survivors, as neurons in the CA2 subfield are generally considered to be the most resilient to injury. However, the CA2 subfield is also the least well studied, and its role in cognitive processing has only recently begun to be understood (Jones and McHugh, 2011). Interestingly, a neuroimaging study of early AD found that CA2 atrophy was more strongly associated with MCI and progression to dementia than CA1 atrophy (Apostolova *et al.*, 2010). Together these findings suggest an important role for CA2 neurons in cognitive function, and my results suggest that reduced neuronal volume may be a mechanism relating this sub-regional hippocampal atrophy to cognitive impairment in the early stages of dementia.

Corrections for multiple testing between the neuronal volume results and cognitive scores using the Bonferroni adjustment resulted in only the correlation between CA2 neuronal volumes and recent memory achieving statistical significance. However, this adjustment may be overly strict resulting in increased false-negative results . For this reason, and because exploratory studies such as this require a flexible approach for design and analysis resulting in large numbers of tests, the use of appropriate multiple test adjustments in exploratory studies is difficult and controversial (Thomas, 1998). Therefore, it has been suggested that in this kind of study, interpretation of 'significant' results may be considered as exploratory results which would require further testing in confirmatory studies to confirm the hypotheses (Bender and Lange, 2001). Therefore, interpretation of the 'significance' of all results should be carefully considered. However, in this situation, I believe the risk of dismissing potentially important results when using strict multiple test adjustments in exploratory research outweighs the implications of reporting a simple coincidence.

3.5.2 Neuronal volumes and densities in different disease processes

Braak stages and CERAD scores were negatively correlated with CA1 neuron density, but there was no relationship between CA1 neuronal volume and AD pathology. Conversely, CA2, CA4 and ECV neuronal volumes were negatively correlated with AD pathology, but there was no relationship with neuron density. This is consistent with the well documented loss of CA1 neurons in AD and literature suggesting tangle burden is related to neuronal death (Zarow *et al.*, 2005). The relationship between AD burden and neuronal volumes, but not densities, in the other subfields indicates that these neurons were affected by AD processes, but they did not cause neuronal death. Reduced neuronal volume may simply reflect damage to neurons caused by disease processes, or alternatively they may reflect increased damage to remote susceptible neurons which communicate with these neurons (i.e. CA1), resulting in loss of targets and deafferentation. This may have caused the retraction of processes and loss of axo-dendritic arbour from the CA2/CA3/CA4 neurons, which has previously been implicated in the cause of neuronal volume loss (Hanks and Flood, 1991; Harrison and Eastwood, 2001).

There were no relationships between neuronal volumes or densities and ratings of CVD burden, which was surprising as neuronal volumes and densities were significantly decreased in pathologically confirmed PSD (VaD) and VaD subjects who had no other significant neurodegenerative disease pathology. This may therefore reflect limitations of the rating system which was not able to detect subtle changes in local vasculature which may have had a direct impact on hippocampal neurons. Alternatively, volume loss may have developed in neurons that lost inputs from cells that died as a result of spatially and temporally distant ischaemic lesions, which would be difficult to relate to hippocampal neuronal changes.

Neuronal volumes and densities were consistently most severely reduced in the MD group in all regions analysed, indicating that the presence of multiple disease processes exacerbated the mechanisms causing neuronal volume loss. These findings therefore suggest a possible mechanism through which coexistence of these pathologies can have an additive effect on cognitive decline (Snowdon *et al.*, 1997; Pasquier *et al.*, 1998). Furthermore, my findings of reduced neuronal volumes in different causes of dementia build on previous research which has found decreased neuronal volumes in the hippocampus in AIDS dementia and in the prefrontal cortex in late-life depression (Sá *et al.*, 2000; Khundakar *et al.*, 2009). Together, these studies suggest that reduced neuronal volumes are associated with cognitive dysfunction caused by various different disease aetiologies.

It was reassuring to find that ECV neuronal volumes were only reduced in MD and AD groups compared to controls, as this was consistent with the well-described involvement of the entorhinal cortex in AD (Schönheit *et al.*, 2004). The clear distinction between the disease groups studied confirmed the robustness of the 3D stereological technique as it clearly identified the differential vulnerability of different neurons within the hippocampal formation to AD and CVD processes.

3.5.3 Comparison with previous studies

CA1 neuronal volumes were 28.3% reduced in AD subjects compared to controls, which falls within the range of previous reports in AD (25% - 39%) (Rinne *et al.*, 1987; Riudavets *et al.*, 2007). Riudavets et al. found that CA1 neuronal volumes were only 9.8% reduced in MCI patients compared to controls, suggesting that the degree of

neuronal volume loss was related to severity of cognitive impairment, in agreement with the findings of negative relationships between CAMCOG scores and neuronal volumes in this study. Neuronal volumes in AIDS dementia subjects were found to be 31% reduced in CA3 and 30% reduced in CA1 compared to controls, without any neuron loss (Sá *et al.*, 2000). My results therefore provide further evidence that neuronal volume loss can occur in regions without neurodegeneration.

Only one previous study had investigated neuronal volumes in VaD using 3D stereological techniques prior to this study. Zarow et al. found a non-significant (6%) reduction in CA1 neuronal volume in AD compared to non-AD subjects, but no reduction in neuronal volume in VaD subjects (Zarow *et al.*, 2005). However they analysed only six VaD cases, compared to the 15 PSD and 22 PSND subjects in this project, which may have limited detection of statistically significant results. Furthermore, this study generally found greater differences in neuronal volumes between controls and dementia groups. This may have also contributed towards their finding of no relationship between neuronal volumes and cognitive function in AD, whereas I found neuronal volumes in the CogFAST subjects were positively correlated with CAMCOG scores. However, there was an average of 2 years between cognitive testing and death in the study by Zarow et al.; compared to just 7.6 months (±2SE = 1.7) in the CogFAST study, which meant CAMCOG scores from the CogFAST study were a more reliable indicator of cognitive status at death, and were more likely to relate to the observed neuronal changes.

Neuron density in the CA1 subfield was reduced in stroke survivors, VaD, MD and AD groups, in agreement with previous literature describing loss of CA1 neurons in AD and VaD (West *et al.*, 1994; Kril *et al.*, 2002b; Rössler *et al.*, 2002).

3.5.4 Limitations of neuronal volume and density measurements

Neuron density was used as a measure of neuron loss because tissue sections were only able to be taken from predefined paraffin-embedded blocks with a fixed starting point, which prevented the strict sampling procedure necessary to conduct Cavalieri calculations and estimate the total cell number within the whole hippocampus using the 'fractionator' method (Gundersen *et al.*, 1988). Density measures are based on the relationship between the numerator (the cell counts) and denominator (the

extracellular matrix), so the effect of differential tissue processing cannot be ruled out. However, all sections were processed and handled in a standardized manner allowing comparisons to be made between subjects.

Another possible factor confounding neuronal density results is the influence of tissue atrophy (Rössler *et al.*, 2002). All the dementia types studied are associated with MTL atrophy. Therefore, if tissue atrophy had influenced results by bringing surviving neurons closer together then my findings would have underestimated neuron loss. Despite these limitations, my results were consistent with the literature describing significant loss of CA1, but not CA2 neurons in VaD and AD (West *et al.*, 1994; Kril *et al.*, 2002b). Previous reports of neuron loss in AD have ranged from 12% to 86% (Rössler *et al.*, 2002). I found CA1 neuronal densities were 33% reduced in AD (17% reduced in both PSND and PSD subjects, 22% reduced in VaD, and 44% reduced in MD) which lies near the middle of this range.

A further potentially confounding variable was variation in the coronal level at which sections were cut. As hippocampal tissue is highly sought after, in some situations sections had to be taken from more posterior blocks nearer level 20-21 according to the Newcastle Brain Map. However, when neuronal density and volume were compared in control sections from level 18 and level 21, there was no indication of any relationship between neuronal measurements and coronal level. Further studies to investigate changes in neuronal volume and density throughout the hippocampus would be required to establish the influence of coronal level on neuronal density and volume in healthy controls.

3.5.5 Neuronal volumes in middle-aged and elderly controls

It was surprising not to find any differences in neuronal volumes between middle-aged and elderly controls. I had reasoned that pathological processes of ageing; such as accumulation of neurodegenerative and vascular disease pathology and hippocampal atrophy, would have resulted in reduced neuronal volumes with age. Additionally, age-associated neuronal atrophy had previously been reported in aged primates (Smith *et al.*, 1999). However, my study was limited as it only sampled a very small and quite variable group of 'younger' controls, ranging from 27 – 59 years old. To establish whether neuronal volumes are affected with increasing age would require a larger

study of subjects under 40 years old, ideally without any age-associated neurodegenerative pathology. It would be interesting to compare 'pathology free' and 'normal ageing pathology' cognitively normal controls at all ages, to explore whether age-associated pathology influences neuronal volumes. As elderly subjects can have significant Alzheimer's-type pathology without cognitive decline (Esiri *et al.*, 2001), one could postulate that these individuals would maintain neuronal volumes as a mechanism to maintain cognitive function.

3.5.6 Neuronal volumes were reversibly reduced in acute cerebral hypoperfusion

In the baboon model of acute cerebral hypoperfusion, CA1 and CA2 neuronal volumes were reduced from 1 – 14 days after the occlusion surgery, whereas 28 day neuronal volumes were similar to sham animals. This suggests that neuronal volumes were initially reduced in response to the hypoxic insult, but recovered normal neuronal volumes by 28 days. The relationship between the percentage of pyknotic neurons and neuronal volume suggested that the reduction in neuronal volume reflected a reversible pyknotic change, which was not surprising as one of the criteria for identifying pyknotic neurons was a shrunken cytoplasm. Interestingly, there did not appear to be any differences in neuronal volumes between the ipsi- and contra-lateral hemispheres, indicating that CA1 and CA2 neurons in both hemispheres were affected by cerebral hypoperfusion. There did not appear to be any significant loss of CA1 neurons within this time period.

Interpretation of these findings was limited due to the lack of statistical analysis and small numbers investigated. This model was also not a true model of stroke, so cannot be directly related to the long-term changes observed in the CogFAST cohort. Despite this, these results provide further evidence that cerebrovascular disease could cause neuronal volume loss, and indicate that hippocampal neuronal volume loss occurs as a reversible acute response to hypoxia. However, it is not known whether these volume changes were associated with cognitive decline, or whether there were long-term changes in neuronal volume or density.

3.6 Conclusions

These observations provide novel evidence that reduced hippocampal neuronal volumes in CA1-4 were associated with cognitive impairment in post-stroke survivors, and were likely to reflect mechanistic changes contributing to cognitive decline. As neuronal volumes were also reduced in CA subfields in AD, VaD and mixed dementia, this mechanism appears to be involved in cognitive decline in brain disorders with CVD and AD. Subjects with mixed dementia had greater neuronal volume and density loss, indicating that co-existence of both disease mechanisms exacerbated neuronal damage.

These results also suggest that reduced neuronal volume may be an important cellular substrate of hippocampal atrophy observed in neuroimaging studies of these disorders, occurring independently to or preceding neurodegeneration.

Chapter 4. Neurodegenerative Processes in Stroke Survivors

4.1 Introduction

The previous chapter described how reductions in hippocampal neuronal volumes were associated with dementia caused by CVD and AD, and that neuronal volumes were correlated with post-stroke cognitive function. As all dementia groups exhibited neuron loss and reduced neuronal volumes in the CA1 subfield this suggested that dysfunctional and degenerating neurons in this subfield contributed to cognitive impairment. Although no significant neuron loss was observed in CA2, CA3 or CA4 in dementia subjects, reduced neuronal volumes in these subfields were also associated with poorer cognitive function, suggesting that neuronal function in these regions was also impaired.

All the dementia subjects studied had CVD or AD which suggests that vascular or neurodegenerative disease mechanisms caused these neuronal changes. CA1 neuronal densities, and CA2, CA4 and ECV neuronal volumes were related to Braak stage and/or CERAD scores, indicating that the burden of AD pathology may have contributed to neurodegeneration and neuronal dysfunction in these subjects. However, these neuropathological ratings were derived from global assessment of the whole brain, and did not reflect subtle differences in local pathological burden within the hippocampus. Therefore, the next stage of this project aimed to further elucidate the role of neurodegenerative disease mechanisms in the hippocampus in causing neuronal volume and density changes and contributing to post-stroke cognitive decline.

4.1.1 Hippocampal Alzheimer's-type pathology

I reasoned that AD pathology may be related to neuronal volume loss through the pathogenic effects of Aβ and hyperphosphorylated tau on neuronal processes and synapses. Neuronal soma shrinkage is thought to reflect a loss of axo-dendritic arbour, as neuronal soma size is related to amount of cellular machinery needed to support the neuronal processes (Harrison and Eastwood, 2001). Both Aβ plaques and tau pathology are associated with damage to neuronal processes and synapse loss.

Therefore, the local burden of AD pathology may be related to neuronal soma volume loss and cognitive function in the hippocampus through damage to neuronal structural and functional connectivity.

Numerous studies have implicated Aβ in synaptic pathology in AD (Parihar and Brewer, 2010), and synapse loss is the best pathological correlate of cognitive decline in AD (Terry *et al.*, 1991). Soluble oligomers of Aβ have been shown to have a direct toxic effect at synapses (Walsh and Selkoe, 2007), however it is unclear whether Aβ deposits are responsible for synapse loss, or whether synaptic changes precede plaque formation (Parihar and Brewer, 2010). Under normal conditions, Aβ is thought to be released to provide negative feedback at excitatory synapses (Kamenetz *et al.*, 2003). Therefore, when levels of Aβ are chronically high in AD, synapses are depressed and synaptic plasticity is impaired. Studies of transgenic (APP) mouse models of AD have shown that Aβ plaques cause loss of spines and atrophy of nearby dendrites (Tsai *et al.*, 2004; Spires *et al.*, 2005). Therefore, greater burden of Aβ pathology in hippocampal parenchyma is likely to indicate damaged and disrupted neuronal processes, loss of synapses and impaired synaptic plasticity, which may be related to decreased neuronal soma volumes and neuronal dysfunction.

As 95% of abnormal tau pathology is found in neuropil threads or dystrophic neurites (Mitchell *et al.*, 2000), the burden of hyperphosphorylated tau pathology is directly related to damaged neuronal processes. The critical step in tau-mediated neurodegeneration is believed to be the initial disruption of the ability of tau to bind to and stabilize microtubules, which results in impaired axonal transport and increased cytosolic concentration of tau. High concentrations of cytosolic tau then stimulate misfolding and formation of tau aggregates (pretangles and paired helical filaments), which sequester normal tau and other proteins involved in stabilizing microtubules. This further exacerbates the disassembly of microtubules and leads to synapse loss and retrograde neurite degeneration (Alonso *et al.*, 1996; Ballatore *et al.*, 2007). Large aggregates form NFTs and neuropil threads (NTs) which also act as a physical obstruction to neuronal transport, further impairing neuronal function and leading to neuronal death. Therefore, the presence of greater numbers of tangles and threads in

the neuropil is a sign of greater damage to hippocampal neuronal circuitry, which is likely to be reflected in reduced neuronal volumes and neuron loss.

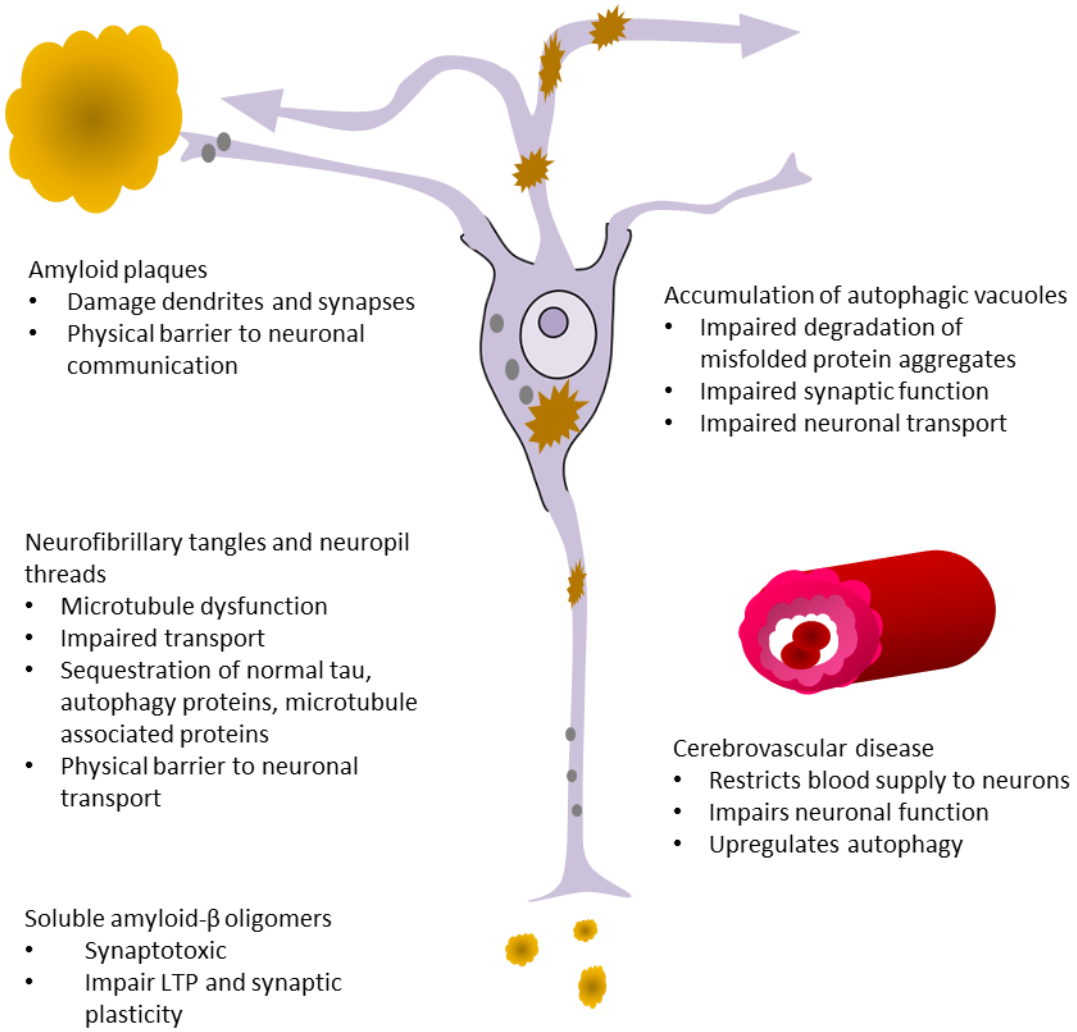

Figure 4.1. Diagram of the key mechanisms in cerebrovascular disease, Aβ and tau pathology relating to neuronal dysfunction and autophagy.

4.1.2 Dysfunctional autophagy in AD and CVD

Dysfunctional autophagy has been implicated in AD, ischemia and ageing, and autophagy has a role in maintaining neuronal function and morphology. Autophagy may influence neuronal soma volume through its role in regulating the morphology of neuronal processes and synapses (Xu *et al.*, 2012). For example, autophagy has been

shown to be involved in axonal remodelling under normal and excitotoxic conditions (Wang *et al.*, 2006). In healthy neurons, AVs form at synapses and carry proteins along neurites to be degraded in lysosomes in the soma. If the transport system becomes impaired, for example due to development of NTs and microtubule dissociation, this leads to swellings and build-up of AVs in axons and dendrites (Nixon, 2007). There is considerable evidence that AD is associated with deficiencies in autophagy, with AV build-up particularly evident in hippocampal neurons (Nixon and Yang, 2011). In AD subjects, accumulated autophagic markers have been shown to co-localise with tau-immunopositive dystrophic neurites and NFTs (Ma *et al.*, 2010). Therefore, accumulation of AVs in AD is thought to be due to impaired transport and clearance (Nixon, 2006; Nixon, 2007), indicative of defects in the autophagic pathway rather than upregulated autophagy. The pathological effect of accumulated of AVs in AD is exacerbated as AV membranes are thought to be a source of increased Aβ production (Yu *et al.*, 2005). Several mechanisms have been implicated in the cause of autophagic dysfunction and pathology in AD, including reduced levels of Beclin-1 (Pickford *et al.*, 2008), autophagy proteins being sequestered by abnormal protein aggregates, impaired trafficking and fusion with the lysosome, and impaired autophagolysosomal maturation (Levine and Kroemer, 2008).

Another protein which has been suggested to have a pathogenic role in autophagy dysfunction and Alzheimer's disease is P62, a regulatory protein involved in protein homeostasis (Salminen *et al.*, 2012). P62 binds directly to LC3 and can target organelles for autophagic degradation, and has a role in regulating the degradation of ubiquitinated tau (Ramesh Babu *et al.*, 2008). A recent study has shown that increased levels of LC3 and P62 in hippocampal neurons and neuronal processes were associated with memory impairments in aged mice (Soontornniyomkij *et al.*, 2012), providing further evidence for a relationship between autophagy dysfunction and neurodegeneration in ageing and cognitive decline. Studies also indicate that P62 has a role in synaptic plasticity, as P62 knock-out mice have significantly reduced levels of pre-synaptic protein synaptophysin, develop NFTs, and exhibit memory impairment after six months (Ramesh Babu *et al.*, 2008). Another study has shown that P62 is involved in surface translocation of receptors in hippocampal synaptic plasticity (Jiang

et al., 2009). However, it is not known whether the pathological involvement of P62 in autophagic and neuronal dysfunction is only related to AD processes, or whether it is also involved in pathogenesis of CVD-mediated neurodegeneration.

Autophagy in CVD

Although there have been numerous recent studies of autophagy in AD, there are fewer studies of autophagy in relation to CVD and no previous studies in post-stroke dementia. Despite the relative lack of studies of autophagy in CVD, there is growing evidence that autophagy is enhanced following cerebral ischemia, and is stimulated in response to energy deficits, hypoxia, endoplasmic reticulum stress and oxidative stress (Xu *et al.*, 2012). Cell culture studies have shown that cells lose mass by autophagy when subjected to prolonged glucose, oxygen and growth factor withdrawal, and then fully recover when they were returned to optimal conditions (Lum *et al.*, 2005; Levine and Kroemer, 2008). As CVD causes similar conditions by restricting blood supply to neurons, autophagy could be a mechanism contributing to reduced neuronal volume in dementia. A study using a rat two vessel occlusion (2-VO) model of transient forebrain ischemia found a pathological increase in autophagic vacuoles in hippocampal neurons after ischemia, and suggested that the resultant accumulation of proteins could be a possible cause multiple organelle damage and delayed neuronal death (Liu *et al.*, 2010). This suggests that hippocampal neurons are particularly susceptible to autophagic dysfunction in ischemia, and supports my hypothesis that autophagy may contribute to neuronal changes in stroke survivors and VaD. Autophagic dysfunction in hippocampal neurons during cerebral ischemia has also been reported in models of neonatal hypoxia-ischemia, where levels of LC3-II and Beclin-1 were increased (Zhu *et al.*, 2005; Carloni *et al.*, 2008; Xu *et al.*, 2012). Increased Beclin-1 was also reported in the penumbra of a rat MCAO model, although not all Beclin-1 upregulating cells also showed increases in LC3 (Rami *et al.*, 2008). However, interpretation of these results is difficult as it is unclear whether an increase or decrease in autophagy markers reflects mechanisms contributing to cell death or survival. Studies have suggested that the role of autophagy in neurodegeneration after ischemia is likely to depend on the brain region affected, maturity, severity of ischemia and timing of therapeutic interventions (Xu *et al.*, 2012).

4.2 Aims

This study compared the burden of amyloid-β and hyperphosphorylated tau pathology in the hippocampus of stroke survivors, controls, VaD and AD subjects, to determine whether AD processes were related to neuronal morphological and density changes in non-demented and demented stroke survivors, VaD, MD and AD subjects.

Although the role of autophagy dysfunction in AD is becoming well studied, fewer studies have investigated the role of autophagy in cerebrovascular disease. As autophagy is involved in regulating neuronal morphology, is implicated in ageing and the pathogenesis of AD, and is altered after ischemia, levels of autophagy proteins LC3, Beclin-1 and P62 were investigated to explore dysfunctional autophagy as a possible mechanism causing neuronal soma shrinkage and cognitive impairment in post-stroke dementia. This study compared changes to CA1 and CA2 neurons as they are differentially vulnerable to neurodegenerative disease processes.

4.3 Materials and methods

4.3.1 IHC and image analysis

Immunohistochemical staining for AT8, 4G8, LC3, Beclin-1 and P62 was carried out according to the protocol described in section 2.6 (Table 2.3). The antibody to LC3 recognised both LC3-I and LC3-II. Image analysis of LC3, Beclin-1 and P62 immunostaining was carried out using Image Pro as described in section 2.7.2 (page 48), generating values for percent per area (%PA) stained and mean integrated optical density (IOD, stain intensity). Images were taken at 10X magnification with a numerical aperture 0.3. Six images of the CA1 were taken where possible, evenly distributed across the proximal-distal axis. The whole CA2 subfield was imaged.

4.3.2 Semi-quantitative rating of hippocampal Aβ pathology

A parallel study had previously quantified burden of hippocampal AD pathology in CogFAST subjects using image analysis techniques (unpublished data). Therefore, I used established semi-quantitative methods to quickly rate hippocampal AD pathological burden.

The burden of Aβ pathology was rated in sections stained using the 4G8 antibody, using a 0-4 scoring system described by (Thal *et al.*, 2006) (Figure 4.2 A). This method involved rating and characterising the development of Aβ in the MTL, which mirrors the development of Aβ pathology throughout the brain (Thal *et al.*, 2006). This system took into account the type of amyloid pathology, location and total amount of Aβ:

- Neuritic plaques were rated in layers III and V of the neocortex, the EC, pyramidal layers of the hippocampus and subiculum, and molecular layer of the dentate gyrus.
- Fleecy amyloid was rated in the inner layers of the EC, the CA1 and subiculum.
- Band-like amyloid was rated in the subpial temporal and entorhinal molecular layers.

Whilst applying these criteria it became clear that within each phase, particularly 3 and 4, there was a great deal of variation in the burden of Aβ deposition. Therefore, I further sub-divided each phase to generate an intuitive 12 stage rating system, allowing more sensitive detection of differences between cases whilst maintaining quick and easy rating of pathology (Figure 4.2 B). Representative images of Aβ pathology at each stage are shown in Figure 4.3...

4.3.3 Semi-quantitative rating of hippocampal tau pathology

Hyperphosphorylated tau pathology was semi-quantitatively rated in sections stained for AT8 using criteria described in (Lace *et al.*, 2009) (**Error! Reference source not found.**). Ratings were based on a 0-3 scale (none, mild, moderate, severe) in the DG, CA4, CA3, CA2, CA1, subiculum, EC and transentorhinal cortex, taking into account:

- Tau positive neuropil threads
- Tau positive neurons (tangles and pretangles)
- Neuritic plaques
- White matter neuropil threads

4.3.4 Statistical analyses

Ordinal data (AD pathology ratings) were compared using Mann-Whitney U test and Spearman's rank correlation. LC3 and Beclin-1 data were normally distributed whereas

P62 data did not follow a normal distribution. Data were therefore analysed using parametric and non-parametric tests as described in section 2.10 (page 61).

Thal Stage	Modified Thal Stage	Amyloid deposits in:
1	1	Temporal cortex
2	2	EC (fleecy in inner layers) and subiculum
	3	CA1 and more in subiculum & EC
3	4	Increasing density of deposits in:
	5	• Molecular layer of DG
	6	• White matter
	7	• CA1 to temporal cortex
4	8	Increasing density of deposits in:
	9	• CA4
	10	• White matter
	11	• EC

Figure 4.2 Thal staging (Thal *et al.*, 2006) of amyloid β and criteria for modified Thal Stages. EC = entorhinal cortex, DG = dentate gyrus.

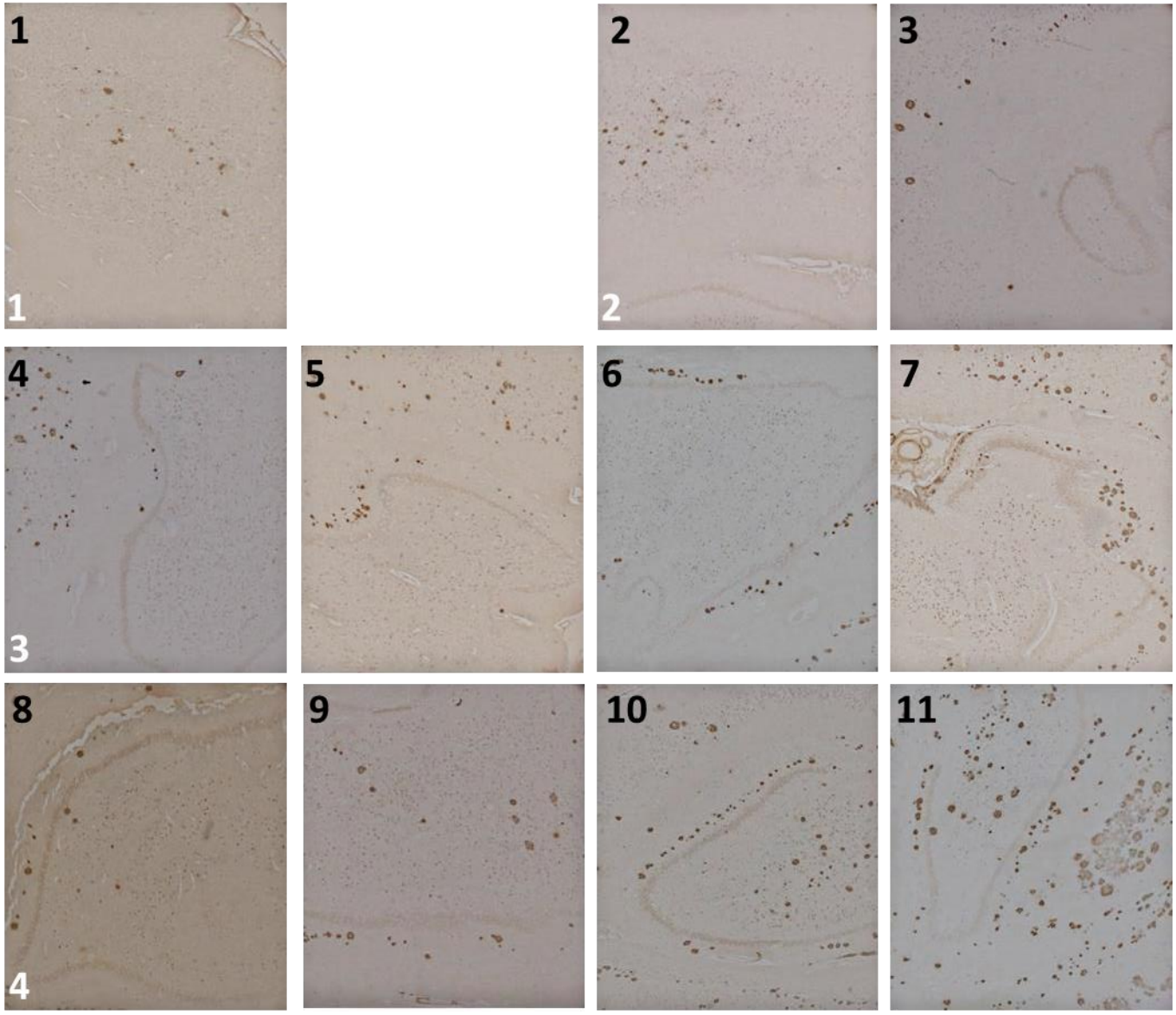

Figure 4.3. Representative images of hippocampal Aβ pathology stained using 4G8, taken at 2.5x magnification. Thal stages are numbered 1-4 in white, modified Thal stages are numbered 1-11 in black.

4.4 Results

4.4.1 AD pathology

Demographics of subjects analysed are shown in Table 4.1. Fixation length was significantly different between groups [F = 2.96 (5, 66) p = 0.018], and the MD group had longer fixation length than PSD (p = 0.015). There were no correlations between AD pathological burden and age, PMD or fixation length.

Group	n	Age, years (range)	PMD, hours (range)	Fixation, weeks (range)
Controls	11	80.1 (72-91)	21.3 (14-24)	14 (8-20)
PSND	22	83.5 (78-94)	48.3 (24-96)	11.3 (2-32)
PSD	13	87.3 (80-98)	45.4 (10-96)	7.2 (4-12)
VaD	16	86.9 (76-97)	43.3 (24-63)	9.1 (4-16)
MD	13	85.9 (72-94)	43.3 (24-63)	16.6 (3-40)
AD	13	83.3 (70-91)	56 (24-72)	9 (6-20)

Table 4.1 Demographics of subjects studied for Aβ and tau pathology. Slightly fewer subjects were analysed for tau pathology (Controls n = 10, PSND n = 19, PSD n = 10, VaD n = 13, MD n = 13, AD n = 11).

AD and mixed dementia groups had greater pathological burden of Aβ and tau than all other groups using Thal staging, modified Thal staging and Tau staging ($p < 0.05$). Tau pathological burden was not different between PSND and PSD groups, and they were not different to elderly controls or VaD. However, it was interesting to find that the PSD group had significantly lower Aβ burden than PSND subjects and controls (Figure 4.4). Frequency tables for rating of amyloid and tau pathology are presented in Appendix Table 8.6.

The different methods used to quantify the burden Aβ and tau pathology were highly correlated (Table 4.2). There were no correlations between AD pathological burden and CAMCOG scores, age, PMD or fixation length.

Modified Thal staging of Aβ pathology was negatively correlated with CA1 neuron density (r = -0.607, p = 0.005) and ECV neuron volume (r = -0.55, p = 0.018). There

were trends to negative correlations between Thal stage and CA1 neuron density (r = -0.419, p = 0.083) and CA4 neuron density (r = -0.434, p = 0.07). Tau stage was weakly negatively correlated with CA1 neuron density (r = -0.325, p = 0.007), and neuron volume in CA4 (r = -0.36, p = 0.011), CA2 (r = -0.339, p = 0.007) and ECV (r = - 0.496, p = 0.002).

		Lace Stage (tau)	Thal Stage (Aβ)	Modified Thal Stage (Aβ)	Braak Stage (tau)
Thal Stage	R	.607			
	P	.028	NA		
Modified Thal	R	.702	.903		
	P	.005	<.001	NA	
Braak Stage	R	.872	.770	.797	
	P	<.001	<.001	<.001	NA
CERAD score	R	.664	.813	.873	.702
	p	.013	<.001	<.001	<.001

Table 4.2. Correlations between different methods used to rate Alzheimer type pathology. Pale blue indicates p < 0.05, dark blue indicates p < 0.01.

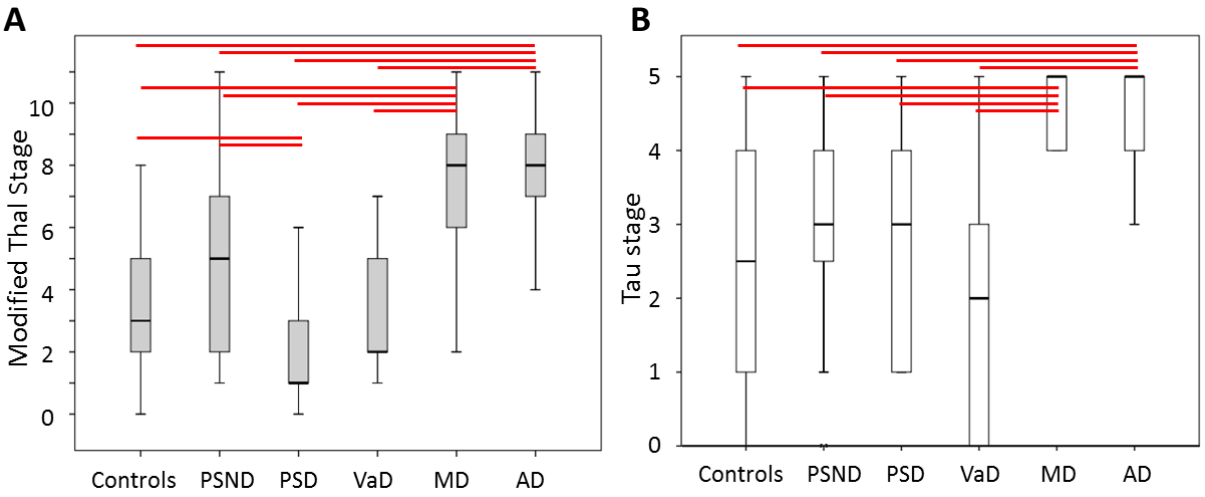

Figure 4.4. Box plots of semi-quantitative ratings of Aβ (A) and hyperphosphorylated tau staining (B) in the CA1. Red lines show differences between groups (Mann-Whitney U test p<0.05).

PSD subjects pathologically classified as 'mixed dementia' had modified Thal stages between 1-6 (1, 3, 4, 4, 6), whereas PSD subjects classified as 'VaD' were between 0-2

(0, 0, 1, 1, 1, 1, 2, 2). The MD group generally had much higher modified Thal stages than the PSD 'MD' (2, 5, 6, 6, 7, 8, 8, 9 9, 9, 11, 11, 11), indicating that the PSD MD subjects did not have equivalent levels of amyloid deposition in the hippocampus as the stroke-free MD subjects.

It was also interesting to observe that Braak staging did not always reflect burden of hippocampal tau pathology, demonstrated in Figure 4.5 where a PSND subject with Braak stage 1 had greater number of tau immunopositive neurons and neurites than a PSND subject with Braak stage 5.

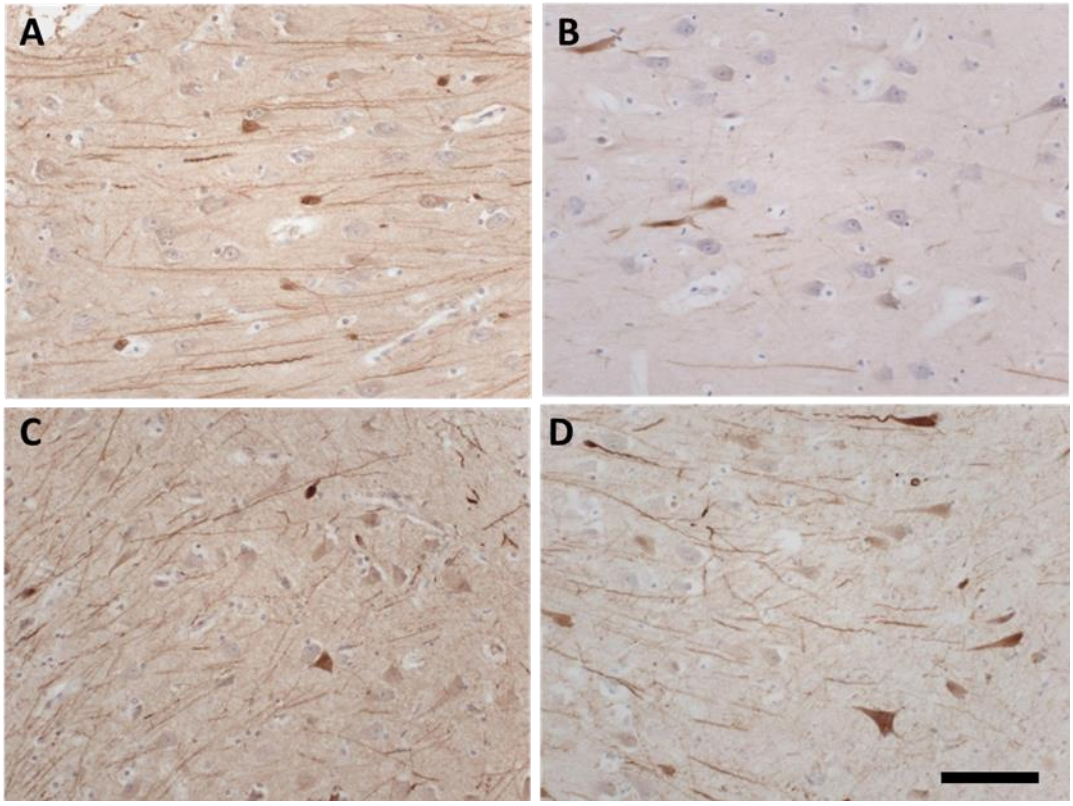

Figure 4.5. Representative images demonstrating the variability of AT8-positive staining in the CA1 in subjects with different Braak scores. A = PSND, Braak stage 1; B = PSND, Braak stage 5, C = PSD, Braak stage 3; D = AD, Braak stage =6.Scale bar = 50um.

4.4.2 Autophagy markers

Group demographics for subjects analysed using LC3 and Beclin-1 are shown in Table 4.3, and P62 in Table 4.4. There were no significant differences in age, PMD or fixation length between groups studied for LC3, Beclin-1 or P62 analysis.

Group	n	Age, years Mean (range)	PMD, hours Mean (range)	Fixation, weeks Mean (range)
Controls	8	82.4 (74-94)	34 (15-67)	9 (1-16)
PSND	8	83.1 (78-89)	32 (11-48)	3(2-5)
PSD	8	84 (80-89)	47 (10-81)	3 (2-5)
AD	6	81 (70-91)	35 (6-72)	8 (5-20)

Table 4.3 Demographics of subjects investigated using LC3 and Beclin-1.

Group	n	Age, years Mean (range)	PMD, hours Mean (range)	Fixation, weeks Mean (range)
Controls	6	82.4 (74-94)	34 (15-67)	10 (6-16)
PSND	6	83.4 (78-89)	37 (11-76)	9 (3-20)
PSD	10	84.1 (76-93)	42 (10-81)	9 (2-26)
AD	7	82.4 (70-91)	40 (6-72)	9 (6-20)

Table 4.4. Demographics of subjects investigated using P62.

There were no significant differences in LC3 or Beclin-1 %PA or IOD between groups in CA1 or CA2 (Figure 4.6 A and B). Numerical values of mean IOD and %PA are presented in Appendix Table 8.7. P62 CA1 %PA was significantly different across all groups [H (3) = 7.934, p = 0.047] (Figure 4.6 C). The AD group had significantly greater P62 CA1 %PA than controls (p = 0.012) and trends to greater %PA compared to PSND (p = 0.081) and PSD (p = 0.094). However, when one outlier in the AD group was removed, these differences were no longer significant (p = 0.093). CA2 P62 mean IOD was also significantly different across all groups [H (3) = 5.04, p = 0.007]. AD had significantly greater CA2 IOD than PSND and PSD (p = 0.021 and p = 0.007 respectively). When the PSD group was divided based upon pathological diagnosis, there was a trend to PSD (MD) subjects having higher CA2 mean IOD than PSD (VaD) (p = 0.072).

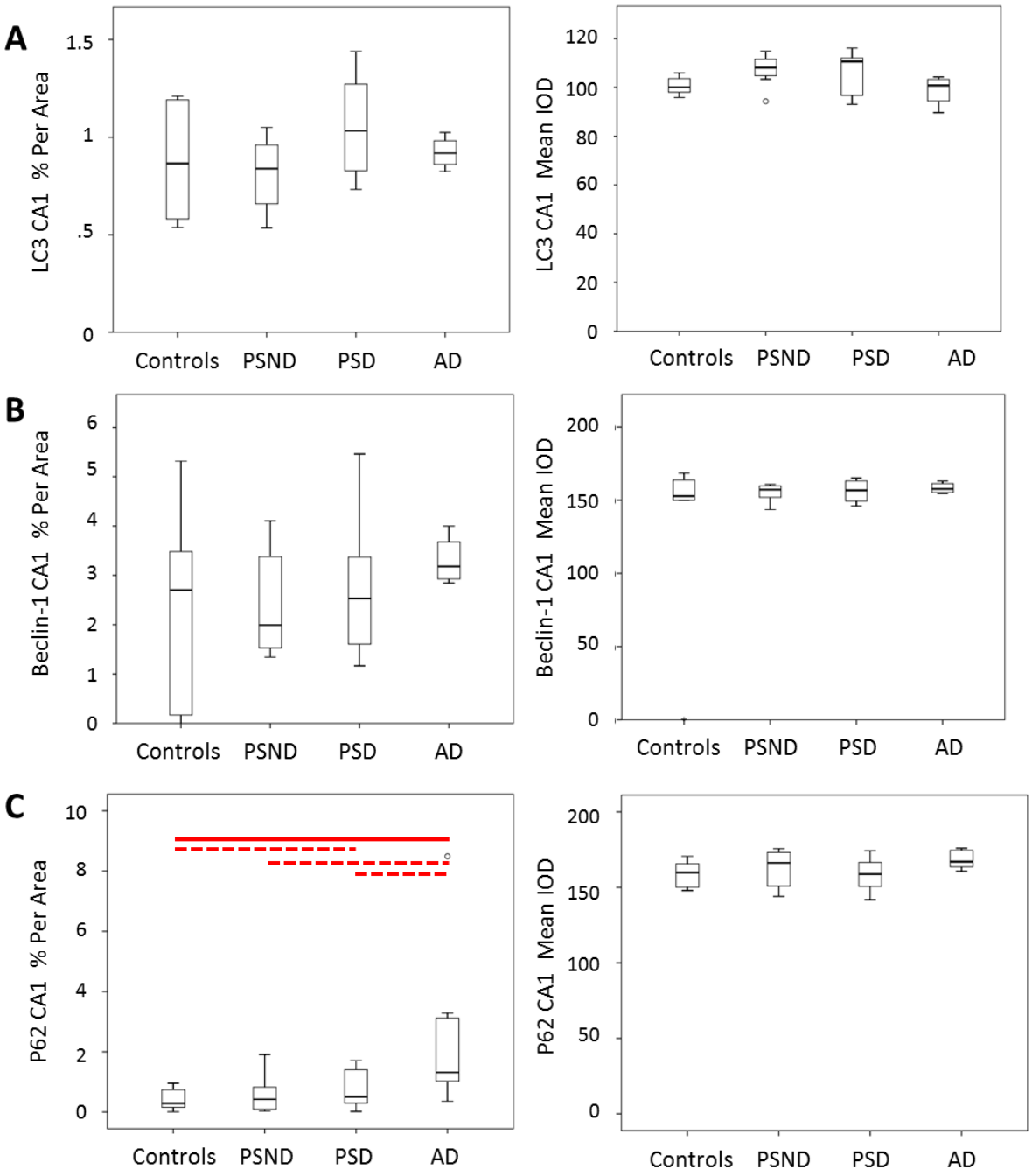

Figure 4.6. Box plots showing CA1 % Per Area and Mean IOD results for A, LC3; B, Beclin-1; C, P62. Red lines indicate significant differences $p < 0.05$, dashed lines indicated $p < 0.1$.

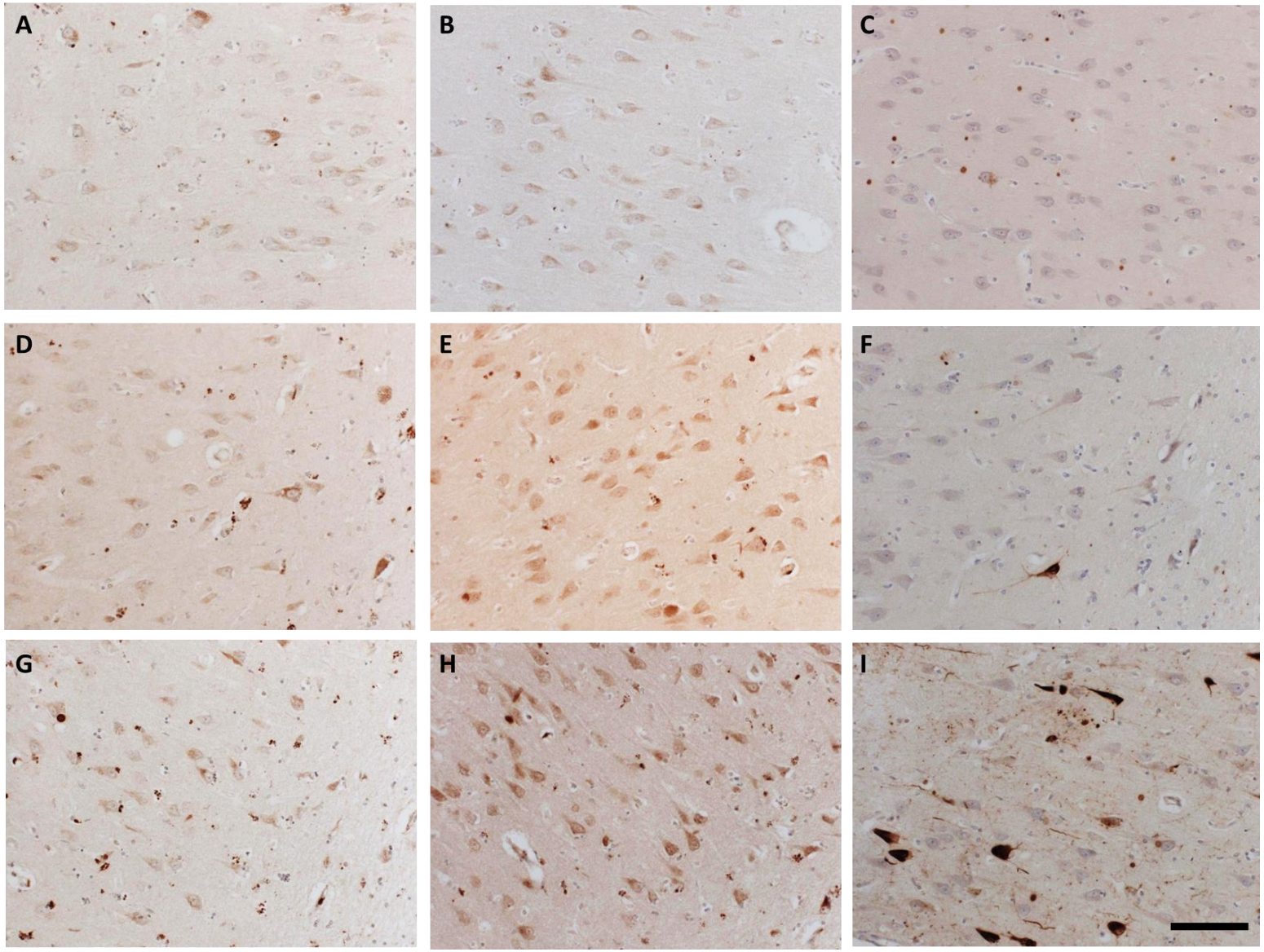

Figure 4.7
Representative images of CA1 stained for LC3 (A, D, G), Beclin-1 (B, E, H) and P62 (C, F, I) in PSND (A, B, C) PSD (D, E, F) and AD (G, H, I). Bar = 50µm

4.4.3 Correlations between autophagy markers

Correlations between the three autophagy proteins were investigated as I hypothesised that subjects with dysfunctional autophagy would have accumulation of all three markers. There were strong positive correlations between CA1 and CA2 LC3 %PA and IOD measurements, which remained significant after correction for multiple testing. Beclin-1 IOD in CA1 and CA2 also remained significantly correlated after adjustment. P62 staining was less well correlated with the markers of autophagy, and not well correlated between and within subfields (Table 1.1 Comparison of the development and distribution of Amyloid-β and tau pathology in AD. * = from (Thal *et al.*, 2002), ** = from (Braak and Braak, 1991).

).

			LC3				Beclin-1				P62			
Spearman's Rho			CA1 %PA	CA1 IOD	CA2 %PA	CA2 IOD	CA1 %PA	CA1 IOD	CA2 %PA	CA2 IOD	CA1 %PA	CA1 IOD	CA2 %PA	CA2 IOD
LC3	CA1 %PA	R	NA											
		p												
	CA1 IOD	R	.107	NA										
		p	.603											
	CA2 %PA	R	.593	-.337	NA									
		p	.002	.107										
	CA2 IOD	R	-.282	.715	-.710	NA								
		p	.182	.00001	.0004									
Beclin -1	CA1 %PA	R	.545	.050	.426	-.205	NA							
		p	.004	.810	.038	.336								
	CA1 IOD	R	.510	-.228	.346	-.257	.583	NA						
		p	.008	.263	.098	.225	.002							
	CA2 %PA	R	.200	-.047	.209	-.075	.405	.504	NA					
		p	.349	.828	.328	.728	.049	.012						
	CA2 IOD	R	.332	-.359	.393	-.398	.357	.777	.576	NA				
		p	.113	.085	.057	.054	.087	<.00001	.003					
P62	CA1 %PA	R	-.129	-.215	-.144	-.257	.003	.278	.132	.499	NA			
		p	.549	.314	.523	.248	.990	.188	.559	.018				
	CA1 IOD	R	.389	-.046	.381	-.004	.345	.201	-.048	-.042	-.155	NA		
		p	.060	.832	.080	.986	.099	.345	.832	.853	.469			
	CA2 %PA	R	-.249	-.271	-.052	-.088	-.326	.142	-.027	.197	.503	-.081	NA	
		p	.276	.234	.823	.703	.149	.540	.907	.391	.020	.726		
	CA2 IOD	R	.271	-.166	.187	-.192	.452	.251	.278	.395	.213	.331	-.383	NA
		p	.234	.471	.417	.404	.040	.273	.223	.077	.354	.142	.086	

Table 4.5. Correlations between LC3, Beclin-1 and P62 image analysis results. Light grey highlights correlations significant at $p < 0.05$. Dark grey highlight correlations that remained significant after correcting for multiple testing ($p < 0.00074$).

4.4.4 Clinicopathological correlations

P62 CA1 IOD was negatively correlated with modified Thal score (r = -0.651, p = 0.03) and there was a trend to a positive correlation with Tau stage (Lace) (r = 0.581, p = 0.078). When the outlier in the AD group was removed, P62 CA1 IOD was positively correlated with Tau stage (r = 0.621, p = 0.006) and CERAD score (r = 0.513, p = 0.004). P62 CA2 IOD was correlated with Braak stage (r = 0.496, p = 0.022), and there were trends to significant correlations with CERAD score (r = 0.418, p = 0.067), and modified Thal score (r = 0.639, p = 0.064). LC3 CA2 IOD was negatively correlated with CERAD score (r = -0.444, p = 0.038), and modified Thal score (r = -0.651, p = 0.03) and there was a trend to negative correlation with tau stage (r = -0.589, p = 0.073). There were no correlations between Beclin-1 and AD pathology.

Global vascular pathology scores were negatively correlated with Beclin-1 CA1 IOD (r = -0.849, p = 0.004) and there was a trend with P62 CA2 %PA (r = -0.721, p = 0.068). LC3 CA1 IOD was positively correlated with vascular pathology scores (r = 0.689, p = 0.04).

CAMCOG scores were negatively correlated with LC3 CA1 IOD (r = -0.715, p = 0.03) and memory scores were negatively correlated with LC3 CA1 %PA (r = -0.528, p = 0.052), and there was a trend with P62 CA1 IOD (r = -0.621, 0 = 0.074). There were no correlations between autophagy markers and age or fixation, however PMD was positively correlated with LC3 IOD in CA1 and CA2 (r = 0.398, p = 0.044 and r = 0.569, p = 0.004 respectively).

4.5 Discussion

4.5.1 Hippocampal AD pathology

As expected, hippocampal Alzheimer's pathological burden was highest in the AD and MD groups. However, it was surprising to find that the PSD group had significantly lower amyloid-β pathology than PSND and control groups, and that amyloid-β and tau pathology were not related to post-stroke cognitive impairment. This may be because stroke survivors with significant pre-existing AD pathology were less likely to be included in the CogFAST study, as they were less likely to recover full cognitive function after stroke. The higher mean amyloid burden in PSND group may reflect better

recovery or compensatory mechanisms in response to the ischaemic insult and AD processes, which was also reflected in greater neuronal volumes.

The use of the modified Thal staging of Aβ pathology allowed identification of further relationships between Alzheimer's type lesions and neuronal volume and CA1 neuronal density changes. A parallel study recently quantified Aβ pathology within hippocampal subfields using image analysis techniques, and also found that the PSND group had greater Aβ pathology than PSD group (unpublished results). This therefore validated the modified Thal staging system as a quick and easy rating scale sensitive enough to detect subtle differences in hippocampal pathology between subjects, unlike the simpler four-stage Thal or CERAD scores.

It was interesting to find that the PSD subjects pathologically diagnosed as MD did not have as great Aβ pathology as the stroke-free MD group using the modified Thal scores. Again, this may be because stroke survivors with severe pre-existing AD pathology were unlikely to have recovered normal cognitive function after the additional insult of ischaemic stroke. Furthermore, AD processes are insidious and develop over many years. If AD processes were triggered by ischemia, yet the mean survival time post-stroke was 6.72 years (Allan *et al.*, 2011), this may not have been long enough to develop late-stage AD pathology in the hippocampus.

There were no differences in the burden of tau pathology between post-stroke, VaD or control subjects, although tau stage was related to CA1 neuronal density and neuronal volumes in CA2, CA4 and ECV. Therefore, Lace et al.'s method of rating hippocampal tau burden was successful in identifying relationships between neuronal densities and volumes with AD pathology. The finding that tau pathology, but not amyloid burden, was related to CA1 neuron density was in agreement with previous literature relating tau pathology and CA1 neuronal death (Gómez-Isla *et al.*, 1997). The finding that greater tau burden was associated with reduced neuronal volumes may reflect tau-mediated degeneration of neurites in support of the hypothesis that reduced neuronal soma volume reflects reductions in axo-dendritic arbour.

All methods of rating AD pathological burden were positively correlated, confirming consistent rating of lesion burden and supporting current understanding of the relationship between development of tau and Aβ pathology through the brain in AD. However, it was interesting to find several subjects where the burden of hippocampal tau pathology was not directly related to the overall tau pathology burden according to Braak stages (Figure 4.5).This supports the importance of determining local burden of Alzheimer's type pathology in relation to local neuronal changes, and may indicate that those subjects had a different pattern of development of tau pathology across the brain.

Taken together, these results suggested that Alzheimer type pathology was not the most important factor contributing to post-stroke cognitive decline and hippocampal dysfunction in this cohort, as the PSND subjects had a greater burden of Aβ pathology than PSD subjects, and there was no difference in severity of tau pathology. This also provides further evidence in support of the discrepancies between Aβ pathology and cognition (Terry *et al.*, 1991; Braak and Braak, 1996). The finding that tau pathology was correlated with CA1 neuron loss and CA2/3/4 neuronal volumes suggests a potential role for tau-mediated neurodegeneration as a mechanism causing neuronal volume loss in post-stroke and ageing-related dementia.

4.5.2 Autophagy markers

There were no differences in LC3 or Beclin-1 %PA or mean IOD in CA1 or CA2 between any of the groups studied. This was surprising as levels of autophagy markers had previously been shown to accumulate in AD (Nixon, 2007; Ma *et al.*, 2010). However, ageing, AD and hypoxic/ischaemic may stimulate differing autophagic responses or dysfunction, for example ageing is associated with decreased autophagy proteins, while early AD (but not late AD) is associated with an increase, and hypoxic response is associated with upregulated autophagy. Therefore, in this group of elderly subjects with mixed pathologies, the net effect may be difficult to relate to one degenerative process.

This complexity was reflected in the conflicting clinicopathological correlations with LC3 and Beclin-1. CA2 LC3 IOD was inversely associated with AD pathological burden,

in agreement with previous studies demonstrating that the accumulation of autophagic markers is highest earlier in AD (Ma *et al.*, 2010). However, Beclin-1 levels were not associated with AD pathology, and there were conflicting correlations between LC3 and Beclin-1 levels and global CVD burden; increased LC3 CA1 IOD but decreased Beclin-1 CA1 IOD were associated with greater burden of CVD lesions. Furthermore, there were surprisingly few correlations between autophagy markers, as I had hypothesised that dysfunctional autophagy would result in increased levels of all autophagy markers. This suggests that there may have been differential effects at different stages of the autophagy pathway. As LC3 and Beclin-1 are involved in the early stages of autophagy, it remains unclear whether autophagy was upregulated or impaired in relation to CVD processes in these dementia subjects. Furthermore, the correlations between LC3 IOD and PMD suggests that LC3 may have had been affected during cell death processes, which should be taken into consideration when attempting to draw conclusions from these results.

An additional factor that made these results difficult to interpret was the loss of neurons in CA1. As subjects in the disease groups had significantly reduced CA1 neuronal density, autophagy marker %PA measurements could appear reduced even if they were actually present in a high proportion of the surviving neurons. A previous study has suggested that autophagy markers build up in neurons targeted for neurodegeneration (Ma *et al.*, 2010), implying that surviving neurons have non-impaired autophagy and therefore low levels of autophagy markers. This may be one reason why few differences or correlations were found with %PA results, as neurons with pathological autophagy dysfunction may have already been lost.

P62 levels were related to AD pathology but not cerebrovascular disease. The AD group had greater P62 %PA in CA1 and IOD in CA2 than the other groups studied, and P62 levels were related tau stages, modified Thal scores and CERAD scores in the CA1 and CA2. However, greater burden of Aβ pathology was associated with more intense P62 staining in CA2, but less intense P62 staining in CA1. This apparent disparity may be due to more severe AD pathology causing neurodegeneration in CA1 but not CA2. Greater burden of AD processes would result in loss of severely impaired neurons in CA1 and therefore loss of intense P62 staining, whereas CA2 neurons appear to resist neurodegeneration, despite development of intracellular NFT and P62 aggregates.

PSD cases pathologically diagnosed as MD had greater P62 IOD than PSD-VaD subjects. Together with the finding of greater intensity of P62 staining in AD subjects this support previous studies which have found that P62 is robustly present in tau aggregates (Kuusisto *et al.*, 2002; Salminen *et al.*, 2012). Although in most subjects P62 staining was restricted to intense cytoplasmic staining, some AD cases also had thread-like positive staining in the neuropil (Appendix Figure 8.3). Furthermore, some subjects had darkly stained extracellular circular structures similar to those seen in argyrophilic grain disease (Scott and Lowe, 2007). This wasn't limited to cases with AD or mixed dementia, as it was also observed in two controls (Braak 3 and 2), one PSND (Braak 1), and three PSD subjects (two MD and one VaD), suggesting different disease mechanisms may also be involved in these subjects.

4.6 Conclusions

These results suggest that Alzheimer's type pathology was not the most important disease mechanism contributing to post-stroke cognitive decline in this cohort, as although there were no differences in tau pathology burden, PSND subjects had greater Aβ pathology than PSD. Investigation of autophagy as a potential mechanism relating disease pathology to neuronal volume and density changes yielded contradictory results that were difficult to interpret. In agreement with previous studies, LC3 was higher in early stages of AD, however the relationship between LC3, Beclin-1 and vascular lesions appears to be complex. P62 was associated with AD pathology, but not necessarily related to markers of autophagy LC3 or Beclin-1. Determining the role of autophagy in CVD will require strictly controlled experiments without effects of other neurodegenerative or cellular stress mechanisms such as post-mortem delay which may influence up- or down-regulation of autophagy markers.

Chapter 5. Hippocampal Dendritic Changes in Post-Stroke and Ageing-Related Dementias

5.1 Introduction

Neuronal soma volume is thought to reflect the amount of cellular machinery needed to support the axonal and dendritic arbour (Harrison and Eastwood, 2001). I therefore hypothesised that the observed decreases in neuronal soma volumes in post-stroke and ageing related dementia were associated with a loss of or reduced complexity of dendritic arbour. Other studies have previously suggested that reduced neuronal soma volume is related to dendrite loss and tissue atrophy even without neuron loss (Selemon and Goldman-Rakic, 1999). This 'reduced neuropil hypothesis' proposed that cortical tissue atrophy in schizophrenia was caused by shrinkage of neuronal soma volumes and interneuronal space, as studies had reported neuronal soma volume loss (Rajkowska *et al.*, 1998) and dendritic spine loss in association with thinning of the prefrontal cortex (Selemon and Goldman-Rakic, 1999). As PSD subjects in the CogFAST study were found to have greater MTL atrophy and smaller hippocampal neuronal volumes than PSND (Firbank *et al.*, 2007), I reasoned that dendritic arbour and synapse loss may have contributed to neuronal volume reductions and cognitive impairment after stroke.

5.1.1 Dendrites and dendritic spines

Dendrites are the major site of neuronal excitatory inputs and make thousands of dynamic connections with other neurons. Dendrites of hippocampal pyramidal neurons contain numerous characteristic small protrusions called dendritic spines, which are the sites of excitatory synapses with passing axons **Error! Reference source not found.**(Harris *et al.*, 1992). Dendritic spines are typically characterized by a mushroom shape, with a fine neck and bulbous head which contains the post-synaptic sites of excitatory synapses (Harris, 1999). The number and morphology of dendritic spines is related to afferent activity (Jia *et al.*, 2012), and reflects the stability and strength of responses (Holtmaat *et al.*, 2006). This structural plasticity of dendritic spines therefore mirrors synapse function and plasticity, where long term potentiation is associated with spine enlargement and long-term depression with spine shrinkage

(Kasai *et al.*, 2010). It is now widely believed that dynamic changes in spine density, size and strength form the biological bass of learning and memory in the brain (Spronsen and Hoogenraad, 2010).

As the size, extent and branching patters of dendrites directly influences the number and function of synapses, it is unsurprising that human and animal studies have found that dendritic alterations are important pathological features contributing to cognitive dysfunction and dementia (Cotter *et al.*, 2000; Penzes *et al.*, 2011). Indeed, dysfunctional neuronal communication has been suggested to be the underlying cause of many psychiatric and neurological diseases (Selkoe, 2002; Spronsen and Hoogenraad, 2010). This theory has been supported by numerous reports of disruptions to spine size, shape and number in disorders associated with deficits in information processing (Penzes *et al.*, 2011). However, dendrites and dendritic spines are highly dynamic which presents particular challenges to studying them in post-mortem tissue.

5.1.2 Techniques used to study dendrite morphology: Golgi staining

The Golgi method remains the preferred method for visualizing the fine structure of dendrites and dendritic spines (Golgi, 1873). The Golgi method is now broadly used to describe a group of techniques based on the original silver impregnation method. These techniques use potassium dichromate in the first step of impregnation, then tissue is immersed in silver nitrate and fine crystals of silver chromate are formed within the tissue, resulting in dark brown/black staining of <5% of neurons **Error! Reference source not found.**(Rosoklija *et al.*, 2003). This technique allows unique visualisation of the profile of the entire dendritic arbour and dendritic spine morphology in fixed tissue, and has been a vital tool in our understanding of dendrites in health and dendritic changes in disease. However, the chemical basis of Golgi staining remains poorly understood, raising concerns about the capricious and inconsistent staining results, and the apparently random selective staining of only ~5% of neurons (Špaček, 1989). These inconsistencies have been suggested to be due to factors affecting Golgi impregnation such as pre-mortem agonal state (Flood, 1993) or post-mortem delay (Buell, 1982).

Studies aspiring to use Golgi staining in human post-mortem studies are limited by the availability of entire blocks of appropriate tissue which has been briefly fixed but not paraffin-embedded. Sufficient quantities of appropriate tissue are therefore scarce in brain bank settings where tissue is stored for long periods of time, although recent advances have been made in using Golgi techniques in thin tissue sections rather than whole blocks (Levine *et al.*, 2013). However, hippocampal tissue from the CogFAST cohort was stored frozen or in paraffin-embedded blocks and was therefore inappropriate for a Golgi study of dendritic changes in delayed PSD. Therefore, alternative methods to investigate dendrites and dendritic spines were explored.

5.1.3 Techniques used to study dendrite morphology: MAP2 IHC

Immunohistochemical staining for the dendritic protein microtubule-associated protein 2 (MAP2) allows visualization of dendrites in paraffin-embedded tissue for morphological and quantitative investigation. Microtubule associated proteins (MAPs) are a major group of cytoskeletal proteins involved in regulating neuronal morphology, of which MAP2 is the most abundant in the brain. MAP2 has a critical role in regulating the structure and function of dendrites, as it stabilizes dendritic microtubules by forming cross-bridges between microtubules and other cytoskeletal components (Yanagihara *et al.*, 1990; Conde and Cáceres, 2009). MAP2 therefore has an important role in determining the number, stability and location of synapses, and MAP2 expression has been shown to be related to dendritic outgrowth, branching and remodelling (Liu *et al.*, 2005). Changes to MAP2 have been suggested to underlie pathological alterations in neuronal morphology (Cotter *et al.*, 2000), as degraded or dysfunctional MAP2 would result in impaired interactions between cytoskeletal proteins, leading to microtubule disassembly and degradation of dendrites (Liu *et al.*, 2005).

5.1.4 Dendritic changes after ischemia

Studies have reported a reduction in hippocampal MAP2 immunoreactivity in human and animal models of hypoxia; including after transient global ischemia caused by cardiac arrest in patients (Akulinin and Dahlstrom, 2003), in a gerbil model of transient cerebral ischemia (Kitagawa *et al.*, 1989; Yanagihara *et al.*, 1990; Yoshimi *et al.*, 1991), and in a two-vessel occlusion (2-VO) rat model, where reduced hippocampal MAP2

mRNA and protein levels were also related to spatial memory impairments (Liu *et al.*, 2005). Rapid loss of MAP2 immunoreactivity has also been reported in damaged brain areas following hypoxia and ischemia in rodent models of stroke (Zhang *et al.*, 1999; Kitano *et al.*, 2004), and in an in vitro model of acute transient focal ischemia (Pastori *et al.*, 2007).

MAP2 is known to be particularly vulnerable in ischaemic injury, which indicates that dendrites are particularly susceptible to ischaemic damage (Yan *et al.*, 2013). The vulnerability of dendrites to ischaemic injury has been suggested to be related to excitotoxic increases in intracellular calcium concentration, which activates calcium-dependent proteases which degrade MAP2, leading to a rapid disassembly of microtubules (Yanagihara *et al.*, 1990). However, some evidence suggests the acute loss of MAP2 immunoreactivity in dendrites after hypoxia reflects MAP2 relocation to neuronal soma rather than degradation (Hoskison and Shuttleworth, 2006), although either response indicates dendritic dysfunction. Therefore, I hypothesised that greater loss of MAP2 immunoreactivity would indicate greater hypoxic injury to neurons, and may be a mechanism related to cognitive impairment in PSD and ageing-related dementias.

In contrast to dendritic MAP2 studies, an in-vivo intracellular recording and staining methods in rat model of transient forebrain ischemia reported acute increases in dendritic length up to 48 hours after ischemia, finding significant outgrowth of mid-section dendrites from CA1 neurons after ischemia (Ruan *et al.*, 2006). As 90% of CA1 neurons were previously shown to undergo delayed neuronal death under these experimental conditions, dendritic outgrowth was suggested to contribute to excitotoxic cell death due to the increased receptive field of CA1 neurons. This outgrowth was suggested to be stimulated by increased CA3 activity activating NMDA receptors on mid-section CA1 dendrites via the Schaeffer collaterals, which is known to promote dendritic branching (Ruan *et al.*, 2006). They also found a dramatic increase in the number of neurons with disoriented dendrites after ischemia (i.e. basal dendrites arising from apical dendritic trunks and vice versa), suggesting that mechanisms involved in regulating dendritic outgrowth were impaired.

These findings appear to contradict those from studies demonstrating a loss of hippocampal MAP2 after ischemia. Furthermore, a Golgi study of chronic cerebral hypoperfusion in 2-vessel occlusion (2VO) rats found that CA1 dendritic length and arborization started to decrease four weeks after surgery, while spine loss and memory impairments were detectable two weeks post-surgery (Jia *et al.*, 2012). Although not entirely contradictory, these inconsistent reports of dendritic increases and decreases after hypoxic-ischaemic injury may reflect differences in the methods and time courses used in these studies to quantify dendrites. As the loss of MAP2 indicates disintegration of dendritic microtubules and therefore dendritic dysfunction, MAP2 may allow more insight into the functionality of dendrites after ischemia than simple structural observations.

Interestingly, Golgi studies have reported increases in dendritic arborization in the CA1 neurons of diabetic rats (Martanez-Tellez *et al.*, 2005) and pyramidal neurons of the prefrontal cortex in rat model of chronic hypertension (Vega *et al.*, 2004), suggesting a possible vascular mechanism causing dendritic outgrowth. Studies have also reported increased MAP2 immunoreactive dendritic length in the CA1, CA2, CA3 and subiculum in schizophrenia (Cotter *et al.*, 2000), but reduced MAP2 neuronal expression and reduced dendrite numbers in dlPFC in autism (Mukaetova-Ladinska *et al.*, 2004).

These variable findings of relationships between MAP2 levels in relation to cognitive dysfunction and ischemia suggested interpretation of studies using MAP2 would be challenging. However, the MAP2 was the best available marker to study dendrites in the tissue available, and was therefore the best way to continue investigations into the cause of neuronal volume reductions. To complement this work, I therefore also began investigation into post-synaptic proteins that would be found in dendrites and dendritic spines.

5.1.5 Synapse loss in AD and stroke

There is considerable evidence supporting synaptic dysfunction as an important mechanism preceding and contributing to neuronal death in AD (Selkoe, 2002; Arendt, 2009), also discussed in Chapter 4. The hippocampus is particularly vulnerable to synapse loss, with numbers of synapses in the hippocampus of AD patients reported to be reduced by 44-55%, and 18% reduced in MCI patients (Scheff *et al.*, 2007). There is

consistent evidence of dendritic spine loss in AD (Penzes *et al.*, 2011), and a recent protein immunoblot study found reduced levels of hippocampal PSD-95 in patients with amnestic MCI (Sultana *et al.*, 2010), in agreement with previous studies also reporting decreased PSD-95 in AD (Gylys *et al.*, 2004; Love *et al.*, 2006). However, a quantitative immunohistochemical study in AD reported an increase in entorhinal cortex PSD-95, and more punctate and filamentous staining particularly in the CA1 (Leuba *et al.*, 2008).

The relationship between synapse loss and cognition in AD may not be as straightforward as initially thought. There is evidence of a biphasic change in pre- and post-synaptic markers in AD, as studies have found an initial increase in synaptic markers in early stages of AD followed by a decrease as the disease progresses (Arendt, 2009). Increases in presynaptic protein synaptophysin (Mukaetova-Ladinska *et al.*, 2000), postsynaptic protein drebrin (Counts *et al.*, 2006), and postsynaptic protein PSD-95 (Leuba *et al.*, 2008) have been found in early AD and amnestic MCI and were suggested to indicate synaptic reorganization as a possible compensatory response to maintain neuronal function. However, other studies have found levels of pre-synaptic proteins such as SNAP25 and synaptophysin were reduced in the brains of AD patients (Schnaider Beeri *et al.*, 2012).

Few studies have investigated synaptic changes post-stroke. A recent study of a rodent stroke mode (rat transient middle cerebral artery occlusion) did not find any neuron loss or synaptic marker changes in the hippocampus 30 days post-stroke, although hippocampal long-term-potentiation was reduced and correlated with impairments in learning and memory (Li *et al.*, 2013). A study of a mouse model of stroke found that even after severe ischemia (<10% blood supply), spine and dendrite structure could be mostly recovered when reperfusion occurred within 60 minutes (Zhang *et al.*, 2005), indicating that dendritic damage caused by ischemia/hypoxia can be reversed if blood flow is promptly restored. In a model of chronic cerebral hypoperfusion, memory deficits were related to reduced levels of post-synaptic protein PSD-95 and pre-synaptic marker synaptophysin 30 days after the occlusion surgery (Wang *et al.*, 2010), indicating that chronic hypoxia resulted in reduced synapse density. A previous quantitative immunohistochemical study within the CogFAST cohort found lower levels of the dendritic spine protein drebrin in the hippocampus of PSD compared to non-

demented stroke survivors, indicating loss of dendritic spines (A. Hamdan, unpublished data). However, it was unclear whether the loss of drebrin was due to loss of dendritic spines, loss of dendrites or both.

5.2 Aims

This project aimed to investigate dendritic changes in the hippocampus in order to establish whether loss of dendritic extent was related to neuronal volume loss and cognitive impairment in delayed PSD. As it was not possible to assess the dendritic arbour using Golgi techniques, IHC for the dendrite-specific protein MAP2 was used to visualize and quantify dendrites. 2D image analysis techniques were used to investigate neuronal immunoreactivity in the pyramidal layer of CA1 and CA2.

During image analysis of CA1 and CA2 neuronal soma it became apparent that there were differences in MAP2 dendritic staining in the stratum radiatum, where the greatest density of dendrites are found in the hippocampus. Furthermore, 2D analysis at low magnification was not able to distinguish staining of fine dendrites from background staining. Therefore, a novel 3D technique was used to quantify dendritic length-density in the CA1 stratum radiatum at 100x magnification. The CA1 stratum radiatum contains the apical dendrites of CA1 neurons, which generally receive inputs through the Perforant path (from EC) and from CA3 neurons more distant from the CA1 (Ishizuka *et al.*, 1990). Synapses in this regions are highly plastic and are thought to have an critical mechanistic role in memory and learning (Kerchner *et al.*, 2012). Therefore, a reduction in MAP2 immunopositive dendrites in this region would reflect a fundamental disruption to the hippocampal circuitry resulting in impaired function.

Patterns of immunohistochemical staining for post-synaptic proteins PSD-95 and drebrin were also investigated in relation to MAP2 dendritic staining, to explore whether there was any relationship between MAP2 staining and other post-synaptic proteins found in dendrites. Immunohistochemical staining for these proteins was also investigated in tissue from the perfusion-fixed baboon model to investigate how post-mortem delay may have influenced staining and results. Levels of PSD-95 and presynaptic proteins synaptophysin and SNAP-25 were quantified in subjects from the CogFAST cohort using protein immunoblotting techniques, as accurate quantification

of these proteins by low-power image analysis is difficult due to their abundance in the neuropil and lack of contrast to background staining.

5.3 Materials and methods

5.3.1 IHC

IHC staining for MAP2, PSD-95 and drebrin was carried out in 10µm thick paraffin-embedded hippocampal sections as described in section 2.6. Three 30µ thick sections were stained for MAP2 for 3D stereological analyses of dendritic length-density.

5.3.2 Image Pro analysis of MAP2 in the pyramidal layer

MAP2 staining in the pyramidal layer of CA1 and CA2 neurons was quantified using Image Pro analysis in images taken at X20 magnification as described in section 2.7.2. Cases were selected with relatively short fixation (<9 weeks) as fixation was believed to influence staining.

5.3.3 Novel 3D analysis of dendritic length density in the stratum radiatum

Dendritic length-density was quantified using a novel 3D stereological technique in the CA1 stratum radiatum (described in section 2.7.6). Cases were selected with short post-mortem delay (PMD) to minimize the effect of PMD on staining variability.

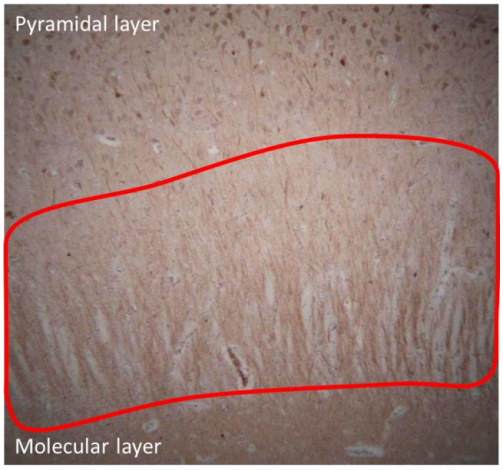

Figure 5.1. The CA1 stratum radiatum in a section stained for MAP2.

5.3.4 Investigation of CA layers stained for MAP2 and other post-synaptic proteins

Clear differences in MAP2 distribution and staining intensity were observed during previous MAP2 analyses. Therefore a semi-quantitative rating scale (0-3) was used to

rate different patterns of staining in layers of the CA1 to quickly determine whether unusual staining was associated with clinicopathological variables. Regions and characteristics rated were:

- Mottled/patchy stratum moleculare
- 'Stringy' stratum radiatum,
- Intensity of soma staining in the pyramidal layer (Figure 5.5).

MAP2 staining patterns were also visually compared with sections stained for post-synaptic proteins PSD-95 and drebrin in human tissue, and drebrin in baboon tissue. Representative images are shown in results.

5.3.5 Protein immunoblots of synaptic markers

Levels of pre- and post-synaptic markers PSD-95, synaptophysin and SNAP-25 were quantified by protein immunoblot according to protocols described in section 2.8. 20µg of protein was loaded into each well for each experiment.

5.3.6 Statistical analysis

Age, PMD and MAP2 staining data were normally distributed. Therefore, group means were compared using ANOVA with post-hoc Tukey's test for pairwise comparison. Fixation length was analysed using non-parametric tests. Western blot results were non-normally distributed and analysed using non-parametric tests.

5.4 Results

5.4.1 MAP2 2D image analysis

Demographic details of subjects analysed using MAP2 with 2D Image Pro techniques are presented in Table 5.1. There were no significant differences in age, PMD or fixation time between groups.

	N	**Age, years** Mean (range)	**PMD, hrs** Mean (range)	**Fixation time, weeks** Mean (range)	**Braak stage** Median (range)	**CERAD,** Median (range)
Controls	6	82 (72-98)	42 (23-59)	8 (8)	3 (1-3)	0.5 (0-1)
PSND	9	84 (78-89)	42 (19-96)	7 (5-12)	3 (1-5)	1 (0-2)
PSD	7	87 (80-96)	53 (10-96)	7 (6-8)	2 (0-4)	0 (0-1)
AD	9	83 (76-91)	47 (6-72)	7 (6-8)	5 (4-6)	3 (3)

Table 5.1 Demographics of subjects analysed with 2D Image Pro analysis of MAP2 immunostaining.

There were no differences in MAP2 %PA (% of stained pixels in the area of interest) or IOD (intensity of stain) in neuronal soma in the CA1 or CA2 between controls, PSND, PSD and AD groups. Group means are presented in Appendix Table 8.8. CA2 IOD appeared to be reduced in the PSND group compared to PSD and other groups, however this did not reach significance (Figure 5.2A). There was considerable variation in neuronal MAP2 staining within groups (demonstrated in Figure 5.3 and Appendix Figure 8.4). MAP2 CA1 %PA was positively correlated with CA2 %PA ($r = 0.596$, $p = 0.003$). CAMCOG scores were negatively correlated with MAP2 CA2 IOD ($r = -0.603$, $p = 0.02$) and there was a trend to negative correlation with CA1 IOD ($r = -0.473$, $p = 0.075$). MAP2 CA1 and CA2 %PA were negatively correlated with PMD ($r = -0.444$, $p = 0.02$ and $r = -0.473$, $p = 0.02$ respectively) (Figure 5.2 B). There were no correlations with AD pathology, fixation or age.

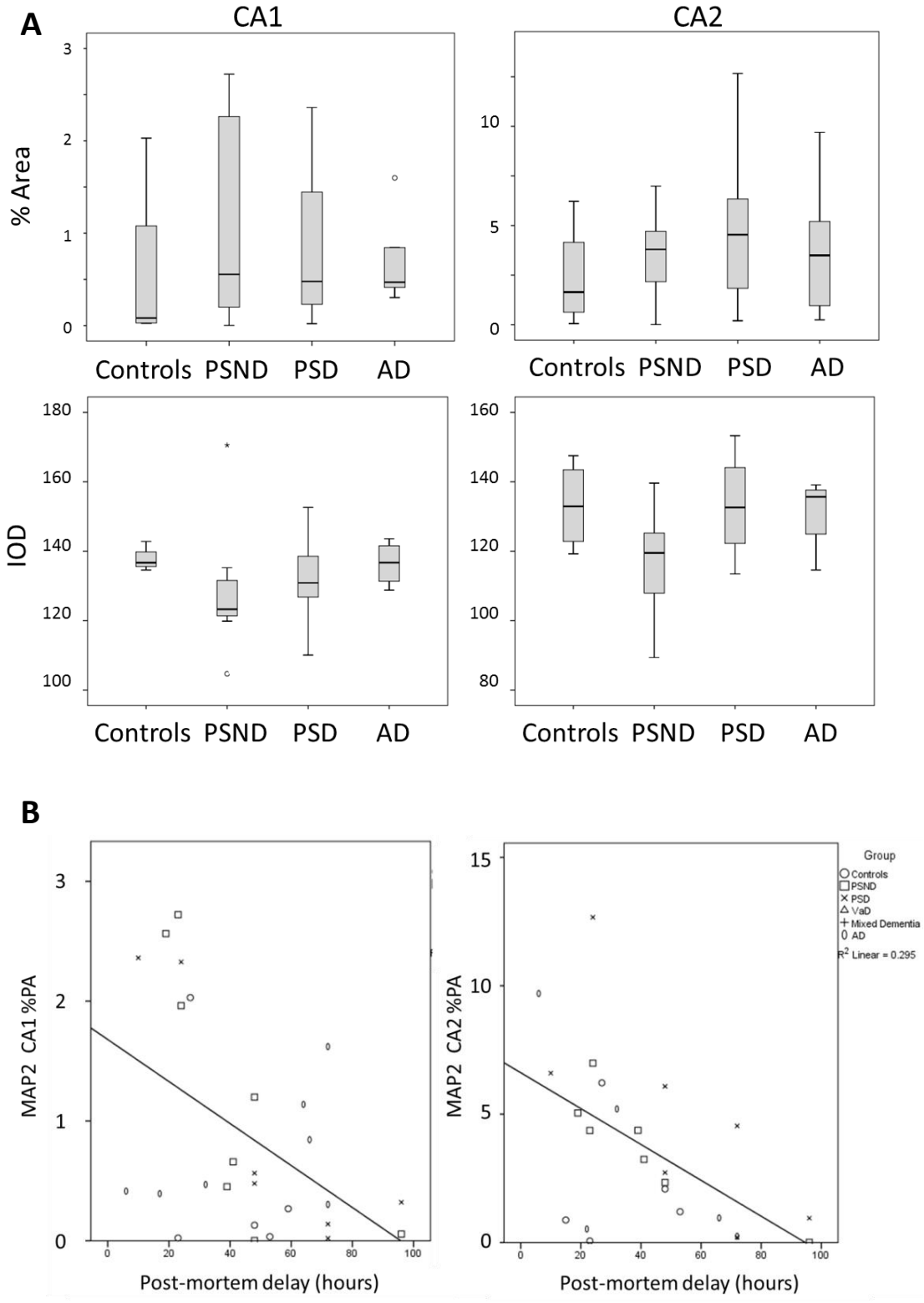

Figure 5.2 A, Box-plots of CA1 and CA2 MAP2 % Area (%PA) staining and IOD; B, Negative correlations between MAP2 %PA and post-mortem delay.

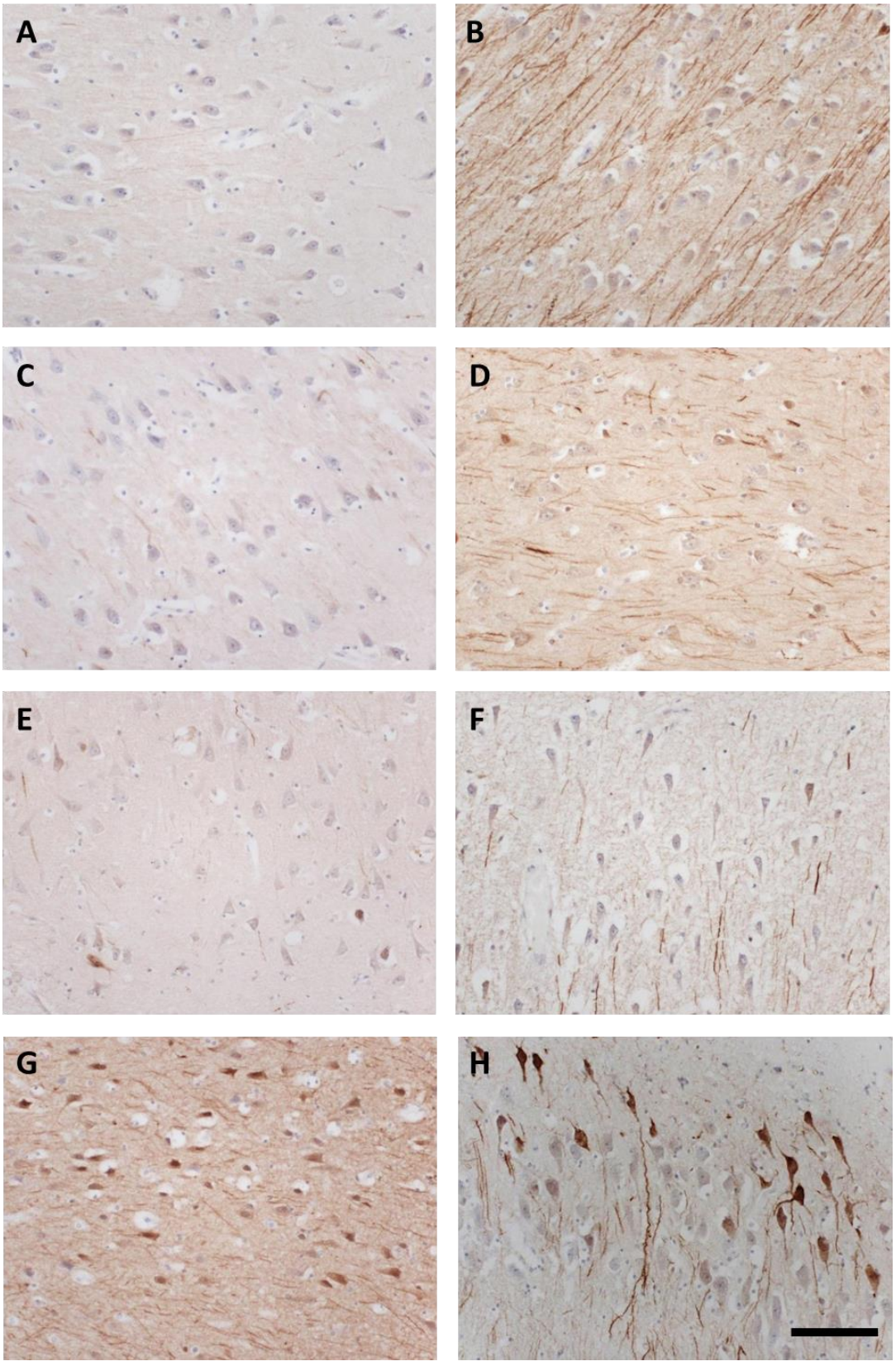

Figure 5.3. Images demonstrating variability in CA1 MAP2 staining in the pyramidal layer between subjects within the same group. A, B = Controls; C, D = PSND; E, F = PSD; G, H = AD. Scale bar = 100µm.

5.4.2 MAP2 dendritic length density

Demographic details of subjects analysed using MAP2 with 3D stereology to measure dendritic length density are presented in Table 5.3. There were no differences in age, or fixation length between groups. There was a trend in the VaD group having significantly longer PMD compared to PSD group ($p = 0.053$). The coefficient of error (CE) of dendritic length density measurements was 0.066 (±2SE = 0.002), demonstrating high level of accuracy.

	N	**Age, years** Mean (range)	**PMD, hrs** Mean (range)	**Fixation time,** Mean weeks (range)	**Braak.** Median (range)	**CERAD,** Median (range)
Controls	8	81 (71-91)	33 (22-67)	22 (5-105)	3 (0-5)	0 (0-3)
PSND	8	86 (80-92)	29 (10-48)	10 (5-20)	2 (1-3)	0.5 (0-1)
PSD	6	88 (82-95)	22 (10-42)	7 (4-12)	3 (2-4)	1.5 (0-2)
VaD	8	84 (71-97)	48 (24-76)	19 (5-52)	2 (1-4)	1 (0-2)
AD	8	82 (70-91)	34 (16-64)	11 (2-24)	5 (4-6)	3 (3)

Table 5.2. Demographics of subjects studied using 3D stereology to quantify dendritic length-density.

There were no differences in CA1 dendritic length-density (DLD) between groups (Figure 5.4). Numerical values for the group mean DLD are presented in Appendix Table 8.8. DLD was negatively correlated with post-stroke memory scores ($r = -0.746$, $p = 0.013$) and fixation length ($r = -0.343$, $p = 0.038$). There were no correlations with Braak stage, CERAD scores, CAMGOG scores or neuronal volume or density results. There were no correlations between DLD and 2D measurements of MAP2 immunopositive staining in the pyramidal layer.

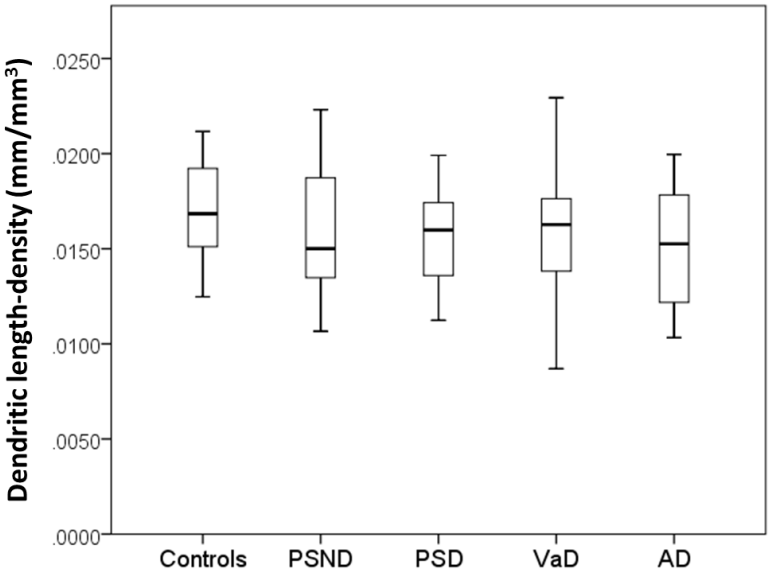

Figure 5.4. Dendritic length density in CA1 stratum radiatum.

5.4.3 Visual investigation of MAP2 and post-synaptic markers

There were no clear relationships between the patterns of MAP2 staining in layers of the hippocampus and disease groups, PMD or fixation length. Representative images of different patterns of staining are shown in Figure 5.5.

Variability in PSD-95 immunostaining between subjects was particularly striking, as several subjects had little/no positive staining, which was not related to PMD, fixation or Braak stage (Figure 5.6 E, F). Surprisingly, strong drebrin immunoreactivity was found in the neuronal soma, rather than in the dendrites as expected (Figure 5.6 C, D).

When sections were viewed at lower power, immunoreactivity was more uniform across hippocampal layers stained for drebrin and PSD-95 than MAP2.

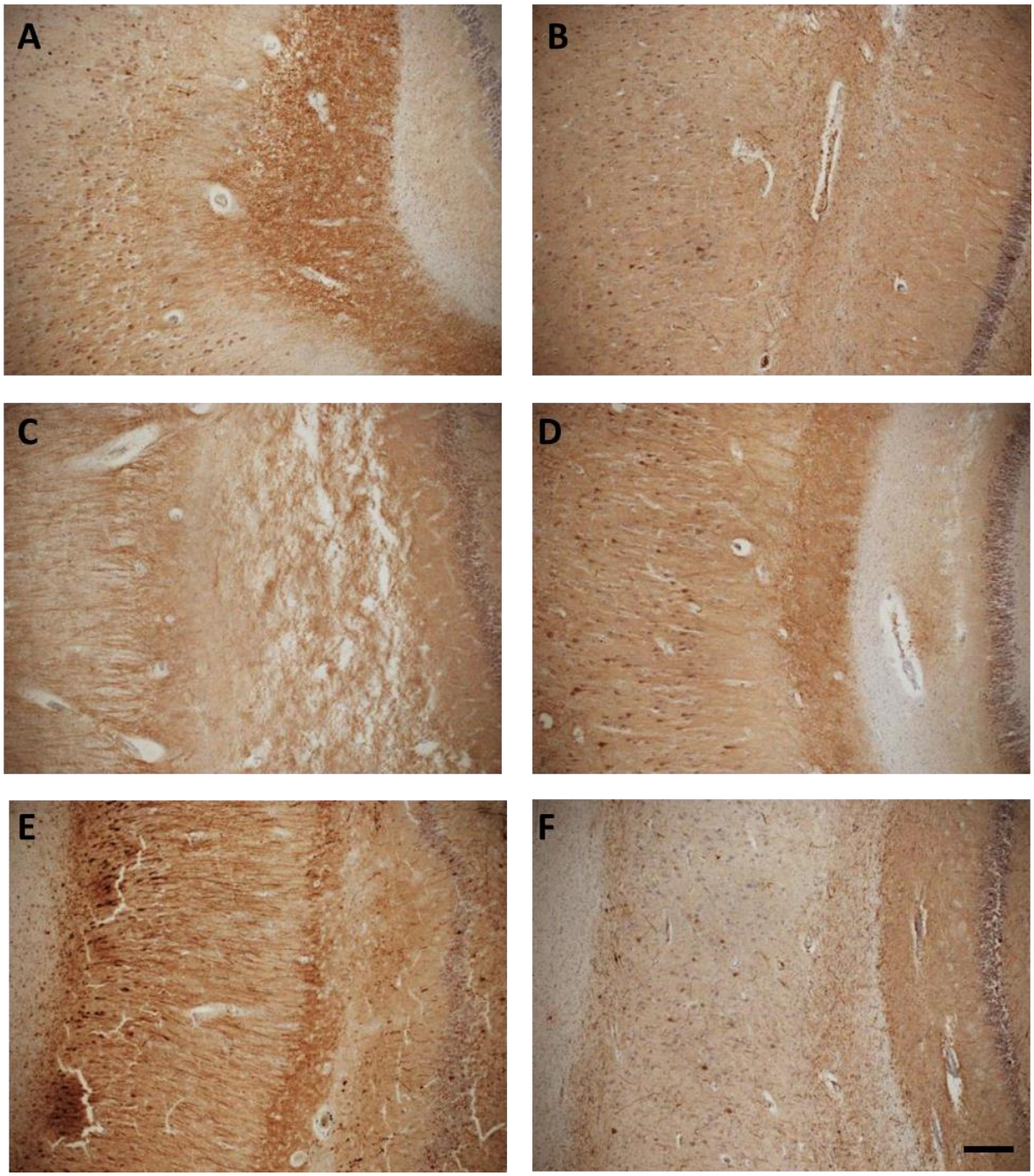

Figure 5.5 Representative images of the different types of hippocampal layer staining using MAP2. A, mottled stratum radiatum; B, Even staining across all layers; C, Patchy stratum moleculare, pale neuronal staining; D, solid stratum molecular of CA layer, pale stratum moleuclare of DG, dark neuronal staining; E, 'Stringy' stratum radiatum; F Few MAP2 positive dendrites in stratum radiatum. Scale bar = 200µm.

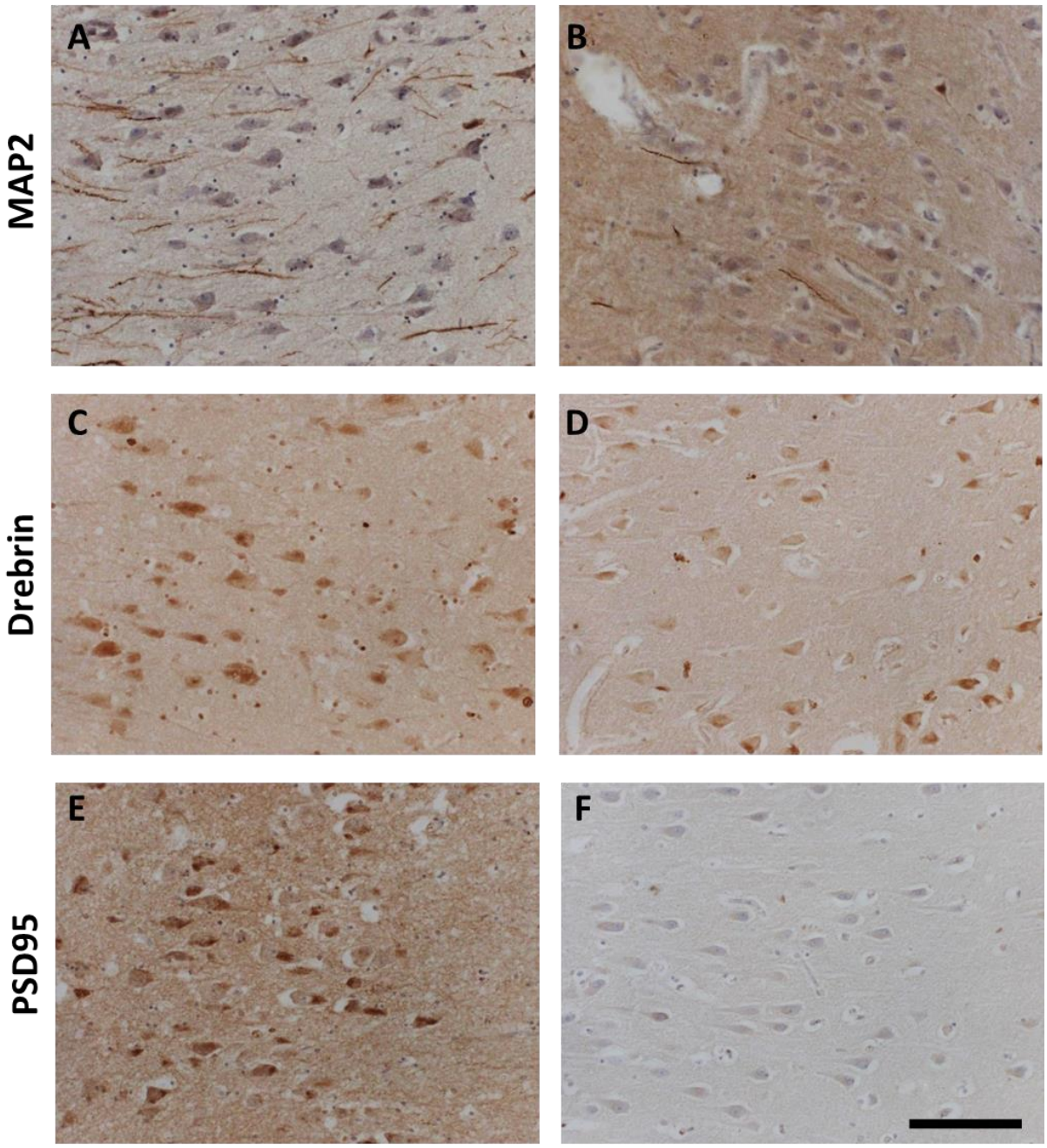

Figure 5.6 Variability in pyramidal layer staining for MAP2 (A, B), Drebrin (C, D) and PSD-95 (E, F) in two PSND subjects with similar PMD, fixation length and Braak stage; A, C, E PMD = 48h, Fixation = 7 weeks, Braak stage = 3; B, D, F PMD = 46h, Fixation = 12 weeks, Braak stage = 3. Scale bar = 100µm

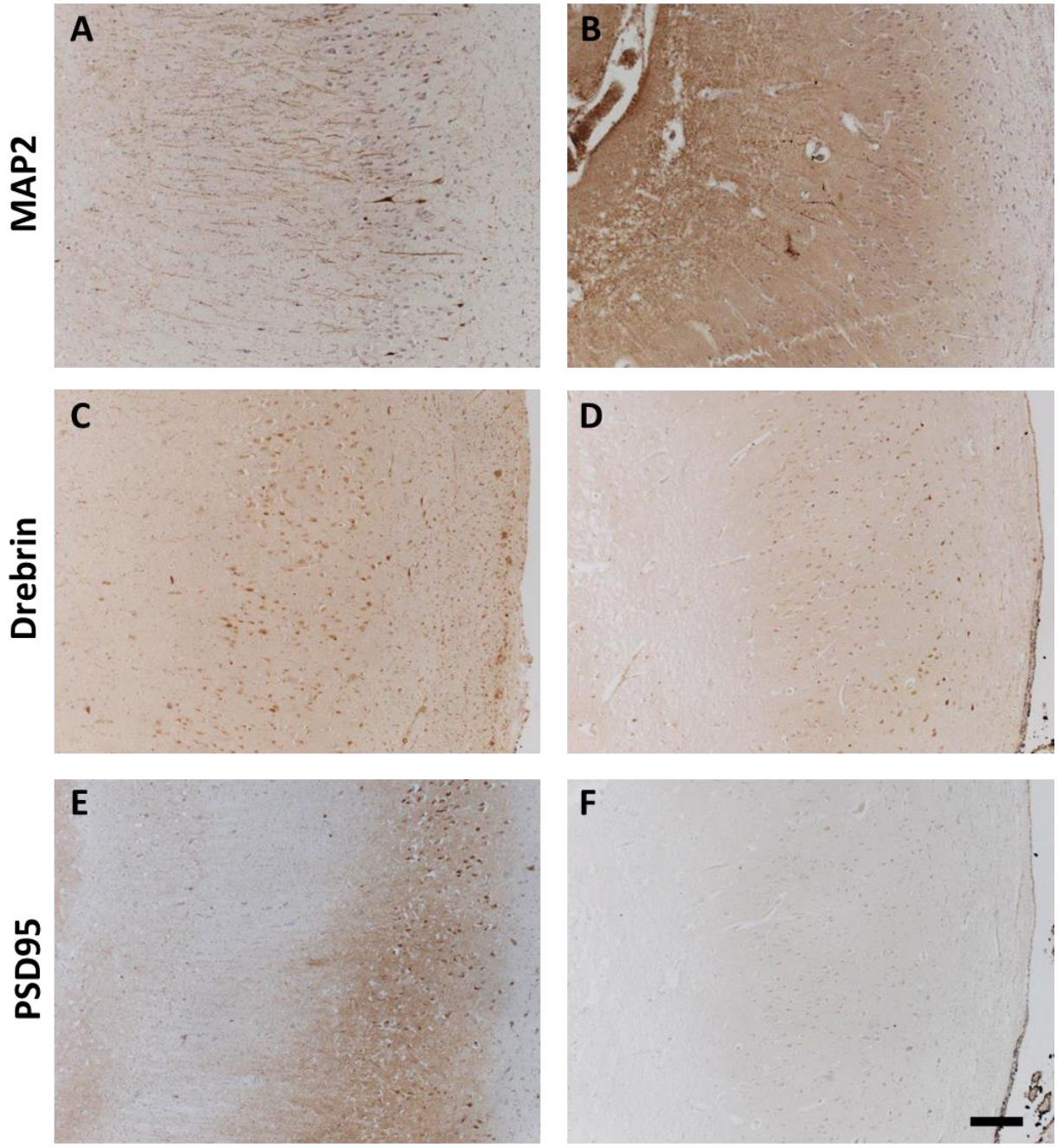

Figure 5.7 Variability in staining for MAP2 in hippocampal layers; (A, B), Drebrin (C, D) and PSD-95 (E, F) in two PSND subjects with similar PMD, Fixation and Braak stage; A, C, E PMD = 48h, Fixation = 7 weeks, Braak stage = 3; B, D, F PMD = 46h, Fixation = 12 weeks, Braak stage = 3. Scale bar = 200µm

5.4.4 MAP2 and drebrin staining in perfused non-human primate model

To investigate the possible effect of PMD on results of studies investigating post-synaptic proteins and dendrites, staining patterns were visually compared to those in the perfused baboon model. In the sham and 7 day animals, MAP2 dendritic staining appeared generally more intense and uniform across the hippocampal layers (Figure 5.8 A). Dendritic staining was clearer than in human tissue when viewed at high power (Figure 5.8 B).

Interestingly, there were considerable differences in drebrin staining compared to the human tissue, as there was greater staining in the neuropil than neuronal soma, in contrast to human tissue where drebrin staining was concentrated in neuronal soma (compare Figure 5.6 C and D with Figure 5.8 E-H). However, in the animals which have previously been found to have greatest neurodegenerative neuronal changes at 7-days post-surgery, there was intense neuronal soma staining in a few neurons at the CA1/CA2 border (Figure 5.8 G, H).However, there were little changes to MAP2 staining between sham and 7-day animals (Figure 5.8 A-D).

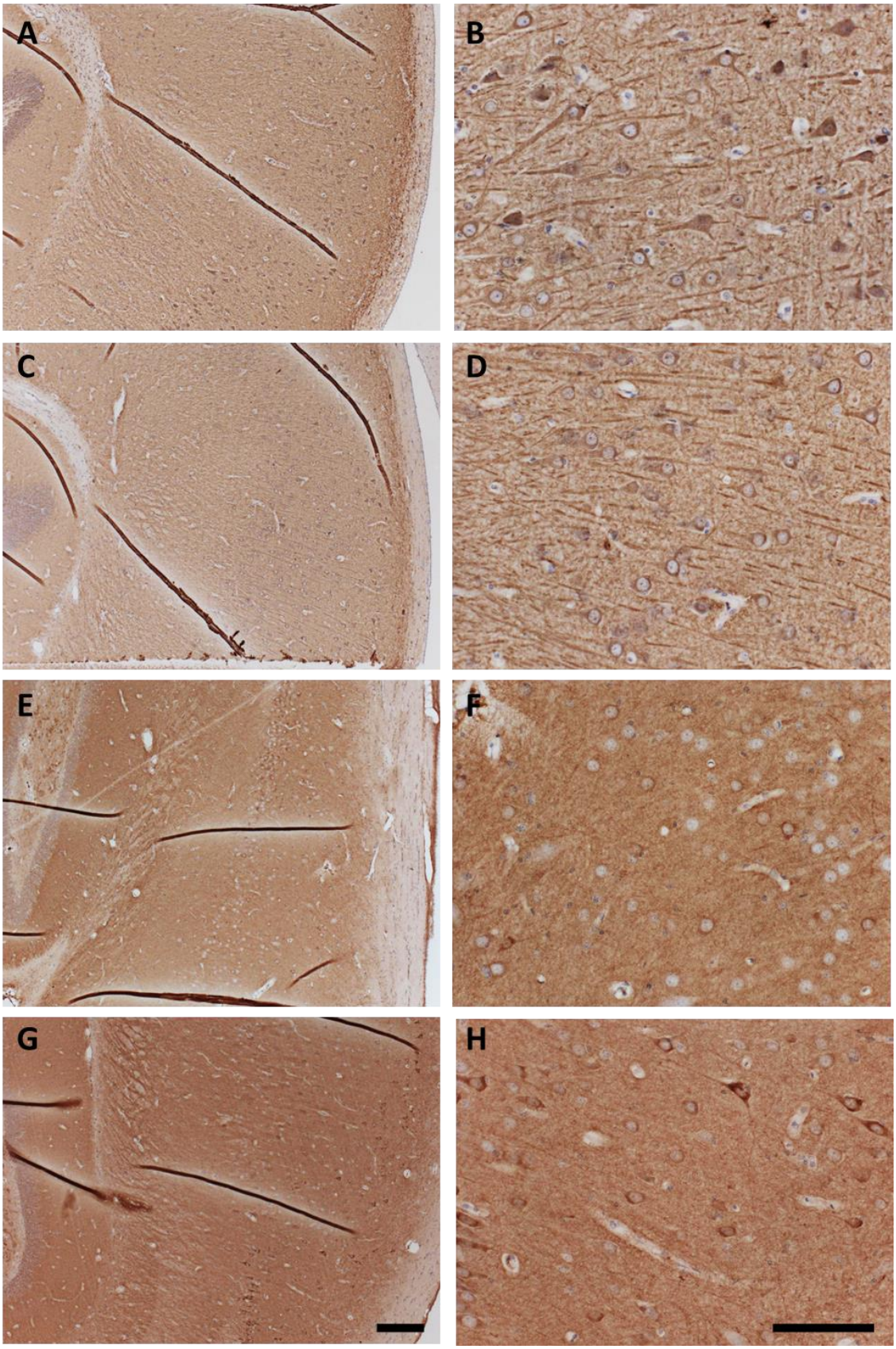

Figure 5.8 A, B, MAP2 staining in sham baboon; C, D, MAP2 staining in 7-day baboon; E, F, drebrin staining in sham baboon; G, H, drebrin staining in 7-days post-surgery baboon. A, C, E scale bar = 200µm; B, D, F scale bar = 100µm.

5.4.5 Protein immunoblots of synaptic markers

Group demographics of subjects analysed using protein immunoblotting techniques are presented in Table 5.3. There were no differences in age or PMD between groups.

	N	**Age, years** Mean (range)	**PMD, hrs** Mean (range)	**Braak Stage** Median (range)	**CERAD,** Median (range)
Controls	8	80 (72-91)	23 (10-34)	3 (0-4)	0 (0-1)
PSND	12	85 (78-94)	24 (10-34)	1 (1-4)	0 (0-2)
PSD	12	86 (75-98)	31 (10-76)	2.5 (0-6)	1.5 (0-3)
AD	8	81 (70-91)	22 (6-37)	5 (4-6)	3 (2-3)

Table 5.3. Demographics of subjects analysed for synaptic proteins in frozen hippocampal tissue.

There were no differences in mean relative band intensity for PSD-95 or synaptophysin between groups. There was a trend to the PSND group having greater mean band intensity (IOD) for SNAP25 than control group ($p = 0.069$) (Figure 5.4). SNAP25 IOD was positively correlated with PSD-95 IOD ($r = 0.509$, $p = 0.001$) and memory scores ($r = 0.619$, $p = 0.018$).

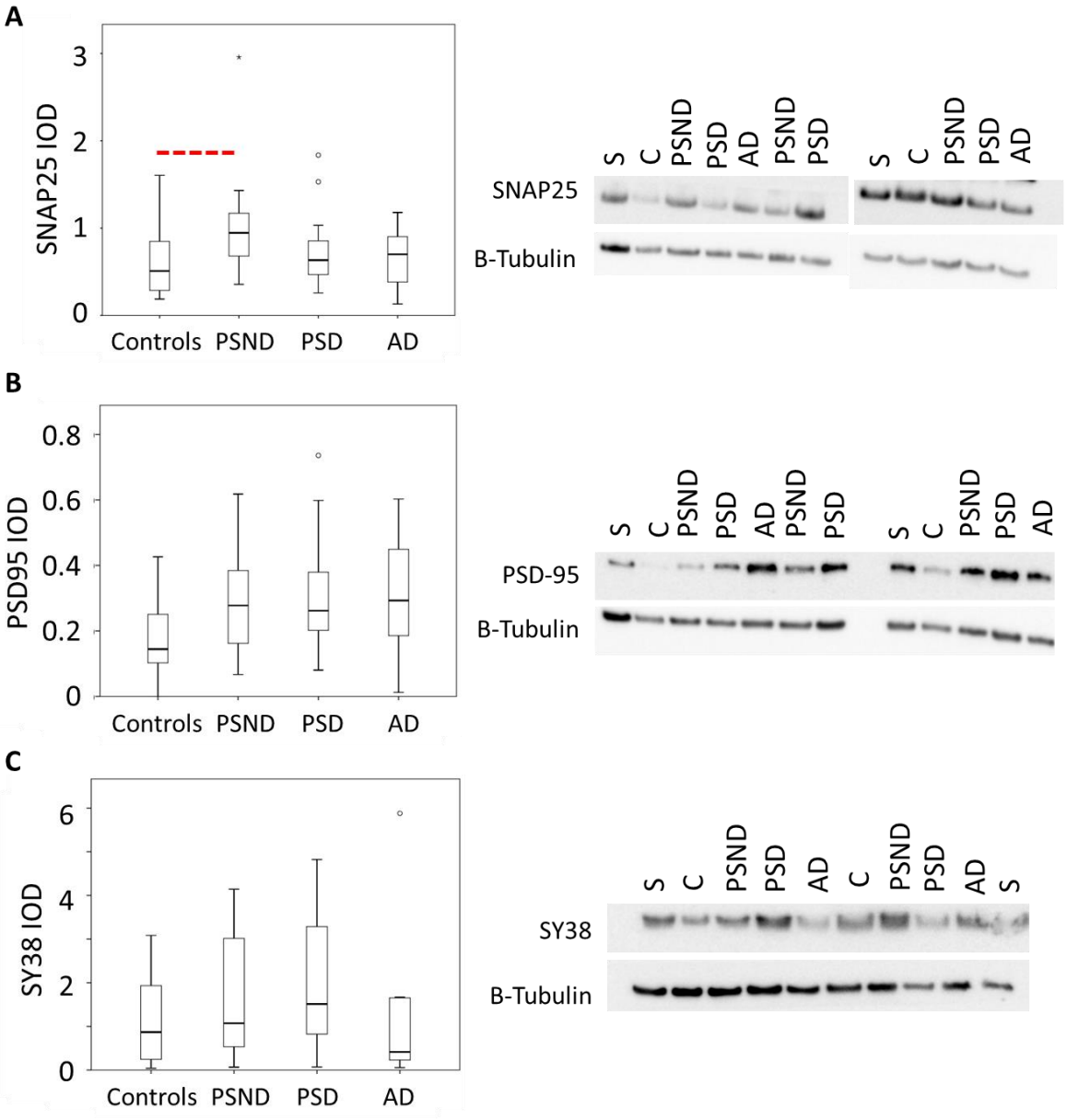

Figure 5.9. Box-plot and representative protein immunoblots probed for A, pre-synaptic protein SNAP-25; B, Post-synaptic protein PSD-95; C, Pre-synaptic protein synaptophysin. Dotted red line indicates trend to significant difference ($p < 0.1$). S = loading standard, C = control.

5.5 Discussion

5.5.1 MAP2 in the pyramidal layer

This investigation revealed that there was considerable variation in MAP2 immunopositive staining in the pyramidal layer between subjects, as demonstrated in Figure 5.3 and reflected in the broad spread of area positively stained for MAP2 (% PA) between subjects. These results were surprising as I expected to find a reduction in MAP2 staining in the post-stroke groups compared to controls and AD, reflecting dendritic damage due to the effects of hypoxic/ischaemic injury from the stroke or other cerebrovascular disease mechanisms. I reasoned that as analysis was restricted to the pyramidal layer of CA1 and CA2, this may be because results were largely based on soma staining rather than dendritic staining. Therefore, it was surprising to find negative correlations between CA1 and CA2 %PA and PMD, as increasing PMD has previously been shown to cause reduced dendritic MAP2 staining but increased soma staining (Schwab *et al.*, 1994). However, Schwab et al.'s study of MAP2 and PMD only examined changes up to 8 hours post-mortem; therefore loss of MAP2 may continue in neuronal soma during longer PMD, as PMD in these subjects reached up to 96 hours. This study was also limited as quantification of MAP2 immunopositive staining using standard image analysis techniques was difficult at 20X magnification as it was impossible to distinguish background staining from fine dendrites in the neuropil.

5.5.2 MAP2 dendritic length density in the stratum radiatum

To address these issues, I adapted a 3D stereological technique previously used to quantify vascular length density (Burke *et al.*, 2013), to quantify dendritic length density of MAP2 positive dendrites in the stratum radiatum. To my knowledge, this technique had not previously been attempted. In contrast to the 2D analysis at low power, even small MAP2 positive dendrites were easily identifiable at 100x magnification, appearing as fine dark brown threads running through the tissue (Figure 2.7). Dendrites in the stratum radiatum were numerous, permitting analysis of large numbers of dendrites to achieve acceptable coefficient of error values.

Although the variability of results within groups was reduced compared to 2D methods, no significant differences in dendritic length density were detected between

groups. However, the disease group means were lower than the control group mean in agreement with previous studies which have reported loss of MAP2 immunoreactivity after ischemia and in AD. Due to the time-consuming nature of the study, exclusion of subjects with longer post-mortem delay, and requirement of relatively large amounts of tissue, numbers of subjects analysed were small. Addition of greater numbers of subjects to be analysed using this technique may improve the power to generate statistically significant differences.

However, addition of further subjects for analysis may not easily resolve significant differences between groups as the issue of variability in MAP2 staining between subjects within the same disease group remains. Visual inspection of different patterns and intensity of staining in the different hippocampal layers did not reveal any relationships with disease groups, fixation or PMD. As there is considerable literature describing rapid loss of hippocampal MAP2 after ischaemic injury, these differences may result from other factors causing hypoxic/ischaemic damage and subsequent changes to MAP2 distribution in the CA1. Possible factors likely to affect MAP2 staining include subsequent strokes, cause of death and pre-mortem agonal state. Furthermore, few previous studies have reported long-term changes to MAP2 after ischemia. Although loss of MAP2 immunoreactivity may be an early marker of ischaemic damage (Kühn *et al.*, 2005), long-term compensatory mechanisms involving dendritic plasticity may restore MAP2 levels in some stroke survivors.

Furthermore, ageing and neurodegenerative diseases have been associated with increased MAP-2, which in turn has also been associated with cognitive impairment (Mukaetova-Ladinska *et al.*, 2000; Haley *et al.*, 2010; VanGuilder *et al.*, 2011). The conflicting effects of reduced MAP2 immunoreactivity after ischemia or post-mortem interval may be countered by increases in MAP2 immunoreactivity in response to other neurodegenerative disease or age-related mechanisms. Currently, the relationship between MAP2 immunoreactivity, dendrite loss or dysfunction, post-mortem delay, ischemia and cognitive function is not well understood. The unknown influence of these factors on these results therefore limits the interpretation of these findings.

A 7-Telsa MRI study recently reported that thinning of the CA1 stratum radiatum was related to memory impairments in early AD (Kerchner *et al.*, 2012), in agreement with autopsy findings that the stratum radiatum contains greater levels of AD pathology than the pyramidal layer, which is thought to cause apical dendrite degeneration and stratum radiatum thinning in AD (Braak and Braak, 1997; Thal *et al.*, 2000). High-resolution neuroimaging studies of CVD and stroke survivors may therefore be able to provide more accurate insight into dendritic changes in the stratum radiatum in the pathogenesis of VaD and delayed PSD.

There are no previous studies reporting use of 3D stereology to analyse dendritic length density. The most similar previous study investigated dendrites in subjects with schizophrenia using 14µm thick hippocampal sections stained for MAP2 and non-phosphorylated MAP2. However, this study estimated dendritic length using linear probes in 2D analysis (Cotter *et al.*, 2000). They also measured dendrites within the pyramidal layer, which includes both apical and basal dendrites, in contrast to my study of only apical dendrites. Cotter et al. found an increase in MAP2 immunoreactive dendritic length in the CA1 and subiculum of schizophrenic subjects compared to controls, although their results contrasted with previous studies reporting reduced MAP2 expression in schizophrenia (Rosoklija *et al.*, 2005). These conflicting findings were attributed to PMD, although they are also likely to reflect the previously discussed issues around current understanding of the relationship between MAP2 levels and cognition in post-mortem studies of human tissue.

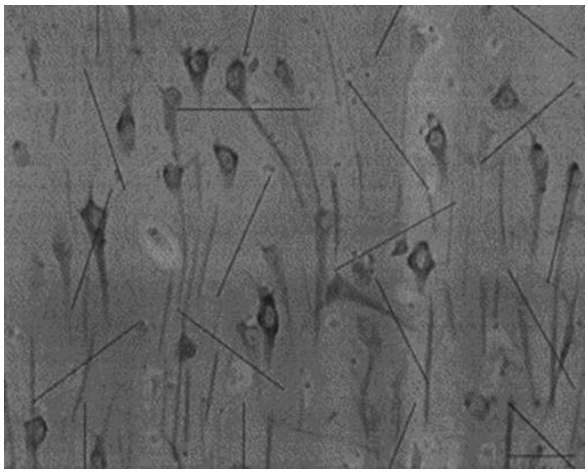

Figure 5.10. Representative image of CA1 pyramidal layer stained for non-phosphorylated MAP2 from (Cotter *et al.*, 2000). Lines represent linear probes. Scale bar = 50µm.

5.5.3 MAP2 and AD pathology

Results from 2D and 3D analysis of MAP2 immunopositive dendrites were not related to AD pathology (Braak stage or CERAD score) (as demonstrated in Figure 8.5). However, previous studies have reported a biphasic change in MAP-2 levels in AD where subjects with Braak stage 4 had the highest MAP-2 staining before it dropped off in Braak stages 5 and 6 (Mukaetova-Ladinska *et al.*, 2000), which would hinder the detection of a linear relationship between MAP2 and AD pathology stage. When the MAP2 data were divided by Braak stage, there was no evidence of a biphasic change although MAP2 was generally lower in Braak stages greater than 4. This is likely to be due to the greater loss of CA1 neurons in subjects with greater tau pathology burden. Previous studies have also suggested that abnormally hyperphosphorylated tau sequesters MAP2 in aggregates, however I did not find evidence of this as intensity of MAP2 staining was not related to Braak stage (Iqbal and Grundke-Iqbal, 1997).

5.5.4 Visual investigation of MAP2, drebrin and PSD-95 staining

There were sometimes striking differences in the appearance of MAP2 staining between subjects. This was due to darker, lighter, or patchier staining in different layers of the CA subfields and dentate gyrus. I initially thought this may reflect loss of MAP2 immunoreactivity due to the effect of PMD; however I could not find a consistent effect related to PMD. I was then interested to know whether staining for other dendritic proteins, specifically post-synaptic proteins involved in the structure and function of dendritic spines, would also display similar staining patterns within and between subjects.

Drebrin staining was relatively consistent and restricted to neuronal soma, which was surprising as drebrin is a protein involved in regulating dendritic spine morphology and function (Ivanov *et al.*, 2009). PSD-95 staining was also unusual. As PSD-95 is the most abundant scaffolding protein found at dendritic spines, I expected to find high density of staining in all CA layers (Chen *et al.*, 2011b). However, PSD-95 staining ranged from dark staining of the pyramidal layer and molecular layer, to almost non-existent staining. This did not appear to be directly related to PMD, fixation or Braak stage, suggesting that other factors, such as additional disease mechanisms or pre-mortem agonal state may have had significant impact on these proteins.

To further elucidate the importance of PMD in the distribution of immunoreactive staining for MAP2 and drebrin, I compared the staining patterns with those in hippocampal sections from the perfused baboon cohort. Identical antibodies and IHC protocols were used for human and baboon tissue, and generated similar staining results. Therefore it is unlikely that any differences observed were due to differences in species. The MAP2 staining appeared fairly similar to human staining, although the sham animals had very even staining across all layers, suggesting that the appearance of clearly defined layers reflects pathological change in the human tissue. Although it is difficult to draw any conclusions from the MAP2 work, these differences suggest that the loss of uniform staining in the human cohort may reflect a change in connectivity in response to disease mechanisms.

The drebrin staining was completely different in the baboon hippocampus, with very little staining in neuronal soma and intense staining in the neuropil. In the 7-day animals, where greatest neuronal volume loss was observed, a few neurons at the CA1/CA2 border had dark staining in the soma which suggests that appearance of drebrin in the soma may reflect pathological response to hypoxic damage. Interestingly, a stereological study of Golgi stained neurons found that CA1 neurons near CA2 had significant loss of total dendritic length and branching in AD (Hanks and Flood, 1991), suggesting that these neurons may be particularly vulnerable to dendritic damage.

A previous study investigated drebrin immunoreactivity in pyramidal layers of CA1 and CA2 in stroke survivors from the CogFAST cohort. This study indicated that there were reduced levels of drebrin in PSD compared to PSND subjects. However, interpretation of these results is limited as the study did not investigate levels of drebrin in the stratum radiatum, where the level of protein would be assumed to reflect the number of dendritic spines and therefore synapses. Further studies would be required to determine whether the accumulation of drebrin in neuronal soma reflects a post-mortem artefact or pathological response.

5.5.5 Pre- and post-synaptic proteins in frozen hippocampal tissue

Levels of proteins determined by immunoblot analysis also demonstrated variability between groups which prevented the detection of statistically significant differences

between groups. Although analysis of frozen tissue removes the possibility of tissue fixation and processing affecting protein immunogenicity, these dynamic synaptic proteins are likely to be more significantly affected by post-mortem delay or other factors that could have influenced protein levels. A previous immunoblot study of glutamatergic synaptic proteins in VaD and PSND also did not find any differences in the levels of pre-synaptic protein synaptophysin, in agreement with my results (Kirvell *et al.*, 2010). They reported correlations between CAMCOG scores and VGLUT1 (vesicular glutamate transporter 1) concentration in the dlPFC and inferior temporal cortex (Kirvell *et al.*, 2010). VGLUT1 is a pre-synaptic protein involved in long-term potentiation and memory, therefore the authors suggested that upregulation of VGLUT1 was associated with preserved cognitive function in patients with CVD.

I found that SNAP-25 levels were increased in PSND compared to control subjects, and appeared higher in PSND compared to PSD subjects. Therefore, upregulation of SNAP-25 may have occurred as a compensatory response to maintain connectivity in surviving hippocampal neurons. However, previous studies have suggested that SNAP-25 may be deposited at degenerating presynaptic terminals (Ishimaru *et al.*, 2001). Previous studies have also shown that synaptophysin and SNAP-25 levels fluctuated in a gerbil model of stroke (5 minutes bilateral common carotid artery occlusion). Western blot and immunohistochemical quantification of these proteins in the CA1 found that protein levels were decreased at day 2 post-surgery, but increased (130-140%) of control levels at day 14 (Ishimaru *et al.*, 2001), in agreement with previous studies reporting increased SNAP-25 immunoreactivity after hippocampal injury, including ischemia and kainite-induced neuronal damage, that resulted in selective neuronal loss (Marti *et al.*, 1998). Therefore, the functional consequences of the perceived increase in SNAP-25 in PSND subjects are unclear.

Interpretation of my findings in frozen hippocampal tissue were limited as it is assumed that the ratio of the area of different subfields was the same between all subjects studied. However, depending on the shape, size and plane that the hippocampal sections were taken from, some subjects may have had a greater amount of tissue from the CA1, whereas others may have had a larger CA4 etc. Therefore, although these results inform us on the level of each protein within the hippocampal formation at that coronal level, they do not indicate changes to specific regions or

subregions such as the CA1 or stratum radiatum. When planning this study, I had initially hoped to sub-dissect the CA1 subfield only. However, this would not have generated great enough protein yields for analysis. A future study could try laser capture microdissection of neurons to establish protein or mRNA levels within neurons from specific subfields. However, this will not eliminate the issues associated with post-mortem delay, and as only the neuronal soma could easily be dissected (i.e. not the dendrites), results will still require careful interpretation.

5.6 Conclusions

Dendrites, dendritic spines and synapses may be one of the most challenging structures to study due to their dynamic plasticity. The changes that these structures undergo during post-mortem interval before fixation, and during different pre-mortem agonal conditions, are not well characterized or understood. This makes it very difficult to draw any specific conclusions from post-mortem studies attempting to quantify dendrites and synaptic markers, and is likely to be major contributor to the conflicting findings in the literature. Furthermore, it has been suggested that measuring dendritic extent at one point in time may not accurately reflect neuronal function, as the ability of dendrites and spines to remain plastic is critical to maintaining neuronal function. Therefore, the measured extent of dendrites in static post-mortem material may not be a useful measure of the functional integrity of that neuron (Flood, 1993).

This study did not find any differences in dendritic proteins or dendritic length-density between PSD and PSND subjects or in VaD or AD. Results suggested that MAP2 immunostaining may be affected by PMD; however there were no differences in mean PMD between groups, and differences in MAP2 staining intensity and distribution could not be solely attributed to PMD. Therefore, these differences may also reflect reorganization of dendrites in response to pathogenic processes associated with disease, cause of death or pre-mortem agonal state. Difficulties interpreting these results were compounded by poor understanding of the functional implications of increased/decreased MAP-2 immunoreactivity on cognitive function. Similar results were found with post-synaptic markers drebrin and PSD-95 using both IHC and

molecular techniques. Further studies to establish the stability of these proteins during the post mortem interval would ensure correct interpretation of findings.

This study established a new technique to quantify dendritic changes using a 3D stereological technique to measure dendritic length density in 30µm thick sections stained for MAP2. However, the usefulness of this technique relies on being able to correctly interpret the findings. Therefore, future studies using this technique could be tested in brain tissue from rapid autopsies or carried out in perfusion fixed tissue from animal models where post-mortem autolysis can be controlled, to ensure that changes to dendritic length density accurately reflect pathogenic processes.

Chapter 6. Hippocampal white matter changes and involvement of astrocytes and microglia

6.1 Introduction

I previously explored potential changes in the structure and function of hippocampal neurons in relation to disease mechanisms that may have contributed to cognitive impairment after stroke. In this study I investigated axonal damage in the hippocampus as a possible mechanism contributing to reduced neuronal volume and cognitive dysfunction. As neuroglia also play a critical role in neuronal and synaptic function and survival, pathological changes to astrocytes and microglia were also examined to assess potential mechanisms contributing to the pathogenesis of delayed PSD.

6.1.1 White matter changes in the alveus

Myelinated axons from hippocampal neurons in the CA subfields form the alveus, a well-defined white matter tract which runs along the transverse axis of the hippocampal formation (Figure 6.1). This relatively simple arrangement with single layers of pyramidal neurons and connective circuitry running along the transverse axis has allowed the organization of hippocampal axonal connections to be better characterized than any other functionally connected cortical areas (Cenquizca and Swanson, 2007). Axons from CA1 neurons project to the alveus where they bifurcate to extend one branch through the fornix to cortical regions, and the other branch to the subiculum and entorhinal cortex. There are also numerous local collateral branches within the CA1 subfield (Cenquizca and Swanson, 2007). Axons from CA2 neurons also project to the alveus, although their projections have been less well characterized. Physiological studies indicate that the majority of CA2 axons projecting to the CA1 terminate in the stratum oriens close to the pyramidal layer, and provide strong synaptic input to the CA1 (Jones and McHugh, 2011; Shinohara *et al.*, 2012). As the alveus contains axons originating from neurons in the hippocampal pyramidal layers, this allows investigation into white matter changes in relation to neuronal and pathological changes previously characterized within these CA subfields.

Few studies have previously examined changes to the white matter of the alveus in stroke or dementia. An MR diffusion tensor imaging (DTI) study of transient neonatal hypoxia-ischemia detected changes to the white matter in the alveus which were associated with severe hippocampal volume loss 24 hours after ischemia (Stone *et al.*, 2008). Another neuroimaging study found changes to the MRI signal in the alveus of middle cerebral artery (MCA) occluded rats 24 after surgery, which was suggested to indicate remote oedema (Izumi *et al.*, 2002). These findings indicate that the white matter of the alveus undergoes pathological changes following hypoxia, which may reflect the well-characterized vulnerability of hippocampal neurons to hypoxic-ischaemic insults. In addition, studies have indicated that axons can become damaged by hypoxic-ischaemic injury through mechanisms independent of the neuronal soma (Pantoni *et al.*, 1996), and oligodendrocytes in the white matter are known to be particularly vulnerable to ischaemic injury and glutamate excitotoxicity (Giaume *et al.*, 2007). Therefore, loss of oligodendrocytes and changes to axonal structure may result in impaired functional connectivity and white matter degeneration without corresponding loss of neuronal cell bodies.

Axonal dysfunction is implicated in AD as the aggregation of hyperphosphorylated tau causes impaired axonal transport. Axonal dysfunction may be a fundamental consequence of AD processes as mouse models of AD overexpressing mutant forms of APP, Presenilin-1 and/or tau demonstrate defective axonal transport (Gallagher *et al.*, 2012). Neuroimaging studies have found evidence of impaired functional connectivity in regions associated with hippocampal axonal projections in amnestic MCI patients, including the hippocampus, parahippocampal gyrus, thalamus and amygdala (Stebbins and Murphy, 2009; Carmeli *et al.*, 2013). These impairments are likely to reflect early pathological changes in hippocampal projection neurons which are affected early in disease progression. As the disease becomes more severe and these neurons degenerate, the hippocampal formation becomes isolated from its inputs and outputs, resulting in worsening of memory impairments (Hyman *et al.*, 1984). Therefore, a similar situation may arise in CVD where susceptible neurons and axons are lost after hypoxic-ischaemic injury, resulting in loss of connections to and from the hippocampus. Therefore, I reasoned that loss of and damage to the white matter in the alveus, indicating impaired structural connectivity of hippocampal neurons, may

contribute to cognitive impairment and be associated with reduced soma volume and/or reduced neuronal density in stroke survivors.

Typically, post-mortem microscopic studies of white matter damage in CVD and dementia have investigated the loss of or damage to myelin as an indicator of axonal damage and dysfunction (Deramecourt *et al.*, 2012; Smallwood *et al.*, 2012). These studies frequently use the histological dye Luxol fast blue (LFB), which stains myelinated axons deep blue (Figure 6.1 B). Areas of pale staining or no staining therefore reflect destruction of the myelin and white matter infarcts (Deramecourt *et al.*, 2012). Although it is not well understood whether loss of myelin reflects loss of axons, it is assumed that loss of myelin will at least indicate areas of axonal dysfunction and impaired functional connectivity, due to the slowing or loss of signal transmission. To complement this technique, it can be useful to also use immunohistochemistry for myelin components or axonal proteins. Degraded myelin basic protein (dMBP) is a pathologically exposed epitope of myelin basic protein (MBP) which is detected in areas of demyelination, white matter damage and focal ischaemic damage (Ihara *et al.*, 2010). IHC to dMBP has been shown to stain degenerating myelin sheaths and abnormal appearing oligodendrocytes in damaged areas in VaD and hereditary forms of VaD (Yamamoto *et al.*, 2009; Ihara *et al.*, 2010).

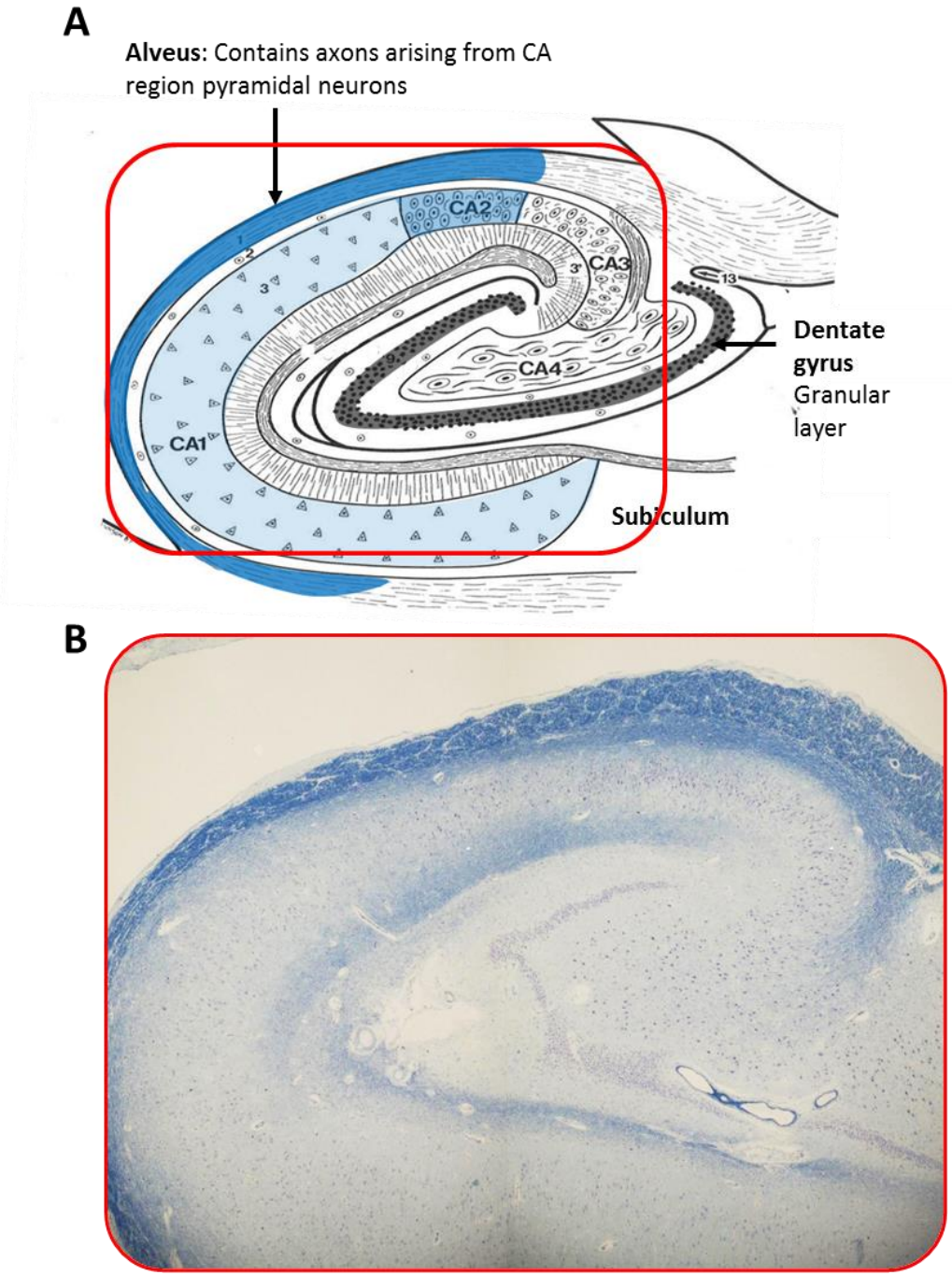

Figure 6.1 A, Diagram of the alveus in the hippocampal formation (dark blue), adapted from (Duevernoy, 2005); B, Image of a hippocampal section stained using LFB to visualize myelin in the alveus, with CFV counterstain to visualize neuronal cell bodies in the pyramidal layers and dentate gyrus.

6.1.2 Neuroglia in stroke and AD

Astrocytes

The integral role of astrocytes in maintaining neuronal function during ischaemic injury and their involvement in synaptic plasticity and neuronal connectivity suggests that astrocytes are likely to be involved in the pathogenesis of the hippocampal neuronal changes investigated in my previous studies. Astrocytes are believed to contribute to the selective vulnerability of neuronal populations such as the CA1 to ischemia, however their precise role remains unclear (Nedergaard and Dirnagl, 2005).

Pathological increases in numbers of reactive astrocytes (astrogliosis) forms part of the brain's defence system to contain lesions and aid remodelling of affected neuronal circuitry (Sofroniew, 2009). Reactive astrogliosis describes a spectrum of astrocytic cellular changes; from mild, reversible changes which are likely to resolve the initial trigger, to an extreme response to tissue lesions and inflammation where astrocytes proliferate, overlap, and form glial scars. The activation of astrocytes has been suggested to contribute to neuronal dysfunction and degeneration, as when astrocytes become reactive their normal supportive functions become impaired (Sofroniew, 2009).

Hippocampal astrogliosis has been reported in animal models of stroke preceding and continuing after neurodegeneration in the CA1 (Tanaka *et al.*, 1992; Briones *et al.*, 2006; Okada *et al.*, 2013). An increase in the number of reactive astrocytes was found in the hippocampus of a rodent model of chronic cerebral hypoperfusion 10 weeks after surgery, which was correlated with impairments in glutamate uptake and cognitive impairment (Vicente *et al.*, 2009). In AD, there is an abnormal increase in the number of reactive astrocytes around Aβ plaques, which take up substantial amounts of Aβ-42 and neuronal debris, and may ultimately cause the astrocytes to lyse forming small GFAP-rich astrocytic amyloid plaques (Nagele *et al.*, 2004).

These findings implicate astrogliosis in the pathogenesis of delayed PSD through activation and/or possible dysfunction after hypoxic injury and neurodegenerative disease processes. Therefore, I investigated changes to the numbers of astrocytes and reactive astrocytes in the hippocampus in relation to neuronal and clinicopathological findings in the CogFAST cohort.

Historically, immunohistochemical studies on astrocytes have used antibodies to GFAP, a cyto-architectural protein found in the main branches of reactive astrocytes, to detect astrocytes. However, GFAP is therefore not a marker of all astrocytes as it is not expressed in non-reactive astrocytes in healthy brain tissue (Sofroniew and Vinters, 2010). Studies using GFAP may have led to the over-estimation of the proliferation of astrocytes in response to brain lesions, as perceived increases in numbers of GFAP-positive astrocytes may have simply reflected increased numbers of activated astrocytes, though the total number remained unchanged (Barreto *et al.*, 2011). Recent studies have identified the protein Aldh1L1 (also known as 10-formyltetrahydrofolate dehydrogenase (FDH)), as a highly specific marker for astrocytes expressed in most if not all astrocytes in healthy tissue (Barres, 2008; Cahoy *et al.*, 2008). This relatively new marker therefore allows more reliable investigations into astrocyte numbers in neurodegenerative disease (compare Figure 6.2 A and B). However, no markers have yet been proven to be entirely specific for and ubiquitously expressed in all astrocytes (Oberheim *et al.*, 2012). At the time of planning this study, there were no previous reports of Alhd1L1-posisitve astrocytes in dementia studies.

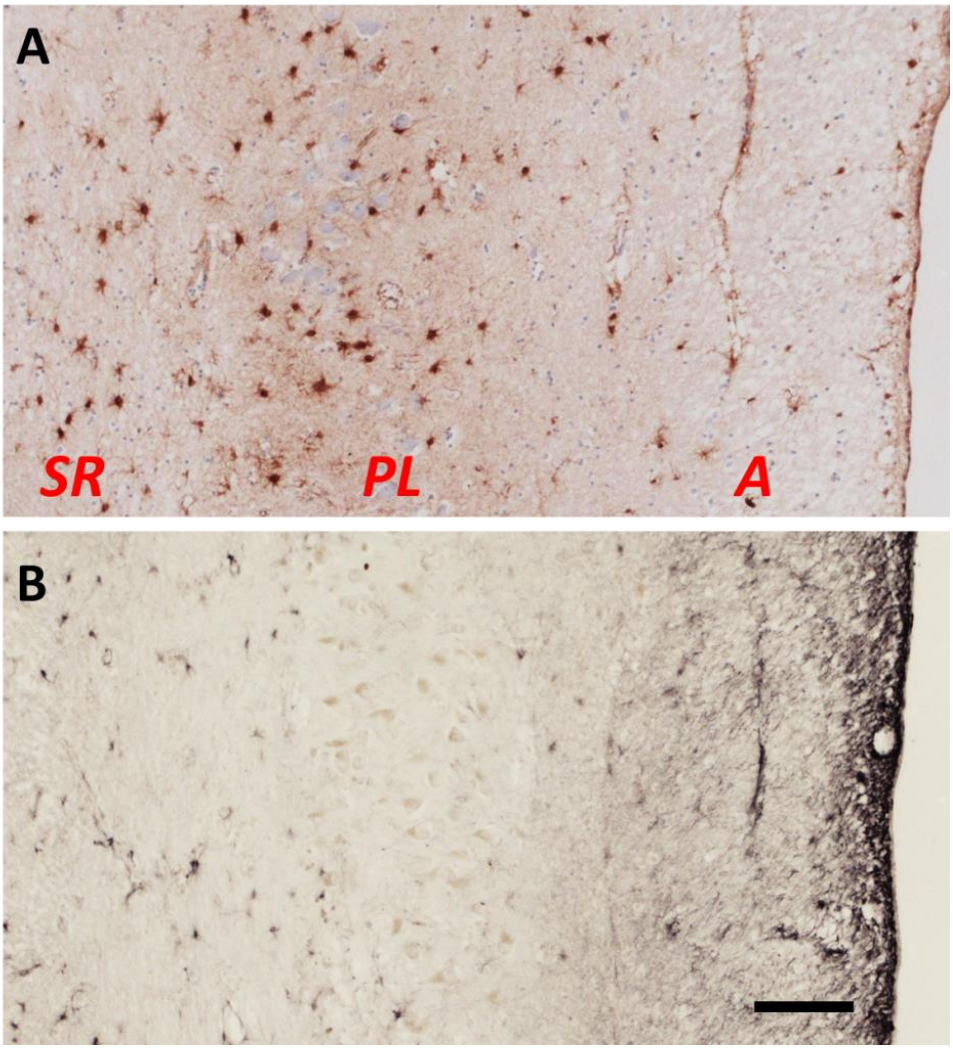

Figure 6.2. Comparing methods to identify astrocytes in the CA2 subfield of a control subject. A, using antibodies to Aldh1L1, DAB stained brown with a very pale hematoxylin counterstain; B, antibodies to GFAP, nickel-DAB stained black, with no counterstain although neurons are still visible in the pyramidal layer as pale brown. There are noticeably fewer astrocytes positive for GFAP (B) than Aldh1L1 (A), particularly in the pyramidal layer. SR = stratum radiatum, PL = pyramidal layer, A = alveus. Scale bar = 100µm.

Microglia

Microglia can also influence neuronal survival after injury through their dual role in neuroprotective and neurotoxic processes. Ramified microglia have a neuroprotective role in releasing neurotrophic factors and removing excess glutamate and cell debris from the neuropil (Vinet *et al.*, 2012), and when activated, microglia are involved in lesion repair and tissue remodelling (Perego *et al.*, 2011). However, activated microglia can also promote neurotoxicity, blood-brain barrier dysfunction and oedema through the release of inflammatory components such as IL-1β, TNF-α, proteases and reactive oxygen species (Nedergaard and Dirnagl, 2005). Aβ plaques also stimulate a neurotoxic

inflammatory response in microglia, which is considered to have an important role in causing neurodegeneration in AD (Akiyama *et al.*, 2000; Meraz Rios *et al.*, 2013). One antigen commonly used to identify activated microglia is CD68, a lysosomal protein expressed during active phagocytosis. Microglia have been shown to engulf Aβ (Meraz Rios *et al.*, 2013) and degenerating neurons, which may have a beneficial effect in removing irreversibly damaged neurons after injury. I hypothesised that an increase in CD68 immunoreactivity would be associated with poorer cognitive outcome after stroke, reflecting activation of microglia in response to greater cerebrovascular and/or neurodegenerative injury in elderly stroke survivors.

6.2 Aims

Damage to the white matter in the alveus was investigated using LFB stained sections to assess myelin integrity and antibodies to dMBP to assess myelin breakdown and pathological accumulation in oligodendrocytes. Based on the known vulnerability of white matter to CVD, hippocampal neuron loss and volume reductions in PSD, VaD and AD, and disruptions to hippocampal connectivity contributing to cognitive dysfunction in these disorders, I reasoned that greater white matter damage would be found in stroke subjects who developed delayed PSD compared to controls and non-demented stroke survivors from the CogFAST cohort. I was also interested in determining whether the white matter was differentially affected in CVD and AD.

As neuronal function is now widely believed to rely on neuroglial support, I investigated astrocyte numbers and activation of astrocytes and microglia in the hippocampus of post-stroke and ageing-related dementia subjects.

I hypothesised that loss of astrocytes may be related to secondary neuronal cell death after stroke, and therefore investigated total astrocyte numbers using IHC to Aldh1L1 to visualize both activated and non-activated astrocytes. The number of activated astrocytes was also investigated using IHC to GFAP, to elucidate whether there was differential astrocyte activation in PSD and PSND subjects, and elderly subjects with VaD and AD. As astrocytes have a critical role in regulating synapses and white matter changes, Aldh1L1-positive and GFAP-positive astrocytes densities were separately

analysed for different layers of the hippocampus (the CA1 and CA2 pyramidal layer (PL), stratum radiatum (SR), alveus, and CA3 and CA4 pyramidal subfields) to determine whether astrocytes in different layers were differentially affected in post-stroke survivors, VaD and AD.

Microglia are implicated in the pathogenesis of delayed neuronal death after ischemia and in the pathogenesis of AD. Therefore, I investigated levels of reactive CD68-positive microglia to assess whether differences in microglial responses were associated with different cognitive outcomes and pathological processes in post-stroke survivors, VaD and AD subjects.

6.3 Methods

6.3.1 Histological and IHC staining

Sections were stained using Luxol fast blue with Cresyl fast violet counterstain as described in section 2.5.2. Immunohistochemistry for degraded myelin basic protein (dMBP), astrocyte markers glial-fibrillary acidic protein (GFAP) and Aldh1L1, and microglia marker CD68 were performed according to protocol described on 2.6. GFAP was visualized using nickel-DAB to increase the contrast and make it easier to identify astrocyte cell bodies.

6.3.2 Image analysis

LFB

LFB staining in the alveus was assessed using Image Pro to calculate %PA and IOD staining in the CA1 and CA2 as described on section 2.7.3. Images were taken at 10X magnification, and areas of a standardized size were analysed from the CA1 and CA2 alveus, and ECV white matter. Myelin index was also calculated as described on section 2.7.3 and in (Yamamoto *et al.*, 2009), from low power scanned images of the hippocampal formation, within which the white matter tract around the CA2-CA1 was delineated for analysis as one region of interest.

dMBP in the alveus and neurons

dMBP staining was assessed in the alveus using Image Pro as described in section 2.7.2

from images taken at 20X magnification. Based on previous investigation using LFB, the alveus was analysed as one area of interest rather than sub-dividing into CA1 and CA2. Unexpected intense neuronal soma staining was found in the pyramidal layers of the CA regions, and was investigated using Image Pro analysis of dMBP immunopositive staining in the CA1 and CA2 pyramidal subfields. Semi-quantitative rating of myelin integrity (Figure 6.3) and dMBP staining (Figure 6.4) in the alveus and pyramidal layer was also conducted based on a 0-3 scale.

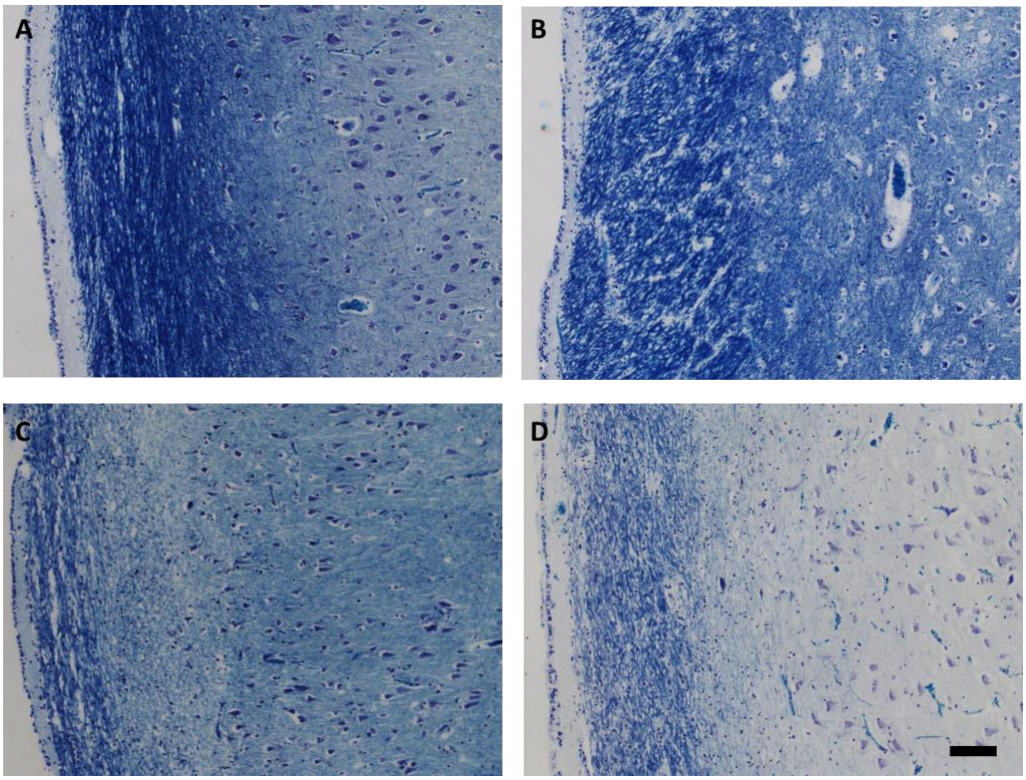

Figure 6.3. Representative images of the alveus stained using LFB to visualize myelin. A, PSND; B, PSD; C, PSD; D PSND. Scale bar = 100µm.

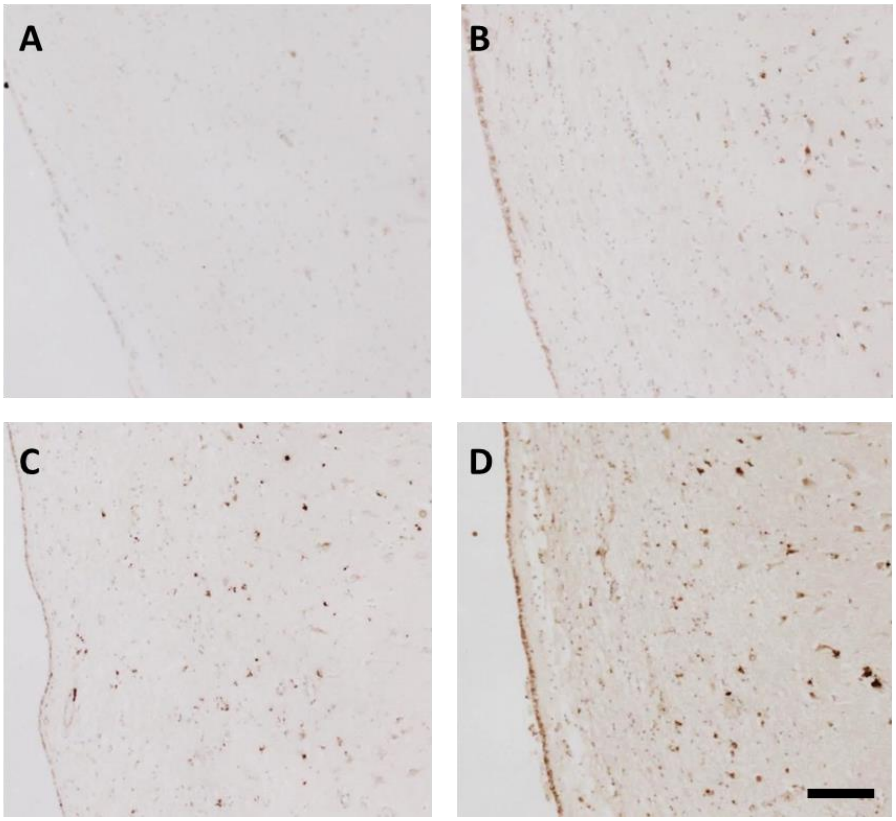

Figure 6.4 Representative images of dMBP staining rating in the alveus (CA1). A, 0 = none; B, 1 = mild; C, 2 = moderate; D, 3 = severe. Scale bar = 100µm.

Neuronal Pyknosis Rating

As pyknotic-appearing neurons had been related to neuronal volumes in the non-human primate (baboon) model, the severity of the number pyknotic appearing neurons were visually rated on a 4 point scale from 0 (no pyknotic appearing neurons) to 3 (many/all pyknotic appearing neurons) in the human cohort (Figure 6.5), stained using H & E as described in section 2.5.3.

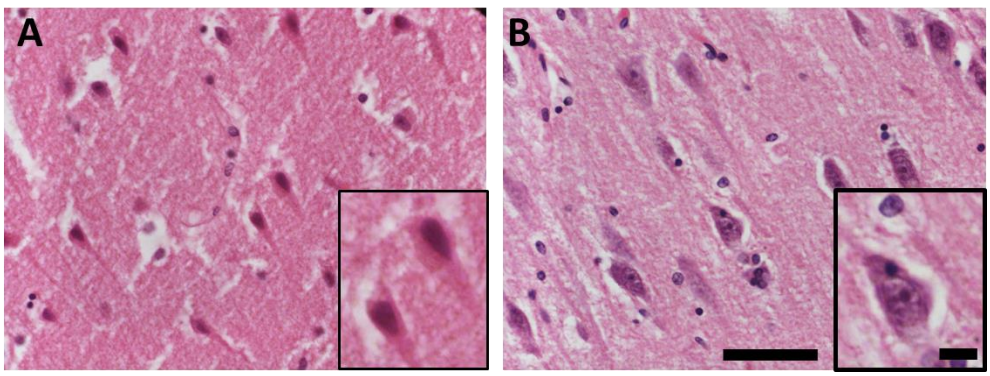

Figure 6.5 Pyramidal neurons in the CA1 stained using H&E. A, Pyknotic appearing pyramidal neurons (PSD); B, normal appearing pyramidal neurons with clear nucleolus (PSND). Scale bar large images = 50µm, small images = 10µm.

Astrocyte Density

Astrocyte density was calculated using a counting grid as described in section 2.7.4, where each grid square had an area equivalent to 0.08mm^2 (283.3 x 283.3µm) (Figure 2.5). Astrocyte counts were performed in the CA1 and CA2 alveus, pyramidal layer and stratum radiatum, the CA3 pyramidal layer and whole CA4 subfield. The mean number of astrocytes per grid square was calculated from which the number of astrocytes per 0.8mm^2 was calculated and expressed as astrocyte density.

6.3.3 Statistical analysis

PMD, fixation length and measures of LFB and dMBP staining were not normally distributed and were therefore analysed using non-parametric tests. Associations between ratings and dementia status were analysed using χ^2 test with Phi and Cramer's V. GFAP-positive astrocyte counts were normally distributed and analysed using parametric tests, whereas Aldh1L1-positive astrocyte counts were non-normally distributed and analysed using non-parametric tests. CD68 group demographics and data were normally distributed and analysed using parametric tests as described in section 2.1.

6.4 Results

6.4.1 White matter changes in the alveus

Demographics of subjects studied for LFB, dMBP and pyknosis are shown in Table 6.1. There were no differences in age, PMD or fixation length between groups.

Group	**N**	**Age** Mean (range)	**Fixation length, weeks** Mean (range)	**PMD, hours** Mean (range)	**Braak Stage** Median (range)	**CERAD score** Median (range)
Controls	7	83.5 (74-94)	10.1 (6-16)	31 (15-67)	2 (0-4)	0 (0-1)
PSND	10	83.3 (78-89)	8.9 (3-20)	36.7 (11-76)	2 (1-4)	2 (1-2)
PSD	12	84.4 (76-93)	9.1 (2-26)	41.9 (10-81)	3 (0-6)	2 (0-3)
AD	8	82.4 (70-91)	9 (6-20)	41.1 (6-72)	5 (4-6)	3 (3-3)

Table 6.1 Demographics of groups analysed for LFB, dMBP and pyknosis rating studies.

LFB analyses

There were no differences in myelin staining between groups in CA1 or CA2 (%PA, mean IOD or myelin index) (Figure 6.6 A, B). There were no correlations between myelin staining and CAMCOG scores, Braak stage, CERAD score, age, PMD or fixation. EC mean IOD was negatively correlated with Braak stage and CERAD score ($r = -0.505$ $p = 0.002$ and $r = -0.478$ $p = 0.007$ respectively). There were no associations between semi-quantitative rating of myelin loss (LFB staining patchiness) and dementia status or dMBP stain rating (Figure 6.7). Frequency tables of myelin ratings are presented in Appendix Table 8.9.

CA1 LFB IOD was positively correlated with CA1, CA2 and CA4 neuronal volumes ($r = 0.401$, $r = 0.512$ and $r = 0.445$ respectively, all $p < 0.05$). CA2 LFB IOD was also positively correlated with CA1, CA2 and CA4 neuronal volumes ($r = 0.437$, $r = 0.474$, $r = 0.515$, $p < 0.05$) and was negatively correlated with CA2 neuronal density ($r = -0.4$, $p = 0.043$).

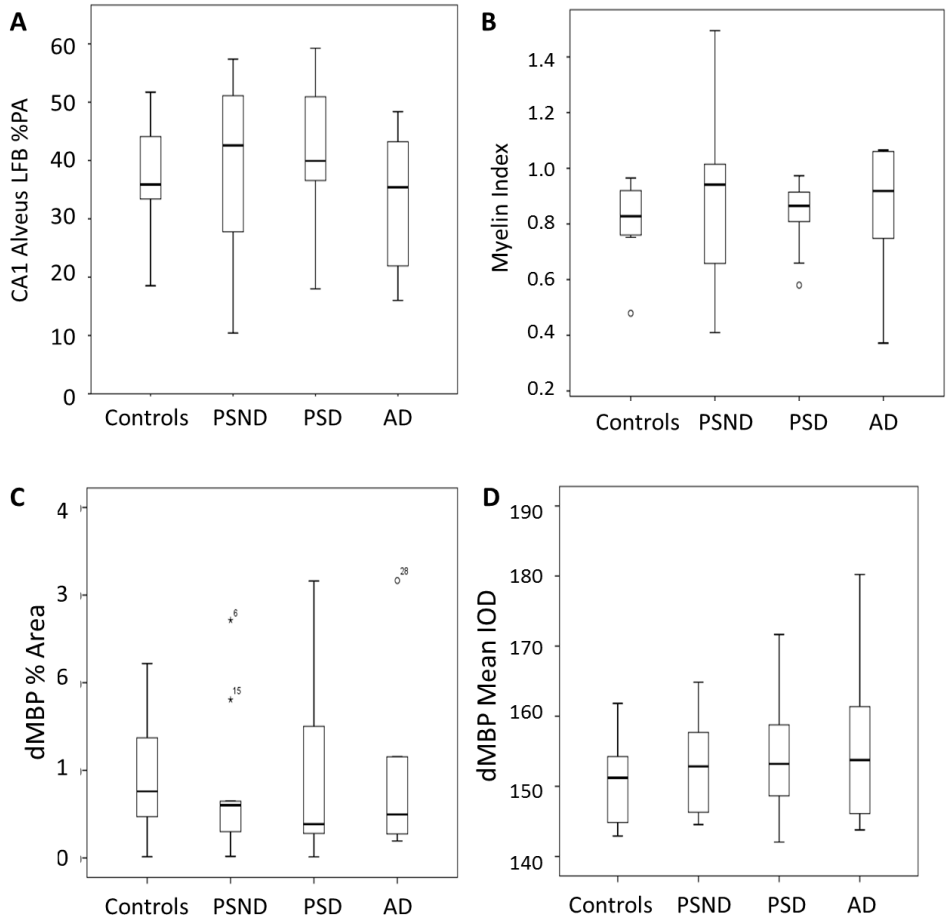

Figure 6.6 A, Area of myelin stained using LFB in the alveus adjacent to CA1 (%PA); B, and CA2 (%PA); C, Area of the CA1 alveus immunoreactive for dMBP (%PA); D, Mean intensity (IOD) of dMBP staining in the CA1 alveus.

dMBP analyses

There were no differences in dMBP %PA or IOD staining in the alveus between groups (Figure 6.6 C, D). There were no correlations between dMBP immunoreactivity and Braak stage, CERAD score, CAMCOG score, fixation time or age, however dMBP IOD in the alveus was negatively correlated with PMD ($r = -0.428$, $p = 0.014$).

dMBP %PA staining was negatively correlated with temporal lobe vascular pathological burden ($r = -0.564$, $p = 0.019$) and CA4 neuronal density ($r = -0.458$, $p = 0.032$). There were no correlations between myelin staining (LFB %PA, IOD or myelin index) and dMBP staining (%PA or IOD) (Figure 6.6). dMBP staining rating was not associated with dementia status.

6.4.2 Neuronal dMBP staining

There were no differences in dMBP %PA or mean IOD in the CA1 or CA2 pyramidal layers between groups (Figure 6.6). CA2 dMBP IOD was positively correlated with Braak stage (r = 0.416, p = 0.002) and CERAD score (r = 0.528, p = 0.003). There were no correlations between dMBP neuronal staining and CAMCOG scores, PMD, fixation, or age. Neuronal dMBP staining was positively correlated with dMBP staining in the alveus (Table 6.2). There were no associations between dementia status and neuronal dMBP staining rating.

			CA1		CA2		Alveus	
			%PA	IOD	%PA	IOD	%PA	IOD
CA1	%PA	r	-					
		p						
	IOD	r	0.22	-				
		p	0.235					
CA2	%PA	r	0.789	0.256	-			
		p	<0.001	0.164				
	IOD	r	0.487	0.61	0.491	-		
		p	0.006	<0.001	0.005			
Alveus	%PA	r	0.576	0.283	0.445	0.569	-	
		p	0.002	0.153	0.02	0.002		
	IOD	r	0.313	0.406	0.352	0.619	0.532	-
		p	0.112	0.036	0.072	0.001	0.002	

Table 6.2 Correlations between dMBP staining in the alveus and neuronal soma (pyramidal layer). Dark grey highlights correlations p < 0.001, light grey highlights p < 0.05.

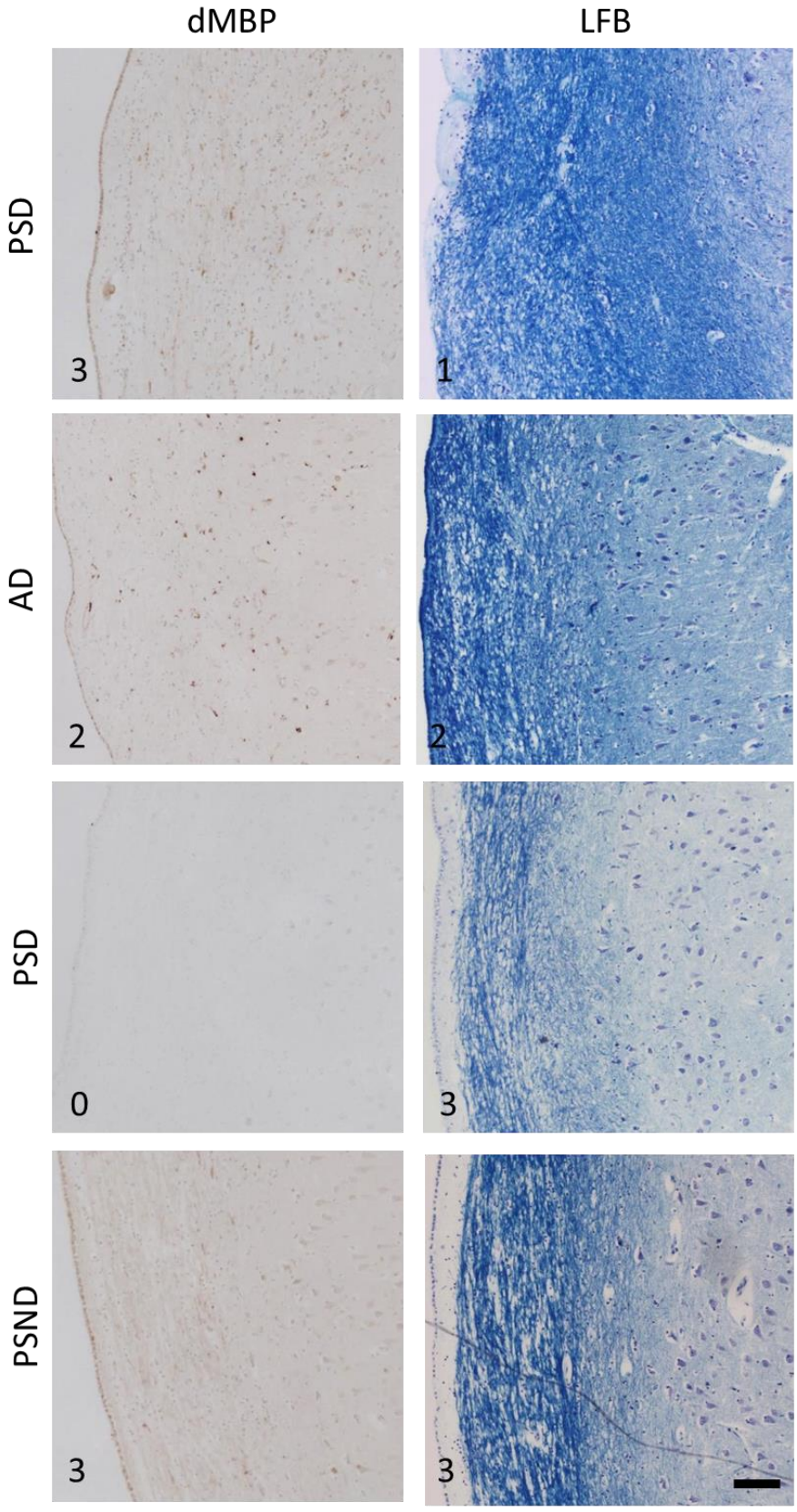

Figure 6.7 Comparison of dMBP immunopositive staining and LFB myelin staining in serial sections from the same cases. Numbers indicate rating score where 0 = none, 1 = mild, 2 = moderate, 3 = severe. There were no relationships between dMBP and myelin damage. Scale bar = 100µm.

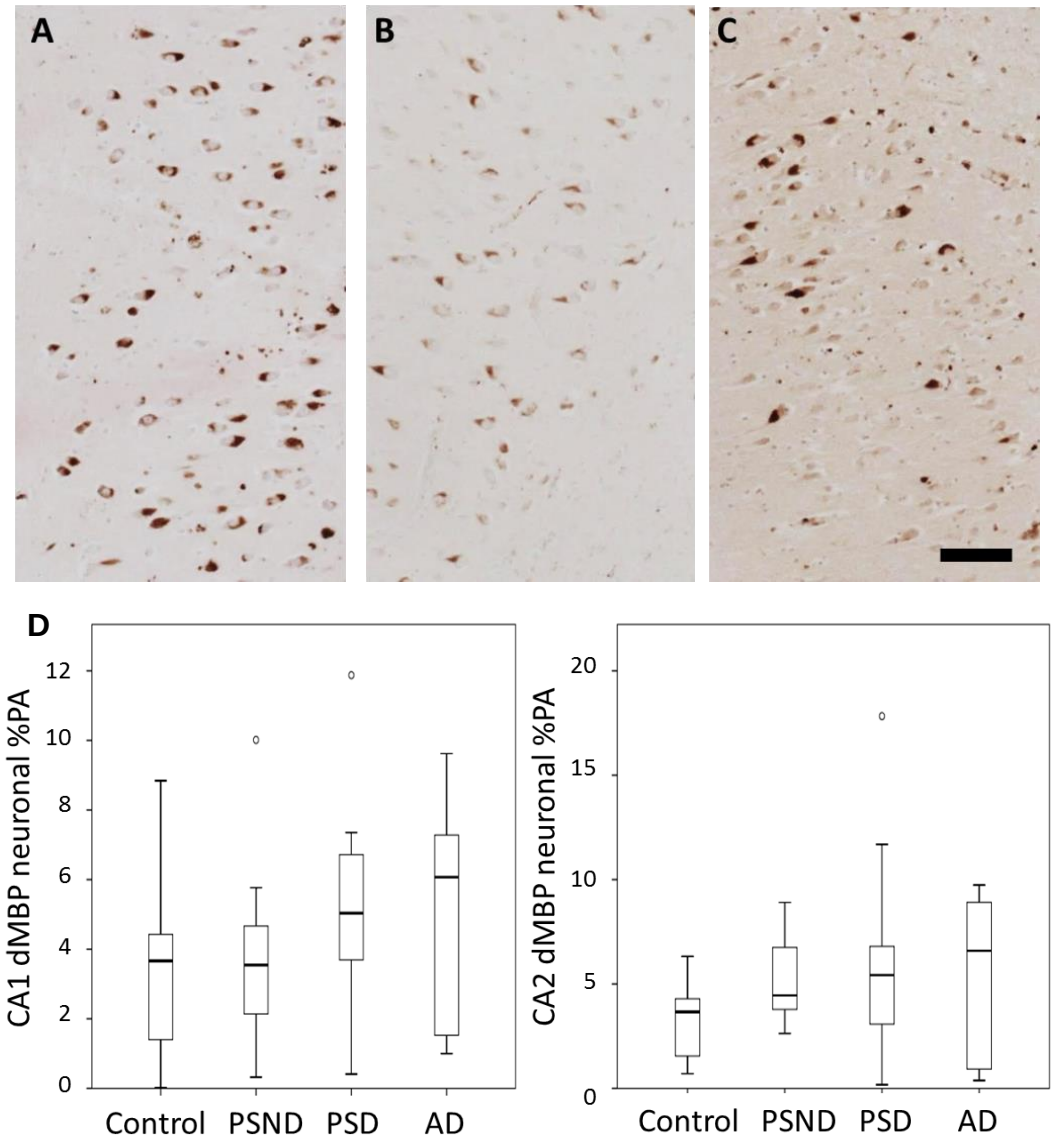

Figure 6.8. Immunopositive dMBP staining in soma of CA1 neurons in controls (A, B) and PSD (C), Scale bar = 50µm; D, box plots of neuronal dMBP immunoreactivity in CA1 and CA2.

6.4.3 Neuronal pyknosis rating

There were no differences in pyknosis rating between groups, and no correlations between pyknosis rating and clinical or pathological features including neuronal volumes and densities. There was a broad spread of ratings in the disease groups, although all control cases were rated as 0 or 1.

6.4.4 Astrocyte density

Demographics of subjects analysed for astrocyte counts are shown in Table 6.3. There were no significant differences in mean age, PMD or fixation between groups.

Group	**N**	**Age, years** Mean (range)	**Fixation length, weeks** Mean (range)	**PMD, hours** Mean (range)	**Braak Stage,** Median (range)	**CERAD score,** Median (range)
Controls	8	81.8 (74-91)	10 (6-16)	34 (15-67)	N/A	N/A
PSND	9	84.4 (79-89)	9 (3-20)	41.8 (11-76)	2 (1-4)	2 (0-2)
PSD	11	83.6 (76-93)	11 (5-26)	39.6 (10-81)	3 (0-6)	2 (0-3)
AD	7	82.6 (70-91)	9 (6-20)	36.7 (6-72)	5 (4-6)	3 (3)

Table 6.3. Group demographics of subjects analysed using astrocyte counts.

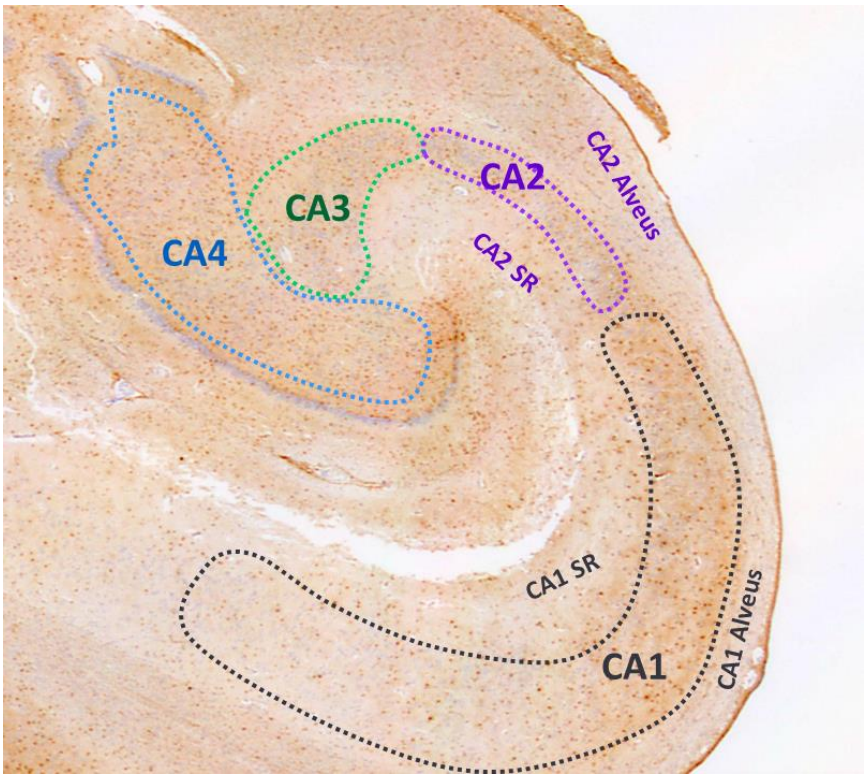

Figure 6.9. Diagram showing the areas where astrocyte densities were calculated. Section from a PSND subject, stained to visualize Aldh1L1.

GFAP-positive astrocytes

There were no significant differences in GFAP-positive astrocyte densities between groups in any regions sampled. Group mean astrocyte densities are presented in Appendix Table 8.10. There was a trend to a difference in CA2 GFAP-positive astrocyte density in the pyramidal layer [F = 2.387 (df 24), p= 0.085] (Figure 6.10 A). GFAP-positive astrocyte densities were positively correlated between regions analysed (see Appendix page 193 for values). There were no correlations with CAMCOG scores, age, PMD or fixation.

There were positive correlations between GFAP-positive astrocyte densities and AD pathological burden; astrocyte density in the CA1 and CA2 pyramidal layer (PL) and CA2 stratum radiatum (SR) was correlated with Braak stage (all r >0.42, p < 0.05), and CA2 PL astrocyte density was correlated with CERAD score (r = 0.504, p = 0.012). Conversely, there were negative correlations between GFAP-positive astrocyte density and vascular pathological burden; CA1 PL and SR was correlated with global (r = -0.82, r = 583) and temporal lobe vascular pathological burden (r = -0.582, r = -0.672 all p = < 0.05), and CA3 PL astrocyte density was negatively correlated with global vascular pathology burden (r = - 0.607, p = 0.036).

GFAP-positive astrocyte density in the CA1 SR was negatively correlated with dendritic length-density (r = -0.709, p = 0.007). There were positive correlations between GFAP-positive astrocyte density and neuronal volumes and densities: CA1 and CA2 alveus astrocyte densities were positively correlated with CA1 neuronal volumes (r = 0.524, r = 0.572 p < 0.02) and CA4 neuronal volumes (r = 0.609, r = 0.574, p< 0.02); CA2 SR astrocyte densities were positively correlated with CA4 and ECV neuronal density (r = 481, r = 0.528, p<0.05). GFAP-positive astrocyte density in the CA2 PL was negatively correlated with ECV neuronal volumes (r = -0.833, p < 0.001).

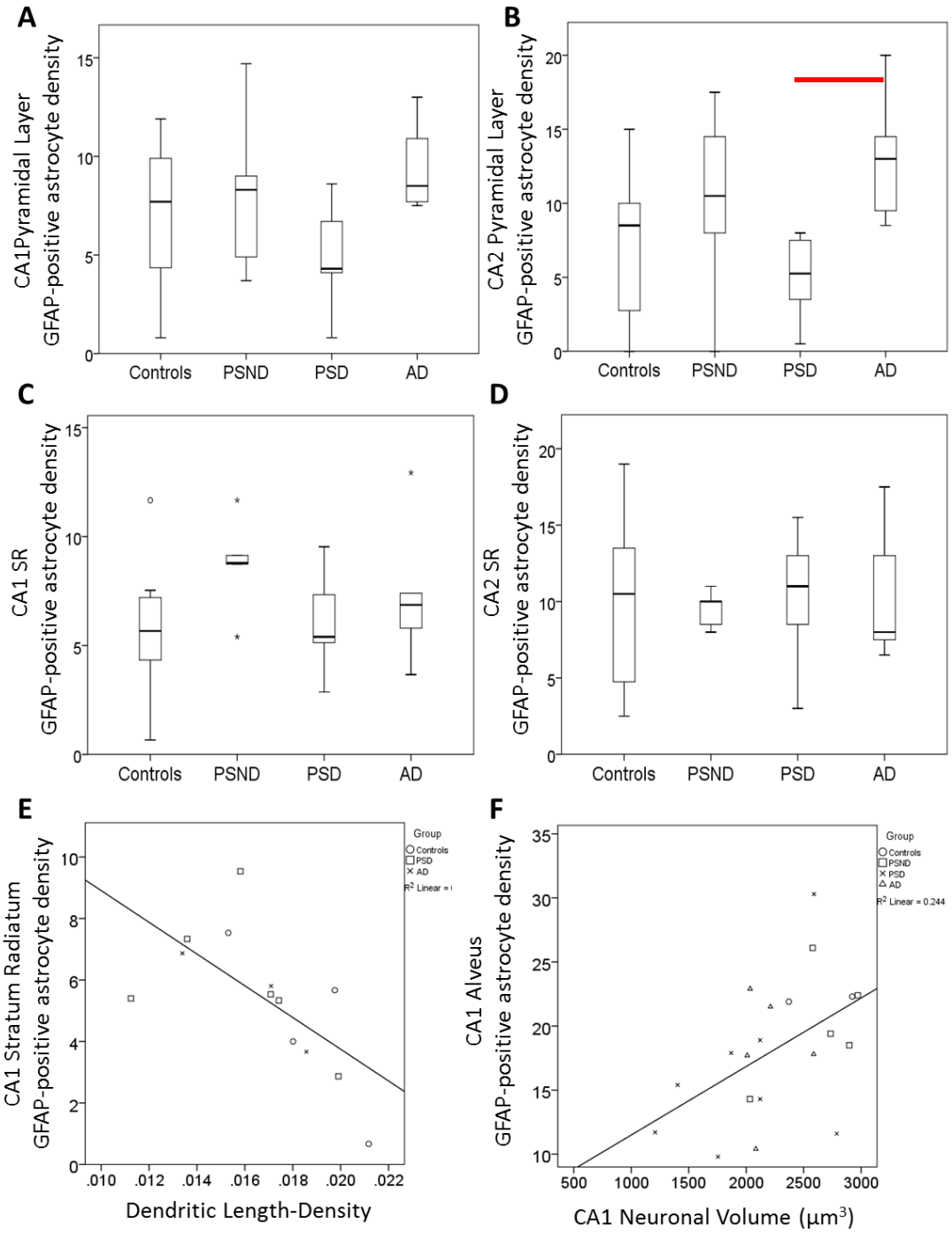

Figure 6.10. GFAP-positive astrocyte density in A, CA1 pyramidal layer; B, CA2 pyramidal layer; C, CA1 stratum radiatum; D, CA2 stratum radiatum; E, Negative correlation between GFAP-positive astrocyte density and dendritic length density in the CA1 stratum radiatum; F, Positive correlation between astrocyte density and CA1 neuronal volume. Dotted red lines indicate trend to significant difference ($p < 0.1$), solid red lines indicate significant difference ($p < 0.05$).

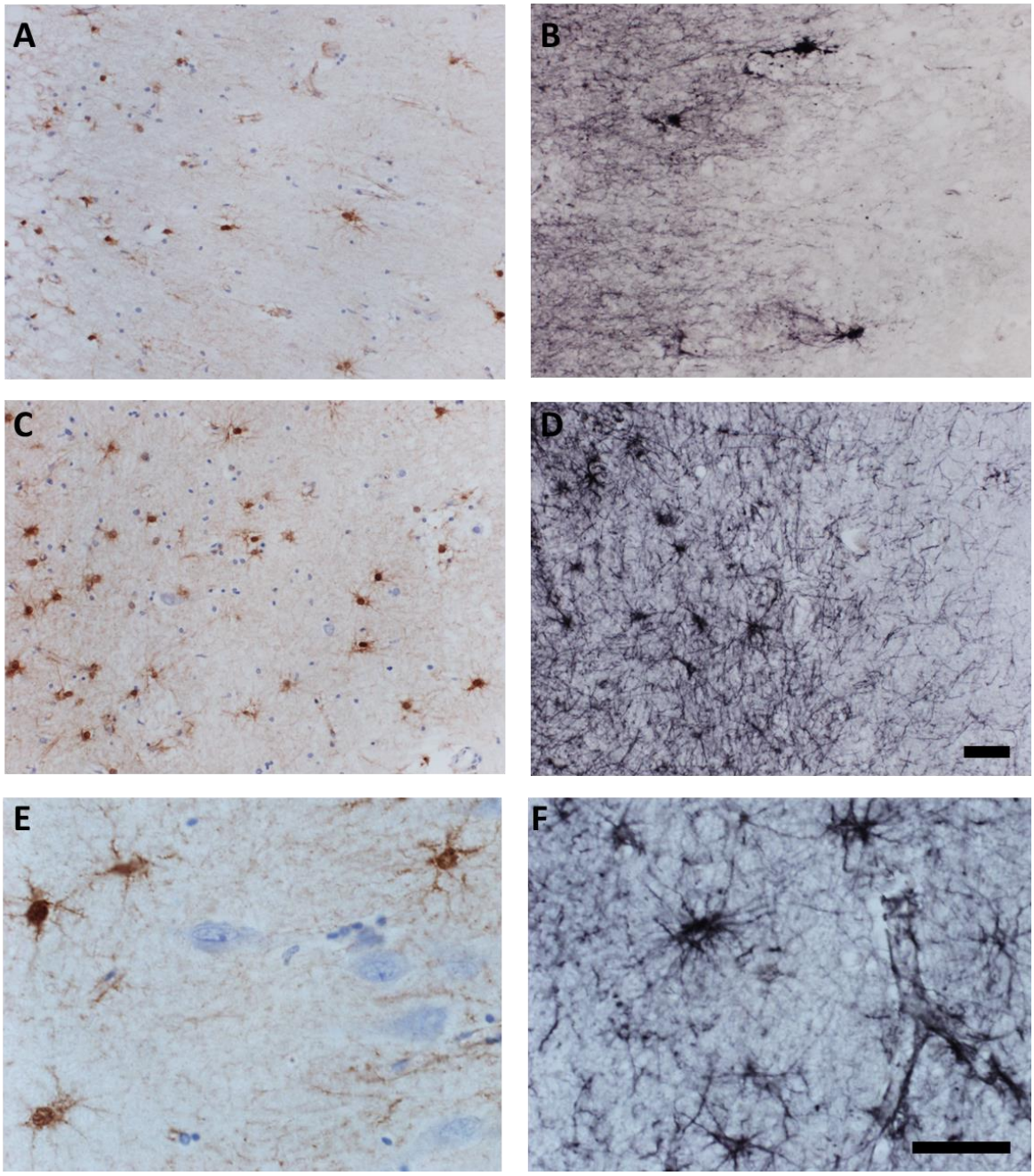

Figure 6.11 Representative images of Aldh1L1-positive astrocytes stained brown using DAB (A, C, E) and GFAP-positive astrocytes stained black using nickel-DAB (B, D, F). A and B are from the CA1 stratum radiatum / moleculare of an AD subject; C and D are from the CA1 stratum radiatum / moleculare of a PSND subject; E and F are high-power representative images of Aldh1L1-positive astrocytes and GFAP-positive astrocytes in the CA1 of the PSND subject. Scale bar in A-D = 100µm, E-F = 50µm.

Aldh1L1-positive astrocyte density

There were no differences in Aldh1L1-positive astrocyte densities between groups in any of the regions studied (Figure 6.12). There was a trend to the PSD group having greater Aldh1L1-positive astrocyte density than controls in the CA1 stratum radiatum ($p = 0.069$), and the AD group having greater astrocyte density than PSND in the CA4 ($p = 0.054$) (Figure 6.10 C). Aldh1L1-positive astrocyte densities were positively correlated between regions (see Appendix page 193 for values). There were no correlations with CAMCOG scores, Braak stage, CERAD score, age, PMD or fixation.

Aldh1L1-positive astrocyte densities were negatively correlated with vascular pathological burden; CA1 and CA2 pyramidal layer astrocyte density with global vascular pathology ($r = -0.487$, $p = 0.04$ and $r = -0.603$, <0.001) (Figure 6.12 D), and CA2 pyramidal layer with temporal lobe vascular pathological burden ($r = -0.595$, $p = 0.009$).

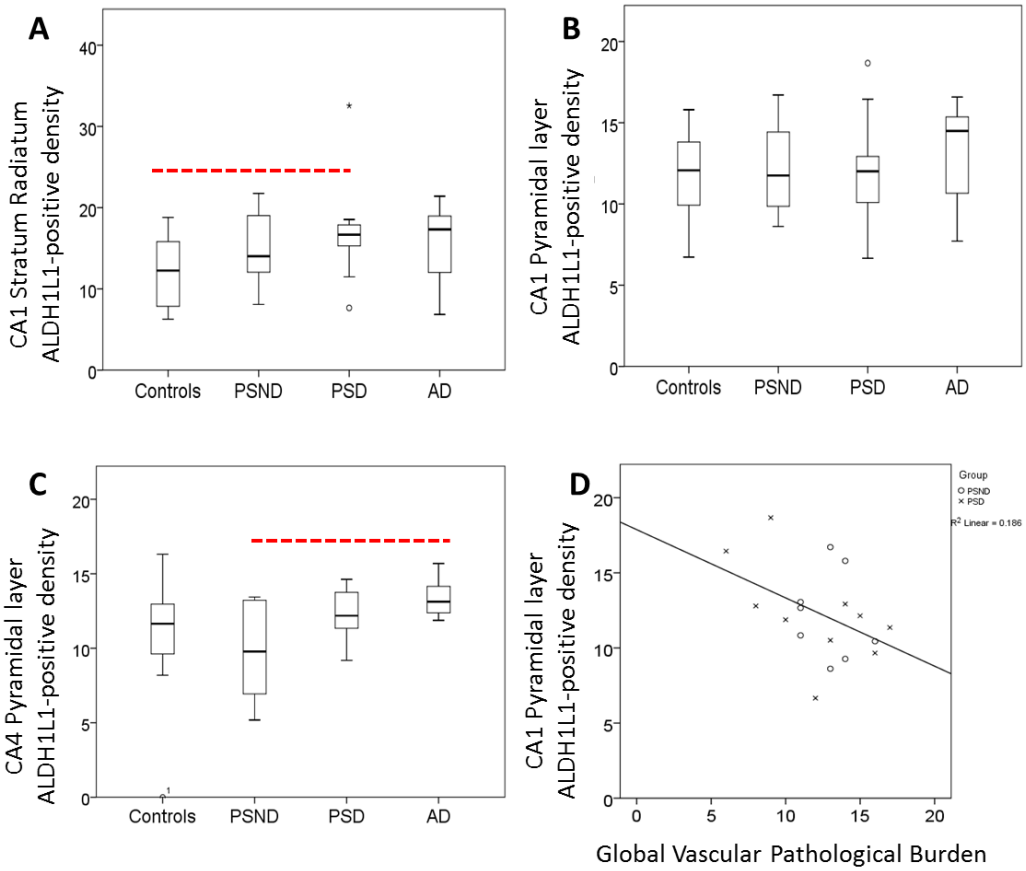

Figure 6.12. Aldh1L1-positive astrocyte densities in the CA1 stratum radiatum (A) and pyramidal layer (B), and CA4 (C); D, Correlation between CA1 pyramidal layer Aldh1L1-positive astrocyte density and global vascular pathological burden.

Aldh1L1 versus GFAP-positive astrocyte densities

Aldh1L1-positive astrocyte densities were different to GFAP-positive astrocyte densities in all layers analysed ($p < 0.001$). In the CA1 SR, CA1 PL and CA2 SR, Aldh1L1 positive astrocyte densities were 2-3 fold greater than GFAP, whereas in the CA1 and CA2 alveus GFAP-positive densities were around twice as high as Aldh1-L1 (Figure 6.13).The ratio of Aldh1L1 : GFAP – positive astrocyte densities in the CA1 SR and PL were higher in the PSD group than the PSND group ($p = 0.012$ and $p = 0.06$), and higher than the AD group in the CA1 PL ($p = 0.004$)(Figure 6.13).

Aldh1L1-positive astrocyte densities in the CA1 pyramidal layer (PL) were positively correlated with GFAP-positive astrocyte densities in the CA1 PL, SR, and CA2 PL ($r > 0.4$, $p < 0.5$). Aldh1L1-positive astrocyte densities in the CA2 PL were positively correlated with GFAP-positive astrocyte densities in the CA1 and CA2 PL, and CA1 and CA2 SR ($r > 0.4$, $p < 0.05$).

GFAP-positive and Aldh1L1-positive astrocyte densities were significantly greater in the CA1 and CA2 pyramidal layer than the alveus ($p < 0.001$), though there was no difference in densities between the CA1 and CA2 pyramidal layer and the stratum radiatum.

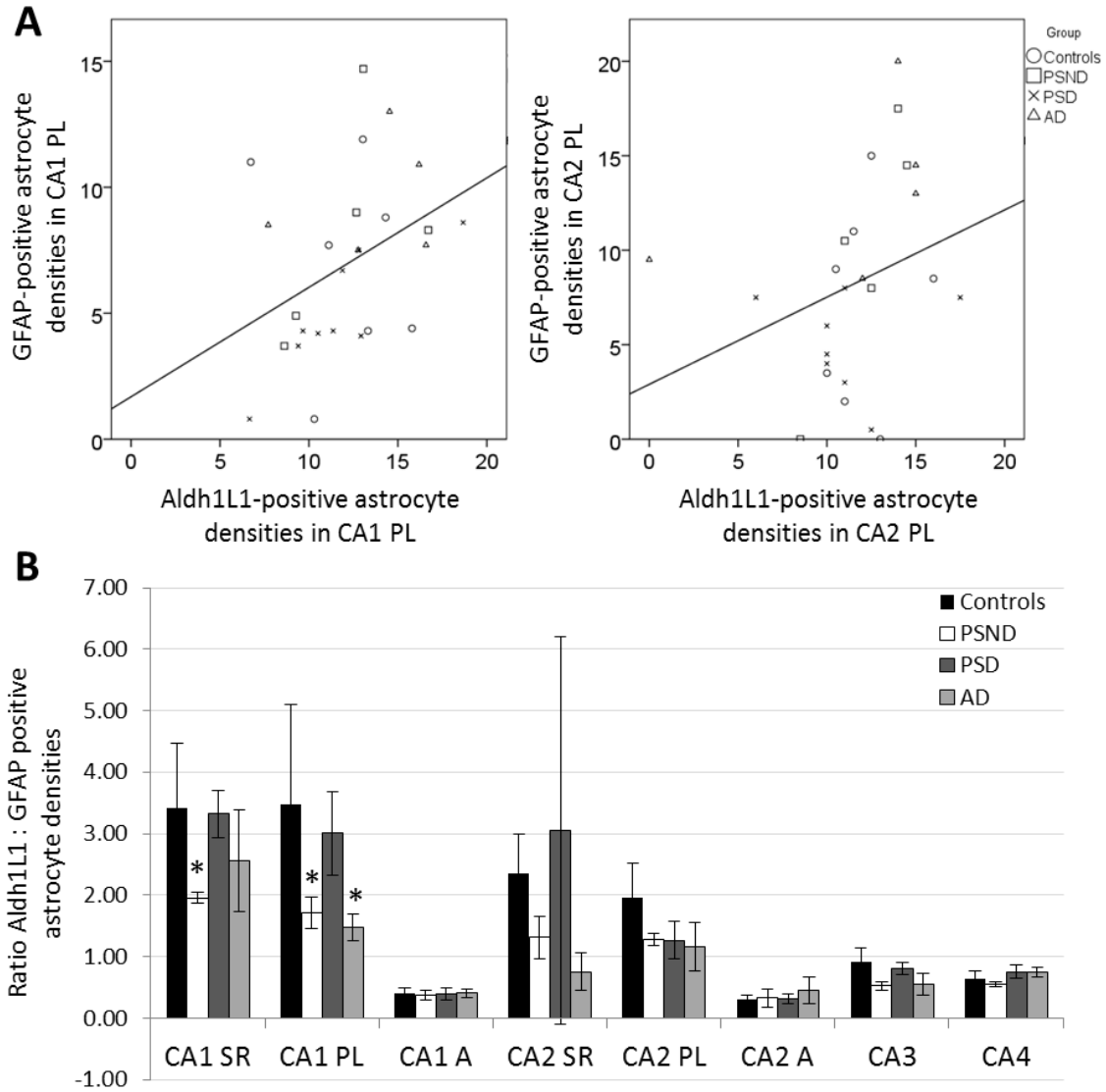

Figure 6.13 A, Correlations between Aldh1L1- and GFAP-positive astrocyte densities in CA1 and CA2; B, Graph showing ratio of Aldh1L1 : GFAP positive astrocyte densities in the different layers analysed. Asterisks indicate significant difference to the PSD group. SR = stratum radiatum, PL= pyramidal layer, A = alveus.

6.4.5 Microglia

Demographics of subjects analysed using CD68 for activated macrophages are shown in Table 6.4. There were no differences in age, PMD or fixation between groups.

	N	**Age, years** Mean (range)	**PMD, hours** Mean (range)	**Fixation length, weeks** Mean (range)	**Braak stage,** Median (range)	**CERAD score,** Median (range)
Controls	6	84.4 (7494)	38.6 (15-67)	10 (6-16)	2.4 (1-3)	0 (0)
PSND	7	85.2 (81-89)	39 (11-76)	9 (5-16)	2.8 (2-4)	1.6 (1-2)
PSD	8	85 (80-89)	59 (24-81)	8 (2-18)	2.3 (1-4)	1.4 (0-3)
AD	9	82.3 (70-91)	31 (6-72)	10 (8-20)	5 (4-6)	3 (3)

Table 6.4. Group demographics of subjects analysed using CD68 to visualise activated microglia.

There was a trend to CA1 CD68 IOD being different across groups [$F(20) = 0.273$, $p = 0.077$], and there was a trend to the AD group having greater CA1 IOD than controls ($p = 0.059$) (Figure 6.14 C). CA1 IOD was correlated with CA2 IOD ($r = 0.706$, $p = 0.001$), and CA1 and CA2 IOD were correlated with CERAD scores ($r = 0.504$, $p = 0.024$ and $r = 0.463$, $p = 0.053$) and Braak stage ($r = 0.436$, $p = 0.048$ and $r = 0.442$, $p = 0.058$). CA1 CD68 %PA was negatively correlated with CA1 neuron density ($r = -0.473$, $p = 0.011$). There were no correlations with CAMCOG scores, vascular pathological burden, age, PMD or fixation.

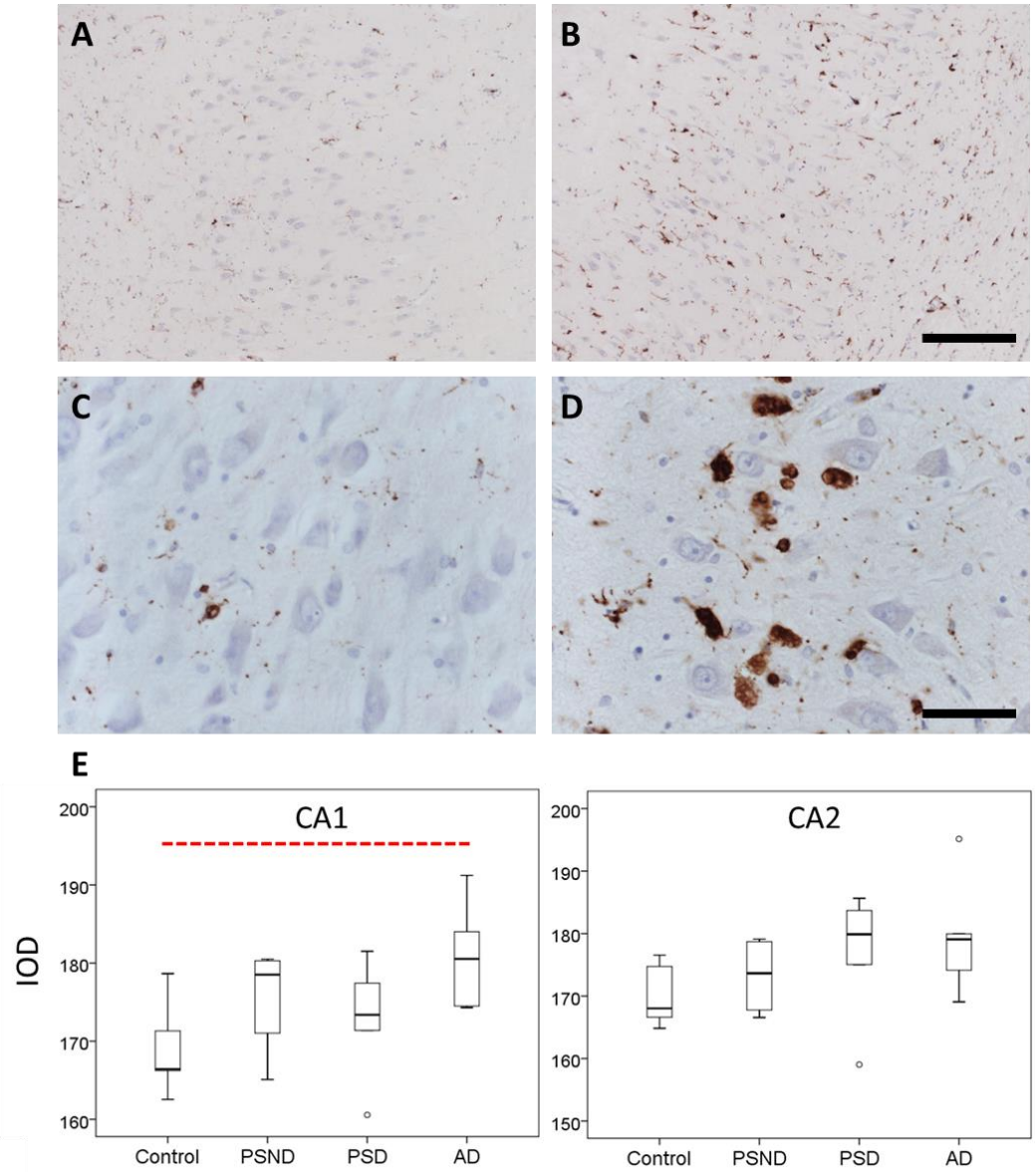

Figure 6.14. Representative images of CD68 immunostaining in the CA1 of PSND (A, C) and AD subject (B, D). A-B Scale bar = 100µm, C-D Scale bar = 50µm. E, Box-plots of CD68 mean IOD in the CA1 and CA2. Dotted line indicates trend to significant difference (p = 0.059).

6.5 Discussion

6.5.1 White matter damage

This study did not find any differences in myelin integrity in the alveus between the PSD and PSND groups using LFB staining for myelin or dMBP for degraded myelin basic protein. Furthermore, myelin and dMBP levels were not related to post-stroke CAMCOG scores or dementia status. The considerable variation in myelin staining between subjects within groups, particularly the controls, may have masked actual disease related differences. Some subjects in the elderly control group exhibited similar pathological white matter changes in the alveus to post-stroke and AD subjects, which may have reflected age-associated white matter damage. Histopathological studies have shown white matter damage, including myelin pallor, loss of white matter fibres, and malformation of myelin sheaths, is a common feature in normal ageing (Marner *et al.*, 2003; Gunning-Dixon *et al.*, 2009). As there does not appear to be significant neuron loss with ageing, damage to white matter is therefore likely to underlie the general slowing of cognition consistently found with increasing age (Marner *et al.*, 2003). Memory function declines with age (Peich *et al.*, 2013), therefore this may be related to myelin loss in the alveus causing slowing or loss of axonal communication in the hippocampal circuitry.

Although there were no clear associations between LFB myelin staining and cognitive status, there was considerable variability in myelin staining between subjects. Myelin staining was positively correlated with neuronal volumes in the CA1, CA2 and CA4, which suggests that subjects with reduced neuronal volumes had fewer myelinated axons in the alveus, in agreement with my hypothesis that reduced neuronal volumes may be related to axonal arbour. The AD group had the lowest mean LFB %PA staining in CA1 and CA2, which is likely to reflect secondary axonal degeneration due to hippocampal neurodegeneration and axonal damage caused by AD pathology. Similarly, Braak and CERAD scores were only related to LFB staining in the EC white matter, reflecting the well-described selective vulnerability of EC neurons to AD processes.

Mean dMBP immunostaining was also similar between groups with a broad spread of results within each group. Levels of dMBP did not appear to be directly related to

neuronal volumes or AD pathology, which may be because dMBP staining in white matter is more closely related to oligodendrocyte than neuronal dysfunction. Furthermore, areas with low LFB staining may have already undergone severe myelin loss and axon degeneration, therefore there was less myelin was available to be degraded and accumulate as dMBP. Therefore, accumulation of greater amounts of dMBP may precede myelin loss after white matter injury. Interestingly, the area stained for dMBP was related to temporal lobe vascular pathological burden, which fits with current understanding of axonal and oligodendrocyte susceptibility to hypoxic/ischaemic damage (Giaume *et al.*, 2007), as subjects with greater cerebrovascular pathology had greater dMBP. A previous study found that dMBP levels were inversely related to the size of oligodendrocytes in the frontal white matter of VaD subjects (Ihara *et al.*, 2010). It would therefore be interesting to determine whether there were reductions in oligodendrocyte number and/or size in the alveus of subjects with greater myelin damage. However, dMBP levels were negatively correlated with PMD, which suggests results may be influenced by PMD and should therefore be interpreted with caution.

It was surprising to find intense dMBP staining in the soma of neurons in the CA subfields. This staining was also not found to be different between disease groups or related to cognitive status; however the stain intensity was related to AD pathological burden in the CA2, and was positively correlated with dMBP levels in the alveus. This suggests that dMBP may be taken up by neurons and accumulated in the neuronal soma, possibly becoming sequestered with protein aggregates associated with AD processes. DMBP-positive immunostaining was also found in neuronal soma in the cortex, and appeared more intense in subjects with more intense hippocampal staining (as shown in Appendix Figure 8.6). However, neuronal staining using dMBP has not previously been reported and was expected to only be found in the white matter and oligodendrocytes, therefore the functional implications of these findings are unclear.

LFB analyses were limited as the hematoxylin counterstain meant that oligodendrocyte and astrocyte nuclei within the alveus were included in the myelin stain analyses. However, the presence/absence of these nuclei also reflects mechanisms contributing to myelin and axonal integrity, as loss of oligodendrocytes would result in demyelination and axonal dysfunction. Variability in the intensity of LFB stain may have

influenced results, although the myelin index calculations were carried out to normalize LFB staining differences. Stains for axonal proteins such as tau may be useful markers to complement studies of this kind and determine whether myelin loss reflects axon degeneration.

Pyknosis ratings were variable within groups, although all control subjects were rated as 0 or 1. It was interesting not to find any relationship between the severity of pyknotic-appearing neurons and neuronal volume or density measures, as reduced neuronal volumes in the baboon model were related to pyknosis and cytoplasm shrinkage was a possible mechanism contributing to neuronal volume loss in the dementia subjects. Further investigation of markers of degenerating neurons, such as poly (ADP-ribose) polymerase 1 (PARP) or Fluoro-Jade C, would be needed to establish whether neuronal volume changes indicated cell death mechanisms. However, the finding of neuronal volume loss without significant reductions in neuronal density suggested that these neurons were not degenerating.

6.5.2 Astrocyte densities

Immunohistochemical staining for Aldh1L1 revealed greater numbers of astrocytes than GFAP in the CA1 and CA2 pyramidal layers and stratum radiatum, which confirmed that Aldh1L1 was a broader maker for astrocytes than GFAP. Aldh1L1-positive protoplasmic astrocytes were evenly distributed across the hippocampus, in agreement with the literature describing astrocytes completely tiling the brain and occupying non-overlapping domains (Ogata and Kosaka, 2002; Sofroniew and Vinters, 2010). Surprisingly, the density of GFAP-positive astrocytes in the alveus was greater than Aldh1L1-positive astrocytes. This may suggest that non-astrocytic GFAP-positive cells were counted, as it is known that not all cells that express GFAP are astrocytes (Oberheim *et al.*, 2012). However, GFAP-positive staining was often intense in the white matter of the alveus and close to the surface, making identification of astrocytic cell bodies considerably more challenging (as shown in appendix Figure 8.8), therefore astrocyte counts in the alveus may not have been accurate using GFAP.

There were no significant differences in Aldh1L1-positive astrocytes between groups, although mean densities appeared higher in the CA1 in disease groups than controls. Immunohistochemical staining for GFAP revealed greater differences in reactive

astrocyte densities between groups. The highest density of reactive astrocytes was found in the AD subjects, and GFAP-positive astrocyte density was correlated with AD pathology in the CA1 and CA2 pyramidal layers and stratum radiatum. These findings are in agreement with previous studies demonstrating hippocampal astrogliosis in response to AD pathology, although the precise role of astrocytes in the pathogenesis of AD remains unknown (Grolla *et al.*, 2013).

Conversely, increased vascular pathological burden was related to lower reactive astrocyte density in the CA1 and CA3 pyramidal layers and the CA1 stratum radiatum. As Aldh1L1-positive astrocyte density was also negatively correlated with vascular pathological burden in the CA1 and CA2 pyramidal layers, these findings suggest that CVD processes may result in loss of hippocampal astrocytes. This opposing effect of AD and CVD processes on astrocyte densities may have prevented the detection of clear differences in astrocyte densities in the groups studied, which are likely to have had some degree of both cerebrovascular and neurodegenerative disease pathology.

The ratio of Aldh1L1- to GFAP-positive astrocyte density in the CA1 stratum radiatum and pyramidal layer was greater in the PSD group compared to PSND, with PSD subjects having a similar ratio to controls, whereas the PSND group were similar to AD. This was surprising, as I had hypothesised that PSND would be more similar to controls, reflecting the neuronal volume findings observed in chapter 1. This may therefore reflect differing astrocytic response in the stroke survivors contributing to cognitive decline, or be related to astrocytic activation by greater Aβ pathology in the PSND group. Further investigation of reactive astrocytes in relation to AD pathology may determine whether the density of GFAP-positive astrocytes was primarily influenced by Aβ plaque density.

It was interesting to discover that GFAP-positive astrocyte density was inversely related to dendritic length-density in the CA1 stratum radiatum as I had previously failed to find any markers or factors related to dendritic length density. This finding suggests that astrocytes within this subfield were responding to local dendritic pathological changes, possibly through dendritic remodelling and synaptic function, although reactive astrocytes have also previously been implicated in contributing to neurodegeneration (Tanaka *et al.*, 1992). However, due to the previously discussed

issues using MAP2, this relationship should be considered with caution. The finding that GFAP-positive astrocyte density in the alveus and stratum radiatum was positively correlated with neuronal volumes in CA1, CA2 and CA4, and that astrocyte density in the CA2 stratum radiatum was related to CA1 and ECV neuronal density, suggests that increased numbers of reactive astrocytes were associated with a neuroprotective response to restore neuronal function, in agreement with previous studies (Briones *et al.*, 2006).

This investigation into astrocyte density was limited by the previously discussed limitations associated with 2D estimates of cell densities, and could not take into account possible variations in tissue atrophy. However, due to time constraints, full investigation using 3D stereological analyses was not possible. These results indicate that it would be extremely interesting to use a 3D stereological method to quantify hippocampal astrocyte density and cell body size. Shrinkage of astrocyte volumes and arbour have previously been reported in the EC in models of AD and were suggested to be contribute to the selective vulnerability of the EC to AD pathology (Yeh *et al.*, 2011), whereas reactive astrogliosis is associated with increased astrocyte diameter (Sofroniew, 2009). Double staining using immunofluorescence could be used to identify the number of astrocytes that express both GFAP and Aldh1L1 for further investigation into differences in reactive astrocyte densities between subjects and hippocampal regions in different disease aetiologies. The use of additional astrocyte markers such as S100β and glutamine synthetase will also allow further insight into mechanistic changes to the hetereogeneous population of astrocytes in the hippocampus after stroke.

6.5.3 Microglia

In agreement with published observations, activated microglial markers were related to AD pathological burden. Although there were no significant differences in CD68 immunoreactivity between groups, the AD group had more intense staining than controls and post-stroke subjects in CA1, and staining intensity in CA1 and CA2 was correlated with AD pathology, in agreement with previous studies reporting microglial activation in response to Aβ deposits in the neuropil and vessel walls (Meraz Rios *et al.*, 2013). The finding that greater CD68 staining was related to lower CA1 neuron

density may reflect the role of CD68-positive microglia in phagocytosing neurons in AD (Neher *et al.*, 2012). Based on these observations in CA1, it was therefore surprising to find mean CD68 was highest in the PSD group in the CA2. I did not find any relationships between CD68 and vascular pathology, suggesting that the microglial activation was more closely related to AD pathology. This was supported by the (non-significant) increase in mean CD68 levels in PSND subjects compared to PSD in the CA1, which may reflect the greater burden of Aβ pathology I previously found in the PSND group.

6.6 Conclusions

This study found considerable variation in myelin integrity in the alveus in elderly subjects with and without dementia. Although myelin density and dMBP staining was not related to cognitive status, loss of myelin staining in the alveus was related to neuronal volumes in CA1, CA2, and CA4. This supported my hypothesis that there may be a relationship between neuronal volume loss and impairment in neuronal connectivity, as reduced myelin integrity is likely to reflect loss of, or dysfunctional axonal connections. Conversely, dMBP immunoreactivity was not related to neuronal volumes or LFB staining, but was related to vascular pathological burden in the medial temporal lobe. This suggests that oligodendrocyte damage was greater in subjects with more severe CVD, which is in agreement with literature describing the particular susceptibility of oligodendrocytes to hypoxic-ischaemic damage.

There were no differences in astrocyte or reactive astrocyte densities between the PSD and PSND groups, and they were not related to post-stroke cognitive function. However, IHC to Aldh1L1 identified 2-3 times more astrocytes in the pyramidal layer and stratum radiatum than GFAP, and they were distributed in a homogeneous manner throughout all layers confirming that Aldh1L1 is a more reliable marker for astrocytes. Interestingly, the PSD group had a higher ratio of Aldh1L1 to GFAP-positive astrocytes than the PSND group, which had greater proportion of GFAP-positive astrocytes similarly to AD subjects. This may have reflected the positive relationship between increased density of reactive astrocytes and AD pathology, in agreement with previous studies (Grolla *et al.*, 2013). Astrocyte densities may also have been affected by CVD, as they were negatively correlated with increasing vascular pathology. CD68-

positive microglial immunoreactivity was also related to AD pathology in agreement with previous studies (Nagele *et al.*, 2004; Bolmont *et al.*, 2008).

Chapter 7. Discussion

7.1 Introduction

This study investigated neuronal morphological changes, neurodegenerative pathological mechanisms, and neuroglial responses in the hippocampus of stroke survivors from the CogFAST cohort and attempted to elucidate mechanisms contributing to delayed post-stroke dementia. The key findings of this study are listed below and discussed in detail in the following subsections:

- Hippocampal neuronal soma volumes were 10 – 20% reduced in post-stroke and ageing-related dementia subjects compared to non-demented stroke survivors and controls. Surprisingly, CA1 neuron density was not related to post-stroke cognitive status, and all stroke survivors had reduced neuron density in the CA1 compared to controls. The degree of neuronal atrophy was related to:
    - severity of post-stroke cognitive impairment (CAMCOG scores)
    - burden of hippocampal hyperphosphorylated tau pathology and Braak stage
    - reactive astrocyte density in the alveus and stratum radiatum
    - myelin density in the alveus
- Amyloid-β pathology was not related to cognitive function, and the non-demented stroke survivors had a greater burden of Aβ pathology than PSD subjects.
- Reactive astrocytes and microglia were associated with greater burden of AD pathology. Conversely, astrocyte density was inversely related to the CVD pathological burden.
- Greater burden of CVD pathology in the temporal lobe was related to accumulation of degraded myelin basic protein in the alveus.
- Interpretation of differences in dendritic and synaptic marker levels and distribution were limited due to the poor understanding of the influence of ischemia, agonal and post-mortem conditions.

- Standard markers of autophagy appeared to be differentially affected in AD and CVD; but were not related to cognitive status.

7.2 Neuronal atrophy as a mechanism contributing to cognitive impairment

This study provided novel evidence that neuronal volume reductions were associated with cognitive impairment in PSD, AD, VaD and mixed dementia. As non-demented stroke survivors maintained neuronal volumes similar to controls, and neuronal volumes were related to cognitive test scores, this suggests that reduced neuronal volumes reflected mechanistic changes contributing to cognitive decline. There were no differences in CA1 neuron density between non-demented and demented stroke survivors, which was surprising as neuron loss is believed to contribute to cognitive dysfunction. However, this finding supported the hypothesis that dysfunction in the surviving neurons was an important determinant of cognitive function.

Since the publication of these findings (Gemmell *et al.*, 2012), further studies from other members of the neurovascular research group have found that neuronal volumes were similarly reduced in layers III and V of the dorsolateral pre-frontal cortex (dlPFC) in PSD subjects from the CogFAST cohort , VaD and AD subjects compared to controls and PSND subjects (manuscript in preparation). Neurons in the CA1/subiculum directly innervate the prefrontal cortex via the hippocampo-prefrontal pathway, and the prefrontal cortex is known to have an important role in learning and memory formation (Laroche *et al.*, 2000). Therefore, neuronal volume reductions in the dlPFC may reflect deafferentation from hippocampal neurons lost or impaired by ischaemic-hypoxic or neurodegenerative insults. However, neuronal volumes in the anterior cingulate cortex and orbitofrontal cortex, regions also involved in memory processing and long-term storage, were not reduced in subjects with dementia. Together with my finding that EC neuronal volumes were only reduced in subjects with severe AD pathology, this suggests that neuronal atrophy is not a global effect, but that neurons in different areas of the brain are differentially vulnerable to mechanisms causing these morphological changes.

These findings have interesting therapeutic implications, as they suggest that cognitive function may be preserved or recovered even after significant loss of neurons, when

the surviving neurons maintain normal volumes. Studies to determine the mechanisms protecting neurons from structural and functional decline in stroke survivors may therefore provide the basis for the development of therapeutic strategies to prevent or slow cognitive decline after stroke and in other age-related dementias.

7.3 Investigating mechanisms causing neuronal atrophy

My subsequent studies built on these findings to explore possible mechanisms causing or contributing to neuronal atrophy and dysfunction.

7.3.1 Alzheimer's disease pathology

Hyperphosphorylated tau pathology was related to neuronal densities in CA1 and neuronal volumes in CA2, CA4 and ECV. These findings suggested that tau pathology contributed to neurodegeneration in the CA1 and neuronal dysfunction in the other subfields, which may be due to loss of neuronal connectivity due to CA1 target loss or tau pathology causing neurite dysfunction. These results were in agreement with previous studies demonstrating relationships between tau pathology, CA1 neuron loss and cognitive impairment (Gómez-Isla *et al.*, 1997; Giannakopoulos *et al.*, 2003), but no relationship with amyloid-β pathological burden (Braak and Braak, 1991). The finding that PSND subjects had maintained neuronal volumes despite greater burden of Aβ pathology suggests that neuronal volume could be an indicator of brain reserve, where the surviving neurons had maintained functional connectivity or had upregulated compensatory mechanisms which protected against neuronal dysfunction and loss caused by disease processes. Anatomical differences in dendritic spines and synapses have previously been suggested as possible quantitative measures of brain reserve (Barulli and Stern, 2013), therefore neuronal volumes may reflect similar mechanisms.

7.3.2 Autophagy

As autophagy is highly efficient in healthy neurons, I reasoned that increased staining for autophagy proteins LC3 and Beclin-1 would be associated with cognitive dysfunction in PSD. Accumulation of autophagic vacuoles indicates autophagic stress, neurite damage caused by impaired protein degradation and trafficking, and leads to structural changes and neuronal dysfunction. My findings were generally in agreement

with previous studies demonstrating increased build-up of AVs in subjects with AD (Nixon and Yang, 2011). However the conflicting correlations between LC3 and Beclin-1 with global pathological burden were difficult to interpret. Imbalanced autophagy is implicated in neurodegeneration, and autophagy can become imbalanced due to down- or up-regulation or impaired clearance. Previous studies have suggested that activation of autophagy can promote neuronal survival in the initial stages of ischaemic brain injury (Carloni *et al.*, 2008), although increased LC3 and Beclin-1 are more commonly associated with neuron death due to excessive activation of autophagy (Cherra III and Chu, 2008). Furthermore, chronic impairment in autophagy has been shown to cause axonal and synaptic degeneration, while increased autophagy can lead to neurite retraction and reduced neuronal communication (Cherra III and Chu, 2008). Therefore, the functional significance of finding increased levels of autophagy markers in CVD is unclear. Studies will first need to establish the role of autophagy in hippocampal neurodegeneration and cognitive dysfunction in carefully controlled animal models of stroke and hypoxia, to allow insight into the effects of CVD in the absence of other age-associated disease processes.

7.3.3 Neuronal connectivity; dendrites, dendritic spines and synapses

Neurons represent the fundamental information processing unit in the brain, and their structure influences how information is received and processed to generate action potentials. Therefore, dysfunctional neuronal communication can be assessed through changes to neurite structure or abnormal expression of proteins involved in synaptic transmission. As the extent and complexity of the axo-dendritic arbour is believed to influence neuronal soma volume (Harrison and Eastwood, 2001), and contribute to loss of neuropil volume and tissue atrophy in cognitive impairment (Selemon and Goldman-Rakic, 1999), changes to dendrites and axons were investigated as putative mechanisms contributing to soma volume loss, neuronal dysfunction, hippocampal atrophy, brain reserve and cognitive impairment in stroke survivors who developed delayed PSD.

I hypothesised that dendrites and/or synaptic markers in the stratum radiatum would be reduced in relation to cognitive impairment and neuronal loss and/or neuron atrophy. However, finding an appropriate technique to investigate dendritic changes in

human post-mortem material was particularly challenging. Previous studies of dendrites in human tissue have generally attributed surprising or conflicting findings to post-mortem delay (Schwab *et al.*, 1994; Cotter *et al.*, 2000). This is a reasonable assumption, as it is hard to believe that such plastic structures specialized to constantly dynamically adapt for learning and memory formation do not also undergo significant changes or degradation during the interval between death and fixation. However, the precise effects of post-mortem autolytic processes on dendritic and synaptic markers are not well characterised. One study, (Siew *et al.*, 2004), has previously investigated the stability of synaptic proteins after post-mortem delay up to 72 hours at 20°C and 4°C in rodent and human post-mortem tissue using ELISAs (enzyme-linked immunosorbent assays). They found that synaptophysin levels were stable in rodent and human tissue post-mortem, while levels of PSD-95 and pre-synaptic protein syntaxin were considerably reduced in human frontal cortex from 24 hours post-mortem. This demonstrated that post-mortem delay longer than 24 hours resulted in inter-species and regional differences in synaptic marker stability, and that different synaptic markers may be degraded at different rates. The authors attributed the greater stability of synaptophysin to its multi-transmembrane structure which make it more resistant to degradation (Siew *et al.*, 2004). Further investigation would be required to determine the reliability of interpreting changes in levels of other synaptic markers using IHC in tissue with varying post-mortem delays. In human tissue, I found that the dendritic spine protein drebrin was concentrated in neuronal soma with very little in the stratum radiatum or moleculare. In contrast, drebrin levels were concentrated in the neuropil in the perfusion-fixed non-human primate model, suggesting that drebrin may be moved from dendritic spines to accumulate in the cell body during the post-mortem interval. This has previously been shown with MAP2 and tau, and further demonstrates that microtubules are not stable post-mortem (Schwab *et al.*, 1994).

MAP2 is also known to be particularly sensitive to hypoxic-ischaemic injury, which further complicated interpretation of changes to MAP2-positive dendrites in stroke survivors. Despite these limitations, I used MAP2 as it was the best marker to assess dendritic changes in the paraffin-embedded tissue available. As expected, interpretation of results using MAP2 was difficult. Differences in distribution patterns

and intensity were clearly visible by eye, but did not appear to be directly related to disease pathology, cognitive function, neuronal volume/density changes, or PMD. Similarly, there was variation in the distribution of post-synaptic proteins drebrin and PSD-95 staining. Further work is required to determine the stability of these proteins post-mortem and determine whether these differences reflect disease processes.

Despite these limitations, this study demonstrated a successful new 3D stereological method to assess MAP2-positive dendritic length-density using a spherical probe. Further work will be required to validate the even penetrance of the immunohistochemical stain in 30µm thick sections, as variable staining has been documented as a potential confounding factor for 3D stereology (Mouton, 2002; Melvin and Sutherland, 2010). However, for studies such as mine which compared differences between groups rather than determining absolute numbers of particles, as all sections were processed and stained in the same way, any differences would have affected all sections equally, allowing fair comparisons between subjects. Although interpretation of these results in human post-mortem material face limitations described previously, this technique could be applied to elucidate changes to dendritic length and complexity in relation to neuronal volumes and memory impairments in animal models of stroke with no PMD.

7.3.4 White matter changes in ageing and CVD

Myelin density in the alveus was correlated with neuronal volumes, suggesting that reduced neuronal volume was associated with axon loss or dysfunction. Myelinated axons do not undergo the dynamic plastic changes that dendrites do, therefore allowing more reliable reflection of structures in life. However, myelin density was not related to cognitive status or disease pathology in this study. This was apparent from inspecting only the control group, where there was considerable variation in myelin staining between subjects. Variability in white matter changes in controls has also recently been shown in a DTI study which reported “tremendous individual variation within a single control group” (Aine *et al.*, 2014). Aine et al. also found that control subjects often had a range of vascular risk factors, which had robust effects on brain anatomy and function. This therefore highlights the current lack of understanding of

the functional impact of cerebrovascular lesions and white matter pathology on cognition.

Myelin density was not related to levels of degraded myelin basic protein, although accumulation of dMBP was associated with CVD burden in the temporal lobe. As previously discussed, this may be because reduced myelin staining reflects myelin loss, therefore there is less myelin left to become degraded. The relationship between dMBP and CVD supports current understanding of the particular vulnerability of oligodendrocytes to hypoxic-ischaemic injury. Further studies to investigate the number and functionality of oligodendrocytes may elucidate relationships between myelin staining and dMBP levels, as loss of myelin indicates loss of oligodendrocytes.

7.3.5 Role of astrocytes and microglial activation

The pivotal role of astrocytes in synaptic transmission, vessel function, and the pathogenesis of neurological diseases have only recently begun to be recognized (Sofroniew, 2009; Oberheim *et al.*, 2012). As my central hypothesis focussed on loss of hippocampal neuronal connectivity as a mechanism contributing to delayed PSD, I reasoned that pathological changes to astrocytes were likely to be involved in neuronal and cognitive dysfunction. Therefore, I investigated total astrocyte density using IHC to a new specific marker of astrocytes (Aldh1L1) and reactive astrocytes using GFAP. Astrocyte densities were not related to post-stroke cognitive function or different between PSD and PSND groups, however the positive correlations between reactive astrocyte densities in the alveus and stratum radiatum and neuronal volumes suggested that reactive astrocytes had a neuroprotective role in maintaining neuronal connections. Reactive astrocyte densities were also related to AD pathology, although they were related to Braak stage more than CERAD score, which was surprising as previous studies have reported accumulation of astrocytes undergoing gliosis around Aβ plaques (Rodríguez *et al.*, 2009). There was also increased activation microglia in subjects with greater AD pathology, in agreement with the literature describing increased gliosis in AD (Meraz Rios *et al.*, 2013).

Interestingly, studies of AD have found that astrocytes distant from amyloid plaques develop atrophy, which has been suggested to result in impaired synapse support, synaptic remodelling and disrupted neuronal circuitry (Rodríguez *et al.*, 2009). As my

findings indicated there may be a role for astrocytic activation and/or dysfunction in relation to neuronal changes in post-stroke subjects, it would be interesting to conduct a 3D stereological study of astrocyte density and volumes in the hippocampus of these stroke survivors, for more accurate investigation into the relationships between neuronal volume, connectivity and astrocytes.

7.4 General strengths and limitations

7.4.1 Unique strengths of the CogFAST cohort

The CogFAST cohort is a unique prospective study allowing insight into the disease mechanisms causing delayed post-stroke dementia in elderly subjects. The extensive detailed clinicopathological information made it possible to deduce relationships between neuronal changes and clinical or pathological features. As all subjects were recruited, assessed and all tissue was processed under the same conditions, this allows for reliable comparison between subjects. The large numbers of subjects within the cohort allowed my studies to have good statistical power.

The mean interval between last cognitive test and death was 7.6 months (± 2SE = 1.7), providing a fairly accurate estimate of cognitive status at death. However, it is impossible to know precisely how accurate these measures were, as subjects may have experienced further or rapid cognitive decline between assessment and death. Variability in degree of cognitive impairment in PSD subjects ranged from CAMCOG scores 24 – 80 and PSND subjects from 76 – 99. Therefore, variability in pathological changes would be expected within these groups to account for the variability in cognition. However, this variability may have prevented detection of statistically significant differences between groups, although providing a good range for correlation analyses.

7.4.2 Additional factors to consider

Hippocampal tissue was randomly taken from either the right or left hemisphere depending on which was available. There were no differences in neuronal volumes or densities when data obtained from the right hippocampus was compared to that from

the left ($p > 0.05$). However, the hemisphere tested may have influenced the strength of relationships between memory dysfunction and pathological changes, as studies have found that different aspects of memory processing are more strongly associated with the left or right hippocampus, with the left hippocampus being more involved in context-dependent episodic memory, whereas the right is particularly involved in memory for locations (Burgess *et al.*, 2002).

Although none of the subjects studied had significant hippocampal vascular lesions, there may have been asymmetrical damage to brain tissue caused by larger vascular lesions such as the initial stroke. Therefore, it is possible that the hippocampus on the contralateral hemisphere may have been less damaged by the more distant lesion. However, no significant differences were found between the volumes of left and right hippocampus of subjects who received volumetric MRI (Firbank, M. et al., unpublished data), suggesting that both hemispheres were equally affected.

Furthermore, the number of risk factors (such as hypertension, cardiovascular events etc.) and treatments (antihypertensive, antidepressants, anti-inflammatories) may have also impacted on brain mechanisms contributing to pathological changes. Although assessment of these variables was beyond the scope of my PhD, the detailed information available in the CogFAST cohort allows the influence of these factors to be investigated in future studies.

7.4.3 Limitations associated with human post-mortem studies of age-associated dementia

The use of age-matched controls may limit detection of significant changes compared to disease groups, as elderly cognitively normal subjects can have varying degrees of physiological brain changes due to age-associated vascular lesions or neurodegenerative pathology (Riley *et al.*, 2002; Aine *et al.*, 2014). It is therefore critical that wherever possible, full clinical and neuropathological reports should be available for control subjects to allow selection of appropriate subjects for studies into disease mechanisms. However, although selection of 'pathology-free' controls may provide more insight into disease mechanisms, it will not further current understanding of why some elderly people maintain cognition despite significant 'disease' pathology. The contribution of variation in the burden of age-associated

pathology in different control subjects may have resulted in the often broad spread of results within the control group in my studies. For example, atrophy of the CA1 subfield, which I reasoned may be due to loss of neurons or neuronal volume, has been shown to also occur in cognitively normal elderly individuals (Wang *et al.*, 2003; Mueller *et al.*, 2007).

The limitations of studying tissue with long or variable post-mortem interval were discussed previously, and are not unique to this study. The use of PMD as a measure of autolysis is also limited, as it does not take into account important factors such as temperature (i.e. room temperature compared to storage in a mortuary refrigerator) and tissue pH, which will influence the impact that duration of the interval between death and fixation had on tissue degradation. Therefore, although studies of dendritic and synaptic changes do appear to yield interesting results, interpretation of these findings should be carefully considered and compared with findings in perfusion-fixed animal models to ensure they are not reflecting artefacts of cell death and post-mortem interval.

As with all post-mortem studies we also cannot rule out the possibility that tissue morphology was affected during tissue processing. However all cases in the present study were treated and analysed the same way, particularly the CogFAST subjects which were recruited and processed as one cohort, therefore all groups should have been equally affected allowing valid comparisons to be made.

7.5 Future Directions

7.5.1 Short-term studies

- There are still many unanswered questions regarding neuronal volume changes in ageing and dementia. Further 3D stereological analysis of neurons in young subjects, without age-associated neuropathology or confounding cause of death (e.g. cardiovascular or respiratory disease) will determine whether hippocampal neuronal volume loss also occurs in normal ageing and may contribute to age-associated brain atrophy.

- Investigation of neuronal volumes in cortical regions of the brain that would be expected to have little involvement in pathogenesis of dementia may provide further evidence to determine whether neuronal atrophy only selectively affects vulnerable regions of the brain.
- Three-dimensional stereological analysis of Aldh1L1-positive hippocampal astrocytes in the CA1 pyramidal layer and stratum radiatum will allow more sensitive detection of subtle differences in astrocyte density between subjects and disease states, to determine whether astrocyte densities are reduced in CVD. Analysis of astrocyte volumes may also indicate whether astrocyte function was impaired, as astrocyte shrinkage has been associated with astrocyte and neuronal dysfunction in AD (Rodríguez *et al.*, 2009), or whether astrocytes were reactive with larger soma diameters.
- Immunofluorescent double labelling of astrocytes with antibodies to Aldh1L1 and GFAP will allow further investigation into the putative protective role of reactive astrocytes. This may also indicate whether there is astrocyte proliferation or loss in specific regions such as vulnerable CA subfields or around Aβ plaques.

7.5.2 Medium-term studies

- To investigate differential changes to protein expression within the CA subfields, laser-capture microdissection of individual neurons and/or astrocytes could be used to select individual cells from frozen tissue. However, as only the soma could be expected to be extracted, this method would be suited for comparison of mRNA levels using RT-PCR (reverse transcription polymerase chain reaction). This may allow insight into different gene expression in different neuronal populations and between disease groups. It would be particularly useful to determine the expression of genes involved in dendrite, axonal and synaptic structure and function.
- Changes to protein expression and distribution assessed using IHC techniques within sections with increasing post-mortem delay should be investigated to aid appropriate use of these techniques and more reliable interpretation of findings. Ideally, this should be carried out in subjects with minimal disease pathology, and post-mortem delays up to at least 72 hours. Results should also

be compared with a rodent model to investigate the effects of increasing post-mortem delay as described by (Siew *et al.*, 2004), at 4C and 20C, and perfusion-fixed rodent tissue. Commonly used synaptic and dendritic proteins should be investigated, as well as markers of cell stress and death mechanisms. This resource would also then allow all markers to be assessed before carrying out studies into mechanisms that are likely to be affected by death, PMD or tissue fixation.

7.5.3 Long-term studies

- To establish whether neuronal volumes are related to changes in dendritic arbour after stroke will require tissue from a perfusion-fixed animal model of stroke. Perfusion fixation will allow rapid and uniform preservation of the tissue as close to its natural state as possible. The tissue can then be fixed under the optimal conditions for the technique chosen.
    - Despite the capricious nature of Golgi silver-impregnation techniques, they remain one of the best ways to visualize dendrites and dendritic spines. Recently, Golgi-Cox methods have been optimised for use in 60 – 100µm thick sections (Levine *et al.*, 2013), which could then be used for 3D analysis of dendritic spine length and complexity, in combination with neuronal soma volume measurements. In addition, serial sections could be taken for IHC analysis of local pathological burden.
    - Fluorescent dyes may be used to trace neurite structure in fixed tissue, through electroporation of Lucifer Yellow or biotin analogues or the more recent “DiOlistic labelling”, where microparticles coated with a lipophilic dye are fired at tissue sections. When a particle is embedded in a neuron, the dye diffuses throughout the cell producing fluorescent labelling of the entire structure (Staffend and Meisel, 2001).
    - Following any of the above techniques, computer assisted dendrite and spine tracing through thick tissue sections can be used to generate 3D reconstructions of neuron and dendrite structure for quantitative assessment of dendrite complexity and branching patterns using Sholl analysis (Milosevic and Ristanovic, 2007).

- Ideally, the animal model of stroke would also undergo cognitive testing at different time points after surgery to assess acute and chronic hippocampal morphological changes in relation to memory impairment.

7.6 Conclusions

This project provided novel evidence that reduced hippocampal neuronal soma volume is a pathological substrate of cognitive impairment in post-stroke and ageing-related dementias. Neuronal volumes were reduced ~20% in CA1, CA2, and CA4 in PSD and VaD, and EC layer V neuronal volumes were also reduced in AD and MD subjects. Both cerebrovascular and Alzheimer's disease processes appeared to contribute to this loss of neuronal volume, therefore this study provided novel evidence for a vascular basis of hippocampal neurodegeneration.

Hippocampal neuronal volumes were related to hippocampal tau pathology burden, but amyloid burden was not related to neuronal volumes or post-stroke cognitive function. Greater neuronal volumes were associated with the density of reactive astrocytes in the stratum radiatum and alveus, suggesting that astrocytes had a protective role in maintaining neurite structure and function. This was further supported by the finding of a relationship between reactive astrocyte density in the stratum radiatum and dendritic length-density, although interpretation of dendrite measures was limited by the influence of post-mortem interval and other unknown variables on staining patterns.

Future studies to investigate the role of astrocytes in the pathogenesis of delayed PSD may provide further evidence of a mechanism contributing to neuronal and vascular dysfunction in stroke survivors. Perfusion-fixed animal models of stroke will be required to determine the precise relationship between neuronal volume loss and axo-dendritic arbour in CVD.

Chapter 8. Appendix

		Neuronal Volume (μm^3)		Neuronal Density (neurons/mm^3)	
	Group	**Mean**	**Std. Deviation**	**Mean**	**Std. Deviation**
CA1	Controls	2357.1	470.4	25040.6	7195.0
	All PS	2180.5	452.6	20819.6	4427.0
	PSND	2332.4	344.5	20829.7	4023.0
	PSD	1957.7	509.3	20804.7	5110.7
	VaD	2072.9	333.8	19546.1	3639.4
	Mixed Dementia	2021.3	395.5	14041.6	4180.2
	AD	1926.0	437.2	16703.6	5141.4
CA2	Controls	3072.1	452.9	33947.5	8955.2
	All PS	2787.0	572.3	30957.3	5741.1
	PSND	3002.0	416.2	30311.3	5222.8
	PSD	2396.2	627.0	32131.7	6686.0
	VaD	2634.1	549.2	30250.9	4738.5
	Mixed Dementia	2421.9	556.7	28663.2	6634.3
	AD	2515.0	675.9	31076.8	6953.3
CA3	Controls	2513.4	374.6	24228.3	4404.0
	All PS	2151.4	716.7	24281.6	3337.2
	PSND	2447.0	610.6	23842.4	2706.6
	PSD	1997.7	427.8	24800.6	4034.5
	VaD	2254.1	516.2	24024.7	2783.5
	Mixed Dementia	1721.5	317.1	23805.8	5794.6
	AD	2073.1	389.7	22127.8	4572.8
CA4	Controls	3045.5	400.3	14288.3	3839.2
	All PS	2580.4	492.9	13678.2	1996.6
	PSND	2758.8	370.5	13301.6	1626.9
	PSD	2353.3	550.7	14157.5	2382.2
	VaD	2603.4	321.8	13366.3	3485.2
	Mixed Dementia	2046.2	345.0	14315.0	3848.7
	AD	2324.3	364.3	11978.0	1410.7
ECV	Controls	1368.0	324.7	34493.1	6938.4
	All PS	1256.0	255.5	32467.7	5310.3
	PSND	1227.3	211.0	32418.1	5160.8
	PSD	1308.2	326.5	32557.7	5829.2
	VaD	1201.2	186.7	32453.0	4570.8
	Mixed Dementia	922.9	127.0	28969.6	6563.3
	AD	1050.6	155.0	29551.8	6156.9

Table 8.1 Numerical values for neuronal volume and density measures. PS = post-stroke; Std. = standard.

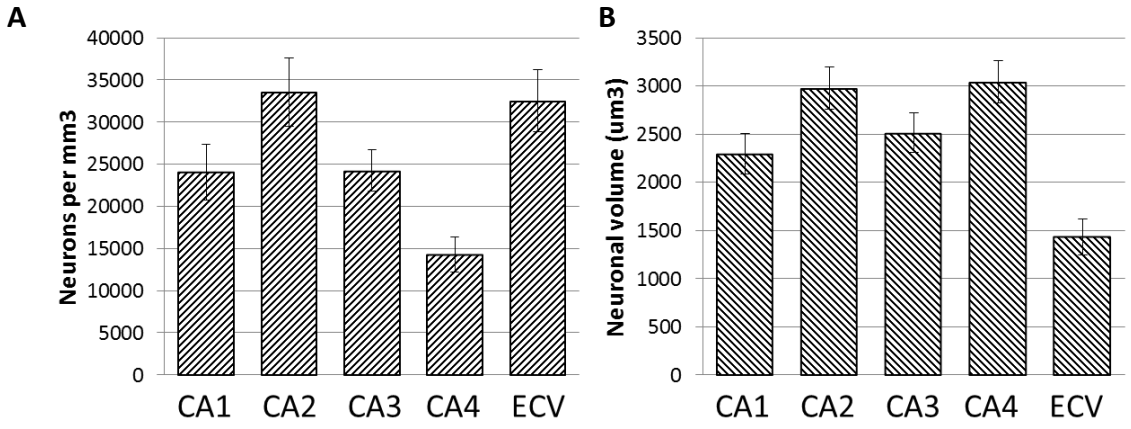

Figure 8.1. Neuronal densities (A) and volumes (B) in hippocampal subfields of controls. Error bars ±2SE.

	CA1 Vol	CA2 Vol	CA3 Vol	CA4 Vol	ECV Vol
PSND	99.0	97.7	90.4	90.6	89.7
PSD	83.1	78.0	79.5	77.3	95.6
VaD	87.9	85.7	89.7	85.5	87.8
Mixed	85.8	78.8	68.5	67.2	67.5
AD	81.7	81.9	82.5	76.3	76.8

Table 8.2. Hippocampal neuronal volumes in CA1-4 and ECV as percentage of control means.

	CA1 Dens	CA2 Dens	CA3 Dens	CA4 Dens	ECV Dens
PSND	83.2	89.3	98.4	93.1	94.0
PSD	83.1	94.7	102.4	99.1	94.4
VaD	78.1	89.1	99.2	93.5	94.1
Mixed	56.1	84.4	98.3	100.2	84.0
AD	66.7	91.5	91.3	83.8	85.7

Table 8.3 Hippocampal neuronal densities in CA1-4 and ECV as percentage of control means.

	CA3	CA2	CA1	ECV
CA4	r=0.718, p<0.001	r=0.627, p<0.001	r=0.462, p<0.001	r=0.373, p=0.001
CA3	-	r=0.555, p<0.001	r=0.386 p<0.001	r=0.325, p=0.005
CA2	-	-	r=0.406, p<0.001	r=0.311, p=0.012
CA1	-	-	-	r=0.231, p=0.05

Table 8.4. Correlations between neuronal volumes in hippocampal subfields CA1- CA4.

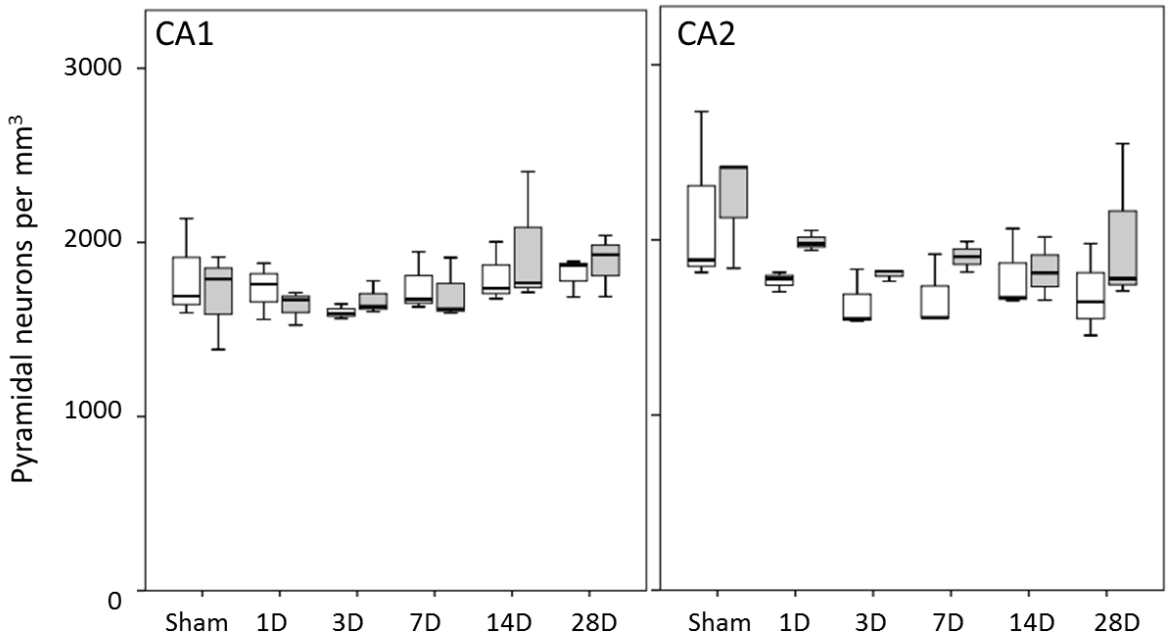

Figure 8.2. Neuronal densities in a baboon model of cerebral hypoperfusion at different survival times post-surgery; 1D = 1 day, 2D = 2 day, 3D = 3 day, 7D = 7 day, 14D = 14 days, 28D = 28 days post-surgery. White bars = left hemisphere (contralateral to surgery), grey bars = right hemisphere (ipsilateral to surgery).

	Group	Right		Left	
		Mean	Std. Deviation	Mean	Std. Deviation
CA1 neuron density (neurons/mm^3)	Sham	16965.8	2773.9	18080.8	2885.0
	1 Day	16355.8	979.5	17326.3	1627.2
	3 day	16711.2	948.7	16000.4	423.6
	7 day	17085.3	1776.1	17495.1	1713.2
	14 day	19621.9	3852.6	18055.9	1735.5
	21 day	20110.6	6751.5	18048.1	4238.6
	28 day	18855.7	1798.5	18153.5	1120.4
CA1 neuron volume (μm^3)	Sham	2964.8	546.2	3043.5	1457.7
	1 Day	1944.4	602.7	2133.7	753.5
	3 day	1913.0	659.6	1754.4	718.6
	7 day	1900.7	607.9	1859.5	582.5
	14 day	1693.3	428.7	1497.8	345.8
	21 day	2314.7	474.3	2705.0	1118.2
	28 day	2707.3	606.0	2466.6	40.0
CA2 neuron density (neurons/mm^3)	Sham	22234.9	3340.1	21443.0	5112.8
	1 Day	19908.4	575.1	17657.1	568.2
	3 day	18030.8	337.7	16388.7	1676.9
	7 day	19039.8	875.9	16768.1	2094.3
	14 day	18277.5	1809.1	17962.7	2326.6
	21 day	22493.3	5859.4	18854.5	3372.6
	28 day	20122.6	4663.3	16934.6	2651.8
CA2 neuron volume (μm^3)	Sham	2627.8	996.0	2688.0	667.8
	1 Day	2098.2	135.1	2101.4	27.0
	3 day	2057.6	371.7	1953.7	402.6
	7 day	2146.4	573.9	2098.7	666.3
	14 day	1936.3	604.4	1891.6	434.0
	21 day	2820.7	250.3	2932.0	143.6
	28 day	2746.0	467.1	2740.5	621.8

Table 8.5 Numerical values for neuronal volume and density measures in baboon model cohort. Right = right hippocampus, left = left hippocampus.

Modified Thal stage (amyloid)

Group	Stage	Frequency	Valid Percent	Cumulative Percent
Controls	0	2	18.2	18.2
	1	0	.0	18.2
	2	2	18.2	36.4
	3	2	18.2	54.5
	4	2	18.2	72.7
	5	0	.0	72.7
	6	2	18.2	90.9
	8	1	9.1	100.0
PSND	0	0	.0	.0
	1	3	13.6	13.6
	2	5	22.7	36.4
	3	1	4.5	40.9
	4	2	9.1	50.0
	5	5	22.7	72.7
	6	2	9.1	81.8
	7	3	13.6	95.5
	8	1	4.5	100.0
PSD	0	2	14.3	14.3
	1	6	42.9	57.1
	2	2	14.3	71.4
	3	1	7.1	78.6
	4	2	14.3	92.9
	5	0	.0	92.9
	6	1	7.1	100.0
VaD	0	0	.0	.0
	1	2	12.5	12.5
	2	7	43.8	56.3
	3	2	12.5	68.8
	4	1	6.3	75.0
	5	1	6.3	81.3
	6	0	.0	81.3
	7	3	18.8	100.0
Mixed Dementia	2	1	7.7	7.7
	5	1	7.7	15.4
	6	2	15.4	30.8
	7	1	7.7	38.5
	8	2	15.4	53.8
	9	3	23.1	76.9
	11	3	23.1	100.0
AD	4	1	7.7	7.7
	6	2	15.4	23.1
	7	1	7.7	30.8
	8	3	23.1	53.8
	9	3	23.1	76.9
	10	1	7.7	84.6
	11	2	15.4	100.0

Lace stage (tau)

Group	Stage	Frequency	Valid Percent	Cumulative Percent
Controls	0	3	30.0	30.0
	1	1	10.0	40.0
	2	1	10.0	50.0
	3	2	20.0	70.0
	4	2	20.0	90.0
	5	1	10.0	100.0
PSND	0	3	15.8	15.8
	1	1	5.3	21.1
	2	1	5.3	26.3
	3	8	42.1	68.4
	4	3	15.8	84.2
	5	3	15.8	100.0
PSD	0	1	10.0	10.0
	1	3	30.0	40.0
	3	4	40.0	80.0
	5	2	20.0	100.0
VaD	0	4	30.8	30.8
	1	2	15.4	46.2
	2	2	15.4	61.5
	3	3	23.1	84.6
	4	1	7.7	92.3
	5	1	7.7	100.0
Mixed Dementia	3	1	7.1	7.1
	4	4	28.6	35.7
	5	9	64.3	100.0
AD	2	1	9.1	9.1
	3	1	9.1	18.2
	4	3	27.3	45.5
	5	6	54.5	100.0

Table 8.6 Frequency tables for ratings of amyloid and tau pathology.

		%PA		IOD	
	Group	**Mean**	**Std. Deviation**	**Mean**	**Std. Deviation**
LC3 CA1	Controls	0.00831	0.00289	102.5	4.7
	PSND	0.00813	0.00184	107.2	6.4
	PSD	0.00980	0.00274	105.5	8.2
	AD	0.00957	0.00110	97.5	6.2
LC3 CA2	Controls	0.01590	0.00499	103.4	10.2
	PSND	0.01390	0.00113	106.4	7.4
	PSD	0.01685	0.00313	105.7	8.0
	AD	0.01708	0.00218	94.8	9.9
Beclin-1 CA1	Controls	2.30688	1.80221	136.4	55.6
	PSND	2.40621	1.11512	155.3	6.1
	PSD	2.82310	1.70090	158.2	6.2
	AD	3.34838	0.52319	158.3	3.7
Beclin-1 CA2	Controls	8.49895	1.74246	161.0	11.0
	PSND	8.00919	2.33600	162.5	10.1
	PSD	8.53998	1.83073	163.5	6.3
	AD	8.61105	1.97772	167.4	5.7
P62 CA1	Controls	1.63461	3.25593	157.9	10.0
	PSND	1.35384	2.06469	159.8	11.8
	PSD	0.99538	0.84991	159.5	10.6
	AD	2.63617	2.79693	168.5	6.5
P62 CA2	Controls	2.72984	2.54887	157.5	13.9
	PSND	2.08923	2.76588	150.6	9.0
	PSD	1.96987	1.16177	150.7	6.5
	AD	3.16026	3.76433	168.4	12.1

Table 8.7 Numerical values for image analysis of autophagy markers LC3, Beclin-1 and P62 in CA1 and CA2. %PA = percentage of the area of interest positively stained; IOD = integrated optical density (intensity of stain); Std = standard.

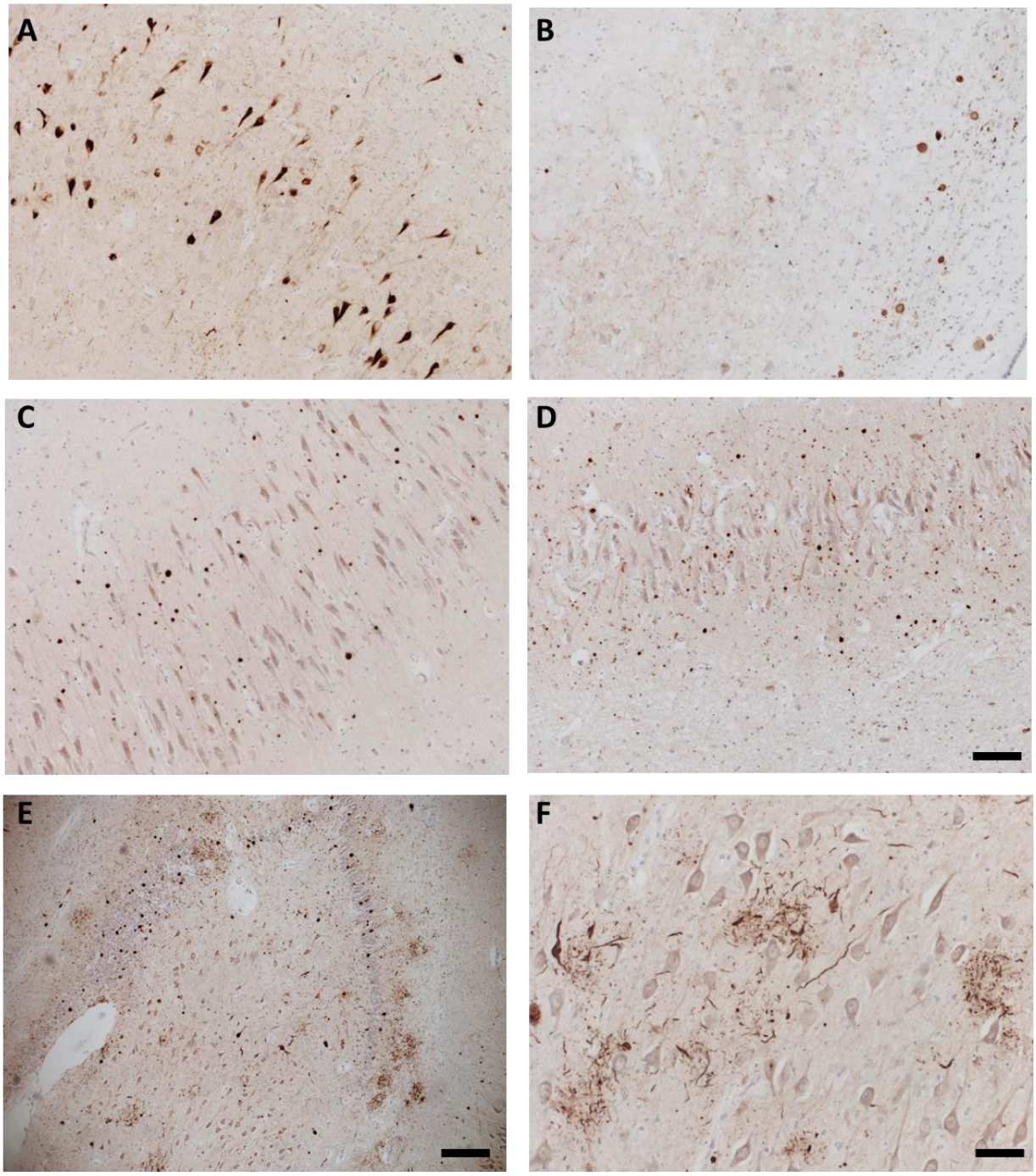

Figure 8.3 Unusual and different patterns of P62 staining. A, AD outlier (high IOD); B, spherical staining in the alveus of a PSD subject; C, intense spherical staining in the CA1 of a PSND subject; D, spherical staining in the CA2 of a control subject; E, Plaque-like staining in an AD subject; F, tangle like staining in the CA2 of an AD subject. Scale bar A-D = 100µm, E = 200µm, F = 50µm.

	Group	Mean	Std. Deviation
CA1 DLD	Controls	.01700	.00289
	PSND	.01592	.00379
	PSD	.01569	.00301
	VaD	.01580	.00443
	AD	.01510	.00348
MAP2 CA1 %PA	Controls	.497	.862
	PSND	1.202	1.092
	PSD	.887	1.012
	AD	.740	.489
MAP2 CA1 IOD	Controls	140.3	6.7
	PSND	131.2	19.7
	PSD	132.1	13.8
	AD	140.1	8.6
MAP2 CA2 %PA	Controls	2.089	2.420
	PSND	3.764	2.205
	PSD	4.823	4.226
	AD	3.326	4.095
MAP2 CA2 IOD	Controls	133.6	11.0
	PSND	116.4	16.4
	PSD	133.1	15.0
	AD	133.5	10.9

Table 8.8 Numerical values for MAP2 dendritic length-density (DLD) and image analysis. %PA = percentage of area of interest positive stained; IOD = integrated optical density; Std. = standard.

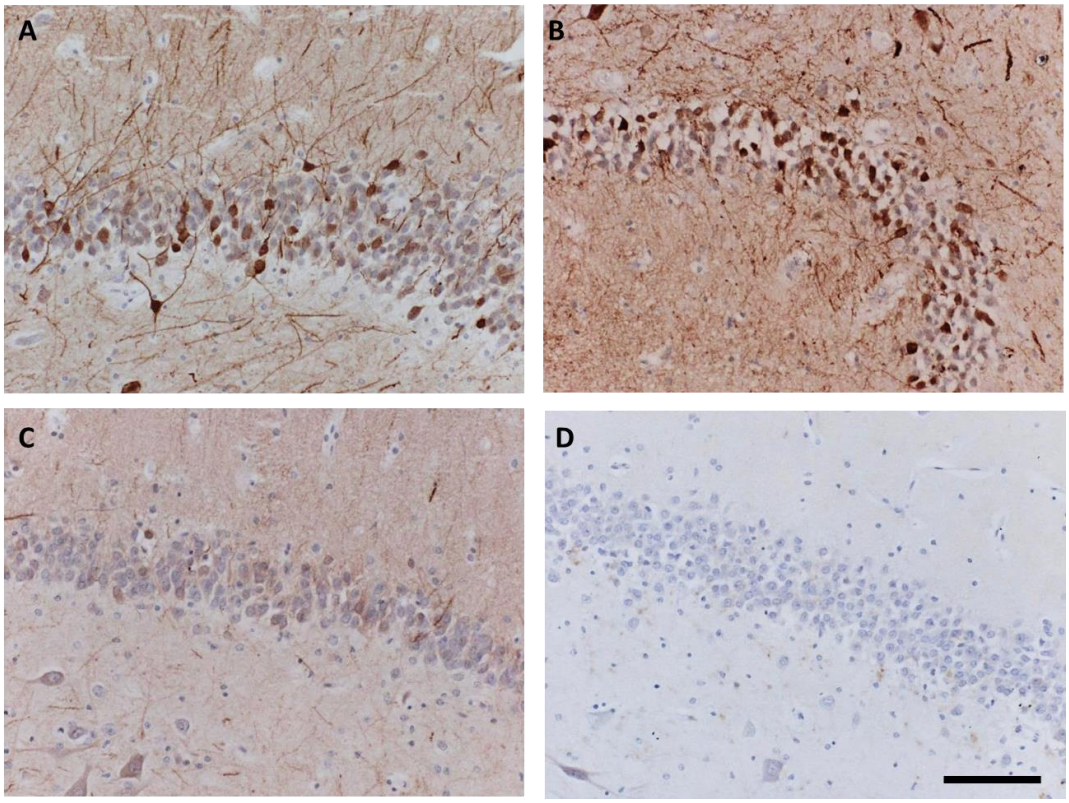

Figure 8.4. Differences in dentate gyrus staining for MAP2. A, control; B, PSD; C and D, PSND. Scale bar = 100µm.

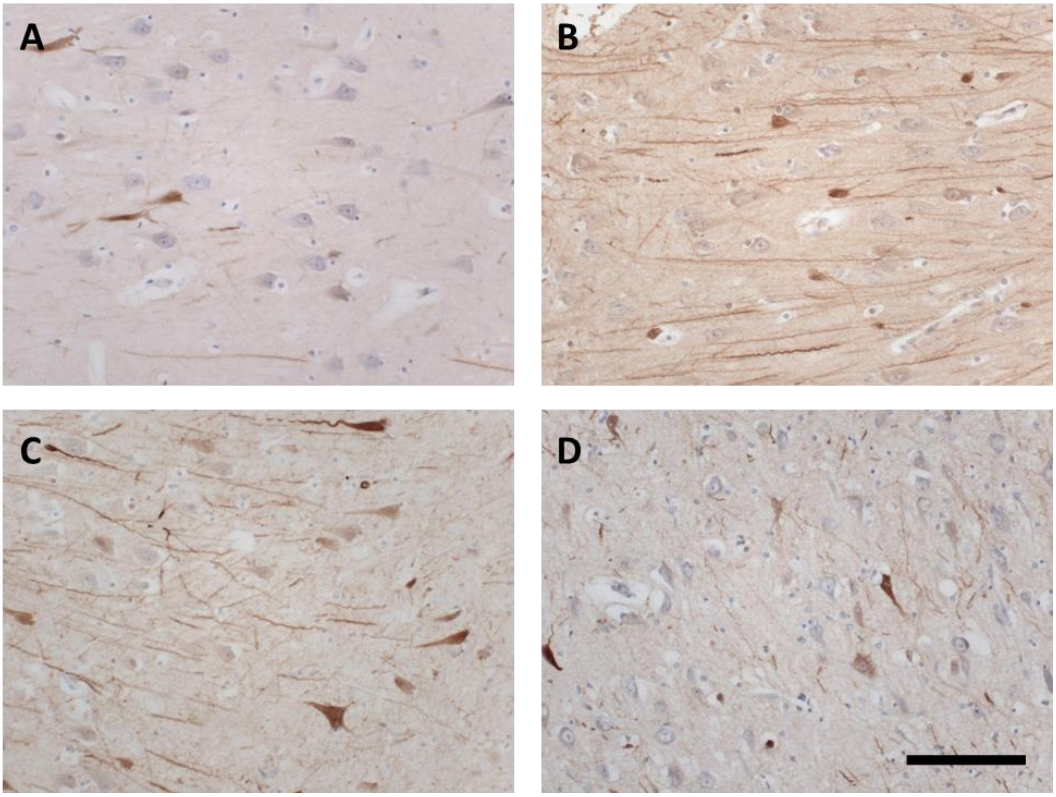

Figure 8.5 Images of subjects with different MAP2 staining and different Braak stages: A = PSND, Braak stage 5; B = PSND, Braak stage 1; C and D = AD, Braak stage 6.

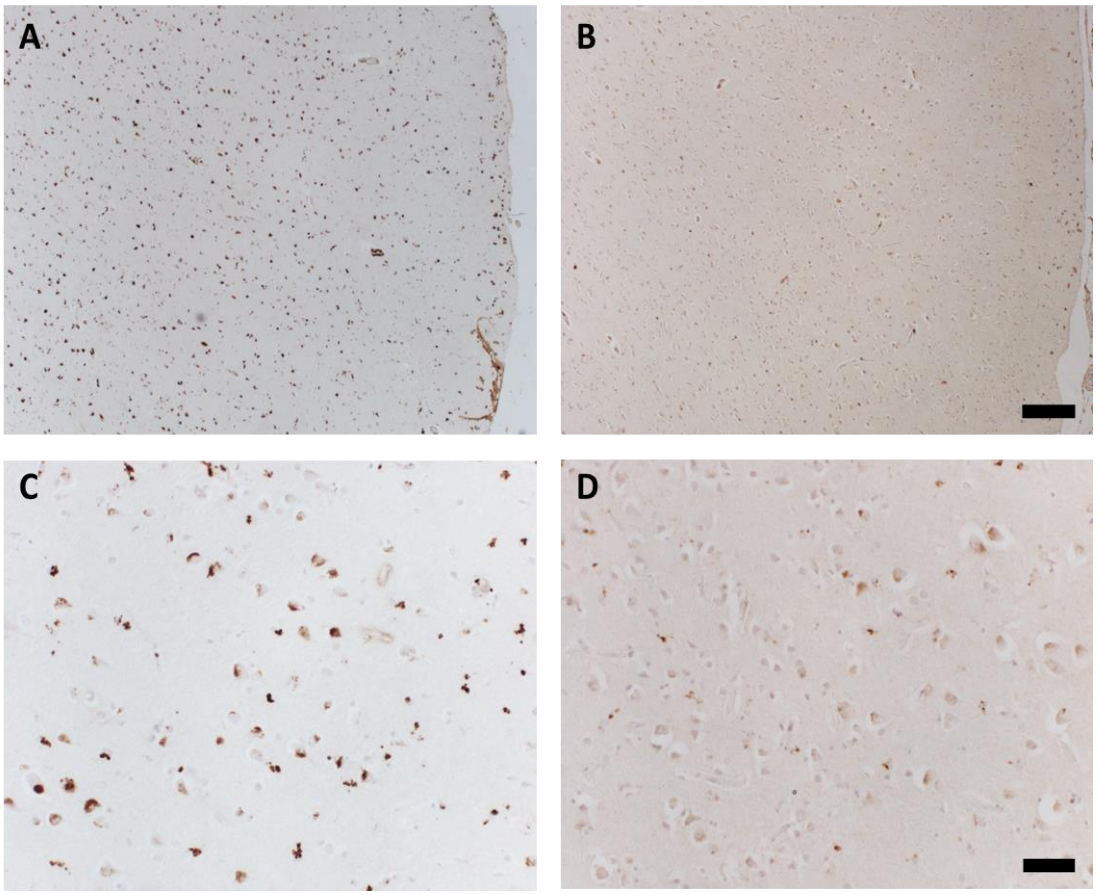

Figure 8.6. dMBP-positive neurons in the temporal cortex of control subjects with intense hippocampal dMBP neuronal immunostaining (A, C) and pale/little hippocampal dMBP neuronal immunostaining (B, D). A-B, Scale bar = 100µm, C-D scale bar = 50µm.

LFB rating

Group	Rating	Frequency	Valid Percent	Cumulative Percent
Controls	1	3	42.9	42.9
	2	2	28.6	71.4
	3	1	14.3	85.7
	4	1	14.3	100.0
PSND	0	2	20.0	20.0
	1	4	40.0	60.0
	3	2	20.0	80.0
	4	2	20.0	100.0
PSD	0	5	45.5	45.5
	1	2	18.2	63.6
	2	1	9.1	72.7
	3	2	18.2	90.9
	4	1	9.1	100.0
AD	1	3	37.5	37.5
	2	4	50.0	87.5
	3	1	12.5	100.0

dMBP rating

Group	Rating	Frequency	Valid Percent	Cumulative Percent
Controls	1	2	33.3	33.3
	2	2	33.3	66.7
	3	2	33.3	100.0
PSND	0	1	10.0	10.0
	1	4	40.0	50.0
	2	2	20.0	70.0
	3	3	30.0	100.0
PSD	0	1	10.0	10.0
	1	2	20.0	30.0
	2	5	50.0	80.0
	3	2	20.0	100.0
AD	0	1	14.3	14.3
	1	2	28.6	42.9
	2	2	28.6	71.4
	3	2	28.6	100.0

Table 8.9 Frequency tables for ratings of myelin integrity in the alveus.

Region	Group	Aldh1L1		GFAP	
		Mean	Std. Deviation	Mean	Std. Deviation
CA1 SR	Controls	12.11	4.52	5.87	3.40
	PSND	15.00	4.64	8.75	2.23
	PSD	16.80	6.07	5.87	2.28
	AD	15.37	5.54	7.33	3.44
CA1 PL	Controls	11.77	2.92	6.99	4.00
	PSND	12.17	2.94	8.12	4.30
	PSD	12.04	3.30	5.01	2.48
	AD	12.97	3.54	9.52	2.37
CA1 WM	Controls	5.74	3.49	16.56	3.98
	PSND	6.64	2.55	20.14	4.42
	PSD	6.41	3.09	17.26	6.31
	AD	7.04	2.10	18.06	4.85
CA2 SR	Controls	14.50	4.27	9.79	6.16
	PSND	10.19	6.88	9.50	1.22
	PSD	12.14	6.37	10.29	4.16
	AD	11.43	6.48	10.50	4.65
CA2 PL	Controls	11.50	2.48	7.00	5.36
	PSND	8.63	5.77	10.10	6.72
	PSD	9.86	4.57	5.43	2.67
	AD	11.50	5.25	13.10	4.57
CA2 WM	Controls	5.19	3.43	17.79	2.20
	PSND	4.50	3.95	19.30	5.32
	PSD	4.45	2.76	16.36	6.73
	AD	4.93	2.42	15.80	7.26
CA3	Controls	12.81	4.37	16.36	7.84
	PSND	8.50	5.92	22.10	5.97
	PSD	11.09	5.25	19.50	6.88
	AD	12.00	6.97	18.10	5.73
CA4	Controls	10.60	4.87	17.26	5.55
	PSND	9.81	3.29	21.31	5.29
	PSD	12.14	1.70	19.77	5.84
	AD	13.39	1.39	18.80	4.08

Table 8.10 Numerical data from investigation into Aldh1L1- and GFAP-positive astrocyte densities. Mean = mean astrocyte density per 0.8mm^2; Std = standard; SR = stratum radiatum; PL = pyramidal layer; WM = white matter (alveus).

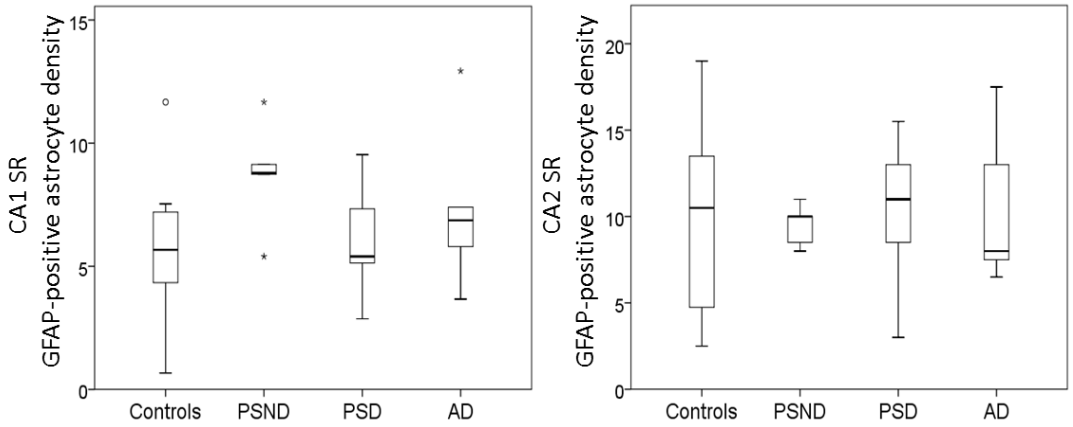

Figure 8.7. GFAP-positive astrocyte density in the CA1 and CA2 stratum radiatum.

GFAP-positive astrocyte counts were positively correlated between regions: CA1 SR (stratum radiatum) – CA2 PL (pyramidal layer), CA3 and CA4; CA1 SR – CA2 PL,; CA1 alveus – CA2 a;lveus, CA3 – CA4 (all $r > 0.43$, $p < 0.05$).

There were positive correlations between CA1 SR – CA1 PL and CA1 alveus; CA1 PL – CA2 PL; CA1 alveus – CA2 alveus; CA2 SR – CA2 PL, CA3 , CA4; CA2 alveus – CA3; CA3 – CA4 (all $p < 0.05$, $r > 0.3$).

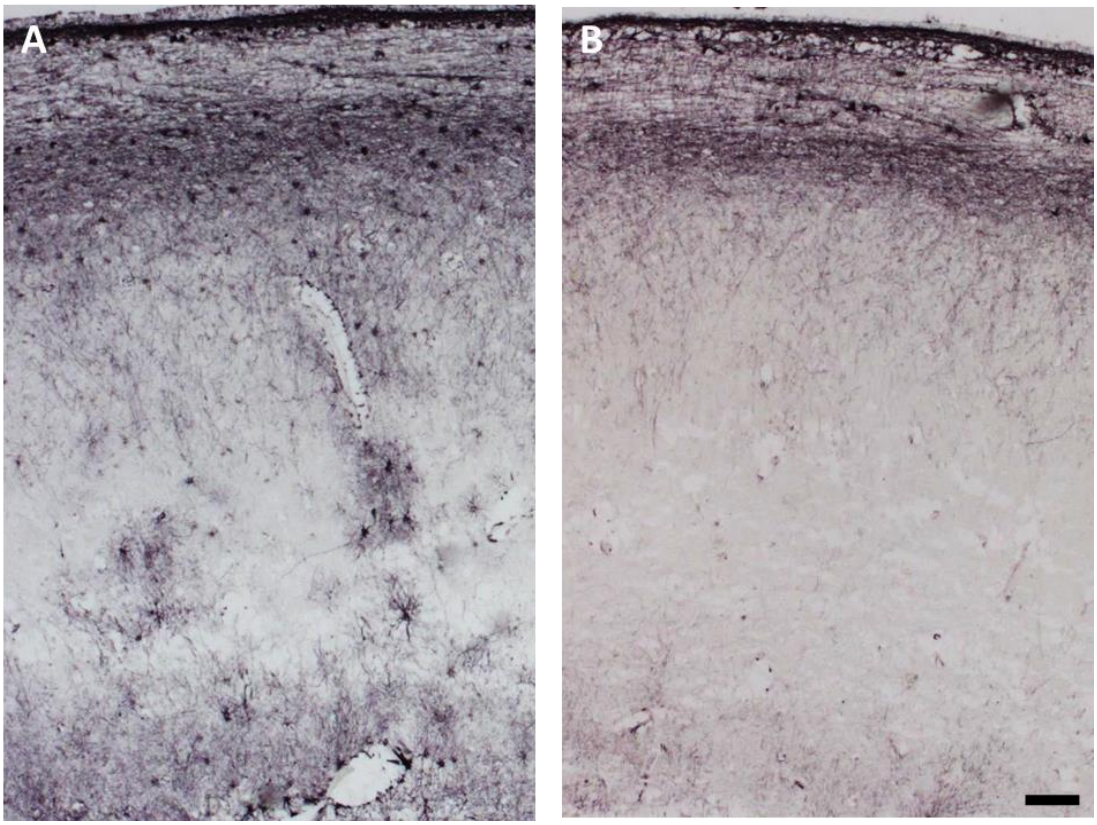

Figure 8.8 Astrocytes in the pyramidal layer and alveus of A) AD subject and B) PSD subject (Braak score 2, CERAD score 0). GFAP was visualized using IHC with Nickel-DAB. Scale bar = 100µm.

References

Aine, C.J., Sanfratello, L., Adair, J.C., Knoefel, J.E., Qualls, C., Lundy, S.L., Caprihan, A., Stone, D. and Stephen, J.M. (2014) 'Characterization of a normal control group: Are they healthy?', *NeuroImage*, 84(0), pp. 796-809.

Akiyama, H., Barger, S., Barnum, S., Bradt, B., Bauer, J., Cole, G.M., Cooper, N.R., Eikelenboom, P., Emmerling, M., Fiebich, B.L., Finch, C.E., Frautschy, S., Griffin, W.S.T., Hampel, H., Hull, M., Landreth, G., Lue, L.F., Mrak, R., Mackenzie, I.R., McGeer, P.L., O'Banion, M.K., Pachter, J., Pasinetti, G., Plata–Salaman, C., Rogers, J., Rydel, R., Shen, Y., Streit, W., Strohmeyer, R., Tooyoma, I., Van Muiswinkel, F.L., Veerhuis, R., Walker, D., Webster, S., Wegrzyniak, B., Wenk, G. and Wyss–Coray, T. (2000) 'Inflammation and Alzheimer's disease', *Neurobiology of Aging*, 21(3), pp. 383-421.

Akulinin, V.A. and Dahlstrom, A. (2003) 'Quantitative Analysis of MAP2 Immunoreactivity in Human Neocortex of Three Patients Surviving After Brain Ischemia', *Neurochemical Research*, 28(2), pp. 373-378.

Alberdi, E., Sánchez-Gómez, M.V. and Matute, C. (2005) 'Calcium and glial cell death', *Cell Calcium*, 38(3–4), pp. 417-425.

Allan, L.M., Rowan, E.N., Firbank, M.J., Thomas, A.J., Parry, S.W., Polvikoski, T.M., O'Brien, J.T. and Kalaria, R.N. (2011) 'Long term incidence of dementia, predictors of mortality and pathological diagnosis in older stroke survivors', *Brain*, 134(12), pp. 3716-3727.

Alonso, A., Grundke-Iqbal, I. and Iqbal, K. (1996) 'Alzheimer's disease hyperphosphorylated tau sequesters normal tau into tangles of filaments and disassembles microtubules', *Nature Medicine*, 2, pp. 783-787.

Altieri, M., Di Piero, V., Pasquini, M., Gasparini, M., Vanacore, N., Vicenzini, E. and Lenzi, G.L. (2004) 'Delayed poststroke dementia: A 4-year follow-up study', *Neurology*, 62(12), pp. 2193-2197.

Amaral, D.G., Scharfman, H.E. and Lavenex, P. (2007) 'The dentate gyrus: fundamental neuroanatomical organization (dentate gyrus for dummies)', in Helen, E.S. (ed.) *Progress in Brain Research*. Elsevier, pp. 3-790.

Americal Psychiatric Association: Diagnostic and Statistical Manual of Mental Disorders, Fourth Edition (2000). 4th Edition edn. Washington, DC.: Americal Psychiatric Association.

Ankarcrona, M., Dypbukt, J.M., Bonfoco, E., Zhivotovsky, B., Orrenius, S., Lipton, S.A. and Nicotera, P. (1995) 'Glutamate-induced neuronal death: A succession of necrosis or apoptosis depending on mitochondrial function', *Neuron*, 15(4), pp. 961-973.

Apaydin, H., Ahlskog, J., Parisi, J.E., Boeve, B.F. and Dickson, D.W. (2002) 'Parkinson disease neuropathology: Later-developing dementia and loss of the levodopa response', *Archives of Neurology*, 59(1), pp. 102-112.

Apostolova, L.G., Green, A.E., Babakchanian, S., Hwang, K.S., Chou, Y.-Y., Toga, A.W. and Thompson, P.M. (2011) 'Hippocampal Atrophy and Ventricular Enlargement in Normal Aging, Mild Cognitive Impairment (MCI), andAlzheimer Disease', *Alzheimer Disease and Associated Disorders*, Publish Ahead of Print, p. 10.1097/WAD.0b013e3182163b62.

Apostolova, L.G., Mosconi, L., Thompson, P.M., Green, A.E., Hwang, K.S., Ramirez, A., Mistur, R., Tsui, W.H. and de Leon, M.J. (2010) 'Subregional hippocampal atrophy predicts Alzheimer's dementia in the cognitively normal', *Neurobiology of Aging*, 31(7), pp. 1077-1088.

Arendt, T. (2009) 'Synaptic degeneration in Alzheimer's disease', *Acta Neuropathologica*, 118(1), pp. 167-179.

Attems, J. and Jellinger, K.A. (2012) *Old Age Psychiatry*. Oxford University Pres.

Baddeley, A. (2001) 'Is stereology unbiased?', *Trends in Neurosciences*, 24(7), pp. 375-376.

Bailey, E.L., Smith, C., Sudlow, C.L.M. and Wardlaw, J.M. (2012) 'Pathology of Lacunar Ischemic Stroke in Humans—A Systematic Review', *Brain Pathology*, 22(5), pp. 583-591.

Ballard, C., Rowan, E., Stephens, S., Kalaria, R. and Kenny, R.A. (2003a) 'Prospective Follow-Up Study Between 3 and 15 Months After Stroke: Improvements and Decline in Cognitive Function Among Dementia-Free Stroke Survivors >75 Years of Age', *Stroke*, 34(10), pp. 2440-2444.

Ballard, C.G., Stephens, S., Kenny, R.A., Kalaria, R.N., Tovee, M. and O'Brien, J. (2003b) 'Profile of Neuropsychological Deficits in Older Stroke Survivors without Dementia', *Dementia and Geriatric Cognitive Disorders*, 16, pp. 52-56.

Ballatore, C., Lee, V.M.Y. and Trojanowski, J.Q. (2007) 'Tau-mediated neurodegeneration in Alzheimer's disease and related disorders', *Nat Rev Neurosci*, 8(9), pp. 663-672.

Banasiak, K.J., Xia, Y. and Haddad, G.G. (2000) 'Mechanisms underlying hypoxia-induced neuronal apoptosis', *Progress in Neurobiology*, 62(3), pp. 215-249.

Baneux, P.J., Garner, D., McIntyre, H.B. and Holshuh, H.J. (1986) 'Euthanasia of rabbits by intravenous administration of ketamine.', *Journal of the American Veterinary Medical Association*, 189(9), pp. 1038-9.

Barba, R., Martinez-Espinosa, S., Rodriguez-Garcia, E., Pondal, M., Vivancos, J. and Del Ser, T. (2000) 'Poststroke Dementia : Clinical Features and Risk Factors', *Stroke*, 31(7), pp. 1494-1501.

Barber, R., Ballard, C., McKeith, I.G., Gholkar, A. and Oâ€™Brien, J.T. (2000) 'MRI volumetric study of dementia with Lewy bodies: A comparison with AD and vascular dementia', *Neurology*, 54(6), pp. 1304-1309.

Barber, R., Gholkar, A., Scheltens, P., Ballard, C., McKeith, I.G. and O'Brien, J.T. (1999) 'Medial temporal lobe atrophy on MRI in dementia with Lewy bodies', *Neurology*, 52(6), pp. 1153-.

Barres, B.A. (2008) 'The Mystery and Magic of Glia: A Perspective on Their Roles in Health and Disease', *Neuron*, 60(3), pp. 430-440.

Barreto, G.E., Sun, X., Xu, L. and Giffard, R.G. (2011) 'Astrocyte Proliferation Following Stroke in the Mouse Depends on Distance from the Infarct', *PLoS ONE*, 6(11), p. e27881.

Barulli, D. and Stern, Y. (2013) 'Efficiency, capacity, compensation, maintenance, plasticity: emerging concepts in cognitive reserve', *Trends in Cognitive Sciences*, 17(10), pp. 502-509.

Bastos-Leite, A.J., van der Flier, W.M., van Straaten, E.C.W., Staekenborg, S.S., Scheltens, P. and Barkhof, F. (2007) 'The Contribution of Medial Temporal Lobe Atrophy and Vascular Pathology to Cognitive Impairment in Vascular Dementia', *Stroke*, 38(12), pp. 3182-3185.

Beauquis, J., Pavía, P., Pomilio, C., Vinuesa, A., Podlutskaya, N., Galvan, V. and Saravia, F. (2013) 'Environmental enrichment prevents astroglial pathological changes in the hippocampus of APP transgenic mice, model of Alzheimer's disease', *Experimental Neurology*, 239(0), pp. 28-37.

Bell, R. and Zlokovic, B. (2009) 'Neurovascular mechanisms and blood–brain barrier disorder in Alzheimer's disease', *Acta Neuropathologica*, 118(1), pp. 103-113.

Bender, R. and Lange, S. (2001) 'Adjusting for multiple testing—when and how?', *Journal of Clinical Epidemiology*, 54(4), pp. 343-349.

Binder, J.R., Desai, R.H., Graves, W.W. and Conant, L.L. (2009) 'Where Is the Semantic System? A Critical Review and Meta-Analysis of 120 Functional Neuroimaging Studies', *Cerebral Cortex*, 19(12), pp. 2767-2796.

Bolmont, T., Haiss, F., Eicke, D., Radde, R., Mathis, C.A., Klunk, W.E., Kohsaka, S., Jucker, M. and Calhoun, M.E. (2008) 'Dynamics of the Microglial/Amyloid Interaction Indicate a Role in Plaque Maintenance', *The Journal of Neuroscience*, 28(16), pp. 4283-4292.

Braak, E. and Braak, H. (1997) 'Alzheimer's disease: transiently developing dendritic changes in pyramidal cells of sector CA1 of the Ammon's horn', *Acta Neuropathologica*, 93(323-325).

Braak, H. and Braak, E. (1991) 'Neuropathological stageing of Alzheimer-related changes', *Acta Neuropathologica*, 82(4), pp. 239-259.

Braak, H. and Braak, E. (1996) 'Evolution of the neuropathology of Alzheimer's disease.', *Acta Neurologica Scandinavica Supplement*, 165, pp. 3-12.

Briones, T.L., Woods, J., Wadowska, M., Rogozinska, M. and Nguyen, M. (2006) 'Astrocytic changes in the hippocampus and functional recovery after cerebral ischemia are facilitated by rehabilitation training', *Behavioural Brain Research*, 171(1), pp. 17-25.

Brown, A.M. and Ransom, B.R. (2007) 'Astrocyte glycogen and brain energy metabolism', *Glia*, 55(12), pp. 1263-1271.

Buell, S.J. (1982) 'Golgi-Cox and rapid golgi methods as applied to autopsied human brain tissue: widely disparate results.', *Journal of Neuropathology & Experimental Neurology*, 41(5), pp. 500-507.

Burgess, N., Maguire, E.A. and O'Keefe, J. (2002) 'The Human Hippocampus and Spatial and Episodic Memory', *Neuron*, 35(4), pp. 625-641.

Burke, M.C.J., Nelson, L., Slade, J.Y., Oakley, A.E., Khundakar, A.A. and Kalaria, R.N. (2013) 'Morphometry of the hippocampal microvasculature in post-stroke and age-related dementias', *Neuropathology and Applied Neurobiology*, pp. n/a-n/a.

Burke, S.N. and Barnes, C.A. (2006) 'Neural plasticity in the ageing brain', *Nat Rev Neurosci*, 7(1), pp. 30-40.

Burton, E.J., Kenny, R.A., O'Brien, J., Stephens, S., Bradbury, M., Rowan, E., Kalaria, R., Firbank, M., Wesnes, K. and Ballard, C. (2004) 'White Matter Hyperintensities Are Associated With Impairment of Memory, Attention, and Global Cognitive Performance in Older Stroke Patients', *Stroke*, 35(6), pp. 1270-1275.

Butler, T.R., Self, R.L., Smith, K.J., Sharrett-Field, L.J., Berry, J.N., Littleton, J.M., Pauly, J.R., Mulholland, P.J. and Prendergast, M.A. (2010) 'Selective vulnerability of hippocampal cornu ammonis 1 pyramidal cells to excitotoxic insult is associated with the expression of polyamine-sensitive N-methyl-d-asparate-type glutamate receptors', *Neuroscience*, 165(2), pp. 525-534.

Cahoy, J.D., Emery, B., Kaushal, A., Foo, L.C., Zamanian, J.L., Christopherson, K.S., Xing, Y., Lubischer, J.L., Krieg, P.A., Krupenko, S.A., Thompson, W.J. and Barres, B.A. (2008) 'A Transcriptome Database for Astrocytes, Neurons, and Oligodendrocytes: A New Resource for Understanding Brain Development and Function', *The Journal of Neuroscience*, 28(1), pp. 264-278.

Canto, C., Wouterlood, F.G. and Witter, M.P. (2008) 'What Does the Anatomical Organization of the Entorhinal Cortex Tell Us?', *Neural Plasticity*, 2008, Article ID 381243, p. 18 [Online] DOI: doi:10.1155/2008/381243.

Capizzano, A., Acion, L., Bekinschtein, T., Furman, M., Gomila, H., Martinez, A., Mizrahi, R. and Starkstein, S. (2004) 'White matter hyperintensities are significantly associated with cortical atrophy in Alzheimer's disease', *Journal of Neurology Neurosurgery and Psychiatry*, 75(6), pp. 822-827.

Carloni, S., Buonocore, G. and Balduini, W. (2008) 'Protective role of autophagy in neonatal hypoxia–ischemia induced brain injury', *Neurobiology of Disease*, 32(3), pp. 329-339.

Carmeli, C., Donati, A., Antille, V., Viceic, D., Ghika, J., von Gunten, A., Clarke, S., Meuli, R., Frackowiak, R.S. and Knyazeva, M.G. (2013) 'Demyelination in Mild Cognitive Impairment Suggests Progression Path to Alzheimer's Disease', *PLoS ONE*, 8(8), p. e72759.

Cenquizca, L.A. and Swanson, L.W. (2007) 'Spatial organization of direct hippocampal field CA1 axonal projections to the rest of the cerebral cortex', *Brain Research Reviews*, 56(1), pp. 1-26.

Chen, J.J., Rosas, H.D. and Salat, D.H. (2011a) 'Age-associated reductions in cerebral blood flow are independent from regional atrophy', *NeuroImage*, 55(2), pp. 468-478.

Chen, Q., He, S., Hu, X.-L., Yu, J., Zhou, Y., Zheng, J., Zhang, S., Zhang, C., Duan, W.-H. and Xiong, Z.-Q. (2007) 'Differential Roles of NR2A- and NR2B-Containing NMDA Receptors in Activity-Dependent Brain-Derived Neurotrophic Factor Gene Regulation and Limbic Epileptogenesis', *The Journal of Neuroscience*, 27(3), pp. 542-552.

Chen, X., Nelson, C.D., Li, X., Winters, C.A., Azzam, R., Sousa, A.A., Leapman, R.D., Gainer, H., Sheng, M. and Reese, T.S. (2011b) 'PSD-95 Is Required to Sustain the Molecular

Organization of the Postsynaptic Density', *The Journal of Neuroscience*, 31(17), pp. 6329-6338.
Cherra III, S.J. and Chu, C.T. (2008) 'Autophagy in neuroprotection and neurodegeneration: A question of balance', *Future Neuroloft*, 3(3), pp. 309-323.
Christiansen, P., Larsson, H.B.W., Thomsen, C., Weislander, S.B. and Henriksen, O. (1994) 'Age-dependent white matter lesions and brain volume chanegs in healthy volunteers', *Acta Radiologica*, 35(2), pp. 117-122.
Colombo, J.A., Quinn, B. and Puissant, V. (2002) 'Disruption of astroglial interlaminar processes in Alzheimer's disease', *Brain Research Bulletin*, 58(2), pp. 235-242.
Colombo, J.A. and Reisin, H.D. (2004) 'Interlaminar astroglia of the cerebral cortex: a marker of the primate brain', *Brain Research*, 1006(1), pp. 126-131.
Conde, C. and Cáceres, A. (2009) 'Microtubule assembly, organization and dynamics in axons and dendrites', *Nature Reviews Neuroscience*, 10(319-332).
Cotter, D., Wilson, S., Roberts, E., Kerwin, R. and Everall, I.P. (2000) 'Increased dendritic MAP2 expression in the hippocampus in schizophrenia', *Schizophrenia Research*, 41(2), pp. 313-323.
Counts, S.E., Nadeem, M., Lad, S.P., Wuu, J. and Mufson, E.J. (2006) 'Differential expression of synaptic proteins in the frontal and temporal cortex of elderly subjects with mild cognitive impairment.', *Journal of Neuropathology & Experimental Neurology*, 65, pp. 592-601.
Cuadros, M.A. and Navascués, J. (1998) 'The origin and differentiation of microglial cells during development', *Progress in Neurobiology*, 56(2), pp. 173-189.
Cumming, T.B. and Brodtmann, A. (2011) 'Can stroke cause neurodegenerative dementia?', *International Journal of Stroke*, 6(5), pp. 416-424.
Davalos, D., Grutzendler, J., Yang, G., Kim, J.V., Zuo, Y., Jung, S., Littman, D.R., Dustin, M.L. and Gan, W.B. (2005) 'ATP mediates rapid microglial response to local brain injury in vivo', *Nature Neuroscience*, 8(752-758).
Davis, R. and Huffman, R. (1968) *A Stereotaxic Atlas of the Brain of the baboon (Papio)*. Department of Physiology, Southwest Foundation for Resrach and Education, San Antonio, Texas.
de Koning, I., van Kooten, F., Dippel, D.W.J., van Harskamp, F., Grobbee, D.E., Kluft, C. and Koudstaal, P.J. (1998) 'The CAMCOG: A Useful Screening Instrument for Dementia in Stroke Patients', *Stroke*, 29(10), pp. 2080-2086.
de la Torre, J.C. (2002) 'Alzheimer Disease as a Vascular Disorder: Nosological Evidence', *Stroke*, 33(4), pp. 1152-1162.
den Heijer, T., der Lijn, F.v., Vernooij, M.W., de Groot, M., Koudstaal, P.J., der Lugt, A.v., Krestin, G.P., Hofman, A., Niessen, W.J. and Breteler, M.M.B. (2012) 'Structural and diffusion MRI measures of the hippocampus and memory performance', *NeuroImage*, 63(4), pp. 1782-1789.
Den Heijer, T., Geerlings, M.I., Hoebeek, F.E., Hofman, A., Koudstaal, P.J. and Breteler, M.M.B. (2006) 'Use of hippocampal and amygdalar volumes on magnetic resonance imaging to predict dementia in cognitively intact elderly people', *Archives of General Psychiatry*, 63(1), pp. 57-62.
Deramecourt, V., Slade, J.Y., Oakley, A.E., Perry, R.H., Ince, P.G., Maurage, C.A. and Kalaria, R.N. (2012) 'Staging and natural history of cerebrovascular pathology in dementia', *Neurology*, 78(14), pp. 1043-1050.
Desmond, D.W., Erkinjuntti, T., Sano, M., Cummings, J.L., Bowler, J.V., Pasquier, F., Moroney, J.T., Ferris, S., Stern, Y., Sachdev, P.S. and Hachinski, V.C. (1999) 'The cognitive syndrome of vascular dementia: implications for clinical trials.', *Alzheimer Disease & Associated Disorders*, 13, pp. S21-9.
Desmond, D.W., Moroney, J.T., Paik, M.C., Sano, M., Mohr, J.P., Aboumatar, S., Tseng, C.L., Chan, S., Williams, J.B.W., Remien, R.H., Hauser, W.A. and Stern, Y. (2000) 'Frequency and clinical determinants of dementia after ischemic stroke', *Neurology*, 54(5), pp. 1124-1131.

Dihné, M., Block, F., Korr, H. and Töpper, R. (2001) 'Time course of glial proliferation and glial apoptosis following excitotoxic CNS injury', *Brain Research*, 902(2), pp. 178-189.
Doetsch, F., Caillé, I., Lim, D.A., García-Verdugo, J.M. and Alvarez-Buylla, A. (1999) 'Subventricular Zone Astrocytes Are Neural Stem Cells in the Adult Mammalian Brain', *Cell*, 97(6), pp. 703-716.
Duevernoy, H.M. (2005) *The Human Hippocampus: Functional Anatomy, Vascularization and Serial Sections with MRI*. Third edn. Springer-Verlag Berlin Heidelberg New York.
Eichenbaum, H. (2003) 'The hippocampus, episodic memory, declarative memory, spatial memory…where does it all come together?', *International Congress Series*, 1250(0), pp. 235-244.
Esiri, M.M., Matthews, F. and Brayne, C. (2001) 'Pathological correlates of late-onset dementia in a multicentre, community-based population in England and Wales', *The Lancet*, 357(9251), pp. 169-175.
'Factsheet: Rarer Causes of Dementia', (2012), *www.alzheimers.org.uk* [Online]. Available at: http://www.alzheimers.org.uk/site/scripts/download_info.php?fileID=1767.
Farkas, E. and Luiten, P.G.M. (2001) 'Cerebral microvascular pathology in aging and Alzheimer's disease', *Progress in Neurobiology*, 64(6), pp. 575-611.
Fellgiebel, A. and Yakushev, I. (2011) 'Diffusion tensor imaging of the hippocampus in MCI and early Alzheimer's disease.', *Journal of Alzheimer's Disease*, 26, pp. 257-62.
Ferrer, I., Kaste, M. and Kalimo, H. (2008) *Greenfield's Neuropathology*. Oxford, UK: Oxford University Press.
Fetler, L. and Amigorena, S. (2005) 'Brain Under Surveillance: The Microglia Patrol', *Science*, 309(5733), pp. 392-393.
Firbank, M.J., Burton, E.J., Barber, R., Stephens, S., Kenny, R.A., Ballard, C., Kalaria, R.N. and O'Brien, J.T. (2007) 'Medial temporal atrophy rather than white matter hyperintensities predict cognitive decline in stroke survivors', *Neurobiology of Aging*, 28(11), pp. 1664-1669.
Firbank, M.J., He, J., Blamire, A.M., Singh, B., Danson, P., Kalaria, R.N. and O'Brien, R. (2011) 'Cerebral blood flow by arterial spin labeling in poststroke dementia.', *Neurology*, 76(17), pp. 1478-84.
Fjell, A.M. and Walhovd, K.B. (2010) 'Structural Brain Changes in Aging: Courses, Causes and Cognitive Consequences', *Reviews in the Neurosciences*, 21(3), pp. 187-222.
Flood, D.G. (1993) 'Critical issues in the analysis of dendritic extent in aging humans, primates, and rodents', *Neurobiology of Aging*, 14(6), pp. 649-654.
Folstein, M.F., Folstein, S.E. and McHugh, P.R. (1975) '"Mini-mental state" : A practical method for grading the cognitive state of patients for the clinician', *Journal of Psychiatric Research*, 12(3), pp. 189-198.
Freeman, S., Kandel, R., Crus, L., Rozkalne, A., Newell, K., Frosch, M.P., Hedley-Whyte, E.T., Locascio, J.J., Lispitz, L. and Hyman, B.T. (2008) 'Preservation of Neuronal Number Despite Age-Related Cortical Brain Atrophy In Elderly Subjects Without Alzhiemer Disease', *Journal of Neuropathology and Experimental Neurology*, 67(12), pp. 1205-1212.
Frisoni, G.B., Fox, N.C., Jack, C.R., Scheltens, P. and Thompson, P.M. (2010) 'The clinical use of structural MRI in Alzheimer disease', *Nat Rev Neurol*, 6(2), pp. 67-77.
Gallagher, J.J., Zhang, X., Ziomek, G.J., Jacobs, R.E. and Bearer, E.L. (2012) 'Deficits in axonal transport in hippocampal-based circuitry and the visual pathway in APP knock-out animals witnessed by manganese enhanced MRI', *NeuroImage*, 60(3), pp. 1856-1866.
Gemmell, E., Bosomworth, H., Allan, L., Hall, R., Khundakar, A., Oakley, A.E., Deramecourt, V., Polvikoski, T.M., O'Brien, J.T. and Kalaria, R.N. (2012) 'Hippocampal Neuronal Atrophy and Cognitive Function in Delayed Poststroke and Aging-Related Dementias', *Stroke*, 43(3), pp. 808-814.
Giannakopoulos, P., Herrmann, F.R.B., T., Bouras, C., Kövari, E., Perl, D.P., Morrison, J.H., Gold, G. and Hof, P.R. (2003) 'Tangle and neuron numbers, but not amyloid load, predict cognitive status in Alzheimer's disease.', *Neurology*, May 13(60 (9)), pp. 1495-500.

Giannakopoulos, P., Hof, P.R., KÃ¶vari, E., Vallet, P.G., Herrmann, F.R. and Bouras, C. (1996) 'Distinct patterns of neuronal loss and Alzheimer's disease lesion distribution in elderly individuals older than 90 years', *Journal of Neuropathology and Experimental Neurology*, 55(12), pp. 1210-1220.
Giaume, C., Kirchoff, F., Matute, C., Reichenbach, A. and Verkhratsky, A. (2007) 'Glia: the fulcrum of brain diseases', *Cell Death and Differentiation*, 14(1324-1335).
Goedert, M.K., A. Crowther, R. A. (2006) 'Tau protein, the paired helical filament and Alzheimer's disease', *Journal of Alzheimer's Disease*, 9, pp. 195-207.
Gokhale, A.M. (1990) 'Unbiased estimation of curve length in 3-D using vertical slices', *Journal of Microscopy*, 159(2), pp. 133-141.
Golgi, C. (1873) 'Sulla struttura della sostanza grigia dell cervello', *Gazz. Med. Lombarda*, 33, pp. 224-246.
Gómez-Isla, T., Hollister, R., West, H., Mui, S., Growdon, J.H., Petersen, R.C., Parisi, J.E. and Hyman, B.T. (1997) 'Neuronal loss correlates with but exceeds neurofibrillary tangles in Alzheimer's disease', *Annals of Neurology*, 41(1), pp. 17-24.
Gorelick, P.B. (2004) 'Risk Factors for Vascular Dementia and Alzheimer Disease', *Stroke*, 35(11_suppl_1), pp. 2620-2622.
Gorelick, P.B. and Nyenhuis, D. (2013) 'Understanding and Treating Vascular Cognitive Impairment.', *CONTINUUM: Lifelong Learning in Neurology*, 19(2), pp. 425-437.
Gosche, K.M., Mortimer, J.A., Smith, C.D., Markesbery, W.R. and Snowdon, D.A. (2002) 'Hippocampal volume as an index of Alzheimer neuropathology: Findings from the Nun Study', *Neurology*, 58(10), pp. 1476-1482.
Grinberg, L.T. and Thal, D.R. (2010) 'Vascular Pathology in the aged human brain', *Acta Neuropathologica*, 119(3), pp. 277-290.
Grolla, A.A., Sim, J.A., Lim, D., Rodriguez, J.J., Genazzani, A.A. and Verkhratsky, A. (2013) 'Amyloid-β and Alzheimer's disease type pathology differentially affects the calcium signalling toolkit in astrocytes from different brain regions', *Cell Death and Disease*, 4(5), p. e623.
Grundman, M., Jack, C., Petersen, R., Kim, H., Taylor, C., Datvian, M., Weiner, M., DeCarli, C., DeKosky, S., Dyck, C., Darvesh, S., Yaffe, K., Kaye, J., Ferris, S., Thomas, R. and Thal, L. (2003) 'Hippocampal volume is associated with memory but not nonmemory cognitive performance in patients with mild cognitive impairment', *Journal of Molecular Neuroscience*, 20(3), pp. 241-248.
Grysiewicz, R. and Gorelick, P. (2012) 'Key Neuroanatomical Structures for Post-Stroke Cognitive Impairment', *Current Neurology and Neuroscience Reports*, 12(6), pp. 703-708.
Gundersen, H.J.G., Bagger, P., Bendtsen, T.F., Evans, S.M., Krobo, L., Marcussen, N., Moller, A., Nielsen, K., Nyengaard, J.R. and Pakkenberg, B. (1988) 'The New Stereological tools: disector, fractionator, nucleator and point sampled intercepts and their use in pathological research and diagnosis', *Acta pathologica, microbiologica et imminologica Scandinavica*, 96(10), pp. 857-81.
Gundersen, H.J.G. and Jensen, E.B. (1987) 'The Efficiency of Systematic Sampling in Stereology and its Prediction', *Journal of Microscopy*, 147, pp. 229-63.
Gunning-Dixon, F.M., Brickman, A.M., Cheng, J.C. and Alexopoulos, G.S. (2009) 'Aging of cerebral white matter: a review of MRI findings', *International Journal of Geriatric Psychiatry*, 24(2), pp. 109-117.
Gylys, K.H., Fein, J.A., Yang, F., Wiley, D.J., Miller, C.A. and Cole, G.M. (2004) 'Synaptic Changes in Alzheimer's Disease: Increased Amyloid-β and Gliosis in Surviving Terminals Is Accompanied by Decreased PSD-95 Fluorescence', *The American Journal of Pathology*, 165(5), pp. 1809-1817.
Halassa, M.M., Fellin, T., Takano, H., Dong, J. and Haydon, P.G. (2007) 'Synaptic Islands Defined by the Territory of a
Single Astrocyte', *The Journal of Neuroscience*, 27(24), pp. 6473-6477.

Haley, G., Kohama, S., Urbanski, H. and Raber, J. (2010) 'Age-related decreases in SYN levels associated with increases in MAP-2, apoE, and GFAP levels in the rhesus macaque prefrontal cortex and hippocampus', *AGE*, 32(3), pp. 283-296.
Hanks, S.D. and Flood, D.G. (1991) 'Region-specific stability of dendritic extent in normal human aging and regression in Alzheimer's disease. I. CA1 of hippocampus', *Brain Research*, 540(1-2), pp. 63-82.
Hara, A. and Mori, H. (2000) 'Novel Apoptotic Evidence for Delayed Neuronal Death in the Hippocampal CA1 Pyramidal Cells After Transient Ischemia', *Stroke*, 31(1), pp. 231-239.
Hardy, J. and Selkoe, D.J. (2002) 'The Amyloid Hypothesis of Alzheimer's Disease: Progress and Problems on the Road to Therapeutics', *Science*, 297(5580), pp. 353-356.
Hardy, J.A. and Higgins, G.A. (1992) 'Alzheimer's disease: the amyloid cascade hypothesis.', *Science*, 256, pp. 184-5.
Harris, K.M. (1999) 'Structure, development, and plasticity of dendritic spines', *Current Opinion in Neurobiology*, 9(3), pp. 343-348.
Harris, K.M., Jensen, F.E. and Tsao, B. (1992) 'Three-dimensional structure of dendritic spines and synapses in rat hippocampus (CA1) at postnatal day 15 and adult ages: implications for the maturation of synaptic physiology and long-term potentiation [published erratum appears in J Neurosci 1992 Aug;12(8):following table of contents]', *The Journal of Neuroscience*, 12(7), pp. 2685-2705.
Harrison, P.J. and Eastwood, S.L. (2001) 'Neuropathological studies of synaptic connectivity in the hippocampal formation in schizophrenia', *Hippocampus*, 11(5), pp. 508-519.
Hawkins, B.T. and Davis, T.P. (2005) 'The Blood-Brain Barrier/Neurovascular Unit in Health and Disease', *Pharmacological Reviews*, 57(2), pp. 173-185.
Holtmaat, A., Wilbrecht, L., Knott, G.W., Welker, E. and Svoboda, K. (2006) 'Experience-dependent and cell-type-specific spine growth in the neocortex', *Nature*, 441, pp. 979-983.
Hoskison, M.M. and Shuttleworth, C.W. (2006) 'Microtubule disruption, not calpain-dependent loss of MAP2, contributes to enduring NMDA-induced dendritic dysfunction in acute hippocampal slices', *Experimental Neurology*, 202(2), pp. 302-312.
Huang, K.-L., Lin, K.-J., Ho, M.-Y., Chang, Y.-J., Chang, C.-H., Wey, S.-P., Hsieh, C.-J., Yen, T.-C., Hsiao, I.-T. and Lee, T.-H. (2012) 'Amyloid deposition after cerebral hypoperfusion: Evidenced on [18F]AV-45 positron emission tomography', *Journal of the Neurological Sciences*, 319(1–2), pp. 124-129.
Hyman, B.T., Van Hoesen, G.W., Damasio, A.R. and Barnes, C.L. (1984) 'Alzheimer's Disease: Cell-Specific Pathology Isolates the Hippocampal Formation', *Science*, 225(225), pp. 1168-70.
Hynd, M.R., Scott, H.L. and Dodd, P.R. (2004) 'Glutamate-mediated excitotoxicity and neurodegeneration in Alzheimer's disease', *Neurochemistry International*, 45(5), pp. 583-595.
Ihara, M., Polvikoski, T.M., Hall, R., Slade, J., Perry, R.H., Oakley, A.E., Englund, E., O'Brien, J.T., Ince, P.G. and Kalaria, R.N. (2010) 'Quantification of myelin loss in frontal lobe white matter in vascular dementia, Alzheimer's disease, and dementia with Lewy bodies', *Acta Neuropathologica*, 119(5), pp. 579-589.
Imura, T., Nakano, I., Kornblum, H.I. and Sofroniew, M.V. (2006) 'Phenotypic and functional heterogeneity of GFAP-expressing cells in vitro: Differential expression of LeX/CD15 by GFAP-expressing multipotent neural stem cells and non-neurogenic astrocytes', *Glia*, 53(3), pp. 277-293.
Ince, P.G. (2001) 'Pathological correlates of late-onset dementia in a multicentre, community-based population in England and Wales', *The Lancet*, 357(9251), pp. 169-175.
Iqbal, K. and Grundke-Iqbal, I. (1997) 'Mechanism of Alzheimer neurofibrillary degeneration and the formation of tangles', *Molecular Psychiatry*, 2(3), pp. 178-180.

Ishimaru, H., Casamenti, F., Uéda, K., Maruyama, Y. and Pepeu, G. (2001) 'Changes in presynaptic proteins, SNAP-25 and synaptophysin, in the hippocampal CA1 area in ischemic gerbils', *Brain Research*, 903(1–2), pp. 94-101.

Ishizuka, N., Weber, J. and Amaral, D.G. (1990) 'Organization of intrahippocampal projections originating from CA3 pyramidal cells in the rat.', *Joural of Computational Neurology*, 295, pp. 580-623.

Ivanov, A., Esclapez, M., Pellegrino, C., Shirao, T. and Ferhat, L. (2009) 'Drebrin A regulates dendritic spine plasticity and synaptic function in mature cultured hippocampal neurons', *Journal of Cell Science*, 122(4), pp. 524-534.

Izumi, Y., Haida, M., Hata, T., Isozumi, K., Kurita, D. and Shinohara, Y. (2002) 'Distribution of brain oedema in the contralateral hemisphere after cerebral infarction: repeated MRI measurement in the rat', *Journal of Clinical Neuroscience*, 9(3), pp. 289-293.

Jellinger, K. (2007) 'The enigma of vascular cognitive disorder and vascular dementia', *Acta Neuropathologica*, 113(4), pp. 349-388.

Jia, H., Zhang, X., Zhang, B., Liu, Y. and Li, J. (2012) 'Dendritic morphology of neurons in medial prefrontal cortex and hippocampus in 2VO rats', *Neurological Sciences*, 33(5), pp. 1063-1070.

Jiang, J., Parameshwaran, K., Seibenhener, M.L., Kang, M.-G., Suppiramaniam, V., Huganir, R.L., Diaz-Meco, M.T. and Wooten, M.W. (2009) 'AMPA receptor trafficking and synaptic plasticity require SQSTM1/p62', *Hippocampus*, 19(4), pp. 392-406.

Johansen, T. and Lamark, T. (2011) 'Selective autophagy mediated by autophagic adapter proteins', *Autophagy*, 7(3), pp. 279-296.

Jokinen, H., Kalska, H., Ylikoski, R., Hietanen, M., Mäntylä, R., Pohjasvaara, T., Kaste, M. and Erkinjuntti, T. (2004) 'Medial temporal lobe atrophy and memory deficits in elderly stroke patients', *European Journal of Neurology*, 11(12), pp. 825-832.

Jones, M.W. and McHugh, T.J. (2011) 'Updating hippocampal representations: CA2 joins the circuit', *Trends in Neurosciences*, 34(10), pp. 526-535.

Jones, R.N., Manly, J., Glymour, M.M., Rentz, D.M., Jefferson, A.L. and Stern, Y. (2011) 'Conceptual and Measurement Challenges in Research on Cognitive Reserve', *Journal of the International Neuropsychological Society*, 17(04), pp. 593-601.

Kalaria, R.N. (2000) 'The role of cerebral ischemia in Alzheimer's disease', *Neurobiology of Aging*, 21(2), pp. 321-330.

Kalaria, R.N. (2010) 'Vascular basis for brain degeneration: faltering controls and risk factors for dementia', *Nutrition Reviews*, 68, pp. S74-S87.

Kalaria, R.N. (2012) 'Cerebrovascular Disease and Mechanisms of Cognitive Impairment: Evidence From Clinicopathological Studies in Humans', *Stroke*, 43(9), pp. 2526-2534.

Kalaria, R.N. and Ballard, C. (1999) 'Overlap between pathology of Alzheimer disease and vascular dementia', *Alzheimer Disease and Associated Disorders*, 13, pp. S115-23.

Kalaria, R.N. and Ihara, M. (2013) 'Dementia: Vascular and neurodegenerative pathways—will they meet?', *Nature Reviews Neurology*, 9, pp. 487-488.

Kalaria, R.N., Kenny, R.A., Ballard, C.G., Perry, R., Ince, P. and Polvikoski, T. (2004) 'Towards defining the neuropathological substrates of vascular dementia', *Journal of the Neurological Sciences*, 226(1–2), pp. 75-80.

Kamenetz, F., Tomita, T., Hsieh, H., Seabrook, G., Borchelt, D., Iwatsubo, T., Sisodia, S. and Malinow, R. (2003) 'APP Processing and Synaptic Function', *Neuron*, 37(6), pp. 925-937.

Karran, E., Mercken, M. and De Strooper, B. (2011) 'The amyloid cascade hypothesis for Alzheimer's disease: an appraisal for the development of therapeutics', *Nature Reviews Drug Discovery*, 10, pp. 698-712.

Kasai, H., Fukuda, M., Watanabe, S., Hayashi-Takagi, A. and Noguchi, J. (2010) 'Structural dynamics of dendritic spines in memory and cognition', *Trends in Neurosciences*, 33(3), pp. 121-129.

Kerchner, G.A., Deutsch, G.K., Zeineh, M., Dougherty, R.F., Saranathan, M. and Rutt, B.K. (2012) 'Hippocampal CA1 apical neuropil atrophy and memory performance in Alzheimer's disease', *NeuroImage*, 63(1), pp. 194-202.

Khundakar, A., Morris, C., Oakley, A., McMeekin, W. and Thomas, A.J. (2009) 'Morphometric analysis of neuronal and glial cell pathology in the dorsolateral prefrontal cortex in late-life depression', *The British Journal of Psychiatry*, 195(2), pp. 163-169.

Kirino, T. (1982) 'Delayed neuronal death in the gerbil hippocampus following ischemia', *Brain Research*, 239(1), pp. 57-69.

Kirvell, S.L., Elliott, M.S., Kalaria, R.N., Hortobágyi, T., Ballard, C.G. and Francis, P.T. (2010) 'Vesicular glutamate transporter and cognition in stroke: A case-control autopsy study', *Neurology*, 75(20), pp. 1803-1809.

Kitagawa, K., Matsumoto, M., Niinobe, M., Mikoshiba, K., Hata, R., Ueda, H., Handa, N., Fukunaga, R., Isaka, Y., Kimura, K. and Kamada, T. (1989) 'Microtubule-associated protein 2 as a sensitive marker for cerebral ischemic damage--Immunohistochemical investigation of dendritic damage', *Neuroscience*, 31(2), pp. 401-411.

Kitano, H., Nishimura, H., Tachibana, H., Yoshikawa, H. and Matsuyama, T. (2004) 'ORP150 ameliorates ischemia/reperfusion injury from middle cerebral artery occlusion in mouse brain', *Brain Research*, 1015(1–2), pp. 122-128.

Kling, M.A., Trojanowski, J.Q., Wolk, D.A., Lee, V.M.Y. and Arnold, S.E. (2013) 'Vascular disease and dementias: Paradigm shifts to drive research in new directions', *Alzheimer's & Dementia*, 9(1), pp. 76-92.

Koehler, R.C., Roman, R.J. and Harder, D.R. (2009) 'Astrocytes and the regulation of cerebral blood flow', *Trends in Neurosciences*, 32(3), pp. 160-169.

Kokmen, E., Whisnant, J.P., O'Fallon, W.M., Chu, C.P. and Beard, C.M. (1996) 'Dementia after ischemic stroke: A population-based study in Rochester, Minnesota (1960-1984)', *Neurology*, 46(1), pp. 154-159.

Korbo, L., Amrein, I., Lipp, H.P., Wolfer, D., Regeur, L., Oster, S. and Pakkenberg, B. (2004) 'No evidence for loss of hippocampal neurons in non-Alzheimer dementia patients', *Acta Neurologica Scandinavica*, 109(2), pp. 132-139.

Kragh, C.L., Ubhi, K., Wyss-Corey, T. and Masliah, E. (2012) 'Autophagy in Dementias', *Brain Pathology*, 22(1), pp. 99-109.

Kril, J., Patel, S., Harding, A. and Halliday, G. (2002a) 'Neuron loss from the hippocampus of Alzheimer's disease exceeds extracellular neurofibrillary tangle formation', *Acta Neuropathologica*, 103(4), pp. 370-376.

Kril, J.J., Hodges, J. and Halliday, G. (2004) 'Relationship between hippocampal volume and CA1 neuron loss in brains of humans with and without Alzheimer's disease', *Neuroscience Letters*, 361(1-3), pp. 9-12.

Kril, J.J., Patel, S., Harding, A.J. and Halliday, G.M. (2002b) 'Patients with vascular dementia due to microvascular pathology have significant hippocampal neuronal loss', *Journal of Neurology, Neurosurgery & Psychiatry*, 72(6), pp. 747-751.

Kühn, J., Meissner, C. and Oehmichen, M. (2005) 'Microtubule-associated protein 2 (MAP2)—a promising approach to diagnosis of forensic types of hypoxia-ischemia', *Acta Neuropathologica*, 110(6), pp. 579-586.

Kuusisto, E., Salminen, A. and Alafuzoff, I. (2002) 'Early accumulation of p62 in neurofibrillary tangles in Alzheimer's disease: possible role in tangle formation', *Neuropathology and Applied Neurobiology*, 28(3), pp. 228-237.

Lace, G., Savva, G.M., Forster, G., de Silva, R., Brayne, C., Matthews, F.E., Barclay, J.J., Dakin, L., Ince, P.G. and Wharton, S.B. (2009) 'Hippocampal tau pathology is related to neuroanatomical connections: an ageing population-based study', *Brain*.

Laroche, S., Davis, S. and Jay, T.M. (2000) 'Plasticity at hippocampal to prefrontal cortex synapses: Dual roles in working memory and consolidation', *Hippocampus*, 10(4), pp. 438-446.

Larsen, G.A., Skjellegrind, H.K., Berg-Johnsen, J., Moe, M.C. and Vinje, M.L. (2006) 'Depolarization of mitochondria in isolated CA1 neurons during hypoxia, glucose deprivation and glutamate excitotoxicity', *Brain Research*, 1077(1), pp. 153-160.
Leal, S.L. and Yassa, M.A. (2013) 'Perturbations of neural circuitry in aging, mild cognitive impairment, and Alzheimer's disease', *Ageing Research Reviews*, 12(3), pp. 823-831.
Lee, A., Lingwood, B.E., Bjorkman, S.T., Miller, S.M., Poronnik, P., Barnett, N.L., Colditz, P. and Pow, D.V. (2010) 'Rapid loss of glutamine synthetase from astrocytes in response to hypoxia: Implications for excitotoxicity', *Journal of Chemical Neuroanatomy*, 39(3), pp. 211-220.
Lee, P.H., Bang, O.Y., Hwang, E.M., Lee, J.S., Joo, U.S., Mook-Jung, I. and Huh, K. (2005) 'Circulating beta amyloid protein is elevated in patients with acute ischemic stroke', *Journal of Neural Transmission*, 112(10), pp. 1371-1379.
Lees, G.J. (1993) 'The possible contribution of microglia and macrophages to delayed neuronal death after ischemia', *Journal of the Neurological Sciences*, 114(2), pp. 119-122.
Leuba, G., Walzer, C., Vernay, A., Carnal, B., Kraftsik, R., Piotton, F., Marin, P., Bouras, C. and Savioz, A. (2008) 'Postsynaptic density protein PSD-95 expression in Alzheimer's disease and okadaic acid induced neuritic retraction', *Neurobiology of Disease*, 30(3), pp. 408-419.
Levine, B. and Kroemer, G. (2008) 'Autophagy in the Pathogenesis of Disease', *Cell*, 132(1), pp. 27-42.
Levine, N.D., Rademacher, D.J., Collier, T.J., O'Malley, J.A., Kells, A.P., San Sebastian, W., Bankiewicz, K.S. and Steece-Collier, K. (2013) 'Advances in thin tissue Golgi-Cox impregnation: Fast, reliable methods for multi-assay analyses in rodent and non-human primate brain', *Journal of Neuroscience Methods*, 213(2), pp. 214-227.
Leys, D., Erkinjuntti, T., Desmond, D.W., Schmidt, R., Englund, E., Pasquier, F., Parnetti, L., Ghika, J., Kalaria, R.N., Chabriat, H., Scheltens, P. and Bogousslavsky, J. (1999) 'Vascular dementia: the role of cerebral infarcts', *Alzheimer's Disease and Associated Disorders*, 13, pp. S38-48.
Leys, D., Hénon, H., Mackowiak-Cordoliani, M.-A. and Pasquier, F. (2005) 'Poststroke dementia', *The Lancet Neurology*, 4(11), pp. 752-759.
Li, W., Huang, R., Shetty, R.A., Thangthaeng, N., Liu, R., Chen, Z., Sumien, N., Rutledge, M., Dillon, G.H., Yuan, F., Forster, M.J., Simpkins, J.W. and Yang, S.-H. (2013) 'Transient focal cerebral ischemia induces long-term cognitive function deficit in an experimental ischemic stroke model', *Neurobiology of Disease*, 59(0), pp. 18-25.
Liu, C., Gao, Y., Barrett, J. and Hu, B. (2010) 'Autophagy and protein aggregation after brain ischemia', *Journal of Neurochemistry*, 115(1), pp. 68-78.
Liu, H.-x., Zhang, J.-j., Zheng, P. and Zhang, Y. (2005) 'Altered expression of MAP-2, GAP-43, and synaptophysin in the hippocampus of rats with chronic cerebral hypoperfusion correlates with cognitive impairment', *Molecular Brain Research*, 139(1), pp. 169-177.
Love, S., Siew, L.K., Dawbarn, D., Wilcock, G.K., Ben-Shlomo, Y. and Allen, S.J. (2006) 'Premorbid effects of APOE on synaptic proteins in human temporal neocortex', *Neurobiology of Aging*, 27(6), pp. 797-803.
Lowry, O.H., Rosebrough, N.J., Farr, A.L. and Randall, R.J. (1951) 'Protein Measurement with the Phenol Reagent', *Journal of Biological Chemistry*, 193, pp. 265-275.
Luengo-Fernandez, R., Leal, J. and Gray, A. (2010) 'Dementia 2010: The economic burden of dementia and associated research funding in the United Kingdom'.
Lum, J.J., Bauer, D.E., Kong, M., Harris, M.H., Li, C., Lindsten, T. and Thompson, C.B. (2005) 'Growth Factor Regulation of Autophagy and Cell Survival in the Absence of Apoptosis', *Cell*, 120(2), pp. 237-248.
Ma, J.F., Huang, Y., Chen, S.D. and Halliday, G. (2010) 'Immunohistochemical evidence for macroautophagy in neurones and endothelial cells in Alzheimer's disease', *Neuropathology and Applied Neurobiology*, 36(4), pp. 312-319.
Maiuri, M.C., Criollo, A. and Kroemer, G. (2010) 'Crosstalk between apoptosis and autophagy within the Beclin 1 interactome', *The EMBO journal*, 29, pp. 515-516.

Mandai, K., Matsumoto, M., Kitagawa, K., Matsushita, K., Ohtsuki, T., Mabuchi, T., Colman, D.R., Kamada, T. and Yanagihara, T. (1997) 'Ischemic damage and subsequent proliferation of oligodendrocytes in focal cerebral ischemia', *Neuroscience*, 77(3), pp. 849-861.

Mariño, G., Madeo, F. and Kroemer, G. (2011) 'Autophagy for tissue homeostasis and neuroprotection', *Current Opinion in Cell Biology*, 23(2), pp. 198-206.

Marner, L., Nyengaard, J.R., Tang, Y. and Pakkenberg, B. (2003) 'Marked loss of myelinated nerve fibers in the human brain with age', *The Journal of Comparative Neurology*, 462(2), pp. 144-152.

Martanez-Tellez, R., Gamez-Villalobos, M.D.J. and Flores, G. (2005) 'Alteration in dendritic morphology of cortical neurons in rats with diabetes mellitus induced by streptozotocin', *Brain Research*, 1048(1-2), pp. 108-115.

Marti, E., Ferrer, I., Ballabriga, J. and Blasi, J. (1998) 'Increase in SNAP-25 immunoreactivity in the mossy fibers following transient forebrain ischemia in the gerbil', *Acta Neuropathologica*, 95, pp. 254-260.

Mayeux, R., Denaro, J., Hemenegildo, N. and et al. (1992) 'A population-based investigation of Parkinson's disease with and without dementia: Relationship to age and gender', *Archives of Neurology*, 49(5), pp. 492-497.

Mayhew, T.M. and Gundersen, H.J.G. (1996) ''If you assume, you can make an ass out of u and me': a decade of the disector for stereological counting of particles in 3D space.', *Journal of Anatomy*, 188, pp. 1-15.

Melkas, S., Oksala, N.K.J., Jokinen, H., Pohjasvaara, T., Vataja, R., Oksala, A., Kaste, M., Karhunen, P.J. and Erkinjuntti, T. (2009) 'Poststroke dementia predicts poor survival in long-term follow-up: influence of prestroke cognitive decline and previous stroke', *Journal of Neurology, Neurosurgery & Psychiatry*, 80(8), pp. 865-870.

Melvin, N.R. and Sutherland, R.J. (2010) 'Quantitative Caveats of Standard Immunohistochemical Procedures: Implications for Optical Disector–based Designs', *Journal of Histochemistry & Cytochemistry*, 58(7), pp. 577-584.

Meraz Rios, M.A., Toral-Rios, D., Franco-Bocanegra, D., Villeda-HernÁNdez, J. and Campos-PeÑA, V. (2013) 'Inflammatory Process in Alzheimer's Disease', *Frontiers in Integrative Neuroscience*, 7.

Milosevic, N.T. and Ristanovic, D. (2007) 'The Sholl analysis of neuronal cell images: Semi-log or log-log method?', *Journal of Theoretical Biology*, 245(1), pp. 130-140.

Mirra, S.S., Heyman, A., McKeel, D., Sumi, S.M., Crain, B.J., Brownlee, L.M., Vogel, F.S., Hughes, J.P., Van Belle, G. and Berg, L. (1991) 'The Consortium to Establish a Registry for Alzheimer's Disease (CERAD). Part II. Standardization of the neuropathologic assessment of Alzheimer's disease', *Neurology*, 41(4), pp. 479-486.

Mishizen-Eberz, A.J., Rissman, R.A., Carter, T.L., Ikonomovic, M.D., Wolfe, B.B. and Armstrong, D.M. (2004) 'Biochemical and molecular studies of NMDA receptor subunits NR1/2A/2B in hippocampal subregions throughout progression of Alzheimer's disease pathology', *Neurobiology of Disease*, 15(1), pp. 80-92.

Mitchell, T.W., Nissanov, J., Han, L.-Y., Mufson, E.J., Schneider, J.A., Cochran, E.J., Bennett, D.A., Lee, V.M.Y., Trojanowski, J.Q. and Arnold, S.E. (2000) 'Novel Method to Quantify Neuropil Threads in Brains from Elders With or Without Cognitive Impairment', *Journal of Histochemistry & Cytochemistry*, 48(12), pp. 1627-1637.

Mizushima, N. (2004) 'Methods for monitoring autophagy', *The International Journal of Biochemistry & Cell Biology*, 36(12), pp. 2491-2502.

Montine, T., Phelps, C., Beach, T., Bigio, E., Cairns, N., Dickson, D., Duyckaerts, C., Frosch, M., Masliah, E., Mirra, S., Nelson, P., Schneider, J., Thal, D., Trojanowski, J., Vinters, H. and Hyman, B. (2012) 'National Institute on Aging–Alzheimer's Association guidelines for the neuropathologic assessment of Alzheimer's disease: a practical approach', *Acta Neuropathologica*, 123(1), pp. 1-11.

Moorhouse, P. and Rockwood, K. (2008) 'Vascular cognitive impairment: current concepts and clinical developments', *The Lancet Neurology*, 7(3), pp. 246-255.

Morrison, J.H., Hof, P.R. and Efrain, C. (2002) 'Chapter 37. Selective vulnerability of corticocortical and hippocampal circuits in aging and Alzheimer's disease', in *Progress in Brain Research*. Elsevier, pp. 467-486.

Mouton, P.R. (2002) *Principles and practices of unbiased stereology*. Baltimore: The John Hopkins University Press.

Mueller, S.G., Chao, L.L., Berman, B. and Weiner, M.W. (2010) 'Evidence for functional specialization of hippocampal subfields detected by MR subfield volumetry on high resolution images at 4 T', *NeuroImage*, 56(3), pp. 851-857.

Mueller, S.G., Stables, L., Du, A.T., Schuff, N., Truran, D., Cashdollar, N. and Weiner, M.W. (2007) 'Measurement of hippocampal subfields and age-related changes with high resolution MRI at 4 T', *Neurobiology of Aging*, 28(5), pp. 719-726.

Mukaetova-Ladinska, E.B., Arnold, H., Jaros, E., Perry, R. and Perry, E. (2004) 'Depletion of MAP2 expression and laminar cytoarchitectonic changes in dorsolateral prefrontal cortex in adult autistic individuals', *Neuropathology and Applied Neurobiology*, 30(6), pp. 615-623.

Mukaetova-Ladinska, E.B., Garcia-Siera, F., Hurt, J., Gertz, H.J., Xuereb, J.H., Hills, R., Brayne, C., Huppert, F.A., Paykel, E.S., McGee, M., Jakes, R., G. Honer, W., Harrington, C.R. and Wischik, C.M. (2000) 'Staging of Cytoskeletal and β-Amyloid Changes in Human Isocortex Reveals Biphasic Synaptic Protein Response during Progression of Alzheimer's Disease', *The American Journal of Pathology*, 157(2), pp. 623-636.

Nagele, R.G., Wegiel, J., Venkataraman, V., Imaki, H., Wang, K.-C. and Wegiel, J. (2004) 'Contribution of glial cells to the development of amyloid plaques in Alzheimer's disease', *Neurobiology of Aging*, 25(5), pp. 663-674.

Nagy, Z., Esiri, M.M., Jobst, K.A., Morris, J.H., F. King, E.M., McDonald, B., Joachim, C., Litchfield, S., Barnetson, L.I.N. and Smith, A.D. (1997) 'The Effects of Additional Pathology on the Cognitive Deficit in Alzheimer Disease', *Journal of Neuropathology & Experimental Neurology*, 56(2), pp. 165-170.

Nave, K. (2010) 'Myelination and support of axonal integrity by glia', *Nature*, 468, pp. 244-252.

Nedergaard, M. and Dirnagl, U. (2005) 'Role of glial cells in cerebral ischemia', *Glia*, 50(4), pp. 281-286.

Neher, J.J., Neniskyte, U. and Brown, G.C. (2012) 'Primary phagocytosis of neurons by inflamed microglia: potential roles in neurodegeneration', *Frontiers in Pharmacology*, 3.

Nimmerjahn, A., Kirchhoff, F. and Helmchen, F. (2005) 'Resting Microglial Cells Are Highly Dynamic Surveillants of Brain Parenchyma in Vivo', *Science*, 308(5726), pp. 1314-1318.

Nixon, R.A. (2006) 'Autophagy in neurodegenerative disease: friend, foe or turncoat?', *Trends in Neurosciences*, 29(9), pp. 528-535.

Nixon, R.A. (2007) 'Autophagy, amyloidogenesis and Alzheimer disease', *Journal of Cell Science*, 120(23), pp. 4081-4091.

Nixon, R.A. and Yang, D.-S. (2011) 'Autophagy failure in Alzheimer's disease—locating the primary defect', *Neurobiology of Disease*, 43(1), pp. 38-45.

O'Brien, J.T., Erkinjuntti, T., Reisberg, B., Roman, G., Sawada, T., Pantoni, L., Bowler, J.V., Ballard, C., DeCarli, C., Gorelick, P.B., Rockwood, K., Burns, A., Gauthier, S. and DeKosky, S.T. (2003) 'Vascular cognitive impairment', *The Lancet Neurology*, 2(2), pp. 89-98.

O'Sullivan, M., Ngo, E., Viswanathan, A., Jouvent, E., Gschwendtner, A., Saemann, P.G., Duering, M., Pachai, C., Bousser, M.-G., Chabriat, H. and Dichgans, M. (2009) 'Hippocampal volume is an independent predictor of cognitive performance in CADASIL', *Neurobiology of Aging*, 30(6), pp. 890-897.

Oberheim, N., Goldman, S. and Nedergaard, M. (2012) 'Heterogeneity of Astrocytic Form and Function', in Milner, R. (ed.) *Astrocytes*. Humana Press, pp. 23-45.

Oberheim, N.A., Takano, T., Han, X., He, W., Lin, J.H.C., Wang, F., Xu, Q., Wyatt, J.D., Pilcher, W., Ojemann, J.G., Ransom, B.R., Goldman, S.A. and Nedergaard, M. (2009) 'Uniquely Hominid Features of Adult Human Astrocytes', *The Journal of Neuroscience*, 29(10), pp. 3276-3287.

Oberheim, N.A., Wang, X., Goldman, S. and Nedergaard, M. (2006) 'Astrocytic complexity distinguishes the human brain', *Trends in Neurosciences*, 29(10), pp. 547-553.
Ogata, K. and Kosaka, T. (2002) 'Structural and quantitative analysis of astrocytes in the mouse hippocampus', *Neuroscience*, 113(1), pp. 221-233.
Okada, T., Kataoka, Y., Takeshita, A., Mino, M., Morioka, H., Kusakabe, K.T. and Kondo, T. (2013) 'Effects of Transient Forebrain Ischemia on the Hippocampus of the Mongolian Gerbil (Meriones unguiculatus): An Immunohistochemical Study', *Zoological Science*, 30(6), pp. 484-489.
Olney, J.W. and Sharpe, L.G. (1969) 'Brain Lesions in an Infant Rhesus Monkey Treated with Monosodium Glutamate', *Science*, 166(3903), pp. 386-388.
Olson, E.E. and McKeon, R.J. (2004) 'Characterization of cellular and neurological damage following unilateral hypoxia/ischemia', *Journal of the Neurological Sciences*, 227(1), pp. 7-19.
Ong, W., Tanaka, K., Dawe, G.S., Ittner, L.M. and Farooqui, A.A. (2013) 'Slow Excitotoxicity in Alzheimer's Disease', *Journal of Alzheimer's Disease*, 35, pp. 643-668.
Pakkenberg, B., Pelvig, D., Marner, L., Bundgaard, M.J., Gundersen, H.J.G., Nyengaard, J.R. and Regeur, L. (2003) 'Aging and the human neocortex', *Experimental Gerontology*, 38(1-2), pp. 95-99.
Pantoni, L. (2010) 'Cerebral small vessel disease: from pathogenesis and clinical characteristics to therapeutic challenges', *The Lancet Neurology*, 9(7), pp. 689-701.
Pantoni, L., Garcia, J.H. and Gutierrez, J.A. (1996) 'Cerebral White Matter Is Highly Vulnerable to Ischemia', *Stroke*, 27(9), pp. 1641-1647.
Parihar, M.S. and Brewer, G.J. (2010) 'Amyloid-β as a Modulator of Synaptic Plasticity', *Journal of Alzheimer's Disease*, 22(3), pp. 741-763.
Parkhurst, Christopher N., Yang, G., Ninan, I., Savas, Jeffrey N., Yates, John R., Lafaille, Juan J., Hempstead, Barbara L., Littman, Dan R. and Gan, W.-B. (2013) 'Microglia Promote Learning-Dependent Synapse Formation through Brain-Derived Neurotrophic Factor', *Cell*, 155(7), pp. 1596-1609.
Pasquier, F., Leys, D. and Scheltens, P. (1998) 'The influence of coincidental vascular pathology on symptomatology and course of Alzheimer's disease.', *Journal of neural transmission*, 54, pp. 117-27.
Pastori, C., Regondi, M.C., Librizzi, L. and de Curtis, M. (2007) 'Early excitability changes in a novel acute model of transient focal ischemia and reperfusion in the in vitro isolated guinea pig brain', *Experimental Neurology*, 204(1), pp. 95-105.
Peich, M.-C., Husain, M. and Bays, P.M. (2013) 'Age-related decline of precision and binding in visual working memory', *Psychology and Aging*, 28(3), pp. 729-743.
Pendelbury, S.T. (2009) 'Stroke-related dementia: Rates, risk factors and implications for future research', *Maturitas*, 64(3), pp. 165-171.
Pendlebury, S.T. and Rothwell, P.M. (2009) 'Prevalence, incidence, and factors associated with pre-stroke and post-stroke dementia: a systematic review and meta-analysis', *The Lancet Neurology*, 8, pp. 1006-18.
Penzes, P., Cahill, M.E., Jones, K.A., VanLeeuwen, J.-E. and Woolfrey, K.M. (2011) 'Dendritic spine pathology in neuropsychiatric disorders', *Nat Neurosci*, 14(3), pp. 285-293.
Perea, G., Navarrete, M. and Araque, A. (2009) 'Tripartite synapses: astrocytes process and control synaptic information', *Trends in Neurosciences*, 32(8), pp. 421-431.
Perego, C., Fumagalli, S. and De Simoni, M.-G. (2011) 'Temporal pattern of expression and colocalization of microglia/macrophage phenotype markers following brain ischemic injury in mice', *Journal of Neuroinflammation*, 8(1), p. 174.
Perry, R.H., Irving, D., Blessed, G., Fairbairn, A. and Perry, E.K. (1990) 'Senile dementia of Lewy body type: A clinically and neuropathologically distinct form of Lewy body dementia in the elderly', *Journal of the Neurological Sciences*, 95(2), pp. 119-139.
Perry, R.H. and Oakley, A.E. (1993) *'Newcastle Brain Map'*. London: Wolfe.

Petito, C.K., Olarte, J.P., Roberts, B., Nowak, T.S. and Pulsinelli, W.A. (1998) 'Selective glial vulnerability following transient global ischemia in rat brain', *Journal of Neuropathology and Experimental Neurology*, 57(3), pp. 231-238.

Pickford, F., Masliah, E., Britschgi, M., Lucin, K., Narasimhan, R., Jaeger, P.A., Small, S.A., Spencer, B., Rockenstein, E., Levine, B. and Wyss-Corey, T. (2008) 'The autophagy-related protein beclin 1 shows reduced expression in early Alzheimer disease and regulates amyloid β accumulation in mice', *Journal of Clinical Investigation*, 118(6), pp. 2190-2199.

Porter, J.T. and McCarthy, K.D. (1996) 'Hippocampal Astrocytes In Situ Respond to Glutamate Released from Synaptic Terminals', *The Journal of Neuroscience*, 16(16), pp. 5073-5081.

Powell, E.M. and Geller, H.M. (1999) 'Dissection of astrocyte-mediated cues in neuronal guidance and process extension', *Glia*, 26(1), pp. 73-83.

Prince, M., Bryce, R., Albanese, E., Wimo, A., Ribeiro, W. and Ferri, C.P. (2013) 'The global prevalence of dementia: A systematic review and metaanalysis', *Alzheimer's & Dementia*, 9(1), pp. 63-75.e2.

Raivich, G. and Banati, R. (2004) 'Brain microglia and blood-derived macrophages: molecular profiles and functional roles in multiple sclerosis and animal models of autoimmune demyelinating disease', *Brain Research Reviews*, 46(3), pp. 261-281.

Rajkowska, G., Miguel-Hidalgo, J.J., Dubey, P., Stockmeier, C.A. and Krishnan, K.R.R. (2005) 'Prominent Reduction in Pyramidal Neurons Density in the Orbitofrontal Cortex of Elderly Depressed Patients', *Biological Psychiatry*, 58(4), pp. 297-306.

Rajkowska, G., Selemon, L.D. and Goldman-Rakic, P.S. (1998) 'Neuronal and glial somal size in the prefrontal cortex: A postmortem morphometric study of schizophrenia and huntington disease', *Archives of General Psychiatry*, 55(3), pp. 215-224.

Ramesh Babu, J., Lamar Seibenhener, M., Peng, J., Strom, A.-L., Kemppainen, R., Cox, N., Zhu, H., Wooten, M.C., Diaz-Meco, M.T., Moscat, J. and Wooten, M.W. (2008) 'Genetic inactivation of p62 leads to accumulation of hyperphosphorylated tau and neurodegeneration', *Journal of Neurochemistry*, 106(1), pp. 107-120.

Rami, A., Langhagen, A. and Steiger, S. (2008) 'Focal cerebral ischemia induces upregulation of Beclin 1 and autophagy-like cell death', *Neurobiology of Disease*, 29(1), pp. 132-141.

Redgrave, P., Prescott, T.J. and Gurney, K. (1999) 'The basal ganglia: a vertebrate solution to the selection problem?', *Neuroscience*, 89(4), pp. 1009-1023.

Riley, K.P., Snowdon, D.A. and Markesbery, W.R. (2002) 'Alzheimer's neurofibrillary pathology and the spectrum of cognitive function: Findings from the Nun Study', *Annals of Neurology*, 51(5), pp. 567-577.

Rinne, J.O., Paljärvi, L. and Rinne, U.K. (1987) 'Neuronal size and density in the nucleus basalis of Meynert in Alzheimer's disease.', *Journal of Neurological Science*, 79(1-2), pp. 67-76.

Riudavets, M.A., Iacono, D., Resnick, S.M., O'Brien, R., Zonderman, A.B., Martin, L.J., Rudow, G., Pletnikova, O. and Troncoso, J.C. (2007) 'Resistance to Alzheimer's pathology is associated with nuclear hypertrophy in neurons', *Neurobiology of Aging*, 28(10), pp. 1484-1492.

Rodríguez, J.J., Olabarria, M. and Chvtal, A.V., A. (2009) 'Astroglia in dementia and Alzheimer's disease', *Cell Death and Differentiation*, 16, pp. 378-385.

Rohn, T.T., Wirawan, E., Brown, R.J., Harris, J.R., Masliah, E. and Vandenabeele, P. (2011) 'Depletion of Beclin-1 due to proteolytic cleavage by caspases in the Alzheimer's disease brain', *Neurobiology of Disease*, 43(1), pp. 68-78.

Román, G.C. (2002a) 'Vascular dementia may be the most common form of dementia in the elderly', *Journal of the Neurological Sciences*, 203–204(0), pp. 7-10.

Román, G.C. (2002b) 'Vascular dementia revisited: diagnosis, pathogenesis, treatment, and prevention.', *Medical Clinics of North America*, (86), pp. 477-99.

Rosoklija, G., Mancevski, B., Ilievski, B., Perera, T., Lisanby, S.H., Coplan, J.D., Duma, A., Serafimova, T. and Dwork, A.J. (2003) 'Optimization of Golgi methods for impregnation of brain tissue from humans and monkeys', *Journal of Neuroscience Methods*, 131(1–2), pp. 1-7.

Rosoklija, G., Toomayan, G., Mancevski, B., Haroutunian, V., Liu, D., Malespina, D., Hays, A.P., Sadig, S., Latov, N. and Dwork, A.J. (2005) 'Altered subicular MAP2 immunoreactivity in schizophrenia.', *Prilozi.*, 26, pp. 13-34.

Rössler, M., Zarski, R., Bohl, J. and Ohm, T. (2002) 'Stage-dependent and sector-specific neuronal loss in hippocampus during Alzheimer's disease', *Acta Neuropathologica*, 103(4), pp. 363-369.

Roth, M., Tym, E., Mountjoy, C.Q., Huppert, F.A., Hendrie, H., Verma, S. and Goddard, R. (1986) 'CAMDEX. A standardised instrument for the diagnosis of mental disorder in the elderly with special reference to the early detection of dementia', *The British Journal of Psychiatry*, 149(6), pp. 698-709.

Rouach, N., Koulakoff, A., Abudara, V., Willecke, K. and Giaume, C. (2008) 'Astroglial Metabolic Networks Sustain Hippocampal Synaptic Transmission', *Science*, 322(5907), pp. 1551-1555.

Ruan, Y.W., Zou, B., Fan, Y., Li, Y., Lin, N., Zeng, Y.S., Gao, T.M., Yao, Z. and Xu, Z.C. (2006) 'Dendritic plasticity of CA1 pyramidal neurons after transient global ischemia', *Neuroscience*, 140(1), pp. 191-201.

Ruitenberg, A., den Heijer, T., Bakker, S.L.M., van Swieten, J.C., Koudstaal, P.J., Hofman, A. and Breteler, M.M.B. (2005) 'Cerebral hypoperfusion and clinical onset of dementia: The Rotterdam study', *Annals of Neurology*, 57(6), pp. 789-794.

Sá, M.J., Madeira, M.D., Ruela, C., Volk, B., Mota-Miranda, A., Lecour, H., Gonçalves, V. and Paula-Barbosa, M.M. (2000) 'AIDS does not alter the total number of neurons in the hippocampal formation but induces cell atrophy: a stereological study', *Acta Neuropathologica*, 99(6), pp. 643-653.

Salminen, A. and Kaarniranta, K. (2009) 'Regulation of the aging process by autophagy', *Trends in Molecular Medicine*, 15(5), pp. 217-224.

Salminen, A., Kaarniranta, K., Haapasalo, A., Hiltunen, M., Soininen, H. and Alafuzoff, I. (2012) 'Emerging role of p62/sequestosome-1 in the pathogenesis of Alzheimer's disease', *Progress in Neurobiology*, 96(1), pp. 87-95.

Sánchez-Gómez, M.V., Alberdi, E., Ibarretxe, G., Torre, I. and Matute, C. (2003) 'Caspase-Dependent and Caspase-Independent Oligodendrocyte Death Mediated by AMPA and Kainate Receptors', *The Journal of Neuroscience*, 23(29), pp. 9519-9528.

Scheff, S.W., Price, D.A., Schmitt, F.A., Dekosky, S.T. and Mufson, E.J. (2007) 'Synaptic alterations in CA1 in mild Alzheimer disease and mild cognitive impairment', *Neurology*, 68(18), pp. 1501-1508.

Scher, A.I., Xu, Y., Korf, E.S.C., Hartley, S.W., Witter, M.P., Scheltens, P., White, L.R., Thompson, P.M., Toga, A.W., Valentino, D.J. and Launer, L.J. (2011) 'Hippocampal morphometry in population-based incident Alzheimer's disease and vascular dementia: the HAAS', *Journal of Neurology, Neurosurgery & Psychiatry*, 82(4), pp. 373-377.

Schmidt, B., Marrone, D.F. and Markus, E.J. (2012) 'Disambiguating the similar: The dentate gyrus and pattern separation', *Behavioural Brain Research*, 226(1), pp. 56-65.

Schmitz, C. and Hof, P.R. (2007) *Brain Ageing: Design-Based Stereology in Brain Ageing Research*. Taylor & Francis Group LLC.

Schnaider Beeri, M., Haroutunian, V., Schmeidler, J., Sano, M., Fam, P., Kavanaugh, A., Barr, A.M., Honer, W.G. and Katsel, P. (2012) 'Synaptic protein deficits are associated with dementia irrespective of extreme old age', *Neurobiology of Aging*, 33(6), pp. 1125.e1-1125.e8.

Schönheit, B., Zarski, R. and Ohm, T.G. (2004) 'Spatial and temporal relationships between plaques and tangles in Alzheimer-pathology', *Neurobiology of Aging*, 25(6), pp. 697-711.

Schousboe, A., Sickmann, H., Walls, A., Bak, L. and Waagepetersen, H. (2010) 'Functional Importance of the Astrocytic Glycogen-Shunt and Glycolysis for Maintenance of an Intact Intra/Extracellular Glutamate Gradient', *Neurotoxicity Research*, 18(1), pp. 94-99.

Schummers, J., Yu, H. and Sur, M. (2008) 'Tuned Responses of Astrocytes and Their Influence on Hemodynamic Signals in the Visual Cortex', *Science*, 320(5883), pp. 1638-1643.

Schwab, C., Bondada, V., Sparks, D.L., Cahan, L.D. and Geddes, J.W. (1994) 'Postmortem changes in the levels and localization of microtubule-associated proteins (tau, MAP2 and MAP1B) in the rat and human hippocampus', *Hippocampus*, 4(2), pp. 210-225.

Scott, I. and Lowe, J. (2007) 'The ubiquitin-binding protein p62 identifies argyrophilic grain pathology with greater sensitivity than conventional silver stains', *Acta Neuropathologica*, 113(4), pp. 417-420.

Scoville, W.B. and Milner, B. (2000) 'Loss of Recent Memory After Bilateral Hippocampal Lesions', *The Journal of Neuropsychiatry & Clinical Neurosciences*, 12, pp. 103-113.

Selemon, L.D. and Goldman-Rakic, P.S. (1999) 'The reduced neuropil hypothesis: a circuit based model of schizophrenia', *Biological Psychiatry*, 45(1), pp. 17-25.

Selkoe, D.J. (2002) 'Alzheimer's Disease Is a Synaptic Failure', *Science*, 298(5594), pp. 789-791.

Shinohara, Y., Hosoya, A., Yahagi, K., Ferecskó, A.S., Yaguchi, K., Sík, A., Itakura, M., Takahashi, M. and Hirase, H. (2012) 'Hippocampal CA3 and CA2 have distinct bilateral innervation patterns to CA1 in rodents', *European Journal of Neuroscience*, 35(5), pp. 702-710.

Siew, L.K., Love, S., Dawbarn, D., Wilcock, G.K. and Allen, S.J. (2004) 'Measurement of pre- and post-synaptic proteins in cerebral cortex: effects of post-mortem delay', *Journal of Neuroscience Methods*, 139(2), pp. 153-159.

Simons, M. and Trajkovic, K. (2006) 'Neuron-glia communication in the control of oligodendrocyte function and myelin biogenesis', *Journal of Cell Science*, 119, pp. 4381-4389.

Smallwood, A., Oulhaj, A., Joachim, C., Christie, S., Sloan, C., Smith, A.D. and Esiri, M. (2012) 'Cerebral subcortical small vessel disease and its relation to cognition in elderly subjects: a pathological study in the Oxford Project to Investigate Memory and Ageing (OPTIMA) cohort', *Neuropathology and Applied Neurobiology*, 38(4), pp. 337-343.

Smith, D.E., Roberts, J., Gage, F.H. and Tuszynski, M.H. (1999) 'Age-associated neuronal atrophy occurs in the primate brain and is reversible by growth factor gene therapy', *Proc. Natl. Acad. Sci. USA*, 96, pp. 10893-10898.

Snowdon, D.A., Greiner, L.H., Mortimer, J.A., Riley, K.P., Greiner, P.A. and Markesbery, W.R. (1997) 'Brain Infarction and the Clinical Expression of Alzheimer Disease: The Nun Study', *JAMA*, 277(10), pp. 813-817.

Sofroniew, M. and Vinters, H. (2010) 'Astrocytes: biology and pathology', *Acta Neuropathologica*, 119(1), pp. 7-35.

Sofroniew, M.V. (2009) 'Molecular dissection of reactive astrogliosis and glial scar formation', *Trends in Neurosciences*, 32(12), pp. 638-647.

Sojkova, J., Beason-Held, L., Zhou, Y., An, Y., Kraut, M.A., Ye, W., Ferrucci, L., Mathis, C.A., Klunk, W.E., Wong, D.F. and Resnick, S.M. (2008) 'Longitudinal Cerebral Blood Flow and Amyloid Deposition: An Emerging Pattern?', *Journal of Nuclear Medicine*, 49(9), pp. 1465-1471.

Soontornniyomkij, V., Risbrough, V.B., Young, J.W., Soontornniyomkij, B., Jeste, D.V. and Achim, C.L. (2012) 'Increased hippocampal accumulation of autophagosomes predicts short-term recognition memory impairment in aged mice', *Age (Dordr)*, 34(2), pp. 305-316.

Špaček, J. (1989) 'Dynamics of the Golgi method: a time-lapse study of the early stages of impregnation in single sections', *Journal of Neurocytology*, 18(1), pp. 27-38.

Spires, T.L., Meyer-Luehmann, M., Stern, E.A., McLean, P.J., Skoch, J., Nguyen, P.T., Bacskai, B.J. and Hyman, B.T. (2005) 'Dendritic Spine Abnormalities in Amyloid Precursor Protein Transgenic Mice Demonstrated by Gene Transfer and Intravital Multiphoton Microscopy', *The Journal of Neuroscience*, 25(31), pp. 7278-7287.

Spronsen, M. and Hoogenraad, C.C. (2010) 'Synapse Pathology in Psychiatric and Neurologic Disease', *Current Neurology and Neuroscience Reports*, 10(3), pp. 207-214.

Spruston, N. (2008) 'Pyramidal Neurons: dendritic structure and synaptic integration', *Nature Reviews Neuroscience*, 9, pp. 206-221.

Staffend, N.A. and Meisel, R.L. (2001) 'DiOlistic Labeling in Fixed Brain Slices: Phenotype, Morphology, and Dendritic Spines', in *Current Protocols in Neuroscience*. John Wiley & Sons, Inc.

Stebbins, G.T. and Murphy, C.M. (2009) 'Diffusion tensor imaging in Alzheimer's disease and mild cognitive impairment', *Behavioural Neurology*, 21(1), pp. 39-49.

Sterio, D.C. (1984) 'The unbiased estimation of number and sizes of arbitrary particles using the disector', *Journal of Microscopy*, 134(2), pp. 127-136.

Stone, B.S., Zhang, J., Mack, D.W., Mori, S., Martin, L.J. and Northington, F.J. (2008) 'Delayed neural network degeneration after neonatal hypoxia-ischemia', *Annals of Neurology*, 64(5), pp. 535-546.

Stroke Statistics 2009 (2009). Foundation, B.H. [Online]. Available at: http://www.bhf.org.uk/publications/view-publication.aspx?ps=1001548.

Sultana, R., Banks, W.A. and Butterfield, D.A. (2010) 'Decreased levels of PSD95 and two associated proteins and increased levels of BCl2 and caspase 3 in hippocampus from subjects with amnestic mild cognitive impairment: Insights into their potential roles for loss of synapses and memory, accumulation of Aβ, and neurodegeneration in a prodromal stage of Alzheimer's disease', *Journal of Neuroscience Research*, 88(3), pp. 469-477.

Swaab, D.F., Hofman, M.A., Lucassen, P.J., Salehi, A. and Uylings, H.B.M. (1994) 'Neuronal atrophy, not cell death, is the main hallmark of Alzheimer's disease', *Neurobiology of Aging*, 15(3), pp. 369-371.

Swanson, L.W. (1982) 'Normal Hippocampal Circuitry', *Neuroscience Research Progress Bulletin*, 20, pp. 624-637.

Tamminga, C.A. (2005) 'The Hippocampus ', *American Journal of Psychiatry*, 162, p. 1 [Online]. Available at: http://ajp.psychiatryonline.org/cgi/reprint/162/1/25.pdf.

Tanaka, H., Araki, M. and Masuzawa, T. (1992) 'Reaction of astrocytes in the gerbil hippocampus following transient ischemia: Immunohistochemical observations with antibodies against glial fibrillary acidic protein, glutamine synthetase, and S-100 protein', *Experimental Neurology*, 116(3), pp. 264-274.

Terry, R.D., DeTeresa, R. and Hansen, L.A. (1987) 'Neocortical cell counts in normal human adult aging', *Annals of Neurology*, 21(6), pp. 530-9.

Terry, R.D., Masliah, E., Salmon, D.P., Butters, N., DeTeresa, R., Hill, R., Hansen, L.A. and Katzman, R. (1991) 'Physical basis of cognitive alterations in Alzheimer's disease: synapse loss is the major correlate of cognitive impairment', *Annals of neurology*, 30(4), pp. 572-580.

Thal, D.R., Capetillo-Zarate, E., Del Tredici, K. and Braak, H. (2006) 'The Development of Amyloid beta Protein Deposits in the Aged Brain', *Sci. Aging Knowl. Environ.*, 2006(6), pp. re1-.

Thal, D.R., Holzer, M., Rüb, U., Waldmann, G., Günzel, S., Zedlick, D. and Schober, R. (2000) 'Alzheimer-Related τ-Pathology in the Perforant Path Target Zone and in the Hippocampal Stratum Oriens and Radiatum Correlates with Onset and Degree of Dementia', *Experimental Neurology*, 163(1), pp. 98-110.

Thal, D.R., Rüb, U. and H., B. (2002) 'Phases of A beta-deposition in the human brain and its relevance for the development of AD.', *Neurology*, 58(12), pp. 1791-800.

Thomas, V.P. (1998) 'What's wrong with Bonferroni adjustments', *BMJ*, 316(7139), pp. 1236-1238.

Toledo, J.B., Arnold, S.E., Raible, K., Brettschneider, J., Xie, S.X., Grossman, M., Monsell, S.E., Kukull, W.A. and Trojanowski, J.Q. (2013) 'Contribution of cerebrovascular disease in autopsy confirmed neurodegenerative disease cases in the National Alzheimer's Coordinating Centre', *Brain*, 136(9), pp. 2697-2706.

Tomlinson, B.E., Blessed, G. and Roth, M. (1970) 'Observations on the brains of demented old people', *Journal of the Neurological Sciences*, 11(3), pp. 205-242.

Tremblay, M.E., Lowery, R.L. and Majewska, A.K. (2010) 'Microglial Interactions with Synapses Are Modulated by Visual Experience', *PLOS Biology*, 8.

Tsai, J., Grutzendler, J., Duff, K. and Gan, W. (2004) 'Fibrillar amyloid deposition leads to local synaptic abnormalities and breakage of neuronal branches', *Nature Neuroscience*, 7(1181-1183).

Tullberg, M., Fletcher, E., DeCarli, C., Mungas, M., Reed, B.R., Harvey, D.J., Weiner, M., Chui, H.C. and Jagust, W.J. (2004) 'White matter lesions impair frontal lobe function regardless of their location', *Neurology*, 63(2), pp. 246-253.

Tulving, E. and Markowitsch, H.J. (1998) 'Episodic and declarative memory: role of the hippocampus.', *Hippocampus*, 8(3), pp. 198-204.

Uh, J., Lewis-Amezcua, K., Martin-Cook, K., Cheng, Y., Weiner, M., Diaz-Arrastia, R., Devous, M., Shen, D. and Lu, H. (2010) 'Cerebral blood volume in Alzheimer's disease and correlation with tissue structural integrity', *Neurobiology of Aging*, 31(12), pp. 2038-2046.

Ukraintseva, S., Sloan, F., Arbeev, K. and Yashin, A. (2006) 'Increasing Rates of Dementia at Time of Declining Mortality From Stroke', *Stroke*, 37(5), pp. 1155-1159.

van Norden, A.G.W., de Laat, K.F., Fick, I., van Uden, I.W.M., van Oudheusden, L.J.B., Gons, R.A.R., Norris, D.G., Zwiers, M.P., Kessels, R.P.C. and de Leeuw, F.-E. (2012) 'Diffusion tensor imaging of the hippocampus and verbal memory performance: The RUN DMC Study', *Human Brain Mapping*, 33(3), pp. 542-551.

van Strien, N.M., Cappaert, N.L.M. and Witter, M.P. (2009) 'The anatomy of memory: an interactive overview of the parahippocampal-hippocampal network', *Nat Rev Neurosci*, 10(4), pp. 272-282.

VanGuilder, H.D., Farley, J.A., Yan, H., Van Kirk, C.A., Mitschelen, M., Sonntag, W.E. and Freeman, W.M. (2011) 'Hippocampal dysregulation of synaptic plasticity-associated proteins with age-related cognitive decline', *Neurobiology of Disease*, 43(1), pp. 201-212.

Vega, E., De JÃ©sus GÃ³mez-Villalobos, M. and Flores, G. (2004) 'Alteration in dendritic morphology of pyramidal neurons from the prefrontal cortex of rats with renovascular hypertension', *Brain Research*, 1021(1), pp. 112-118.

Vicente, É., Degerone, D., Bohn, L., Scornavaca, F., Pimentel, A., Leite, M.C., Swarowsky, A., Rodrigues, L., Nardin, P., Vieira de Almeida, L.M., Gottfried, C., Souza, D.O., Netto, C.A. and Gonçalves, C.A. (2009) 'Astroglial and cognitive effects of chronic cerebral hypoperfusion in the rat', *Brain Research*, 1251(0), pp. 204-212.

Vinet, J., van Weering, H., Heinrich, A., Kalin, R., Wegner, A., Brouwer, N., Heppner, F., van Rooijen, N., Boddeke, H. and Biber, K. (2012) 'Neuroprotective function for ramified microglia in hippocampal excitotoxicity', *Journal of Neuroinflammation*, 9(1), p. 27.

Walsh, D.M. and Selkoe, D.J. (2007) 'Aβ Oligomers – a decade of discovery', *Journal of Neurochemistry*, 101(5), pp. 1172-1184.

Wang, L., Swank, J.S., Glick, I.E., Gado, M.H., Miller, M.I., Morris, J.C. and Csernansky, J.G. (2003) 'Changes in hippocampal volume and shape across time distinguish dementia of the Alzheimer type from healthy aging', *NeuroImage*, 20(2), pp. 667-682.

Wang, Q.J., Ding, Y., Kohtz, S., Mizushima, N., Cristea, I.M., Rout, M.P., Chait, B.T., Zhong, Y., Heintz, N. and Yue, Z. (2006) 'Induction of Autophagy in Axonal Dystrophy and Degeneration', *The Journal of Neuroscience*, 26(31), pp. 8057-8068.

Wang, X., Xing, A., Xu, C., Cai, Q., Liu, H. and Li, L. (2010) 'Cerebrovascular hypoperfusion induces spatial memory impairment, synaptic changes, and amyloid-β oligomerization in rats', *Journal of Alzheimer's disease : JAD*, 21(3), pp. 813-822.

Wardlaw, J.M. (2008) 'What Is a Lacune?', *Stroke*, 39(11), pp. 2921-2922.

Wardlaw, J.M., Sandercock, P.A.G., Dennis, M.S. and Starr, J. (2003) 'Is Breakdown of the Blood-Brain Barrier Responsible for Lacunar Stroke, Leukoaraiosis, and Dementia?', *Stroke*, 34(3), pp. 806-812.

Wardlaw, J.M., Smith, C. and Dichgans, M. (2013) 'Mechanisms of sporadic cerebral small vessel disease: insights from neuroimaging', *The Lancet Neurology*, 12(5), pp. 483-497.

Weller, R., Djuanda, E., Yow, H.-Y. and Carare, R. (2009) 'Lymphatic drainage of the brain and the pathophysiology of neurological disease', *Acta Neuropathologica*, 117(1), pp. 1-14.

West, M.J. (1999) 'Stereological methods for estimating the total number of neurons and synapses: issues of precision and bias', *Trends in Neurosciences*, 22(2), pp. 51-61.
West, M.J., Coleman, P.D., Flood, D.G. and Troncoso, J.C. (1994) 'Differences in the pattern of hippocampal neuronal loss in normal ageing and Alzheimer's disease', *The Lancet*, 344(8925), pp. 769-772.
West, M.J. and Slomanka, L. (2001) '2-D versus 3-D cell counting – a debate ', *Trends in Neurosciences*, 24(7), p. 374.
Wetterling, T., Kanitz, R.-D. and Borgis, K.-J. (1996) 'Comparison of Different Diagnostic Criteria for Vascular Dementia (ADDTC, DSM-IV, ICD-10, NINDS-AIREN)', *Stroke*, 27(1), pp. 30-36.
Wharton, S.B., Brayne, C., Savva, G.M., Matthews, F.E., Forster, G., Simpson, J., Lace, G. and Ince, P.G. (2011) 'Epidemiological Neuropathology: The MRC Cognitive Function and Aging Study Experience', *Journal of Alzheimer's Disease*, 25(2), pp. 359-372.
Xu, F., Gu, J.-H. and Qin, Z.-H. (2012) 'Neuronal autophagy in cerebral ischemia', *Neuroscience Bulletin*, 28(5), pp. 658-666.
Yamamoto, Y., Ihara, M., Tham, C., Low, R.W.C., Slade, J.Y., Moss, T., Oakley, A.E., Polvikoski, T. and Kalaria, R.N. (2009) 'Neuropathological Correlates of Temporal Pole White Matter Hyperintensities in CADASIL', *Stroke*, 40(6), pp. 2004-2011.
Yan, B.C., Park, J.H., Ahn, J.H., Lee, J.-C., Won, M.-H. and Kang, I.-J. (2013) 'Postsynaptic density protein (PSD)-95 expression is markedly decreased in the hippocampal CA1 region after experimental ischemia–reperfusion injury', *Journal of the Neurological Sciences*, 330(1–2), pp. 111-116.
Yanagihara, T., Brengman, J.M. and Mushynski, W.E. (1990) 'Differential vulnerability of microtubule components in cerebral ischemia', *Acta Neuropathologica*, 80(5), pp. 499-505.
Yeh, C.-Y., Vadhwana, B., Verkhratsky, A. and Rodríguez, J.J. (2011) 'Early astrocytic atrophy in the entorhinal cortex of a triple transgenic animal model of Alzheimer's disease', *ASN Neuro*, 3(5), p. e00071.
Yoshimi, K., Takeda, M., Nishimura, T., Kudo, T., Nakamura, Y., Tada, K. and Iwata, N. (1991) 'An immunohistochemical study of MAP2 and clathrin in gerbil hippocampus after cerebral ischemia', *Brain Research*, 560(1–2), pp. 149-158.
Yu, W.H., Cuervo, A.M., Kumar, A., Peterhoff, C.M., Schmidt, S.D., Lee, J.-H., Mohan, P.S., Mercken, M., Farmery, M.R., Tjernberg, L.O., Jiang, Y., Duff, K., Uchiyama, Y., Näslund, J., Mathews, P.M., Cataldo, A.M. and Nixon, R.A. (2005) 'Macroautophagy—a novel β-amyloid peptide-generating pathway activated in Alzheimer's disease', *The Journal of Cell Biology*, 171(1), pp. 87-98.
Zarow, C., Sitzer, T. and Chui, H. (2008) 'Understanding hippocampal sclerosis in the elderly: Epidemiology, characterization, and diagnostic issues', *Current Neurology and Neuroscience Reports*, 8(5), pp. 363-370.
Zarow, C., Vinters, H.V., Ellis, W.G., Weiner, M.W., Mungas, D., White, L. and Chui, H.C. (2005) 'Correlates of hippocampal neuron number in Alzheimer's disease and ischemic vascular dementia', *Annals of Neurology*, 57(6), pp. 896-903.
Zekry, D., Duyckaerts, C., Moulias, R., Belmin, J., Geoffre, C., Herrmann, F.R. and Hauw, J. (2002) 'Degenerative and vascular lesions of the brain have synergistic effects in dementia of the elderly', *Acta Neuropathologica*, 103, pp. 418-487.
Zhang, S., Boyd, J., Delaney, K. and Murphy, T.H. (2005) 'Rapid Reversible Changes in Dendritic Spine Structure In Vivo Gated by the Degree of Ischemia', *The Journal of Neuroscience*, 25(22), pp. 5333-5338.
Zhang, Z.G., Bower, L., Zhang, R.L., Chen, S., Windham, J.P. and Chopp, M. (1999) 'Three-dimensional measurement of cerebral microvascular plasma perfusion, glial fibrillary acidic protein and microtubule associated protein-2 immunoreactivity after embolic stroke in rats: a double fluorescent labeled laser-scanning confocal microscopic study', *Brain Research*, 844(1–2), pp. 55-66.

Zhu, C.-Q., Wang, X., Xu, F., Bahr, B.A., Shibata, M., Uchiyama, Y., Hagberg, H. and Blomgren, K. (2005) 'The influence of age on apoptotic and other mechanisms of cell death after cerebral hypoxia–ischemia', *Cell Death and Differentiation*, 12, pp. 162-176.

Zlokovic, B.V. (2011) 'Neurovascular pathways to neurodegeneration in Alzheimer's disease and other disorders', *Nature Reviews Neuroscience*, 12, pp. 723-738.